

TESIS DOCTORAL



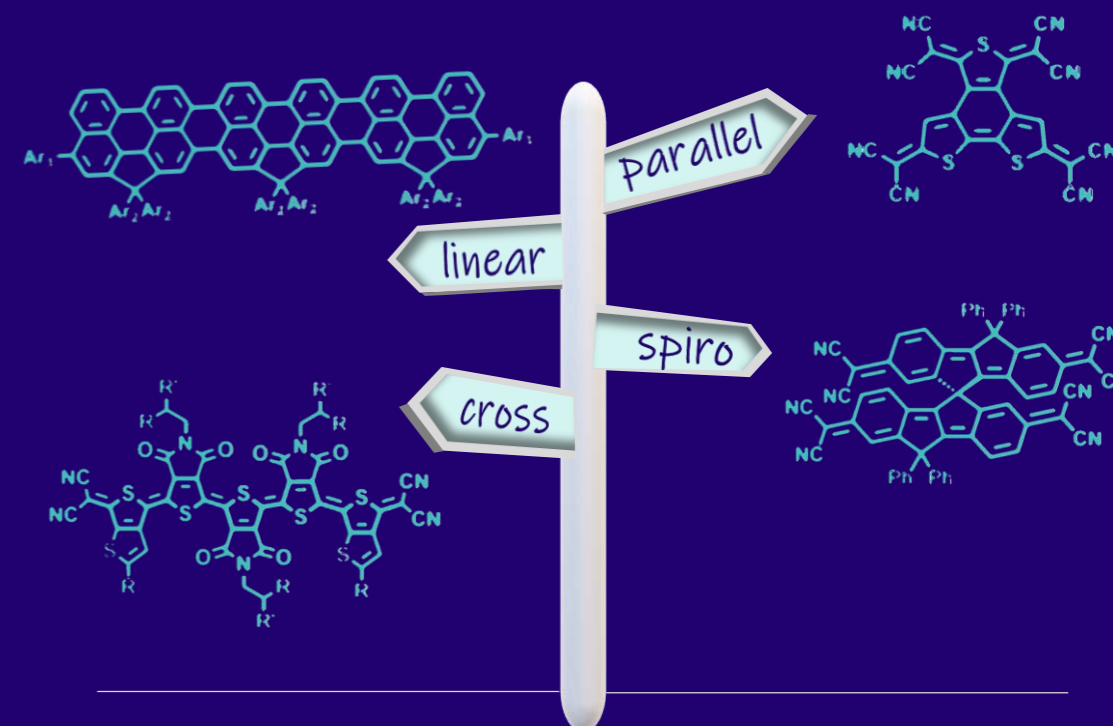
UNIVERSIDAD DE MÁLAGA



Samara Lourdes Medina Rivero

TESIS DOCTORAL

DIRADICALS SHAPED BY DOUBLE π -CONJUGATION: CONTRIBUTION FROM MOLECULAR SPECTROSCOPY



TESIS DOCTORAL

Samara Lourdes Medina Rivero

Diradicals Shaped by Double π -Conjugation:
Contribution from Molecular Spectroscopy



UNIVERSIDAD
DE MÁLAGA

Directores: Juan Casado Cordon y F. Javier Ramírez Aguilar

Departamento de Química-Física, Facultad de Ciencias

2020

Doctorado en Química y Tecnologías Químicas, Materiales y Nanotecnología



DECLARACIÓN DE AUTORÍA Y ORIGINALIDAD DE LA TESIS PRESENTADA PARA OBTENER EL TÍTULO DE DOCTOR

D./Dña SAMARA LOURDES MEDINA RIVERO

Estudiante del programa de doctorado QUÍMICA Y TECNOLOGÍAS QUÍMICAS, MATERIALES Y NANOTECNOLOGÍA de la Universidad de Málaga, autor/a de la tesis, presentada para la obtención del título de doctor por la Universidad de Málaga, titulada: "DIRADICALS SHAPED BY DOUBLE PI-CONJUGATION: CONTRIBUTION FROM MOLECULAR SPECTROSCOPY".

Realizada bajo la tutorización de JUAN CASADO CORDÓN y dirección de JUAN CASADO CORDÓN Y FRANCISCO JAVIER RAMÍREZ AGUILAR (si tuviera varios directores deberá hacer constar el nombre de todos)

DECLARO QUE:

La tesis presentada es una obra original que no infringe los derechos de propiedad intelectual ni los derechos de propiedad industrial u otros, conforme al ordenamiento jurídico vigente (Real Decreto Legislativo 1/1996, de 12 de abril, por el que se aprueba el texto refundido de la Ley de Propiedad Intelectual, regularizando, aclarando y armonizando las disposiciones legales vigentes sobre la materia), modificado por la Ley 2/2019, de 1 de marzo.

Igualmente asumo, ante a la Universidad de Málaga y ante cualquier otra instancia, la responsabilidad que pudiera derivarse en caso de plagio de contenidos en la tesis presentada, conforme al ordenamiento jurídico vigente.

En Málaga, a 24 de ENERO de 2020


Fdo.: SAMARA LOURDES MEDINA RIVERO





UNIVERSIDAD
DE MÁLAGA

AUTOR: Samara Lourdes Medina Rivero

 <http://orcid.org/0000-0003-4490-4813>

EDITA: Publicaciones y Divulgación Científica. Universidad de Málaga



Esta obra está bajo una licencia de Creative Commons Reconocimiento-NoComercial-SinObraDerivada 4.0 Internacional:

<http://creativecommons.org/licenses/by-nc-nd/4.0/legalcode>

Cualquier parte de esta obra se puede reproducir sin autorización pero con el reconocimiento y atribución de los autores.

No se puede hacer uso comercial de la obra y no se puede alterar, transformar o hacer obras derivadas.

Esta Tesis Doctoral está depositada en el Repositorio Institucional de la Universidad de Málaga (RIUMA): riuma.uma.es





UNIVERSIDAD DE MÁLAGA

D. **Juan Casado Cordón**, Catedrático de Universidad, y D. **Francisco Javier Ramírez Aguilar**, Catedrático de Universidad,

Certifican:

Que la memoria presentada por **Samara Lourdes Medina Rivero** bajo el título “**Diradicals Shaped by Double π -Conjugation: Contribution from Molecular Spectroscopy**”, para optar al título de Doctora en Ciencias Químicas por la Universidad de Málaga, ha sido realizada bajo nuestra dirección en los laboratorios del Departamento de Química Física de la Universidad de Málaga.

Considerando que constituye una investigación de alta calidad en el campo de la espectroscopía aplicada de materiales moleculares, se autoriza mediante este escrito su presentación y defensa como Tesis Doctoral en la Facultad de Ciencias de la Universidad de Málaga.

Y para que así conste, firman el presente certificado en Málaga a 24 de Enero de 2020.

Dr. D. Juan Casado Cordón

Dr. D. Francisco Javier Ramírez Aguilar



UNIVERSIDAD DE MÁLAGA

D. **Juan Carlos Otero Fernández de Molina**, Catedrático de Universidad y Director del Departamento de Química Física de la Universidad de Málaga,

Certifica:

Que la Tesis Doctoral titulada “**Diradicals Shaped by Double π -Conjugation: Contribution from Molecular Spectroscopy**”, que constituye la memoria que presenta Dña. **Samara Lourdes Medina Rivero** para optar al título de Doctora en Ciencias Químicas por la Universidad de Málaga, ha sido realizada bajo la dirección de los Doctores D. **Juan Casado Cordón** y D. **Francisco Javier Ramírez Aguilar**, en el Departametno de Química Física de la Universidad de Málaga.

Y para que así conste, firma el presente certificado en Málaga a 24 de Enero de 2020.

Dr. D. Juan Carlos Otero Fernández de Molina

Agradecimientos

Los acontecimientos vividos en el tramo final del desarrollo de esta tesis han hecho que eche la vista atrás con un criterio diferente al de hace solo unos meses. La situación sobrevenida en este año 2020 nos ha obligado a todos a reconsiderar nuestras prioridades y a valorar en su justa medida todos los aspectos que forman parte de nuestro día a día. Todos confiamos en la Ciencia para conseguir pronto una solución que nos permita volver a relacionarnos sin miedos ni restricciones. Ahora más que nunca, permitamos que todos los que la practican puedan hacer su trabajo de forma digna. **Sin Ciencia no hay futuro.**

Con esta memoria finaliza una etapa intensa y llena de nuevas experiencias en la que no ha tenido cabida el aburrimiento. El momento y lugar adecuados han hecho de ella un tiempo inolvidable, pues han permitido que la compartiera con personas que hacen que no quiera cambiar ni uno solo de los momentos vividos.

Los principales responsables de que haya podido disfrutar esta aventura son mis directores, Juan y Javier. Ellos me han dado la oportunidad de iniciarme en el mundo científico y me han guiado en estos primeros años de la mejor forma posible. A Javier, agradecerle que nos aporte siempre equilibrio, alternativas y palabras amables en los momentos críticos. Gracias de nuevo (prometo que será la última) por todo el trabajo de estos últimos meses, en los que nuestros pensamientos estaban en asuntos de mucha mayor importancia, gracias por hacerlo con la minuciosidad que te caracteriza. A Juan, agradecerle todo lo que me ha enseñado y su dedicación completa. Su pasión por la Ciencia hace que los que trabajamos con él veamos la investigación como un modo de vida. Gracias a ellos y a su trabajo hay un futuro después de esta memoria.

Mi agradecimiento también a todos los compañeros y amigos del Departamento de Química-Física y de los Servicios Centrales de Apoyo a la Investigación que han estado conmigo en el día a día y que siempre están dispuestos a ayudar. De entre todos ellos no puedo dejar de destacar a “mis conjurados” (¡me juego la expulsión!). Gracias a Fran, José María, Cristina Capel y Zafra. Me considero la estudiante de doctorado más afortunada por haber compartido con ellos estos años. Gracias por estar siempre conmigo, por apoyarme en los malos momentos (tanto científicos como personales), por tener siempre un buen consejo, por las risas y, por supuesto, por todo lo que me han enseñado (¡incluidos sus “inventos”!). En los mejores recuerdos de esta etapa siempre están ellos presentes. Tienen toda mi admiración, profesional y personal. Tampoco puedo olvidarme de los compañeros de batallas y de buenos momentos: María, Alexandra, Fernando, Luis, Iratxe, Sara y Guzmán. Gracias a Paula y a Zafra, por ser los mejores profesores en el laboratorio. Gracias a Iván Cheng, por la ayuda “orgánica” y por tener siempre un momento para compartir risas y penas.

Una de las mejores oportunidades de la investigación es la posibilidad de conocer personas que comparten tus inquietudes y estilo de vida. Gracias a Nadia por su “brilli-

brilli” y por hacer de las largas jornadas de trabajo para la organización de “la Escuela” tiempo compartido con una amiga. A Bea por su buen humor, incluso cuando todo parece ir mal, y a Ana Claudia, por transmitirnos su paz a las chicas más inquietas de “El Club del Crepe y el Cotilleo”.

One of the best memories of these years is the time in Québec. I am extremely grateful to my labmates in Laval University for their help with the Organic Chemistry and also with the snow! To Cyril, for his guide and for the coffee time! To Anthony and Chloé, because they always have a good plan for the weekend (thank you for showing me the best of the bad weather). Marie, thank you for being always sincere and for your long-distance friendship! (and for your blanket too!). To Ali, for the walks to the residence talking about everything, and to Aurélien, for making me laugh even at -10°C. Thanks to Fred for playing the music during the cold afternoons (best diradical team ever!). Merci beaucoup à tous.

Estos años de trabajo también han servido para forjar amistades que, estoy segura, durarán toda la vida, y para fortalecer otras que me han acompañado desde hace mucho tiempo. Gracias a Irene por abrirme su corazón y por hacerme ver que todos los problemas se pueden superar, gracias por tu perspectiva. Las largas jornadas de despacho junto a Sergio Gámez han hecho que las horas pasen, si no más rápido, sí de forma más agradable. Gracias por ser un gran amigo. A Abel solo puedo decirle que es y será siempre mi otro spin, porque solo con él son posibles “fiestas de la cubeta” y “céntimos de la suerte”. Gracias por su apoyo y su amistad y, sobre todo, por su magia. A Inés le agradezco que sea mi alma gemela, que vea el mundo exactamente igual que yo y que siempre me comprenda. Parece que los acontecimientos más desafortunados siempre nos acompañan, pero vivirlos contigo hace de ellos experiencias para recordar con mucho cariño (¡y humor!). Gracias por ser tan inocente y vergonzosa como yo, gracias por “elegirme” como amiga cuando aún Málaga no era mi hogar y por estos diez años de la mejor amistad. ¡Siempre serás mi mejor compañera de laboratorio! A Iván, porque nuestra amistad ha existido desde que tengo uso de razón. Gracias por tu apoyo, gracias por nunca dejar que el tiempo y la distancia deterioren la mejor de las relaciones. Gracias a Mine, por hacer que me ría siempre de todos mis problemas, y porque, a pesar de los suyos, siempre me regala su sonrisa.

Para el Dr. Zafra no valen los simples agradecimientos, por eso merece un punto aparte. Él ha sufrido todos mis peores momentos, personales y profesionales, de estos años. Nunca se ha cansado de enseñarme (¡incluso cuando no lo entiendo!), tanto en la ciencia como en la vida. A pesar de mi “intensidad”, nunca ha dejado de ayudarme, de aconsejarme y de intentar que esté preparada para las peores situaciones. Sin duda, eres lo mejor que me llevo de esta tesis.

Para el final he dejado a mi familia, porque a ellos egoístamente les he impuesto esta distancia. Gracias a mis hermanos: Benito, Fran y Gustavo, y gracias a mis cuñadas-hermanas: Maica, Olga y Esther. Gracias por cuidarme y quererme siempre como a una hija. Gracias a mis sobrinos: Aldara, Celia, Carla, Paula, Álvaro e Ethan, porque son lo

mejor que tengo. Gracias a Sergio, porque sin él no habría sido posible (especialmente este último tramo, del que él ha sido el principal afectado). Con todo, eres la fuerza motriz. Gracias a Mari y a Pascual, por darme una familia malagueña. Ellos hacen de Málaga un hogar. Por último, gracias a mi madre, porque ella es la que más ha sufrido estos años y porque todo lo que soy es gracias a ella. Espero que esté tan orgullosa de mí como yo lo estoy de ella.

Gracias a todos.

Para mi madre, artífice de todo.

***Para todas las niñas y niños que no tienen acceso a una educación,
porque estamos en deuda con ellos.***

Science involves confronting our “absolute stupidity”
(Martin A. Schwartz, *The Importance of Stupidity in Scientific Research*)

I feel that the greatest reward for doing is the opportunity to do more
(Jonas Salk)

Contents

| | |
|---|----------------|
| I. Introduction | 1—36 |
| I.I. π-Conjugated Organic Systems: Molecules “Born to Purple” | 3—12 |
| I.II. Cross-Conjugated Systems: A (No Longer) Neglected Family of Hydrocarbons | 13—18 |
| I.III. Spiro-Conjugation | 19—22 |
| I.IV. The Aromatic-Quinoidal Nature and the Diradical Character in π-Conjugated Systems | 23—29 |
| II. Goals | 37—44 |
| III. Methodology | 45—72 |
| III.I. Spectrochemical Methods | 47—61 |
| III.II. Complementary Techniques | 62—64 |
| III.III. Quantum Chemistry Calculations | 65—67 |
| IV. Results and Discussion | 73—228 |
| Section A. Linearly π-Conjugated Diradicals | 75—100 |
| 1. The Case of Aromatic and Quinoidal Oligorylenes | 76—100 |
| 1.1 <i>Neutral Species of CP-nR and nR-2N Oligorylenes</i> | 77—94 |
| 1.2 <i>Conclusions</i> | 95—96 |
| Section B. Cross-Conjugated Diradicals | 101—180 |
| 2. The Case of Aromatic Oligothienopyrrolediones: Cross-Conjugated Dianions | 102—130 |
| 2.1 <i>Neutral Species of OTPD_n Oligomers</i> | 103—115 |
| 2.2 <i>Charged Species of OTPD_n Oligomers</i> | 116—125 |
| 2.3 <i>Conclusions</i> | 126—127 |
| 3. The Case of Quinoidal Oligothienopyrrolediones: The Effect of Size | 131—180 |
| 3.1 <i>Neutral Species of 2DQoT Oligomers</i> | 133—146 |
| 3.2 <i>Charged Species of 2DQoT Oligomers. N-Doping</i> | 147—165 |
| 3.3 <i>Cross-Conjugation in Closed-Shell Molecules. Single Molecule Conductance</i> | 166—173 |
| 3.4 <i>Conclusions</i> | 174—175 |
| Section C. Spiro-Conjugated Diradicals | 181—228 |
| 4. The Case of Octacyano Diradicals: Spiro versus Parallel π-Conjugation | 182—228 |
| 4.1 <i>Neutral Species of CPV Family</i> | 183—201 |
| 4.2 <i>Charged Species of CPV Family</i> | 202—221 |
| 4.3 <i>Conclusions</i> | 222—224 |
| V. Concluding Remarks on Polyconjugated Systems | 229—234 |
| VI. Resumen y Conclusiones | 235—252 |
| VII. Appendices | 253—324 |
| VII.I. Acronyms | 255 |
| VII.II. Keywords | 256—257 |



| | |
|--|----------------|
| VII.III. Structures and IUPAC Formulation..... | 258—262 |
| VII.IV. Optimized Geometries..... | 263—266 |
| VII.V. Electron Paramagnetic Resonance (EPR) Spectra..... | 267—269 |
| VII.VI. UV-Vis-NIR Spectroelectrochemical Processes..... | 270—276 |
| VII.VII. Publications..... | 277—324 |

I. INTRODUCTION

I.I. π -Conjugated Organic Systems: Molecules “Born to Purple”

Introduction

Second century A.D., Roman emperor Trajan comes into Rome in triumph to celebrate his conquest on Dacia.^[1, 2] He wore the *toga picta*, completely coloured in Tyrian purple. This dye, only reserved for emperors, is the 6,6'-dibromo substituted indigo (Figure I.1).^[3]

21st century, Tyrian purple and derivatives are tested as functional materials in organic electronic devices, such as Organic Field Effect Transistors (OFFETs).^[4, 5] The evolution in the application of this organic molecule, and many other similar systems, is only explained by the deep knowledge of its chemical structure, and the properties derived from it.

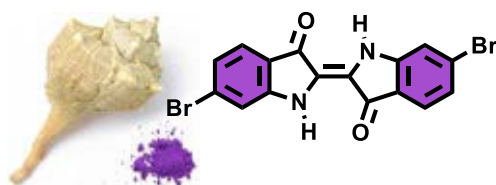


Figure I.1. Chemical structure of 6,6'-dibromoindigo (or Tyrian purple), together with the dye colour and the sea snail from which it is extracted.

Particularly in the case of π -conjugated organic molecules, as Tyrian purple, their structure-properties relation has been extensively studied since their probe as efficient semiconductors, making them potential substitutes of silicon-based electronic materials. The delocalization of the π -electrons through the carbon framework, as the valence electrons are delocalized over the metallic network in conducting metals, is responsible for the

semiconducting features of these systems. Therefore, establishing not only the electron delocalization mechanism and its extension, but also which factors disturb the π -electron density is of utmost importance to enhance the proper performance of these materials and also develop *ad hoc* synthesis for desired application.

However, it is obvious that the abstract concept of π -electron delocalization in organic molecules, that currently any chemist is familiar with, was not known by the Romans, and even today its notion is in some way intuitive.

Nowadays, electron delocalization definition given by the IUPAC Gold Book to describe a π -bond in a conjugated system is a bond which is not localized between two atoms, “instead, each link has a ‘fractional double bond character’ or bond order”.^[6] Also the delocalization energy is included in this definition as “the stabilization of the system compared with a hypothetical alternative in which formal (localized) single and double bonds are present.”^[6] Despite its simplicity once it is outlined, the way to this definition was not trivial and it was reached thanks to plenty of recognised scientists, contributing with right as well as mistaken hypothesis.

A Brief Historical Review

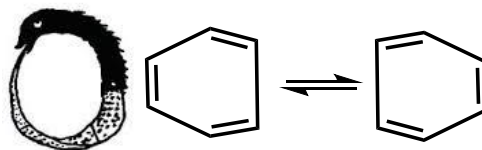
When the focus is on π -electron delocalization phenomenon in conjugated organic molecules, it is unavoidable to

think in benzene. This molecule is the cyclic π -electron delocalized (or aromatic) system par excellence.

Benzene was first isolated in 1825 by Michael Faraday from coal gas. Then, in 1834, the German chemist Eilhard Mitscherlich prepared it from the distillation of the benzoic acid and lime mixture and gave it the name of Benzin, then in English Benzene, (since the benzoic acid was obtained from the benzoin gum) and calculated its molecular weight.^[7] It was in 1855 when the term “aromatic” was employed by August Wilhelm Hofmann to describe the family of benzene and its derivatives, not with the chemical meaning they have today but only in reference to their fragrances.^[8]

Since its C_6H_6 empirical formula was established, several chemical structures were proposed for benzene. However, it was not until 1865 that the cyclic form was contemplated. Friedrich August Kekulé suggested firstly the hexacyclotriene structure for the benzene and then, in 1872, he described it with two *oscillating* mesomeric forms to account for the properties found experimentally, *i. e.*, the empirical equivalence of the six carbon positions, and the persistence of aromaticity upon reactions (Scheme I.1).^[7, 9] Obviously, these forms did not account for the empirical behaviour of benzene, which encourages the search of other possible cyclic structures.

It was Johannes Thiele, in 1899, who addressed the problem of one unique structure that really represents the benzene properties. According to “partial valences” theory, the carbon valences in

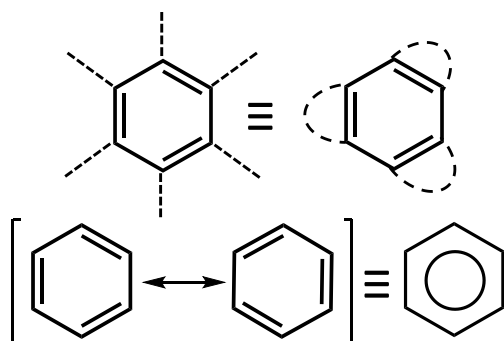


Scheme I.1. Chemical structures of benzene proposed by Kekulé in 1872, together with the vision of the snake biting its tale that gave him the idea. Observe that the equilibrium double arrow indicates the oscillation between the two mesomeric structures. The snake image was taken from The New York Times article “The Benzene Ring: Dream Analysis”.^[10]

benzene were not completely employed in forming the corresponding bonds, explaining the obtention of specific substitution products. By this way, the concept of resonance was somehow evoked, being the resulting chemical structure, indeed, used today (Scheme I.2).^[7, 9, 11]

Finally, in 1929 Kathleen Lonsdale obtained the X-Ray structure of hexamethylbenzene^[12], which demonstrated the identical lengths of the six CC bonds. Her experimental results, together with the formal introduction of the resonance phenomenon and its application to the chemical bonds by Werner Heisenberg and Linus Pauling, respectively, resulted in the description of benzene as an intermediate structure between two mesomeric forms, only differentiated in their electrons positions (Scheme I.2).^[7, 12]

With this short revision of the benzene structure evolution it is clear that π -electron delocalization and π -conjugation resonance are concepts that always come together and are hard to delimit. Turning again to the IUPAC Gold Book, resonance



Scheme 1.2. Chemical structures of benzene proposed by Thiele (*top*), together with the resonance forms and the resonance hybrid of benzene (*bottom*) as described today. Note that now the relationship between the two isomers is through a resonance double headed arrow, denoting that the actual structure is between these two forms.

phenomenon is described as “*the representation of the electronic structure of a molecular entity in terms of contributing structures.*”^[6] Now, in the field of Quantum Chemistry, it also explains “*Resonance among contributing structures means that the wavefunction is represented by 'mixing' the wavefunctions of the contributing structures*”^[6] and indicates that can be used to refer to the delocalization effect itself. In the same way, the resonance energy concept is similar to the delocalization energy description given above, and accounts for the energy difference between the most stable contributing resonance structure and the true chemical structure of the molecule.^[6]

In this sense, the play between the resonance and π -electron delocalization phenomena in π -conjugated organic materials is the origin of their semiconducting properties, and the contribution ratio of the different

resonance structures is the key to manage them.

Linear Carbon-based π -Conjugation

Carbon chains with an alternating CC simple and double bond pattern describe the simplest linear π -electron conjugated systems. These π -electrons are delocalized over the sp^2 framework formed by the C—C σ -bonds. This delocalization is possible by means of the overlapping of the p_π orbitals (or π - π overlapping). The way this delocalization works, and the properties derived from it, can be qualitatively explained by the Linear Combination of Atomic Orbitals approach (LCAO) of Erich Hückel, also known as Hückel Molecular Orbitals (HMO) theory.

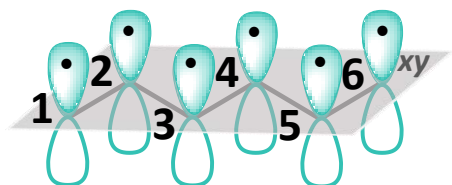
To illustrate the application of the Hückel method to study the electronic structure of π -conjugated organic systems, a simple linearly π -conjugated chain, the 1,3,5-hexatriene, will be described. In the framework of the HMO theory, the following approximations are assumed^[11, 13-15]:

- i. **σ/π separation.** In π -conjugated planar systems, σ orbitals are symmetric respect to the molecular plane (or xy plane) while π orbitals are antisymmetric. As a consequence, they belong to different irreducible representations of the molecular symmetry group, which allows us to assume that the interaction between these two orbitals groups is negligible. σ -orbitals ($2s$, $2p_x$ and $2p_y$ atomic

orbitals of carbon and heteroatoms, regarding only the valence electrons) form the sp^2 molecular framework, while π -orbitals ($2p_z$) constitute an independent system in which the π -electrons are freely delocalized.

With this assumption, the dependence between the energies and wavefunctions of the π -orbitals with those derived from the σ -orbitals vanishes, and only the solutions for the π -system are calculated.

In the case of the 1,3,5-hexatriene, which possesses 44 electrons, only the 6 π -electrons are considered within the HMO frame (see Scheme I.3).



Scheme I.3. Illustration of the $2p_z$ atomic orbitals of 1,3,5-hexatriene forming the π -system in the HMO approximation.

- ii. **The wavefunction.** Considering only the π -system and according to the LCAO approximation, the molecular orbital wavefunction is described as the linear combination of the $2p_z$ atomic orbitals of the sp^2 centres:

$$\Psi = \sum_{i=1}^N c_i \cdot \chi_i \quad \text{I.1.1}$$

Where χ_i refers to the valence atomic $2p_z$ orbitals of a molecule of N centres, and c_i to the atomic coefficients.

- iii. **The atomic orbital basis set is orthonormal.**

- iv. **Parametrization of the interaction integrals.** The interaction integrals are equal to the negative empirical values:

- α_i , when the Hamiltonian acts over the same centre, it is called *Coulomb integral* and is referred to the energy of an electron in the $2p_z$ atomic orbital of the corresponding centre plus the nuclear repulsion energy.
- β_i , when the interaction takes place between two different centres. This is the *resonance integral*, that accounts for the interaction between two atomic orbitals of two different centres and is equal to zero when the two centres are not adjacent. In consequence, β_i introduces the resonance stabilisation effect between two adjacent centres.

- v. **Atomic orbitals belonging to only one type of atom.** When the p_z atomic orbitals forming the π -system correspond to only one type of atom, the parameters α_i and β_i are generalized to the values α and β . This is the case of 1,3,5-hexatriene, where the π -system is formed only by the $2p_z$ atomic orbitals of carbon atoms.

With these approximations, the secular equations and determinant needed to obtain the atomic coefficients (c_i) and energy values (ε) of the atomic orbitals of 1,3,5-hexatriene is simplified to the following expression:

$$\begin{aligned} (\alpha - \varepsilon)c_1 + \beta c_2 &= 0 \\ \beta c_1 + (\alpha - \varepsilon)c_2 + \beta c_3 &= 0 \\ \beta c_2 + (\alpha - \varepsilon)c_3 + \beta c_4 &= 0 \end{aligned}$$

$$\begin{aligned}\beta c_3 + (\alpha - \varepsilon)c_4 + \beta c_5 &= 0 \\ \beta c_4 + (\alpha - \varepsilon)c_5 + \beta c_6 &= 0 \\ \beta c_5 + (\alpha - \varepsilon)c_6 &= 0\end{aligned}$$

I.1.2

$$\begin{vmatrix} \alpha - \varepsilon & \beta & 0 & 0 & 0 & 0 \\ \beta & \alpha - \varepsilon & \beta & 0 & 0 & 0 \\ 0 & \beta & \alpha - \varepsilon & \beta & 0 & 0 \\ 0 & 0 & \beta & \alpha - \varepsilon & \beta & 0 \\ 0 & 0 & 0 & \beta & \alpha - \varepsilon & \beta \\ 0 & 0 & 0 & 0 & \beta & \alpha - \varepsilon \end{vmatrix} = 0$$

I.1.3

To simplify these, each term of the determinant is divided by the parameter β and a new variable x is defined as:

$$x = \frac{\alpha - \varepsilon}{\beta} \quad \text{I.1.4}$$

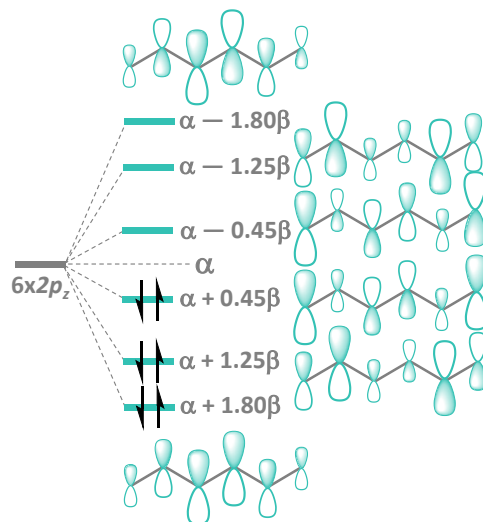
Solving the 6x6 determinant I.1.3 with the expression I.1.4, the energy values of the molecular orbitals of the π -system of 1,3,5-hexatriene are obtained. Once these energies are known the atomic coefficients can be also calculated from expression I.1.2 by imposing the orthonormality condition ($\langle \Psi | \Psi \rangle = 1$). At this point, the Hückel molecular orbitals energy diagram can be described as in Scheme I.4.

Since only the three lowest molecular orbitals are occupied in the ground electronic configuration, the total π -energy (E_π) of the 1,3,5-hexatriene is:

$$E_\pi = 6\alpha + 7.00\beta \quad \text{I.1.5}$$

Besides the total π and the molecular orbital energies, HMO also allows to obtain other significant magnitudes:

- **Resonance or delocalization energy (E_R):** as described above, this energy



Scheme I.4. Molecular orbitals energy diagram of the ground electronic configuration of 1,3,5-hexatriene. Different colour of the orbital lobes indicates different sign, and their sizes correspond to the absolute values of the corresponding atomic coefficients. Observe that the $(\alpha + 0.45\beta)$ molecular orbital constitutes the Highest Occupied Molecular Orbital (HOMO), while the $(\alpha - 0.45\beta)$ one is the Lowest Unoccupied Molecular Orbital (LUMO).

can be estimated from the difference between the E_π of 1,3,5-hexatriene (expression I.1.5) and the energy considering this molecule as three localized single bonds, *i.e.*, as the merge of three ethylene molecules. With the HMO approximation described, E_π of ethylene is:

$$E_\pi = 2\alpha + 2.00\beta \quad \text{I.1.6}$$

Ergo:

$$E_R = (6\alpha + 7.00\beta) - (6\alpha + 6.00\beta) = 1.00\beta \quad \text{I.1.7}$$

This value corresponds to the extra stabilization energy when the 6 π -electrons are delocalized in 1,3,5-hexatriene instead of forming three localized double C=C bonds.

- **Bond order (p_{ij})** of the π -system between two adjacent atoms i and j :

$$p_{ij} = \sum_r n_r \cdot c_{ir} \cdot c_{jr} \quad \mathbf{I.1.8}$$

Subscripts i and j refers to atoms, while r refers to the molecular orbitals. For 1,3,5-hexatriene:

$$p_{1-2} = 0.87$$

$$p_{2-3} = 0.48$$

$$p_{3-4} = 0.79$$

$$p_{4-5} = 0.48$$

$$p_{5-6} = 0.87$$

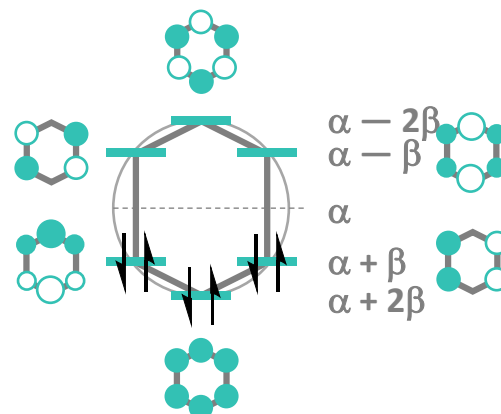
I.1.9

These values indicate the contribution of the π -bond, thus, in 1,3,5-hexatriene, the CC bond between atoms 1 and 2 (or 3 and 4) is not a *pure* double bond (in that case, the bond order should be $p = 1$), and the CC bond between atoms 2 and 3 (or 4 and 5) is not a *pure* single bond ($p = 0$). In consequence, the bond order gives an intuitive picture of the π -electron delocalization. Regarding these values, it can be also observed that the delocalization of the π -electrons is larger in the molecule centre, since the innermost double bond present a shorter p value than the two final double bonds ($p_{1-2} = p_{5-6} > p_{3-4}$).

The HMO approximation can be also applied to cyclic π -conjugated systems, as the benzene molecule. In this case, when solving the diagonalized 6x6 determinant, the energy values for the 6 molecular orbitals obtained from the linear combination of the 6 atomic orbitals are:

$$\varepsilon = \alpha \pm 2\beta, \alpha \pm \beta, \alpha \pm \beta \quad \mathbf{I.1.10}$$

Observe that solutions $\alpha + \beta$ and $\alpha - \beta$ appear twice, *i. e.*, these energy levels are doubly degenerated.



Scheme I.5. Molecular orbitals energy diagram of the ground electronic configuration of benzene. Different colour of the orbital lobes indicates different sign, and their size correspond to the absolute values of the corresponding atomic coefficients. Molecular orbitals are represented in top view for clarity.

The resonance energy in benzene can be calculated from the difference between the total π energy of this molecule and the localized cyclohexatriene:

$$E_{\pi}^{\text{benzene}} = 6\alpha + 8\beta$$

$$E_{\pi}^{\text{cyclohexatriene}} = 6\alpha + 6\beta$$

$$E_R = (6\alpha + 8\beta) - (6\alpha + 6\beta) = 2\beta$$

I.1.11

The larger resonance energy of benzene respect to the 1,3,5-hexatriene (2β and 1β according to expressions **I.1.11** and **I.1.7**, respectively), highlights that not only the π - electron delocalization contributes to the stabilization of the cyclic molecule, but also the σ -framework with strong single C—C bonds and an internal

angle of 120° . The generalization of this extra stabilization for other cyclic π -systems with $4n+2$ π -electrons is the well-known Hückel's rule of aromaticity.^[13, 14, 16]

The Optical Bandgap and the Oligomer Approach

Even with the basic HMO approximation in π -conjugated systems, the enlargement of the delocalization phenomenon when increasing the number of alternating double and single bonds (the size of the π -conjugated framework) is evident. The combination of atomic orbitals in longer π -conjugated molecules (or oligomers, since they use to be composed by repeating units) generates more stabilized unoccupied molecular orbitals and less stabilized occupied molecular orbitals. Given that the π - π overlapping of a greater number of successive molecular orbitals enhances the electron delocalization through the linear path, the π -conjugation effect will increase with the oligomer length.^[17] This hypothesis leads to the conclusion that in an infinite C—C/C=C alternating bonds chain (polyacetylene) the π -electron delocalization will be maximum, provoking a metallic behaviour in this kind of systems. However, this structure is highly unstable and the apparition of chain defects (two consecutive single or double bonds) gives rise to a dimerization distortion (known as Peierls distortion), where two degenerated structures are obtained.^[15, 17, 18] In consequence, a gap between the highest occupied (HOMO) and lowest unoccupied (LUMO) molecular

orbitals energy levels can be described, and a semiconductor character is revealed for polyacetylene.

Therefore, the fact that a finite gap can be *measured* for an infinite polymer leads to the conclusion that there is a determined number of repetitive monomeric units at which the optical properties converge, and hardly differ from those of the hypothetical infinite polymer. This phenomenon is referred as the *effective conjugation length*. The effective conjugation length (n_{ECL}) is defined as the oligomer length at which the wavelength of the absorption maxima is equal or less than 1 nm larger than the one of the previous oligomer.^[19, 20] In this context, all the properties derived from the π -electron delocalization can be considered unaltered from the oligomer with n_{ECL} units, even the heavier polymers. The value of this parameter can be explored by means of the Meier's equations:^[21-23]

$$E(n) = E_\infty + (E_1 - E_\infty)e^{-a(n-1)} \quad \mathbf{1.1.12}$$

$$\lambda(n) = \lambda_\infty + (\lambda_1 - \lambda_\infty)e^{-b(n-1)} \quad \mathbf{1.1.13}$$

Equation **1.1.12** corresponds to the Meier's expression in terms of energy, while equation **1.1.13** is expressed in terms of the absorption wavelength. These equations relate the number of monomeric units (n) with the transition energy or electronic absorption maximum wavelength of the infinite chain (E_∞ and λ_∞ , respectively). E_1 and λ_1 correspond to the data of the first oligomer of the series, and parameters a and b indicate how fast the

limit of convergence is reached.^[21, 22] By fitting the experimental optical data to these exponential equations, the values of E_∞ , λ_∞ and n can be obtained. The number of monomeric units (n) in the limit of convergence ($n \rightarrow \infty$) is the mentioned *effective conjugation length*. In Figure 1.2, the classical Meier's plot of π -conjugated organic oligomers (a family of regioregular oligo(thieno[3,4-b]thiophene)s^[24]) is showed. For this particular system, the maximum absorption wavelength converges to 906 nm at a chain size of 33 monomers, that is, the electronic properties of any oligomer or polymer with $n > 33$ units will be similar to those of the oligomer of this size.

In any case, the discovery of the semiconducting properties of π -conjugated organic polymers has been a turning point in the development of new electronic devices and transformed the study of these systems in an emerging research field. The existence of an effective conjugation length for the semiconducting polymers has brought about the development of the most used methodology to elucidate the electronic and optical properties of these systems: the oligomer approach. The systematic study of the evolution of these properties when lengthening the oligomer size (which is actually the case of the Meier's fitting), from the monomer to a size closer to the effective conjugation length, and their extrapolation to the infinite chain, allows to establish straightforward structure-properties relationships in simpler systems.^[25]

As has been already mentioned, the

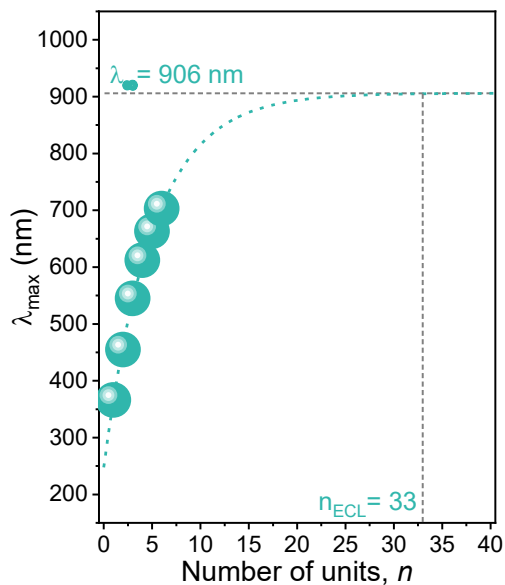


Figure 1.2. Meier's plot fitting of a series of π -conjugated oligo(thieno[3,4-b]thiophene)s together with its effective conjugation length (n_{ECL}) and its corresponding absorption maximum of the infinite chain (λ_∞).

energies of the highest occupied (HOMO) and lowest unoccupied (LUMO) molecular orbitals are crucial in π -conjugated functional materials. The energy difference between these two frontier molecular orbitals, or optical bandgap (E_g), modulates the conducting properties of these systems in the same way as the gap between the valence and the conduction bands govern the behaviour of inorganic semiconductors. For this reason, one of the main goals that must be addressed through the oligomer approach is to obtain structural features that allow a reduction of this optical bandgap.^[25-28] These relations will provide a synthetic guide to obtain π -conjugated systems with tailored properties.

The structural factors that govern the HOMO-LUMO gap are:^[26-28]

1. **The aromaticity or resonance stabilization energy.** As it has been described in the previous section, the molecular orbital energies of the π -systems are linked to the resonance or delocalization energy.

2. **The bond length alternation (BLA) or aromatic/quinoidal tautomerism.**

Bond length alternation (or BLA) parameter is defined as the difference between the lengths of the single and double bonds in a π -conjugated system. Therefore, BLA is directly related to the π -electron delocalization in organic molecules, since this phenomenon provokes the enlarging of the double C=C bonds and the shortening of the single ones.^[29-31] In other words, in highly π -electron delocalized systems the BLA value must be close to zero. This easy relation between the BLA and the π -electron delocalization is why this parameter has been extensively used in the study of the electronic and optical properties of organic π -conjugated oligomers to employ them as functional materials.^[32-36] In these cases, in which only one carbon framework is involved in the delocalization of the π -electrons, BLA diminishes with the number of monomeric units as a consequence of the extension of the π - π overlapping. Consequently, shorter BLA values are related with narrower HOMO-LUMO gaps.

3. **The planarity or rigidity of the system.**

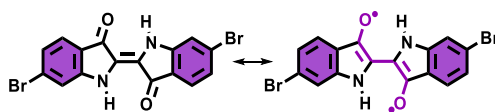
The rigidification of the carbon backbone improves the π - π overlapping between consecutive p_z

orbitals of the π -system, hence, E_g is reduced.

4. **The substituent groups.** In general, electron-withdrawing groups, as cyano units, stabilize the HOMO level, increasing the optical bandgap, while electron-releasing groups rise this level, narrowing E_g .

The evolution of these factors as a function of the π -electron delocalization is relatively easy to study applying the oligomer approach, since longer oligomers generally mean larger π -conjugation. But, what is the behaviour of the electron density when more than one π -conjugated framework occurs in the molecule?

Coming back to our initial example, the 6,6'-dibromoindigo presents two connected benzene rings. However, the π -systems of these two rings are not *electronically connected* due to the presence of an alternative π -conjugated framework that isolates them. The withdrawing character of the Oxygen atoms and the double bond of the carbonyl groups allow the delocalization of the π -electrons towards them, leading to an alternative resonance structure that contributes to the chemical structure of 6,6'-dibromoindigo (and other indigo derivatives). These structures are presented in Scheme 1.6.:



Scheme 1.6. Resonance structures of 6,6'-dibromoindigo. Aromatic rings and the cross-conjugated framework in the diradical resonance structure (*right*) are highlighted in purple.

This second π -conjugated pathway is the motif responsible for the electronic properties of this kind of molecules, with the aromatic benzene rings playing a secondary role.

Two key points in the study of π -conjugated organic molecules are revealed in the resonance structures presented in Scheme I.6:

- i. Alternative π -electron delocalization frameworks can co-exist with the main linearly conjugated sequence. Despite the resonance structures corresponding to the electron delocalization through these pathways may not be the largest contributing forms, their existence can modify significantly the optical, electronic and molecular properties of the system under study.
- ii. These alternative resonance structures are usually described as diradical forms of the molecule of interest. In consequence, diradical properties must be taken into consideration in the study of these polyconjugated systems.

I.II. Cross-Conjugated Systems: A (No Longer) Neglected Family of Hydrocarbons

Cross-Conjugation

Cross-conjugation is present in systems with “three unsaturated groups, two of which although conjugated to a third unsaturated centre are not conjugated to each other”.^[37] In consequence, the two isolated centres conjugated to the third one must be separated by two single bonds to avoid the π -electron conjugation between them. In this regard, the lone pair electrons of heteroatoms (as nitrogen, oxygen or sulphur) can be also considered as unsaturated groups. Cross-conjugated molecules can be also defined as π -conjugated systems in which “two conjugation paths share a multiple bond”.^[38] With these definitions, a general cross-conjugation motif can be described (Figure I.3).

In other words, the cross-conjugated framework can be defined as an alternative π -electron delocalization pathway, orthogonal to the predominant linear one (see Figure I.3). Therefore, a competitive effect is established between the two conjugated sequences, affecting the delocalization of the π -electrons through the linear path and, consequently, the electronic properties derived from the π -system.

Despite the influence of this cross-conjugated framework in the electronic and optical properties of these kind of organic systems has not been extensively studied, this property is relatively common in the organic field. Indeed, some renowned systems in the Chemistry History present cross-conjugation. This is

the case of urea or the already mentioned indigo and its derivatives. In Figure I.3 some examples of cross-conjugated molecules are presented.

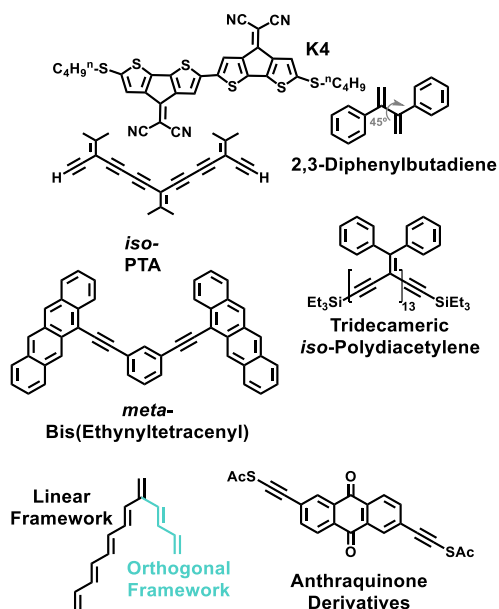
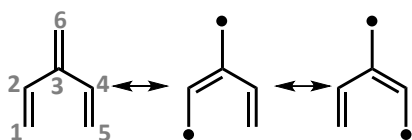


Figure I.3. Examples of cross-conjugated π -systems.

MO Description of Cross-Conjugation

Analogous to the molecular orbitals description of 1,3,5-hexatriene applying the Hückel's approximation, the molecular energy levels diagram of a cross-conjugated system can be also built. For this purpose, the simplest cross-conjugated carbon chain will be considered: the 3-methylene-1,4-pentadiene (or [3]-dendralene, the first oligomer of this series). The resonance forms that contribute to the chemical structure of this molecule are depicted in Scheme I.7:



Scheme 1.7. Resonance structures of 3-methylene-1,4-pentadiene. Observe that C=C bonds 1,2 and 4,5 are conjugated to 3,6, but not between them.

At first sight, it is evident that CC bonds 1,2 and 4,5 do not possess a *pure* double character, and, in the same line, C₂—C₃ and C₃—C₄ are not *pure* single bonds. But what is the character of CC bond 3,6? To which extent it is affected by the *doubly* π-conjugation?

To build the MO energy diagram and obtain the bond orders, the secular equations and determinant of 3-methylene-1,4-pentadiene are described according to the approximations of the HMO theory. In this case the π-system is formed by 6 2p_z atomic orbitals, contributing each one with 1 π-electron, thus 6 molecular orbitals must be obtained.

$$(\alpha-\varepsilon)C_1 + \beta C_2 = 0$$

$$\beta C_1 + (\alpha-\varepsilon)C_2 + \beta C_3 = 0$$

$$\beta C_2 + (\alpha-\varepsilon)C_3 + \beta C_4 + \beta C_6 = 0$$

$$\beta C_3 + (\alpha-\varepsilon)C_4 + \beta C_5 = 0$$

$$\beta C_4 + (\alpha-\varepsilon)C_5 = 0$$

$$\beta C_5 + (\alpha-\varepsilon)C_6 = 0$$

I.2.1

According to that, a 6x6 secular determinant must be solved. In this case, some new resonance integrals (β, in green in expressions I.2.1 and I.2.2) that were not present in the secular equations of

1,3,5-hexatriene, are introduced to account for the 3,6 CC bond.

$$\begin{vmatrix} \alpha-\varepsilon & \beta & 0 & 0 & 0 & 0 \\ \beta & \alpha-\varepsilon & \beta & 0 & 0 & 0 \\ 0 & \beta & \alpha-\varepsilon & \beta & 0 & \beta \\ 0 & 0 & \beta & \alpha-\varepsilon & \beta & 0 \\ 0 & 0 & 0 & \beta & \alpha-\varepsilon & 0 \\ 0 & 0 & \beta & 0 & 0 & \alpha-\varepsilon \end{vmatrix} = 0$$

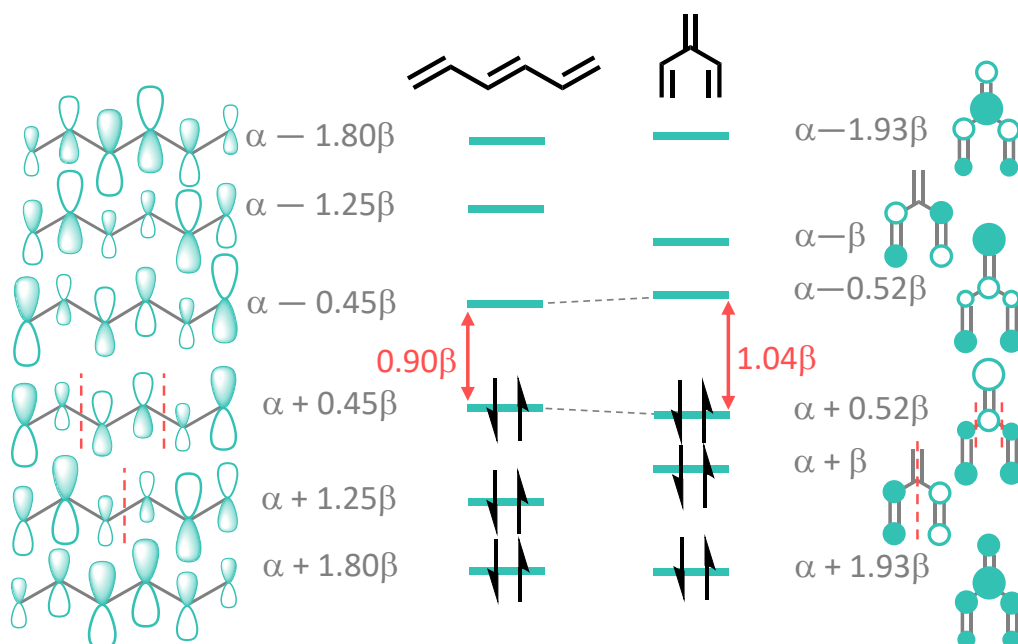
I.2.2

Following the procedure described in the former section for 1,3,5-hexatriene, the energy values and the atomic coefficients can be obtained. The MO energy diagram of 3-methylene-1,4-pentadiene is displayed in Scheme I.8.

As can be seen from the orbitals representation in Scheme I.8, coefficients of C₂, C₃ and C₄ (indicated with the lobes sizes) in HOMO-2, with bonding nature, are larger than those in HOMO, where present an antibonding character. Thus, the resulting π-bonding interaction between these centres evidences the existence of cross-conjugation, or in other words, there is a non negligible contribution of the cross-conjugated resonance forms to the true molecular structure.^[37]

The bond order values, the total π-energy (E_π) and the resonance energy (E_R) can be also obtained, and are presented in Table I.1.

According to these values, some extension of the π-system is over the 2-3 and 3-4 CC bonds *i. e.*, they are not *pure* single CC bonds (36% of π-bond). The



Scheme I.8. Molecular orbitals energy diagram of the ground electronic configuration of linear 1,3,5-hexatriene (*left*) and cross-conjugated 3-methylene-1,4-pentadiene (*right*). Different colour of the orbital lobes indicates different sign, and their size correspond to the absolute values of the corresponding atomic coefficients. Molecular orbitals of 3-methylene-1,4-pentadiene are represented from top view for clarity. Red arrows and numbers indicate the HOMO-LUMO gap, and red, dashed lines highlights the nodal planes.

Table I.1. Bonds Order, total π and resonance energies for linear and cross-conjugated molecules under study.

| Bonds Orders | $p_{1-2} = 0.87$ | $p_{1-2} = 0.88$ |
|-----------------------------|-----------------------|-----------------------|
| | $p_{2-3} = 0.48$ | $p_{2-3} = 0.36$ |
| | $p_{3-4} = 0.79$ | $p_{3-4} = 0.36$ |
| | $p_{4-5} = 0.48$ | $p_{4-5} = 0.88$ |
| | $p_{5-6} = 0.87$ | $p_{3-6} = 0.96$ |
| E_{π} | $6\alpha + 7.00\beta$ | $6\alpha + 6.69\beta$ |
| E_R | 1.00β | 0.69β |

largest double bond character was found for $C_3=C_6$ bond, which corroborates the larger contribution of the non-diradical (or *closed-shell*) resonance form to the ground electronic configuration structure. This conclusion could be also extracted applying the Valence Bond Theory (VBT) according to the resonance forms of 3-methylene-1,4-pentadiene (Scheme I.7). However, this approximation does not account for the larger total π and resonance energies of the linear carbon chain respect to the crossed one. The HMO theory can explain these differences when the nodal planes of the occupied MO are considered. In Scheme I.8, nodal planes in 1,3,5-hexatriene are always placed between carbon atoms, thus the six π -

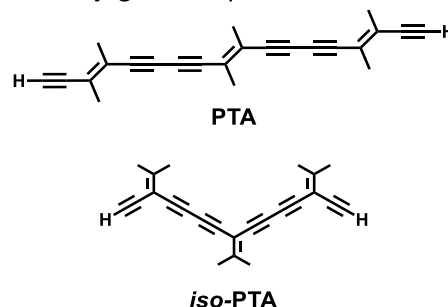
electrons of the six $2p_z$ orbitals contribute to the π -system. However, in the case of 3-methylene-1,4-pentadiene the HOMO-1 level presents a nodal plane in the cross-conjugated atoms (C_3 and C_6), hence these atoms do not contribute to the π -system in this MO. Consequently, only four π -electrons participate in one of the resonance structures of the cross-conjugated molecule, diminishing the total π -energy and, subsequently, the resonance stabilization energy. The shorter π -electron delocalization in 3-methylene-1,4-pentadiene than in 1,3,5-hexatriene is also revealed in the larger HOMO-LUMO gap of the cross-conjugated system, as can be seen in Scheme I.8.

Cross-Conjugation Expression

The presence of an alternative, orthogonal electron delocalization framework in π -conjugated organic systems modifies the properties of the main conjugated sequence. When comparing with linear molecules, these variations are expressed by the following parameters:

1. Bond Length Alternation (BLA). Lüthi *et al.* studied the BLA evolution in a series of linearly conjugated polytriacetylenes (PTAs) and cross-conjugated *iso*-polytriacetylenes (*iso*-PTAs) (see Scheme I.9).^[39] They found that, while for PTAs the BLA diminishes progressively from the dimer to the octamer, with a total reduction of 0.010 Å (calculated at the B3LYP/6-31G** level of theory), in the case of *iso*-PTAs,

BLA does not change significantly from the trimer to larger molecules. The slight elongation observed for the cross-conjugated double C=C bond is ascribed to their participation in the two conjugated sequences.



Scheme I.9. Chemical structures of polytriacetylenes (PTA) and *iso*-polytriacetylenes (*iso*-PTA) from reference [39].

2. Effective Conjugation Length. This parameter is intimately related to the BLA value since it converges at the effective conjugation length.

For PTAs and *iso*-PTAs polymers, the effective conjugation length was determined to be $n_{ECL} = 8$ monomeric units (24 conjugated bonds) for the first one, and $n_{ECL} = 3$ (9 conjugated bonds) for the cross-conjugated system.^[39]

The fact that both parameters, BLA and n_{ECL} values, are shorter for the cross-conjugated oligomers than for the linear ones indicates that the crossed system reaches its maximum π -electron delocalization at shorter oligomer sizes than the corresponding linear molecules. That is, π -conjugation is less effective in cross-conjugated oligomers.

3. HOMO-LUMO Gap. The impact of the two former parameters in the electronic properties of the molecules

under study is observed in the HOMO-LUMO gap. Small BLA and n_{ECL} values, which are almost constant along the oligomeric series, means that the optical band gap remains also invariable when lengthening the oligomer size.

Returning to the PTA and *iso*-PTA oligomers, the linear oligomers present a larger reduction of the optical bandgap with the oligomer size than the corresponding crossed models.^[39] The cross-conjugated sequences make the π -electron density to also delocalize through them, withdrawing it from the linear carbon backbone. By this way, the cross-conjugated sequences reduce the extension of the π -conjugation through the main chain. Consequently, the narrowing of the optical bandgap with the oligomer size is not as significant as for linear molecules.

In Scheme I.8, a comparison between the HOMO-LUMO gap of a linear and cross-conjugated systems is depicted. Despite both molecules present the same number of carbon atoms and double CC bonds (*i. e.*, the same number of π -electrons), the cross-conjugated 3-methylene-1,4-pentadiene displays a larger optical bandgap than the linear 1,3,5-hexatriene.

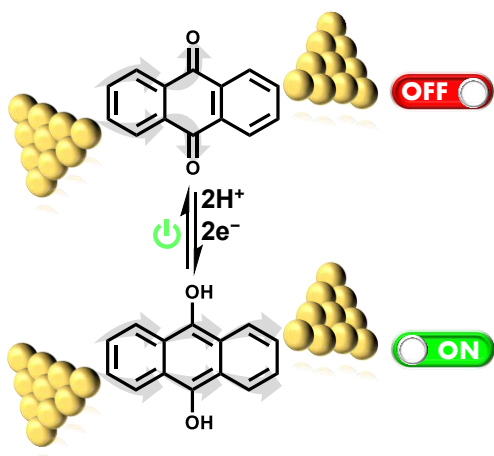
Applications of Cross-Conjugated Systems. Electron Transport

In 1984, Professor Henning Hopfs defined dendralenes as “*a neglected group of highly unsaturated hydrocarbons*”.^[40]

Then, in 2012, the same author reviewed the fast development of this kind of cross-conjugated systems in 27 years.^[41] This evolution was able thanks to the significant advances in the field of organic synthesis, that provided a wider range of substituted and/or longer cross-conjugated π -systems.

Due to the scarce knowledge about their electronic properties, initially the more extended use of cross-conjugated molecules (especially dendralenes) was as building blocks in organic synthesis involving the Diels-Alder mechanism.^[40-43]

However, the application of cross-conjugated systems as functional entities coincides with the development of single molecule electronics. In molecular electronic devices, as single-molecule switches or single-molecule field effect transistors, the charge transport through the molecule of interest is one of the crucial phenomena to assure their correct operation.^[44] In this context, it is evident that the conjugation pattern plays a critical role in the functionality of these devices. A well-known example is the reversible anthraquinone/hydroanthraquinone redox pair, which can switch the conductance by an electrochemical gating. At the starting point with the anthraquinone form, the electron transport through the molecule is interrupted by the cross-conjugated carbonyl groups. The electrochemical reduction to the enol form switches on the electronic linear path through the molecule, increasing the conductance of the system in more than one order of magnitude.^[45-47] In Scheme I.10 this mechanism has been represented.



Scheme 1.10. Representation of the switch off / switch on mechanism in the described anthraquinone/ hydroanthraquinone derivatives systems in single molecular conductance techniques.

The fact that the cross-conjugated form of the molecule switches off the conductance has been ascribed to destructive quantum interferences (QI).^[48, 49] This phenomenon takes place in charge transport when the interference between electron waves propagating through the molecular orbitals are out of phase, destructing or reducing the resulting quantum wave function.^[48, 49]

The use of cross-conjugated molecules as ON/OFF systems in single molecular conductance has not been limited only to anthraquinone derivatives. Tetraphenylethene based molecules or diphenylethene derivatives are some examples of cross-conjugated molecules studied in charge transfer techniques.^[50, 51]

I.III. Spiro-Conjugation

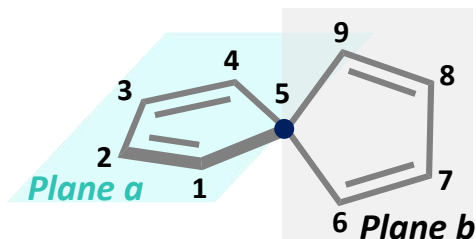
Through-Space Conjugation. Spiro-Conjugation

Linear and cross-conjugation in π -systems have been explained because of the π - π overlapping between the p_z orbitals of adjacent atoms. These interactions, called *through-bond* conjugation, have been described for systems where the CC bonds present an alternance between single and double bonds, *i. e.*, in which all the carbon atoms that participate in the π -delocalization are sp^2 hybridized.

In addition to this through-bond π -conjugation, also several forms of *through-space* delocalization can exist, such as homoconjugation and spiro-conjugation.

In general, *homoconjugation* concept refers to the interaction between two π -systems which are separated by an insulating atom.^[6, 52] This is possible when the appropriate spatial conformation is adopted. When two homoconjugated systems lie in two orthogonal planes with only a tetrahedral atom in common, this specific kind of homoconjugation interaction between the atoms adjacent to the tetrahedral one is called *Spiro-conjugation*.^[15, 53]

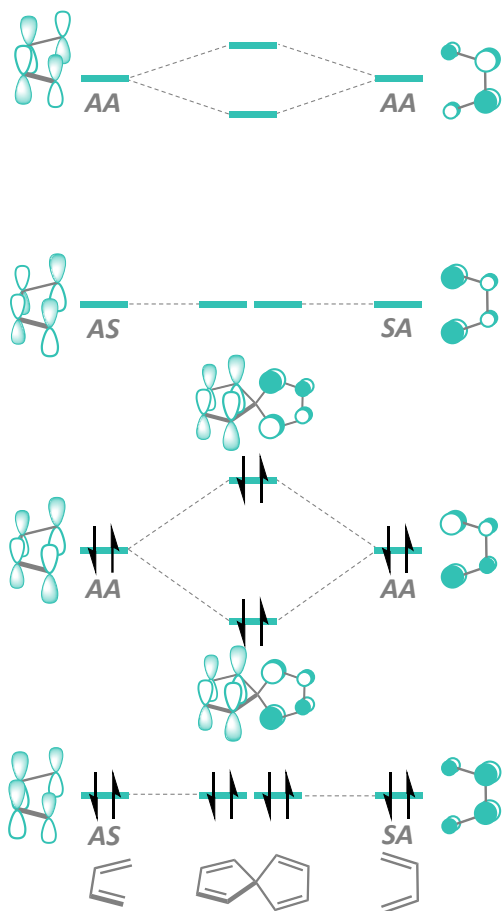
The classical example to study the spiro-conjugation phenomenon is that of two 1,3-butadiene systems held in two orthogonal planes, *i. e.*, the spiro[4.4]nonatetraene, showed in Scheme I.11. In order to understand the spiro interaction between the two perpendicular π -systems, the molecular orbital diagram of the spiro[4.4]



Scheme I.11. Chemical structure of spiro[4.4]nonatetraene. Each 1,3-butadiene system is held in one of the two orthogonal planes *a* and *b*. The tetrahedral carbon (or spiro carbon) is highlighted in blue (C_5).

nonatetraene (Scheme I.12) can be constructed from that of the 1,3-butadiene. In Scheme I.12 the molecular orbitals of the two 1,3-butadiene moieties are also showed. Considering that only MO with the same symmetry can be combined, only those energy levels with antisymmetric behaviour respect to both perpendicular planes (denoted as AA in Scheme I.12) will present interaction. Thus, the AA levels of both 1,3-butadiene moieties are combined producing a stabilized and a destabilized MO in the spiro system.

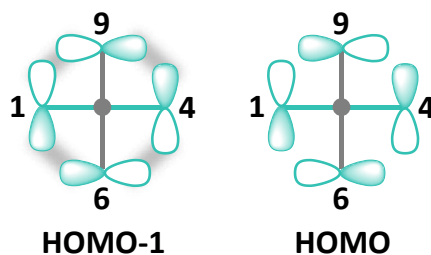
These energy changes upon the AA MO interaction can be easily understood considering the phase relationships between the π -orbitals, as showed in Scheme I.13. When the spatial disposition of both AA MO levels of the 1,3-butadiene moieties makes the π -orbitals to be in phase, a stabilizing interaction occurs between them, forming the HOMO-1 level of the spiro[4.4]nonatetraene. On the other hand, when these orbitals are not in phase, the resulting molecular orbital in the spiro system (the HOMO level) increases its energy. As a consequence of



Scheme I.12. Molecular orbitals energy diagram of the ground electronic configuration of spiro[4.4]nonatetraene (*middle*), built from that of the 1,3-butadiene (*left and right*). Different colour of the orbital lobes indicates different sign, and their sizes correspond to the absolute values of the corresponding atomic coefficients. Molecular orbitals of the π -system in plane *b* are represented in top view. AS: antisymmetric with respect to plane *a* and symmetric with respect to plane *b*; SA: symmetric with respect to plane *a* and antisymmetric with respect to plane *b*; AA: antisymmetric with respect to both planes.

this rise in the HOMO energy, the optical bandgap of the spiro system is narrower than that of the 1,3-butadiene (its non-spiro counterpart).^[15, 53] The energy difference between HOMO-1 and HOMO is

two AA-MO (LUMO+2 and LUMO+3) since in the former pair the coefficients of the spiro-conjugated orbitals are larger.



Scheme I.13. Newman projection of AA-MO of 1,3-butadiene moieties interaction. Only orbitals in phase present through-space conjugation.

Simmons and Fukunaga and also Zeiss *et al.*^[53, 54] studied the MO interaction between the spiro-conjugated moieties in different spiro systems. They found that when both moieties contribute with an even number of double bond and the total number of π -electrons in the spiro molecule is equal to $4N$ (which is the case of spiro[4.4]nonatetraene, with $N=2$), the resulting HOMO level increases its energy with respect to the non-spiro moieties and the E_g is reduced (as it has been already explained in Scheme I.12). However, when the spiro-conjugated groups contribute with an odd number of double bonds, for example in the spiro[2.2]pentadiene (with $4N$ π -electrons, $N=1$), the narrowing of the bandgap is because of the lower energy of the resulting LUMO level. In Table I.2 the effects of the spiro-conjugation in the optical bandgap are summarized for these examples and also for systems in which the spiro-conjugated moieties are constituted one for an odd number of double bonds and the other one with an even number. Depending on these interactions, Simmons and Fukunaga distinguished 4 classes of

Table I.2. Classification of the spiro-conjugated systems according to reference [53] and the effect of the spiro-conjugation in the resulting optical bandgap.

| Class | Double Bonds ^a | | Total number of π -e ^{-b} | HOMO Symmetry ^a | | LUMO Symmetry ^a | | Spiro FMO ^b | | |
|-------|---------------------------|---------|--|----------------------------|---------|----------------------------|---------|------------------------|-------|----------------|
| | Plane a | Plane b | | Plane a | Plane b | Plane a | Plane b | HOMO | LUMO | E _g |
| I | Odd | Odd | 4N | AS | SA | AA | AA | Equal | ↓ E | ↓ E |
| II | Even | Even | 4N | AA | AA | AS | SA | ↑ E | Equal | ↓ E |
| III | Odd | Even | 4N+2 | AA | SA | AS | AA | ↓ E | Equal | ↑ E |
| IV | Even | Odd | 4N+2 | SA | AA | AA | AS | Equal | ↑ E | ↑ E |

^aRefers to the individual moieties.^bRefers to the final spiro-conjugated molecule.

spirenes (spiro-conjugated hydrocarbons).^[53]

Spiro-conjugation Expression

The orthogonal arrangement of two π -conjugated moieties makes them to present independent electronic properties. However, the presence of a spiro linkage between these two systems disturbs the π -electron delocalization in the individual chromophores. Therefore, several parameters are altered in comparison with the non-spiro analogous molecules:

- 1. Optical bandgap (E_g).** From the MO diagram discussion in the above section, it is evident that one of the properties affected by the spiro-conjugation is the optical bandgap and, consequently, the electronic absorption spectrum when the

HOMO→LUMO electron transition is observed. For example, in the case of the spiro[4.4]nonatetraene (spirene class II), the destabilization of the HOMO level upon the spiro linkage provokes a reduction of the optical bandgap (see Scheme I.12). Consequently, the maximum electronic absorption wavelength corresponding to the HOMO→LUMO transition will experiment a bathochromic shift (to shorter energy values) respect to the non-spiro 1,3-butadiene system. The changes in the E_g with the spiro connection as a function of the spirenes class are indicated in Table I.2.

- 2. Bond Length Alternation (BLA).** As a π -conjugation phenomenon, spiro-conjugation decreases the bond length alternation pattern between double and single CC bonds. However, the overlap integral between the spiro-conjugated orbitals represents only the 20% of the value corresponding to the

π - π overlapping between adjacent atoms placed in the same plane.^[53] Thus, the BLA reduction can go unnoticed in already highly delocalized π -systems. Note also that the BLA values can be calculated only for the bonds adjacent to the spiro-conjugated orbitals and not between the spiro-conjugated themselves, since it is a through-space interaction.

Nevertheless, the contribution of each atomic coefficient to the π -system are accessible parameters. Larger coefficient values for the spiro-conjugated atoms mean a larger contribution to the spiro π -electron conjugation.

of the amorphous functional material due to the thermal stress can provoke improper operations of the electronic device, and even its degradation.

- iii. The spiro linkage limits excimer formation, avoiding fluorescence quenching.

For these reasons, spiro-conjugated systems have been used as light-emitting fluorescence dyes^[55, 56], as ambipolar charge transport materials in Organic Light-Emitting Diodes (OLEDs)^[55, 56], Organic Field Effect Transistors (OFETs)^[57] or solar cells,^[58] and have been as well proposed for singlet-fission^[59, 60] experiments.

Applications of Spiro-conjugation

The spiro-bond between two orthogonal π -systems gives rise to a highly steric demanding and rigid structure. This disposition in spiro-conjugated molecules presents several advantages for optoelectronic applications:^[55, 56]

- i. This bulky structure avoids intermolecular interactions (when there is no extension of the conjugated systems) and increases the solubility in comparison with the non-spiro models.
- ii. Also as a consequence of this steric demand and rigidity, these systems present a specific arrangement in the amorphous state that impedes the recrystallization at lower temperatures than the glass transition one. The recrystallization

I.IV. The Aromatic-Quinoidal Nature and the Diradical Character in π -Conjugated Systems

The Aromatic-Quinoidal Tautomerism

The π -conjugated systems presented along this *Introduction* section, and most of the oligomers and polymers derived from them, have a nondegenerate ground electronic configuration, in contrast to polyacetylene.

In the case of oligomeric systems based on aromatic rings, in which the π -electron delocalization is of utmost importance, tautomerization is governed by the higher stabilization energy of the *aromatic form* compared to the *quinoidal* one, because of the already mentioned aromatic or resonance stabilization energy. These *aromatic* and *quinoidal forms* are also resonance structures of the π -conjugated

system under study and represent the two limits of the bond length alternation parameter (BLA), since on going from one to the other the double and single CC bonds must be interconverted. In this way, the potential energy surface of the π -conjugated molecules can be described as a function of the BLA value, presenting the shape showed in Figure I.4.^[35]

In Figure I.4 (black, solid line for an aromatic system), point C corresponds to the more stable aromatic structure, the absolute minimum of the potential energy surface, while the quinoidal tautomer (point B), which presents a BLA value with contrary sign (BLA<0), is a local minimum. Note that this BLA/energy curve is adopted

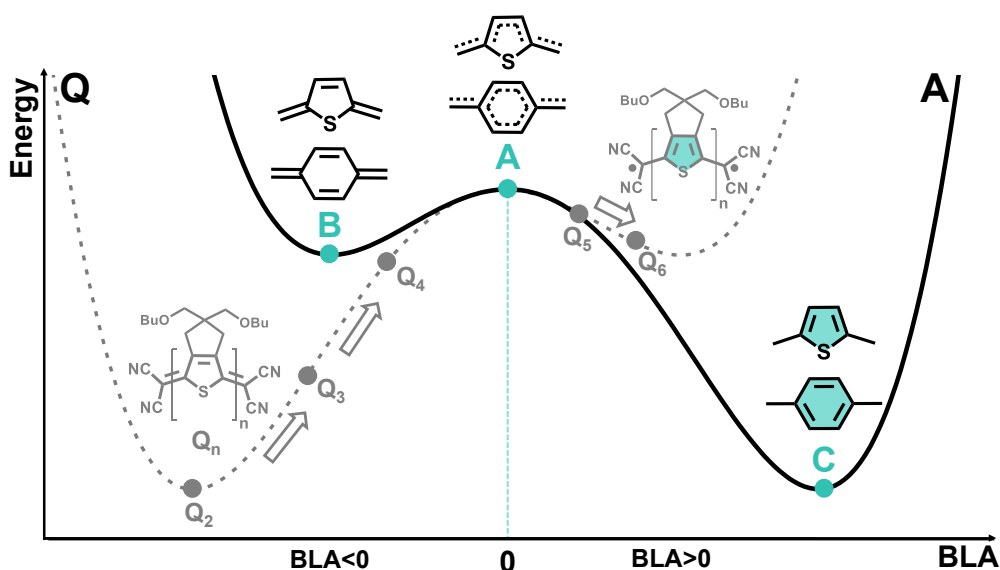


Figure I.4. Generalized BLA-energy curve of the ground electronic configuration of an aromatic (black, solid line) and a quinoidal (grey, dashed line) polymer. Point A corresponds to the fully delocalized electronic structure, while points B and C corresponds to the fully quinoidal and fully aromatic forms, respectively. In grey, the example of the tetracyanoquinoidal oligothiophenes Q_n is represented.

for an aromatic π -conjugated system. The two resonance structures are connected through an energy barrier at BLA=0 (point A): this structure corresponds to the full delocalization of the π -electron density, where no differences exist between double and single CC bonds. The reason why this fully delocalized form constitutes a maximum in the potential energy surface is clear: an infinite chain formed by identical repetitive units (as fully delocalized polyacetylene) is a highly unstable system, and experiments a distortion towards more stable structures (the Peierls dimerization^[15, 17, 18], explained in Section I.I). In polyacetylene, this dimerization gives rise to two degenerated structures in which the double and single CC bonds are interconverted. However, in the case of aromatic or heteroaromatic π -systems, the distorted structures are not degenerated. While the quinoidal tautomer (point B) is stabilized due to the Peierls dimerization, the aromatic one (point C) presents a second stabilization source: the aromatic or resonance stabilization energy. Therefore, the energy difference between points B and C corresponds to the aromatic stabilization energy, that favours the structure C. To transform the aromatic or quinoidal pattern in the other one, a π -bond must be broken, leading to a diradical structure.^[35] Despite the simplicity of this explanation, two important consequences must be extracted:

- i. Diradical structures are involved in the aromatic/quinoidal tautomerism in π -conjugated systems.
- ii. Since this diradical form is obtained surpassing an energy barrier, to carry

out the transformation between both structures (quinoidal \leftrightarrow aromatic) a new source of stabilization energy must come into play. This is the aromatic energy, that accounts for the energy needed to break a double bond, forming the diradical structure, and is usually referred as *driving force*.

All the structures placed between points B and A or C and A constitute intermediate cases, with quinoidal or aromatic character and larger π -electron delocalization than the fully aromatic/quinoidal structures (their absolute BLA values are shorter than those of points B and C).

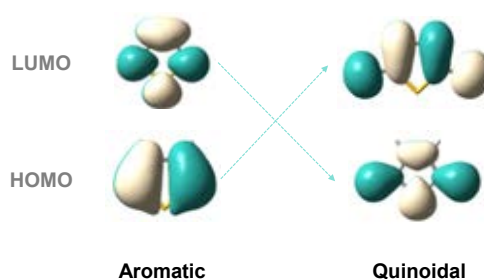
As has been explained in *The Optical Bandgap and The Oligomer Approach* section, shorter BLA values are related with narrower HOMO-LUMO gaps in linearly π -conjugated systems. Thus, intermediate structures between C-A and B-A points will present smaller E_g values. Making use of the oligomer approach, if the π -electron delocalization increases when lengthening the oligomer size, then in the potential energy surface of a specific oligomeric system the monomer will represent the fully aromatic (or quinoidal) form, and the next oligomers will draw the potential curve toward the point A. In other words, for an aromatic system the increasing contribution of the quinoidal resonance form to the chemical structure diminishes the HOMO-LUMO gap.^[17, 61] However, since the fully delocalized structure (point A) is unattainable due to its intrinsic instability, the narrowing trend of the optical bandgap with the oligomer

size is not unlimited, and presents an asymptotic behaviour. Therefore, there is a number of monomeric units at which the optical properties converge and are similar to those of the infinite polymer. By this way, the oligomeric approach is demonstrated, and according to the Meier's equations,^[21-23] parameters corresponding to the infinite chain (E_∞ and λ_∞) correspond to the structure A, the asymptotic value.

An example of this behaviour is the family of tetracyanoquinoidal oligothiophenes Q_n (from $n=2$ to $n=6$)^[33-35] (see Figure I.4, grey, dashed line and grey chemical structures). In these oligothiophenes, the end-capping dicyanomethylene groups assure the quinoidal form of the thiophene rings. Since these electron-withdrawing groups are in the two extremes of the carbon backbone, their effect is diminished towards the molecular centre as the chain is lengthened. According to the spectroscopic study, while Q_2 represents the fully quinoidal system (point B), when lengthening the oligomer size the BLA is diminished, moving closer to the maximum point A (BLA \rightarrow 0). For Q_5 , the aromatic diradical structure is more stable than the quinoidal one, moving to the aromatic well. The energy needed to surpass the barrier is given by the aromatic stabilization of 5 thiophene rings.^[35]

The gap reduction when enlarging the oligomer size (and diminishing the BLA value) takes place simultaneously destabilizing the HOMO and stabilizing the LUMO energy levels. The HOMO level of the aromatic molecule is destabilized

when increasing the contribution of the quinoidal form due to the loss of aromaticity. On the other hand, the aromatic character of the LUMO level of the quinoidal form provokes a stabilization of this FMO with the same change. FMO of an aromatic and a quinoidal thiophene units are depicted in Scheme I.14.

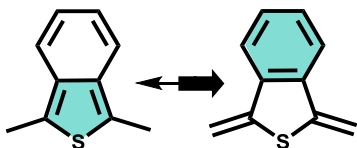


Scheme I.14. Frontier molecular orbitals topologies of the aromatic (*left*) and quinoidal (*right*) monothiophene unit.

According to this discussion, the synthesis of oligomeric structures with an intermediate behaviour between the fully aromatic and the fully quinoidal resonance forms has been used as a successful strategy to obtain low bandgap systems for organic electronic applications.^[61-65] The classical example of this strategy is the polyisothianaphthene, first synthesized by Heeger *et al.* in 1984.^[66] This polymer consists in a polythiophene backbone as a main π -conjugated framework, but the aromatic thiophene units are fused to benzenoid rings, as showed in Scheme I.15.

The higher aromaticity of the benzene ring increases the contribution of this resonance form, conferring a quinoidal character to the thiophene ring. The resulting intermediate chemical structure presents a shorter BLA and the optical bandgap is reduced from 2.0 eV in

polythiophene to 1.0 eV in polyisothianaphthene.^[64, 66] In this system, the *driving force* that pushes the system to the larger-contributing resonance form is the aromaticity gain of the benzene ring.



Scheme 1.15. Resonance structures of the monomeric units of polyisothianaphthene.

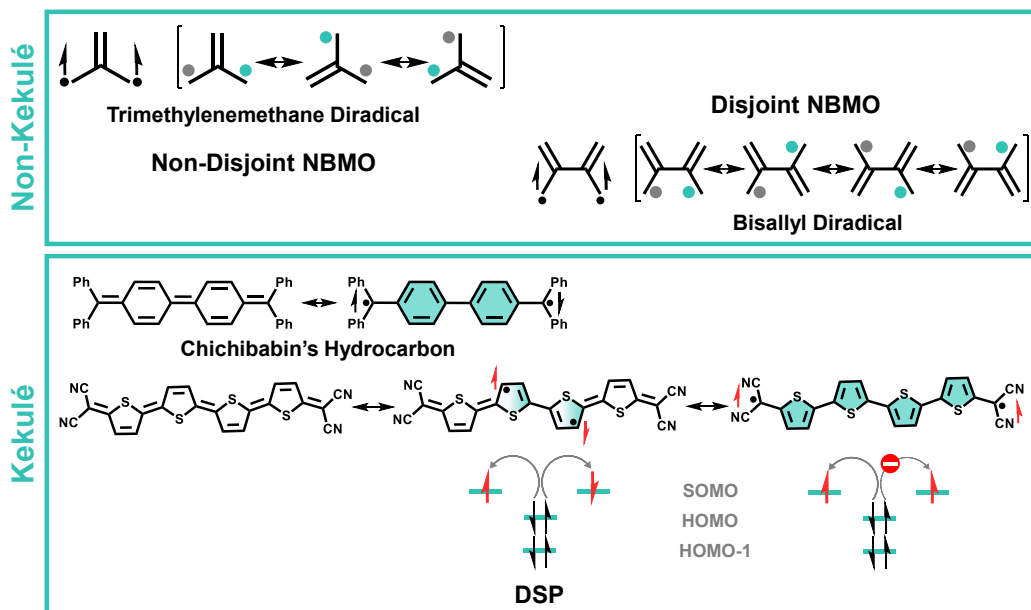
Diradicals. A Qualitative Approximation

According to the discussion of the potential energy surface for aromatic π -conjugated polymers, the rise in the number of monomeric units diminishes the BLA value due to the larger contribution of the quinoidal canonical form. On the other hand, the aromatic \leftrightarrow quinoidal transformation takes place through a diradical species, in which a double bond has been broken to generate two delocalized radical centres. Therefore, there is a number of monomeric units at which the diradical state is favoured *versus* the *completely* bonded form (*i. e.*, the open-shell configuration *versus* de closed-shell one). This diradical structure brings about a narrowing of the optical bandgap, and it is one of the reasons why the open-shell configurations have been a matter of interest in the organic electronics field in the recent years.^[67, 68] This kind of diradicals, whose chemical structures can be also described by a closed-shell canonical form, are referred as *Kekulé*

diradicals. If the two radical centres cannot be accommodated in a π -bond, that is, a closed-shell configuration cannot be drawn, then this is a *Non-Kekulé* diradical. In Scheme 1.16 examples of *Kekulé* (Chichibabin's hydrocarbon) and *Non-Kekulé* (trimethylenemethane and bisallyl structures) diradicals are depicted.

Because of the fact that a different chemical entity, a diradical, is now considered, a new range of properties come into play for π -conjugated molecules. Probably the most important is the accessibility to high-spin organic molecules.^[66, 69] In a diradical species, the ground electronic configuration can be defined as a function of the spin disposition of the two radical centres in the Singly Occupied Molecular Orbitals (SOMOs) as singlet ($S=0$) or triplet ($S=1$) open-shell configurations. According to the Hund's rule of maximum multiplicity,^[70-72] the ground electronic configuration of the diradical species should be a triplet state. This is indeed the case of non Kekulé diradicals and diradicals which present *non-disjoint* non-bonding molecular orbitals (NBMOs). In non-disjoint NBMOs, the electron densities of the radical centres can be located at the same atom (Scheme 1.16, *top*; the two radical centres, grey and green, can be accommodated in the same atom in different resonance structures). Pauli exclusion principle avoids these two electrons with identical spin to be in the same spatial region, minimizing the electron-electron repulsion.^[66, 68]

However, as the SOMOs wavefunctions reduce their spatial overlap, but the



Scheme I.16. Resonance structures of *Non-Kekulé* (top) and *Kekulé* (bottom) diradicals. For the *Non-Kekulé* structures the non-disjoint (for the trimethylenemethane diradical) and the disjoint (bisallyl diradical) NBMO are schematized differentiating each radical centre in different colour. Observe that in non-disjoint NBMO both centres are accommodated in the same atom in any of the resonance structures, while in the disjoint NBMO grey and green radical centre do not share any atom. For the *Kekulé* diradicals also the Double Spin Polarization mechanism is represented.

through-bond interaction is still effective, the NBMOs become more *disjoint*. In this case, the spin densities do not coincide in the same spatial region, and the electron-electron repulsion vanishes (in Scheme I.16, *top*; the two radical centres are not accommodated in the same atom in any of the resonance structures). Now, the singlet and triplet electronic states can be considered degenerated. This situation is of special interest in *Kekulé* diradicals, in which the two radical centres can be connected through a π -conjugated framework (or bridge), according to the corresponding resonance structures.^[67, 73] In this way, electrons in bonding molecular orbitals can be partially localized in the NBMO, *i. e.*, unpaired electrons can conjugate with the π -electrons of the

molecular bridge. If the unpaired electrons present antiparallel spin (singlet diradical), then the two electrons of the bonding MO can delocalize in both NBMOs. Though, if the unpaired electrons are of parallel spin (triplet diradical), then only one of the bonding MO electrons can be located in the NBMO at the same time (Pauli exclusion principle). This phenomenon is represented in Scheme I.16, *bottom*, and accounts for the stabilization of the singlet electronic state respect to the triplet one (that does not change its energy), violating the Hund's rule. Since the π -electrons of the bridge can be delocalized twice in the singlet open-shell configuration, this stabilization is known as the *Double Spin Polarization* (DSP) mechanism.^[67, 72-74]

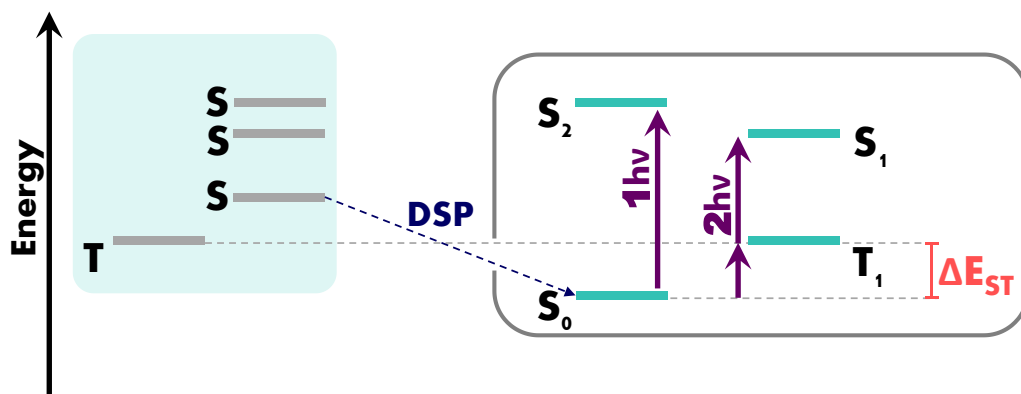
Once the DSP mechanism is activated, the ground electronic configuration of the four possible energy levels of two electrons in two NBMO-diradical system is of singlet character. The energy disposition of these states is known as “the four energy levels diagram” of diradical species, and justifies the different properties arising from the singlet open-shell form. In Scheme I.17 this diagram is qualitatively depicted, while a more detailed description is given in references [67, 75, 76].

According to this diagram, the following properties of singlet open-shell systems can be exploited in the field of organic electronics:

- The already mentioned small energy difference between the singlet and triplet states. The possibility to tune the ground electronic state in *Kekulé* diradicals is given by the energy difference between these two configurations, referred as singlet-triplet gap (ΔE_{ST}). If ΔE_{ST} is small enough, the triplet state can be populated at room temperature.

Therefore, ΔE_{ST} accounts for the strength of the spin coupling between the two radical centres.^[77] The paramagnetic character conferred by the accessibility of the triplet state in the organic diradicals brings the possibility to their use in magnetic applications and spintronic devices.^[67, 77, 78]

- $S_0 \rightarrow S_1$ electronic transition is forbidden by one-photon absorption for symmetry reasons, but it is allowed by multi-photon absorption.^[67, 76] Therefore, singlet open-shell diradicals can experiment two photon absorption processes, constituting an important category of organic nonlinear optical (NLO) materials.^[79, 80]
- When S_1 acquires twice the energy of the triplet state, then singlet fission phenomenon can occur. In this process, the absorption of one photon promotes the system to a singlet excited state that, after an internal conversion process ($S_2 \rightarrow S_1$), can then split in two triplet excited states.^[81]



Scheme I.17. The four energy levels diagram of a singlet open-shell system. The double spin polarization mechanism (DSP), one and two photon absorption processes ($1h\nu$ and $2h\nu$, respectively), and the singlet-triplet energy gap (ΔE_{ST}) are schematized.

In this way, two photogenerated excitons are obtained from only one photon absorption, which is of utmost utility to increase the cell yields in organic photovoltaics.^[82, 83]

The exceptional contribution of the diradical properties to functional materials for organic electronic devices is evident. However, the application of these systems is limited due to their low stability. The inherent high reactivity of diradical systems makes them labile molecules avoiding taking advantage of their outstanding properties. For these reasons, many efforts are focus on the development of robust, air stable diradical species with low ΔE_{ST} .^[67, 84, 85]

DSP mechanism is the reason why most of *Kekulé* diradical systems present a singlet open-shell configuration of their electronic ground state.^[35, 67, 68, 74] However, this effect can be surpassed if the chemical interaction between the two radical centres is minimized. In other words, any factor that interrupts the π -electron conjugation through the bridge will avoid the DSP mechanism and, consequently, the stabilization of the singlet state respect to the triplet. In linearly π -conjugated molecules, the easiest way to disturb the π -electron delocalization through the carbon backbone is the structural distortion. In singlet open-shell systems, deviation from the planarity interrupts the through-bond interaction between the diradical centres, rising the energy of the singlet state and, even, deactivating the DSP mechanism.^[86]

On the other hand, in polyconjugated systems the effective conjugation through the main backbone is interrupted by the presence of alternative, competitive π -conjugated frameworks. In this case, the π -electron density is shifted from the linear conjugated sequence to the secondary pathways, by means of through-bond or through-space phenomena. Therefore, if the system under study is a singlet open-shell diradical, hence the DSP mechanism will be affected by the alternative π -conjugated frameworks.

REFERENCES

- [1] *Trajan's Bridge over the Danube*, M. Serban, *Int. J. Naut. Archaeol.*, **2009**, *38*, 331–342.
- [2] *Trajanic Trees: The Dacian Forest on Trajan's Column*, A. Fox, *Papers of the British School at Rome*, **2019**, *87*, 47–69.
- [3] *Colour from Molecules*, R. J. D. Tilley in *Colour and the Optical Properties of Materials*, R. J. D. Tilley, John Wiley & Sons Ltd, Chichester: England, **2010**, 2nd ed., 309–362.
- [4] *Ambipolar Organic Field Effect Transistors and Inverters with the Natural Material Tyrian Purple*, E. D. Głowacki, L. Leonat, G. Voss, M. A. Bodea, Z. Bozkurt, A. Montaigne Ramil, M. Irimia-Vladu, S. Bauer and N. S. Sariciftci, *AIP Adv.*, **2011**, *1*, 042132.
- [5] *Stability of Selected Hydrogen Bonded Semiconductors in Organic Electronic Devices*, M. Irimia-Vladu, Y. Kanbur, F. Camaioni, M. E. Coppola, C. Yumusak, C. Vlad Irimia, A. Vlad, A. Operamolla, G. M. Farinola, G. P. Suranna, N. Gonzalez-Benitez, M. Carmen Molina, L. F. Bautista, H. Langhals, B. Stadlober, E. D. Głowacki and N. S. Sariciftci, *Chem. Mater.*, **2019**, *31*, 6315–6346.
- [6] *IUPAC. Compendium of Chemical Terminology, 2nd ed. (the "Gold Book")*. Compiled by A. D. McNaught and A. Wilkinson. Blackwell Scientific Publications, Oxford (**1997**). Online version (2019-) created by S. J. Chalk. ISBN 0-9678550-9-8. <https://doi.org/10.1351/goldbook>.
- [7] *The Aromatic Ring*, Doris Kolb, *J. Chem. Educ.*, **1979**, *56*, 334–337.
- [8] *Organic Chemistry*, J. McMurry, Brooks/Cole, Belmont: CA, **2000**, 7th ed.
- [9] *A Different Story of π -Delocalizations: The Distortivity of π -Electrons and Its Chemical Manifestations*, S. Shaik, A. Shurki, D. Danovich and P. C. Hiberty, *Chem. Rev.*, **2001**, *101*, 1501–1539.
- [10] *The Benzene Ring: Dream Analysis*, M. W. Browne, *The New York Times*, Aug. 16, **1988**, Section C, 10.
- [11] *A History of the Structural Theory of Benzene—The Aromatic Sextet Rule and Hückel's Rule*, S. Kikuchi, *J. Chem. Educ.*, **1997**, *74*, 194–201.
- [12] *The Structure of the Benzene Ring in $C_6(CH_3)_6$* , K. Lonsdale, *P. Roy. Soc. A-Math. Phys.*, **1929**, *123*, 494–515.
- [13] *Química Cuántica*, J. Bertran, V. Branchadell, M. Moreno and M. Sodupe, Síntesis, Vallehermoso: Madrid, **2002**, 2nd ed.
- [14] *Atkin's Physical Chemistry*, P. Atkins and J. de Paula, Oxford University Press, USA, **2006**, 8th ed. (Translation of *Editorial Médica Panamericana*).
- [15] *Aromaticity and Other Conjugation Effects*, R. Gleiter and G. Haberhauer, Wiley-VCH, Weinheim: Germany, **2012**.
- [16] *Quantum Contributions to the Benzene Problem*, E. Hückel, *Z. Phys.*, **1931**, *70*, 3–4.

- [17] *Optical Properties of Conducting Polymers*, A. O. Patil, A. J. Heeger and F. Wudl, *Chem. Rev.*, **1988**, *88*, 183–200.
- [18] *Bond Alternation Defects in Long Polyene Molecules*, J. A. Pople and S. H. Walmsley, *Mol. Phys.*, **1962**, *5*, 15–20.
- [19] *Effective Conjugation Length and UV/Vis Spectra of Oligomers*, H. Meier, U. Stalmach and H. Kolshorn, *Acta Polymer.*, **1997**, *48*, 379–384.
- [20] *Conjugation Oligomers with Terminal Donor-Acceptor Substitution*, H. Meier, *Angew. Chem. Int. Ed.*, **2005**, *44*, 2482–2506.
- [21] *Monodisperse Dialkoxy-Substituted Oligo(Phenyleneethynylene)s*, U. Stalmach, H. Kolshorn, I. Brehm and H. Meier, *Liebigs Ann.*, **1996**, *9*, 1449–1456.
- [22] *Effective Conjugation Length and UV/Vis Spectra of Oligomers*, H. Meier, U. Stalmach and H. Kolshorn, *Acta Polymer.*, **1997**, *48*, 379–384.
- [23] *Conjugation Oligomers with Terminal Donor-Acceptor Substitution*, H. Meier, *Angew. Chem. Int. Ed.*, **2005**, *44*, 2482–2506.
- [24] *Multifaceted Regioregular Oligo(thieno[3,4-*b*]thiophene)s Enabled by Tunable Quinoidization and Reduced Energy Band Gap*, F. Liu, G. L. Espejo, S. Qiu, M. Moreno Oliva, J. Pina, J. S. Seixas de Melo, J. Casado, X. Zhu, *J. Am. Chem. Soc.*, **2015**, *137*, 10357–10366.
- [25] *Electronic Materials: The Oligomer Approach*, M. Bürkle, K. Müllen and G. Wegner, Eds.; John Wiley & Sons, LTd: United Kingdom, **2008**.
- [26] *Optical Bandgaps of π -Conjugated Organic Materials at the Polymer Limit: Experiment and Theory*, J. Gierschner, J. Cornil and H.-J. Egelhaaf, *Adv. Mater.*, **2007**, *19*, 173–191.
- [27] *Synthetic Principles for Bandgap Control in Linear π -Conjugated Systems*, J. Roncali, *Chem. Rev.*, **1997**, *97*, 173–205.
- [28] *Molecular Engineering of the Band Gap of π -Conjugated Systems: Facing Technological Applications*, J. Roncali, *Macromol. Rapid Commun.*, **2007**, *28*, 1761–1765.
- [29] *The Alternation of Bond Lengths in Long Conjugated Chain Molecules*, H. C. Longuet-Higgins and L. Salem, *Proc. R. Soc. Lond. A*, **1959**, *251*, 172–185.
- [30] *Synthetic Principles for Bandgap Control in Linear π -Conjugated Systems*, J. Roncali, *Chem. Rev.*, **1997**, *97*, 173–205.
- [31] *Molecular Engineering of the Band Gap of π -Conjugated Systems: Facing Technological Applications*, J. Roncali, *Macromol. Rapid Commun.*, **2007**, *28*, 1761–1765.
- [32] *Relationship Between Band Gap and Bond Length Alternation in Organic Conjugated Polymers*, J. L. Brédas, J. *Chem. Phys.*, **1985**, *82*, 3808–3811.
- [33] *On the Biradicaloid Nature of Long Quinoidal Oligothiophenes: Experimental Evidence Guided by Theoretical Studies*, R. Ponce Ortiz, J. Casado, V. Hernández, J. T. López Navarrete, P. M. Viruela, E. Ortí, K.

Takimiya and T. Otsubo, *Angew. Chem. Int. Ed.*, **2007**, *46*, 9057–9061.

[34] *Quinoidal Oligothiophenes: Towards Biradical Ground State Species*, R. Ponce Ortiz J. Casado, S. Rodríguez González, V. Hernández, J. T. López Navarrete, P. M. Viruela, E. Ortí, K. Takimiya and T. Otsubo, *Chem. Eur. J.*, **2010**, *16*, 470–484.

[35] *Quinoidal/Aromatic Transformation in π -Conjugated Oligomers: Vibrational Raman Studies on the Limit of Rupture of π -Bonds*, P. Mayorga Burrezo, J. L. Zafra, J. T. López Navarrete and J. Casado, *Angew. Chem. Int. Ed.*, **2017**, *56*, 2250–2259.

[36] *Reverse Bond-length Alternation in Cumulenes: Candidates for Increasing Electronic Transmission with Length*, M. H. Garner, W. Bro-Jørgensen, P. D. Pedersen and G. C. Solomon, *J. Phys. Chem. C*, **2018**, *122*, 26777–26789.

[37] *Cross Conjugation*, N. F. Phelan and M. Orchin, *J. Chem. Educ.*, **1968**, *45*, 633–637.

[38] *Cross-Conjugation*, P. A. Limacher and H. P. Luthi, *Comput. Mol. Sci.*, **2011**, *1*, 477–486.

[39] *Through versus Cross Electron Delocalization in Polytriacetylene Oligomers: A Computational Analysis*, M. Bruschi, M. G. Giuffreda and H. P. Lüthi, *ChemPhysChem*, **2005**, *6*, 511–519.

[40] *The Dendralenes: A Neglected Group of Highly Unsaturated Hydrocarbons*, H. Hopf, *Angew. Chem. Int. Ed. Engl.*, **1984**, *23*, 948–959.

[41] *Dendralenes Branch Out: Cross-Conjugated Oligoenes Allow the Rapid Generation of Molecular Complexity*, H. Hopf and M. S. Sherburn, *Angew. Chem. Int. Ed.*, **2012**, *51*, 2298–2338.

[42] *Oligomeric and Polymeric Systems with a Cross-conjugated π -Framework*, M. Gholami and R. R. Tykwinski, *Chem. Rev.*, **2006**, *106*, 4997–5027.

[43] *Cross Conjugation in Polyenes and Related Hydrocarbons: What Can Be Learned from Valence Bond Theory about Single-Molecule Conductance?*, J. Gu, W. Wu, T. Stuyver, D. Danovich, R. Hoffmann, Y. Tsuji and S. Shaik, *J. Am. Chem. Soc.*, **2019**, *141*, 6030–6047.

[44] *Concepts in the Design and Engineering of Single-Molecule Electronic Devices*, N. Xin, J. Guan, C. Zhou, X. Chen, C. Gu, Y. Li, M. A. Ratner, A. Nitzan, J. Fraser Stoddart and X. Guo, *Nat Rev Phys.*, **2019**, *1*, 211–230.

[45] *Observation of Electrochemically Controlled Quantum Interference in a Single Anthraquinone-Based Norbornylogous Bridge Molecule*, N. Darwish, I. Díez-Pérez, P. Da Silva, N. Tao, J. J. Gooding and M. N. Paddon-Row, *Angew. Chem. Int. Ed.*, **2012**, *51*, 3203–3206.

[46] *Electrochemical Control of Single-Molecule Conductance by Fermi-Level Tuning and Conjugation Switching*, M. Baghernejad, X. Zhao, K. Baruël Ørnsø, M. Füeg, P. Moreno-García, A. V. Rudnev, V. Kaliginedi, S. Vesztergom, C. Huang, W. Hong, P. Broekmann, T. Wandlowski, K. S. Thygesen and M. R.

- Bryce, *J. Am. Chem. Soc.*, **2014**, *136*, 17922–17925.
- [47] *Experimental Investigation of Quantum Interference in Charge Transport Through Molecular Architectures*, X. Li, Z. Tan, X. Huang, J. Bai, J. Liu and W. Hong, *J. Mater. Chem. C*, **2019**, *7*, 12790–12808.
- [48] *Quantum Interference Effects in Charge Transport through Single-Molecule Junctions: Detection, Manipulation, and Application*, J. Liu, X. Huang, F. Wang and W. Hong, *Acc. Chem. Res.*, **2019**, *52*, 151–160.
- [49] *Observation of Quantum Interference in Molecular Charge Transport*, J. Liu, C. Guédon, H. Valkenier, T. Markussen, K. S. Thygesen, J. C. Hummelen and S. J. van der Molen, *Nature Nanotech.*, **2012**, *7*, 305–309.
- [50] *Controlling Electron Transfer in Donor-Bridge-Acceptor Molecules Using Cross-Conjugated Bridges*, A. Butler Ricks, G. C. Solomon, M. T. Colvin, A. M. Scott, K. Chen, M. A. Ratner and M. R. Wasielewski, *J. Am. Chem. Soc.*, **2010**, *132*, 15427–15434.
- [51] *The Orbital Selection Rule for Molecular Conductance as Manifested in Tetraphenyl-Based Molecular Junctions*, M. Bürkle, L. Xiang, G. Li, A. Rostamian, T. Hines, S. Guo, G. Zhou, N. Tao and Y. Asai, *J. Am. Chem. Soc.*, **2017**, *139*, 2989–2993.
- [52] *Homoconjugation and Homoaromaticity. IV. The Trishomocyclopropenyl Cation. A Homoaromatic Structure*, S. Winstein and J. Sonnenberg, *J. Am. Chem. Soc.*, **1961**, *83*, 3244–3251.
- [53] *Spiroconjugation*, H. E. Simmons and T. Fukunaga, *J. Am. Chem. Soc.*, **1967**, *89*, 5208–5215.
- [54] *The Spirarenes*, R. Hoffmann, A. Imamura and G. D. Zeiss, *J. Am. Chem. Soc.*, **1967**, *89*, 5215–5220.
- [55] *Spiro Compounds for Organic Optoelectronics*, T. P. I. Saragi, T. Spehr, A. Siebert, T. Fuhrmann-Lieker and J. Salbeck, *Chem. Rev.*, **2007**, *107*, 1011–1065.
- [56] *Spiro Compounds for Organic Electroluminescence and Related Applications*, R. Pudzich, T. Fuhrmann-Lieker and J. Salbeck in *Emissive Materials Nanomaterials. Advances in Polymer Science*, vol. 199 (*Emissive Materials Nanomaterials*), Springer, Heidelberg: Berlin, **2006**, 83–142.
- [57] *From One- to Three-Dimensional Organic Semiconductors: In Search of the Organic Silicon?*, J. Roncali, P. Leriche and A. Cravino, *Adv. Mater.*, **2007**, *19*, 2045–2060.
- [58] *Recent Advances in Spiro-MeOTAD Hole Transport Material and Its Applications in Organic-Inorganic Halide Perovskite Solar Cells*, Z. Hawash, L. K. Ono and Y. Qi, *Adv. Mater. Interfaces*, **2018**, *5*, 1700623.
- [59] *Tuning Singlet Fission in π -Bridge- π Chromophores*, E. Kumarasamy, S. N. Sanders, M. J. Y. Tayebjee, A. Asadpoordarvish, T. J. H. Hele, E. G. Fuemmeler, A. B. Pun, L. M. Yablon, J. Z. Low, D. W. Paley, J. C. Dean, B. Choi, G.

D. Scholes, M. L. Steigerwald, N. Ananth, D. R. McCamey, M. Y. Sfeir and L. M. Campos, *J. Am. Chem. Soc.*, **2017**, *139*, 12488–12494.

[60] *Singlet Fission in Spiroconjugated Dimers*, M. E. Sandoval-Salinas, A. Carreras, J. Casado and D. Casanova, *J. Chem. Phys.*, **2019**, *150*, , 204306.

[61] *Electronic Properties of Vinylene-Linked Heterocyclic Conducting Polymers: Predictive Design and Rational Guidance from DFT Calculations*, B. M. Wong and J. G. Cordaro, *J. Phys. Chem. C*, **2011**, *115*, 18333–18341.

[62] *Rational Design of High Performance Conjugated Polymers for Organic Solar Cells*, H. Zhou, L. Yang and W. You, *Macromolecules*, **2012**, *45*, 607–632.

[63] *Low Bandgap Semiconducting Polymers for Polymeric Photovoltaics*, C. Liu, K. Wang, X. Gong and A. J. Heeger, *Chem. Soc. Rev.*, **2016**, *45*, 4825–4846.

[64] *Development of a Quantum Chemical Descriptor Expressing Aromatic/Quinoidal Character for Designing Narrow-Bandgap π -Conjugated Polymers*, Y. Hayashi and S. Kawauchi, *Polym. Chem.*, **2019**, *10*, 5584–5593.

[65] *Poly(isothianaphthene)*, F. Wudl, M. Kobayashi and A. J. Heeger, *J. Org. Chem.*, **1984**, *49*, 3382–3384.

[66] *Diradicals*, M. Abe, *Chem. Rev.*, **2013**, *113*, 7011–7088.

[67] *Pro-aromatic and Anti-aromatic π -Conjugated Molecules: An Irresistible Wish to Be Diradicals*, Z. Zeng, X. Shi, C. Chi, J. T. López Navarrete, J. Casado and J. Wu, *Chem. Soc. Rev.*, **2015**, *44*, 6578–6596.

[68] *Disjoint Molecular Orbitals in Nonalternant Conjugated Diradical Hydrocarbons*, J. R. Dias, *J. Chem. Inf. Comput. Sci.*, **2003**, *43*, 1494–1501.

[69] *Spin Control in Organic Molecules*, D. A. Dougherty, *Acc. Chem. Res.*, **1991**, *24*, 88–94.

[70] *Quantum Chemistry*, I. N. Levine, Pearson Education S. A., London: United Kingdom, **2001**, 5th ed.

[71] *Modern Spectroscopy*, J. M. Hollas, John Wiley & Sons Ltd, Chichester: England, **2004**, 4th ed.

[72] *The Double (or Dynamic) Spin Polarization in π -Diradicals*, P. Karafiloglou, *J. Chem. Educ.*, **1989**, *66*, 816–818.

[73] *Para-Quinodimethanes: A Unified Review of the Quinoidal-Versus-Aromatic Competition and its Implications*, J. Casado, *Top Curr Chem (Z)*, **2017**, *375*, doi:10.1007/s41061-017-0163-2.

[74] *Organic Diradicals and Polyradicals: From Spin Coupling to Magnetism?*, A. Rajca, *Chem. Rev.*, **1994**, *94*, 871–893.

[75] J. L. Zafra. Birradicales Kekulé. Espectroscopía Raman en la Transición Singlete-Triplete. Ph. D. Dissertation, University of Málaga, 2014. Retrieved

from

<http://hdl.handle.net/10630/8632>.

[76] *Dirradicales: Moléculas “Rotas”*, J. Casado, *An. Quím.*, **2019**, *115*, 371–380.

[77] *Molecular Spintronics*, S. Sanvito, *Chem. Soc. Rev.*, **2011**, *40*, 336–335.

[78] *Air Stable High-Spin Blatter Diradicals: Non-Kekulé versus Kekulé Structures*, X. Hu, L. Zhao, H. Chen, Y. Ding, Y.-Z. Zheng, M.-S. Miao and Y. Zheng, *J. Mater. Chem. C*, **2019**, *7*, 6559–6563.

[79] *Strong Two-Photon Absorption of Singlet Diradical Hydrocarbons*, K. Kamada, K. Ohta, T. Kubo, A. Shimizu, Y. Morita, K. Nakasuji, R. Kishi, S. Ohta, S.-i. Furukawa, H. Takahashi and M. Nakano, *Angew. Chem. Int. Ed.*, **2007**, *46*, 3544–3546.

[80] *Remarkable Two-Photon Absorption in Open-Shell Singlet Systems*, M. Nakano, K. Yoneda, R. Kishi, H. Takahashi, T. Kubo, K. Kamada, K. Ohta, E. Botek and B. Champagne, *J. Chem. Phys.*, **2009**, *131*, 114316.

[81] *Singlet Exciton Fission in Polycrystalline Pentacene: From Photophysics toward Devices*, M. W. B. Wilson, A. Rao, B. Ehrler and R. H. Friend, *Acc. Chem. Res.*, **2013**, *46*, 1330–1338.

[82] *Efficient Singlet Fission Discovered in a Disordered Acene Film*, S. T. Roberts, R. E. McAnally, J. N. Mastron, D. H. Webber, M. T. Whited, R. L. Brutchey, M. E. Thompson and S. E. Bradforth, *J. Am. Chem. Soc.*, **2012**, *134*, 6388–6400.

[83] *Light Harvesting for Organic Photovoltaics*, G. J. Hedley, A. Ruseckas and I. D. W. Samuel, *Chem. Rev.*, **2017**, *117*, 796–837.

[84] *High-Spin Organic Diradical with Robust Stability*, N. M. Gallagher, J. J. Bauer, M. Pink, S. Rajca and A. Rajca, *J. Am. Chem. Soc.*, **2016**, *138*, 9377–9380.

[85] *Air Stable High-Spin Blatter Diradicals: Non-Kekulé versus Kekulé Structures*, X. Hu, L. Zhao, H. Chen, Y. Ding, Y.-Z. Zheng, M.-s. Miao and Y. Zheng, *J. Mater. Chem. C*, **2019**, *7*, 6559–6563.

[86] *Pushing Extended p-Quinodimethanes to the Limit: Stable Tetracyano-oligo(N-annulated perylene)quinodimethanes with Tunable Ground States*, Z. Zeng, M. Ishida, J. L. Zafra, X. Zhu, Y. Mo Sung, N. Bao, R. D. Webster, B. S. Lee, R.-W. Li, W. Zeng, Y. Li, C. Chi,† J. T. Lopez Navarrete, J. Ding, J. Casado, D. Kim, and J. Wu, *J. Am. Chem. Soc.*, **2013**, *135*, 6363–6371.

II. GOALS

II. GOALS

The present Ph.D. Thesis is focused on the study of the electronic and molecular structure of organic systems which present different π -conjugated frameworks, and their effect on the electronic and optical properties with potential applications in organic electronic devices. The availability of several conjugated sequences within a molecular system provokes a different behaviour of the π -electrons with respect to that presented in classical, linearly π -conjugated systems. The knowledge of how these conjugation pathways disturb the π -electron density and the formulation of function-structure relationships can lead to a rational tune of the main π -conjugated framework that brings new functional properties to the organic electronics field which are not accessible in monoconjugated systems.

The presence of different polyconjugated pathways is especially relevant on the limits of rupture of π -bonds, *i. e.*, in molecules with large π -electron delocalization. Consequently, systems with **appreciable diradical character** will be used to evaluate the relative weight and the influence of the different π -conjugated frameworks on the electronic properties. In the development of the present Ph.D. Thesis, open-shell configurations in neutral molecules will be available through the **quinoidal \leftrightarrow aromatic tautomerization**. For this reason, the possible tautomerization along the oligomeric series will be addressed from both quinoidal and aromatic shapes for each

conjugation sequence.

On the other hand, injection or removal of electrons allows us to set up radical centres that can move through the available π -frameworks. Therefore, the electronic and molecular structures of **charged species** in polyconjugated systems will provide useful information about the π -electron delocalization patterns. In addition, the establishment of an *extra* charge arrangement through the different π -conjugated sequences is of utmost importance for its application as functional materials operating under doping conditions.

The general methodology that will be adopted to achieve these purposes is the study along the oligomeric series of two main points:

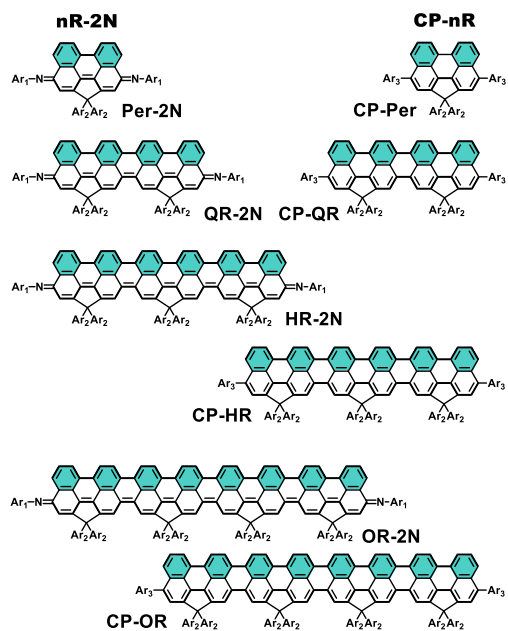
- i) The characterization of the **electronic structure** and the **effective conjugation length** through UV-Vis-NIR electronic absorption and the theoretical description, in terms of energy and topologies, of the frontier molecular orbitals;
- ii) The analysis of the **molecular structure** through vibrational IR and Raman spectroscopies, and the relationships of the spectral trends with the calculated Bond Length Alternation (BLA) patterns, representative of the π -conjugation extension.

In this context, the present Ph.D. Thesis has been organised in three main sections according to the π -conjugated frameworks simultaneously present in the molecules under study.

Section A. Linearly π -Conjugated Diradicals.

In this first section, the study of neutral, linearly π -conjugated oligomeric series is performed. The particular aim of this chapter is to establish a general procedure in the study of π -conjugated systems, and to discriminate the π -electron density behaviour in monoconjugated molecules from closed-shell to diradical species.

For this purpose, two oligorylene families are studied: an **aromatic cyclopenta-ring fused oligorylene (CP-nR)** and a **quinoidal bis(imino)oligorylene (nR-2N)** series, from the monomer (the perylene unit) to the tetramer (or octarylene, regarding the naphthalene moieties). The chemical structures of these two families are depicted in Scheme II.1.



Scheme II.1. Chemical structures of the quinoidal bis(imino)oligorylene (**nR-2N**, left) and aromatic cyclopenta-ring fused oligorylene (**CP-nR**, right) series studied in Chapter 1.

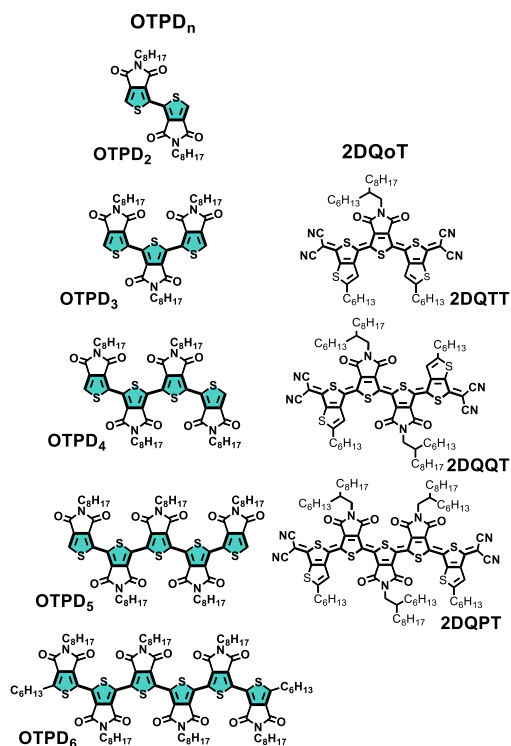
The synthesis of these oligorylene series have been performed by the group of Professor Jishan Wu, from the National University of Singapore (Singapore). These systems constitute nanographene models (graphene nanoribbons), presenting variable semi-conducting or metallic performance depending on the length of the arm-chair edge. The fact that both families describe a closed-shell to singlet open-shell transformation in their neutral forms allows a fully characterization of the π -electron density behaviour in a linear framework for quinoidal and aromatic shapes through UV-Vis-NIR electronic absorption and vibrational spectroscopies.

Section B. Cross-Conjugated Diradicals.

In the second section through-bond conjugation between two orthogonal π -conjugated frameworks, *i. e.* cross-conjugated systems, is investigated. This section is structured in two chapters according to the aromatic and quinoidal forms of the cross-conjugated molecules.

Chapter 2 presents an **aromatic thieno [3,4-c]pyrrole-4,6-dione oligothiophene series (OTPD_n)**, from the dimer to the hexamer ($n = 2-6$) (see Scheme II.2 for the chemical structure).

The introduction of pyrroledione units confers an electron-deficient character to the series. The dione groups of the thieno[3,4-c]pyrrole-4,6-dione (**TPD**) moiety introduce an alternative π -electron conjugated pathway through the carbonyl groups of vicinal **TPD** moieties, crossed to the linear *classical* oligothiophene



Scheme II.2. Chemical structures of the aromatic thieno[3,4-c]pyrrole-4,6-dione oligothiophenes (**OTPD_n**, *left*) and quinoidal tetracyanothienoquinoidal oligothiophenes (**2DQoT**, *right*) series studied in Section B.

conjugated framework. The study of the optical, electronic and structural properties of the neutral and reduced species of these molecules allows a better understanding of the interference between these two crossed conjugated sequences in the electron delocalization and the properties derived from it.

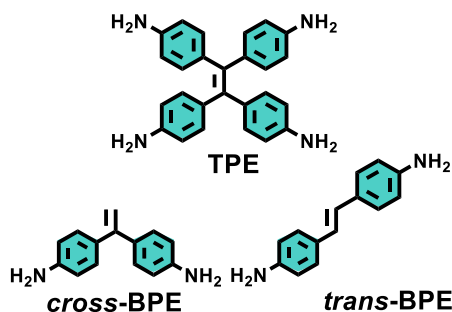
The analogous quinoidal series of the **OTPD_n** molecules, a tetracyanothienoquinoidal oligothiophene family (**2DQoT**), is then studied in Chapter 3. The presence of even and odd number of **TPD** units are responsible of the different cross-conjugation properties of these molecules. Due to their similar structures, results

obtained from both oligothiophene families can be compared. Scheme II.2 shows the chemical structures of the cross-conjugated oligothiophenes series.

For both oligothiophene families, the competition between the two orthogonal π -conjugated frameworks is evaluated for the neutral and reduced species (radical anions and dianions). Since the cross-conjugated units are constituted by electron-withdrawing dione groups, the injection of electrons upon reduction is supposed to activate this alternative π -electron pathway. Substituted-thiophenes are valuable building blocks for π -functional materials since their semiconducting properties can be easily tuned *ad hoc* by changing the substituent groups.

In Chapter 3, together with the **2DQoT** systems, a family of phenyl-substituted ethenes (**nPE**) is investigated as closed-shell systems presenting cross-conjugation features. In particular, tetraphenyl-substituted ethene (**TPE**) specially attracts attention due to its polyconjugated character, allowing *cis*-, *trans*- and cross-conjugation of the π -electrons. The chemical structures of the **nPE** family is presented in Scheme II.3.

Aromatic and quinoidal cross-conjugated oligothiophene series have been synthesized by the group of Professor Xiaozhang Zhu, from the Chinese Academy of Science (Beijing, China), while the synthesis of **nPE** molecules has been carried out by the group of Professor José Luis Segura (Universidad Complutense de Madrid, España).



Scheme II.3. Chemical structures of nPE molecules studied in Chapter 3.

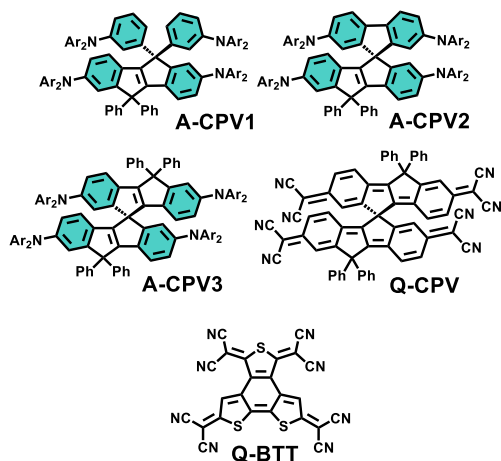
Section C. Spiro-Conjugated Diradicals.

In this final section, the effect of the through-space, intramolecular interactions between π -electron densities on the linear π -conjugation is assessed. For the evaluation of this through-space conjugation, the more appropriate systems are those formed by two spiro-conjugated subunits. The structural rigidity of spiro-compounds, together with their semiconducting properties, make them suitable for their use as charge transport materials.

In Chapter 4, electronic and molecular properties of a family of carbon-bridged phenylene-vinylene (CPV) molecules, in their neutral and charged forms, are elucidated. This family is constituted by three aromatic systems and only one quinoidal spiro-conjugated molecule, Q-CPV. The characterization of the three aromatic molecules is devoted to establishing the best structural features in order to improve the through-space π -conjugation.

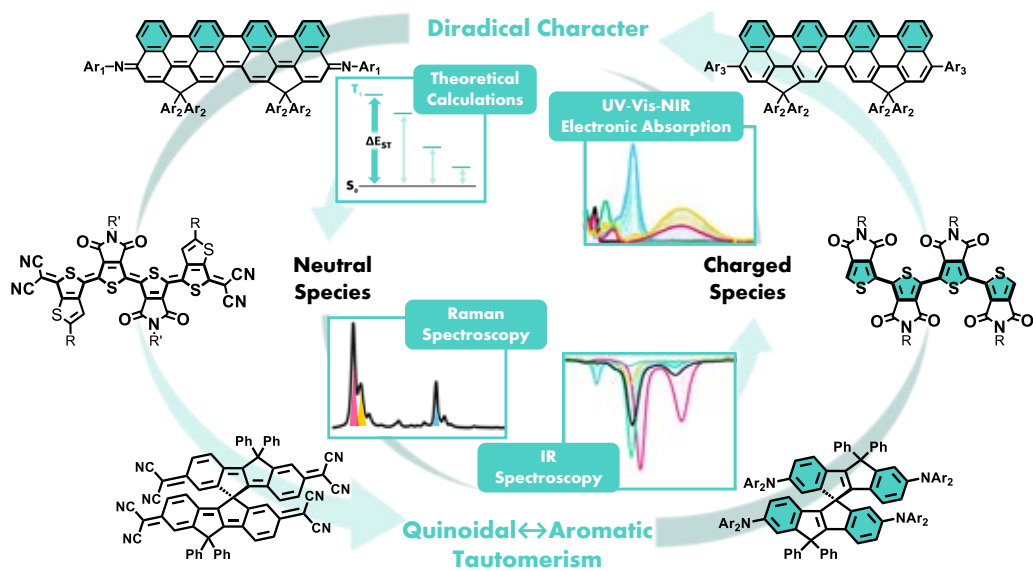
In the case of Q-CPV, the quinoidal shape is provided by the presence of four

dicyanomethylene units. The influence of this feature in the π -electron delocalization properties is also examined in a quinoidal octacyano benzotrithiophene (Q-BTT), in which two parallel π -conjugated pathways through the two dicyanomethylene pairs are observed. Note that a second classification (different from the *through-bond* and *through-space* one) can be established for the spiro Q-CPV and parallel Q-BTT molecules: while the second presents a 2D conjugated core, similar to the case of the cross-conjugated oligothiophenes, Q-CPV is a 3D π -conjugated system.



Scheme II.4. Chemical structures of the molecules forming the spiro-conjugated CPV family, and parallel Q-BTT molecule, studied in Chapter 4.

Scheme II.4 displays the chemical structures of the spiro-conjugated molecules, which were synthesized by the group of Professor Eiichi Nakamura (School of Science, The University of Tokyo, Japan), and the parallel Q-BTT, synthesized by the group of Professor Nazario Martín (Universidad Complutense de Madrid and IMDEA Nanoscience, España).



Scheme II.5. Scheme of the methodology employed in the study of the molecules presented in the present Ph. D. Thesis.

III. METHODOLOGY

III.I. SPECTROCHEMICAL METHODS

III. I.I. Radiation-Matter Interaction and the Electromagnetic Radiation

Spectroscopy is defined as the science that studies the interaction between a material system and the electromagnetic radiation. In *Spectrochemical methods* the systems of interest are atoms and molecules. By measuring the electromagnetic radiation absorbed or emitted by these species their structures and other chemical properties can be elucidated.^[1-2]

The electromagnetic radiation is a form of energy that is transported through space at light velocity, and accordingly with its properties present a double nature.^[2] Phenomena as reflection, refraction or diffraction are characteristic of waves. On the other hand, the absorption and emission processes in which the electromagnetic radiation is involved require its treatment as particles or discrete packets of energy. In this scenario, the different nature of the light generates different kinds of information about the chemical systems under study.

When the electromagnetic radiation is described through its wave nature, it is composed by a magnetic (H) and an electric (E) field perpendicularly disposed. Both components are, in turn, orthogonal to the propagation direction (Figure III.1). Both the electric and the magnetic fields are described by the standard features of a wave: amplitude, wave vector, velocity, frequency and wavelength (depicted in Figure III.1). The wavelength (λ), or frequency (ν), is of utmost importance in

spectroscopy since the different forms of radiation are classified in function of them. The wavelength is defined as the lineal distance between points in phase in two consecutive waves. Frequency is the number of oscillations that take place per time. They are also relevant because they can be related with the characteristic feature of the electromagnetic radiation as a particle: the photon energy. Frequency and wavelength are linked to the energy (E) through the equation:

$$E = h\nu = \frac{hc}{\lambda} \quad \text{III.1.1}$$

where h is the Planck constant (6.626×10^{-34} J·s) and c is the speed of light in the vacuum (2.997×10^8 m/s).

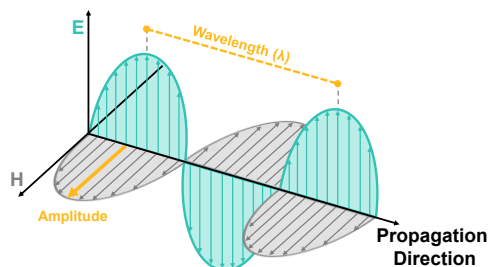


Figure III.1. Plane-polarized electromagnetic radiation. E is the electric field component and H, the magnetic component.

Frequency is often expressed as wavenumber ($\bar{\nu}$), defined as the number of waves per centimetre ($\bar{\nu} = \nu/c$), inversely proportional to the wavelength ($\bar{\nu} = 1/\lambda$). Both ν and $\bar{\nu}$ are used as energy measurements.

According to the wavelength (or frequency), the electromagnetic radiation can be classified in different regions, and this classification is projected to the

| Spin Changes | | Rotational Changes | Vibrational Changes | Electronic Changes | | Nuclear Changes | |
|-----------------|-----------------|--------------------|---------------------|------------------------|--------------------|--------------------|--------------------------------|
| | | | | | | | |
| | 10^{-2} | 1 | 100 | 10^4 | 10^6 | 10^8 | Wavenumber (cm ⁻¹) |
| 10 m | 100 cm | 1 cm | 100 μm | 1000 nm | 10 nm | 100 pm | Wavelength |
| 3×10^6 | 3×10^8 | 3×10^{10} | 3×10^{12} | 3×10^{14} | 3×10^{16} | 3×10^{18} | Frequency (Hz) |
| NMR | EPR | Microwaves | Infrared | Visible Ultraviolet | X Rays | γ Rays | |

Figure III.2. Representation of the different spectroscopies accordingly to the employed electromagnetic radiation region for the sample excitation.

different kinds of spectroscopies (Figure III.2).

In the elemental spectroscopic phenomenon, the atom or molecule absorbs or emits a quantized radiation that carries it from an initial energy state (E_1) to a final state (E_2), an excited state. The chemical information is obtained by the measurement of the intensity either of the absorbed radiation (absorption spectroscopies) or the emitted radiation (emission spectroscopies) as a function of the wavelength or frequency. According to the Einstein equation ($\Delta E = h\nu$), the energy of the absorbed radiation must match the energy difference between the two involved states.

In Figure III.3 the different energy transitions that can take place between the energy levels of a polyatomic molecule are showed. This scheme is known as the *Jablonski diagram*. Attending to the molecular transitions, the different spectroscopies are:^[3]

- **Electronic spectroscopy**, when the electronic function changes. These transitions are depicted in Figure III.3

(blue arrows), and the energy difference between the two electronic states uses to be in the ultraviolet and visible spectral region.

- **Vibrational spectroscopy**, when the vibrational function changes. These functions exclusively depend on the nuclear coordinates, which is also the case of the rotational functions. These less energy transitions (pink arrow in Figure III.3) are generated by the infrared radiation.
- **Rotational spectroscopy**, when the vibrational function changes. These transitions (green arrow in Figure III.3) occur in the microwave and radio-frequency regions.

The Einstein equation is not the unique requirement that must be satisfied in a state change with radiation absorption or emission. The treatment of this phenomenon through the time-dependent Perturbation Theory indicates that the probability of any $\Psi \rightarrow \Psi'$ transition is expressed by the integral:

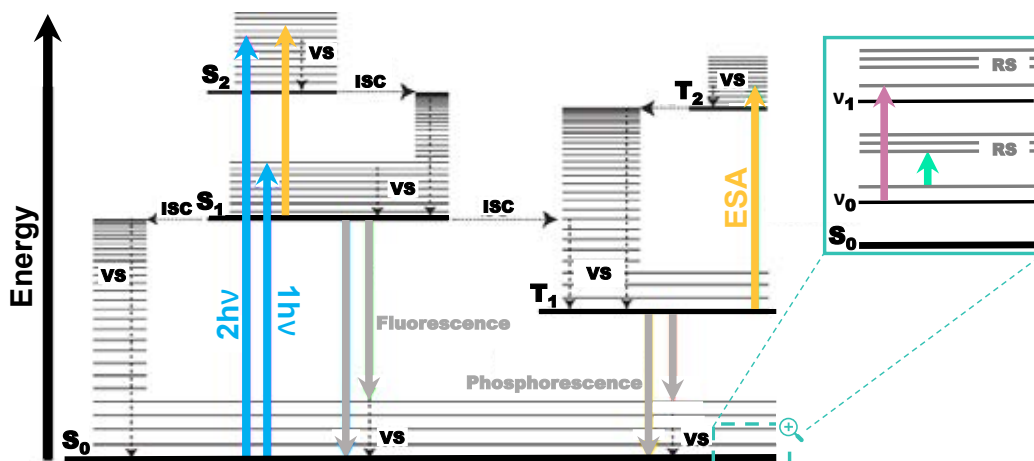


Figure III.3. Jablonski diagram of the energy states of a molecule together with the different possible transitions. S_n : singlet electronic states; T_n : triplet electronic states; VS and v_n : vibrational states; RS: rotational states; ISC: intersystem crossing; ESA: excited state absorption; $h\nu$: photon energy.

$$p = \langle \Psi | \hat{\mu} | \Psi \rangle \quad \text{III.1.2}$$

where $\hat{\mu}$ is the operator associated to the physical mechanism that allows the matter-energy electric or magnetic interaction. From all the possible mechanisms, the electric dipole mechanism is the most intense, and the only one commonly considered.

The set of conditions that Ψ and Ψ' functions must fulfil to make the integral III.1.2 different from zero in the electric dipole mechanism are known as "Selection Rules". Regarding these Selection Rules, only two kinds of transitions exist:

$$\text{Allowed: } \langle \Psi | \hat{\mu} | \Psi \rangle \neq 0$$

$$\text{Forbidden: } \langle \Psi | \hat{\mu} | \Psi \rangle = 0$$

In general, the evaluation of the Selection Rules is made according to the symmetry properties of the state functions. The components of the dipolar electric moment present the same symmetry as the x , y , z vectors. Then, only

those transitions in which the final state presents any of the x , y , z vectors symmetry will be allowed since: i) in order to make III.1.2 integral different from 0, the integrand must be totally symmetric; and ii) the initial state uses to be the ground state (in absorption processes) and, consequently, total symmetric function.^[4, 5]

Nuclear transitions use to fulfil this result rigorously. However, in electronic transitions, the interaction between electrons and nuclei motions, or vibronic coupling, can allow to observe, in electronic absorption spectra, forbidden electronic transitions as weak bands in the electronic spectra.

In this scenario, the techniques employed in the present thesis are electronic absorption spectroscopy and vibrational IR and Raman spectroscopies, principally, as well as electronic paramagnetic resonance.

III.I. II. Electronic Absorption Spectroscopy

Electronic absorption spectroscopy uses as source of excitation an electromagnetic radiation in the UV-Vis-NIR region. The energy of this radiation is able to provoke a transition from the ground electronic state (S_0) to an excited state (S_n).

In the electronic transitions of a polyatomic molecule some considerations must be taken into account:

- i. Since the mass of the nuclei are much larger than those of the electrons, these move faster enough to avoid the nuclei to change their positions appreciably. In other words, in the electronic transition it can be considered that the nuclei positions remain unaltered.^[3, 4] This assumption is known as *the Franck-Condon principle*, and explains the vibronic structure of an electronic band.

Let us consider the case of a diatomic molecule as an example. In the initial state, most of the molecules are in the lowest vibrational state of its ground electronic state. According to the probability distribution (which is given by the square of the vibrational wavefunction, Ψ_{vib}^2 , showed in Figure III.4), the most probable inter-nuclei position is the equilibrium distance, R_e ; then, the electronic transition is more probable to occur at this configuration. Following the Franck-Condon principle, since the inter-nuclei distance does not change during the absorption process, the most probable electronic transition takes place vertically at R_e to the

vibrational excited state in which Ψ_{vib}^2 is maximum for this distance (light blue solid arrow in Figure III.4). Consequently, this transition will give rise to the most intense band in the electronic absorption spectrum. This is the origin of the concept “vertical transition” to refer to an electronic transition in which the nuclei geometry is not changed.^[3, 4]

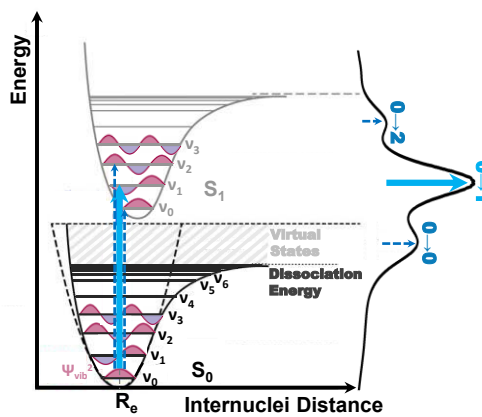


Figure III.4. Morse energy curves for the ground (S_0) and excited (S_1) electronic states of a molecule, together with the corresponding electronic absorption spectrum (right). The probability distribution is presented in pink and purple colours.

- ii. Besides the most probable final vibrational state, the nearest vibrational states also present a considerable probability to find the nuclei at R_e . In consequence, near energy electronic transitions occur, giving rise to the vibronic structure of the electronic band (dark blue dashed arrows in Figure III.4). Usually these transitions are indicated according to the vibrational levels: from the lowest vibrational level of the ground electronic state to the lowest vibrational level of the excited electronic state ($0 \rightarrow 0$ electronic

transition), to the first vibrational level ($0 \rightarrow 1$), to the second ($0 \rightarrow 2$), and so on.

In general, the electronic transitions are described with the molecular orbitals that are involved in the absorption process. The more common molecular orbitals in which the valence electrons of a ground state are accommodated are σ - and π -orbitals for the bonding electrons, and n orbitals for the non-bonding electrons (for example the lone pairs of heteroatoms). The empty molecular orbitals at which the valence electrons can be promoted use to be antibonding σ^* - or π^* -orbitals.

In electronic spectroscopy, the functional groups responsible of the absorptions are named "chromophores". For chromophores with no π nor n orbitals, the only electronic transitions are $\sigma \rightarrow \sigma^*$, which take place with excitation radiation of the far ultraviolet region (high energy transition). These transitions do not use to give as structural information as the $\pi \rightarrow \pi^*$ or $n \rightarrow \pi^*$ ones, which are observed in the visible or near UV region.^[3, 5] For example, the $\pi \rightarrow \pi^*$ electronic transition of the double C=C bond at 180 nm or the $n \rightarrow \pi^*$ transition for the carbonyl group at 290 nm are representative of these chromophores.

When the electronic transference involves molecular orbitals that are essentially centered on localized molecular moieties, the transition is known as *charge transfer*. In general, a charge transfer band increases its intensity when augmenting the distance between the two involved moieties as the transition dipole moment is also increased.^[3, 4]

π -Conjugated Systems

An interesting case of electronic spectroscopy study is π -conjugation. In π -conjugated molecules, the most important electronic transition is the HOMO-LUMO (a $\pi \rightarrow \pi^*$ transition), since it accounts for the semiconducting properties of these materials. A common effect in these systems is that the enlargement of the effective π -conjugated length (for instance, by increasing the number of C=C chromophores), provokes the progressive narrowing of the HOMO-LUMO gap energy. Consequently, the absorption wavelength (λ_{\max}) is shifted to larger values (bathochromic or red-shift displacement).^[6-8] This process is schematized in Figure III.5.

Using the oligomeric approach, the properties derived from the progressive red-shift of the λ_{\max} wavelength when increasing the number of monomeric units can be studied through the Meier's equation.^[9-12]

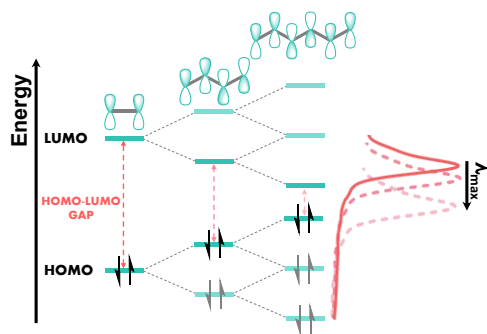


Figure III.5. Representation of the HOMO-LUMO gap evolution when lengthening the oligomer size, and its bathochromic effect on the maximum electronic absorption wavelength.

As previously discussed in the *Introduction* section, the linear fit of the λ_{\max} wavelengths to the Meier's equation

allows to obtain the *effective conjugation length*, the characteristic number of monomeric units at which the oligomer properties converge.

Electronic absorption spectroscopy is also very useful for the study of the charged species of these π -conjugated systems. The progressive reduction/oxidation to the radical monovalent (polaron) and, then, the divalent (bipolaron) charged species lead to well-known electronic absorption patterns (see Figure III.6 for the reduction process). Injection or removal of one electron from a linearly π -conjugated oligomer usually generates two bands in their electronic absorption spectra: the *polaron* structure (pink transitions and

spectrum). In the doublet, the most energy and intense absorption band corresponds to the SOMO \rightarrow LUMO transition, while the second band, placed at lower energies (frequently a broad band in the near IR region), is assigned to the HOMO \rightarrow SOMO.^[13-15] Similar to the electronic absorptions of the neutral molecules, these pair of bands are progressively red-shifted when lengthening the oligomer size as a consequence of the larger π -electron delocalization.

Upon injection or removal of a second electron classical closed-shell divalent species are obtained. They present a single, intense absorption band caused by the HOMO \rightarrow LUMO electron transition

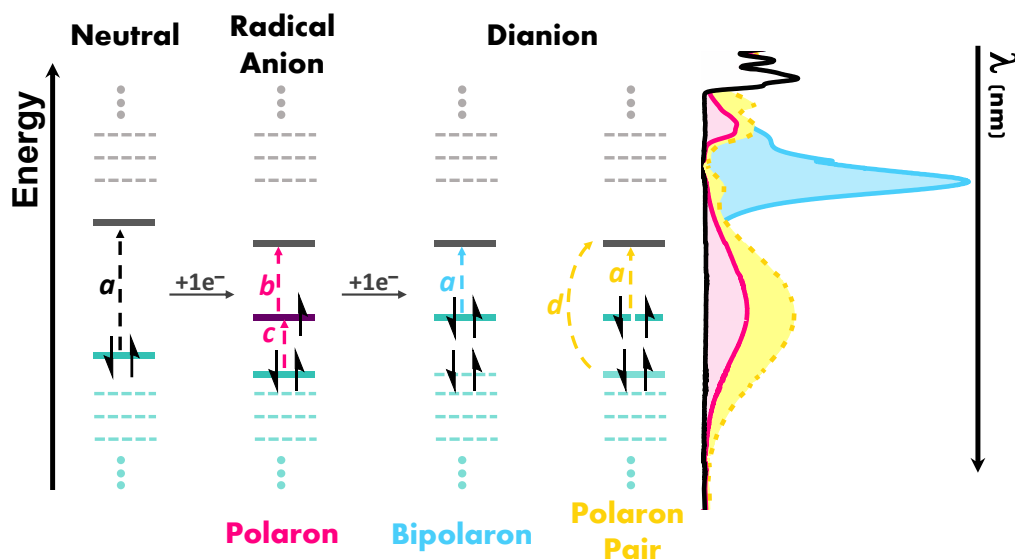
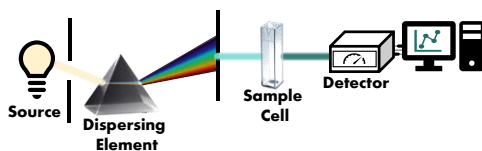


Figure III.6. Schematic electronic structures and transitions of neutral (black), polaron radical anion (pink), bipolaron (light blue) and polaron pair (yellow) dianion species, together with the corresponding electronic absorption band pattern. Dark green states correspond to the HOMO levels; dark grey states correspond to LUMO levels; purple state corresponds to SOMO level; light green and light grey states correspond to HOMO- n and LUMO+ n levels, respectively (electrons in HOMO- n energy levels have been omitted for clarity). Designated electronic transitions are: *a*: HOMO \rightarrow LUMO; *b*: SOMO \rightarrow LUMO; *c*: HOMO \rightarrow SOMO; *d*: HOMO-1 \rightarrow LUMO.

(see Figure III.6, transition and band in blue). The spectral pattern of these species is referred as *bipolaronic* structure.^[13-15] However, divalent species of π -conjugated molecules can also present an open-shell configuration, and are favoured when the spatial overlap of spin orbitals is diminished, that is, in disjoint orbitals. In these cases, the two charges are localized in different parts of the molecule, and they behave as two symmetrical polarons (or two isolated radical cations or anions). For this reason, their electronic spectra are assigned as *segregated polarons*, *side-by-side polarons* or *polaron pair* structure, and they resemble to that of the polaronic pattern: two optical bands, one of them less intense and considerably red-shifted respect to the first one (yellow transitions and spectrum).^[14, 15] These polaron pair structures are, therefore, characteristic of diradical species.

The Experimental Technique

The general components of an electronic absorption spectrophotometer are represented in Scheme III.1:^[2, 5]



Scheme III.1. General scheme of the basic components of an absorption spectrophotometer.

- 1) **Source:** the element that generates the electromagnetic radiation. In electronic absorption consist in several lamps which emit continuum

radiation in different ranges of the UV-Vis-NIR spectrum.

- 2) **Dispersing Element:** a diffraction grating that disperses the radiation into its constituting wavelengths.
- 3) **Sample Cell:** where the sample is placed.
- 4) **Detector:** the component that transforms the radiation in an electrical signal.

The electronic absorption spectra presented in this Ph. D. Thesis have been generally measured solving the sample in CH_2Cl_2 solvent at room temperature, with molar concentration in the range of 10^{-3} - 10^{-5} mol/L. The studied molecules are highly soluble in CH_2Cl_2 solvent (Sigma-Aldrich/Merck, HPLC grade, 99.9%) due to its low polarity (dielectric constant: 8.93) and the alkyl groups present in these oligomers.

Electronic absorption of thin-films was also carried out. To perform these measurements, 10^{-3} mol/L standard solutions in CHCl_3 were spin-coated on glass. In this case, CHCl_3 solvent (Sigma-Aldrich/Merck, HPLC grade, 99.8%) was used to emulate the thermoelectric device.

The spectrophotometers employed in the electronic absorption measurements were:

- **Agilent 8453 UV-Vis spectrophotometer:** with a wavelength range of 190-1100 nm.
- **Cary 5000 UV-Vis-NIR spectrophotometer:** with a wavelength range of 175-3300 nm.

III.I. III. Vibrational Infrared Spectroscopy

In most of the molecules, transitions between vibrational states can be triggered by infrared radiation. Vibrational absorption spectroscopy is therefore called “infrared spectroscopy”.

Any polyatomic molecule of N atoms has $3N-6$ independent vibrational modes ($3N-5$ in the case of linear systems) named *normal modes*. The *normal modes* are collective displacements of all the nucleus that preserve the centre of mass, present the same frequency and are in phase with different amplitudes. According to the electric dipole Selection Rules, to make equation III.1.2 different from 0, μ must change during the vibration.

In this absorption spectroscopy, to obtain an active IR vibration:

- i. The electric dipolar moment of the molecule must change during the relative displacement of the atoms.^[3, 4] For this reason, homonuclear diatomic molecules are inactive in IR spectroscopy.
- ii. Only transitions between two consecutive vibrational states absorb IR radiation ($\Delta v=+1$). Since this selection rule is derived from the harmonic model, and the polyatomic system present anharmonic motions, $\Delta v>1$ are also active. Although with lower intensities. By this way, despite the fundamental transition ($\Delta v=+1$) is the most probable (usually from $v=0$ to $v=1$ at room temperature), also overtones ($\Delta v>1$) can be obtained (less probable as the difference Δv increases).

π -conjugated molecules do not present intense IR absorption due to their small dipole moment. However, this technique is usually employed in the study of π -conjugated molecules bearing strongly polar groups, as carbonyl or cyano groups, which possess characteristic vibrational wavenumbers in spectral region where not other groups absorb. Comparing the behaviour of these IR bands in the oligomeric series allows to determine if a reinforce (if $\bar{\nu}$ is upshifted) or weaken (if $\bar{\nu}$ is downshifted) of the chemical bond takes place.^[6] If these groups are conjugated to the π -framework, also the affectation of the π -electron delocalization can be described.

The Experimental Technique

The most widely employed IR spectrometer is that implementing the Fourier Transform technique (FT-IR). Instead of a dispersing element, the FT-IR spectrometers use a Michelson interferometer to produce an interferogram, which is then transformed in the IR spectrum through a Fourier Transform mathematical treatment.^[2, 3] Through this technique higher spectral resolution in a wider spectral range is obtained.

In this thesis, the IR absorption studies have been performed both with sample in solid state (pellets obtained by diluting the sample in KBr) (Sigma-Aldrich/Merck, FT-IR grade, $\geq 99\%$), and solved in CH_2Cl_2 . Also, IR spectra of thin-film have been measured

by spin-coating the sample solution (in CHCl_3) on a KBr substrate.

These spectra were recorded with the following FT-IR spectrometers:

- **Bruker Tensor 27 FT-IR:** with a wavenumber range of $7500\text{-}370\text{cm}^{-1}$.
- **Vertex FT-IR 70:** with a wavenumber range of $7500\text{-}400\text{ cm}^{-1}$.

III.I. IV. Vibrational Raman Spectroscopy

Despite Raman spectroscopy is also a vibrational technique, its physical nature is clearly different from that of the IR spectroscopy. This fact is evident only considering the phenomena that are detected in each technique: light absorption in IR spectroscopy and light scattering in Raman spectroscopy.

As has been described in the section *Radiation-Matter Interaction and the Electromagnetic Radiation*, the light-matter interaction can be studied through absorption and emission processes. However, photons can also interact with molecules and then be re-emitted from them. This re-emitted radiation is known as scattered light and take place in all the directions. This is the phenomenon on which Raman spectroscopy is based.

In light scattering, the incident radiation distorts the electron cloud around the nuclei to form a short-lived virtual state, and the physical magnitude that produces it is the molecular polarizability. The virtual state does not correspond to any of the vibrational states

of the molecule, and its energy depends on the energy of the light source. The inherent instability of the virtual state makes the *excited photon* to be quickly re-emitted. Depending on the energy of scattered photons, two light scattering processes are described:

1. Scattering without energy exchange. In this case, the energy of the incident and scattered light is similar and, hence, their frequencies too. This elastic radiation, in which the energy is mainly conserved, is named *Rayleigh scattering*.

2. Scattering with energy exchange. During the process it can also occur an energy transfer between the incident photons and the molecule, in a way that the light is scattered with a different energy/frequency. This kind of inelastic interaction is named Raman scattering, and can be classified, in turn, in two emissions:

- **Stokes Raman Scattering:** the energy is transferred from the photons to the molecule; thus, the scattered light is less energy than the incident radiation.
- **Anti-Stokes Raman Scattering:** the energy is transferred from the molecule to the photons, which are emitted with larger energies. This process takes place in molecules which do not come from the lowest vibrational state (ν_0). Since most of the molecule are in the ground state, *i. e.*, the population in ν_0 is

larger than in the excited vibrational states, then the anti-Stokes scattering is much less intense than the Stokes one.

These scattering processes are schematized in Figure III.7. It has to be noted that Raman scattering is a weak phenomenon: only one of 10^6 - 10^8 photons experiments an inelastic scattering.^[16]

In Raman spectroscopy, the molecule is excited with a single frequency radiation (monochromatic radiation), and the scattered light is detected. Since the electron is promoted to a virtual state, the energy of the incident radiation is higher than the energy difference between the vibrational states. This is one of the main differences with the electronic and IR spectroscopies, and it allows the use of several excitation energies.

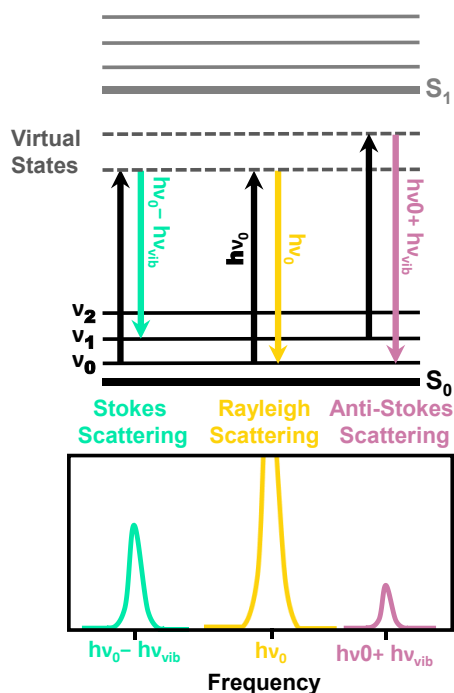


Figure III.7. Representation of the light scattering processes and the resulting vibrational signals.

Once the Raman scattering is described, it can be deduced that the Selection Rules for the Raman transitions are based on the molecular polarizability rather than in the dipole moment. A vibration will be Raman active if it produces a periodic change on the molecular polarizability. Consequently, IR inactive vibrations can present an intense Raman activity and *vice versa*, thus making both vibrational techniques highly complementary.

π -Conjugated Systems: The ECC Mode

As aforementioned, π -conjugated molecules do not present high IR activity, unless substitution with polar functional groups. However, the large polarizability of the π -electron density generated by the alternant double and single CC bonds, makes them suitable systems for Raman studies.

The general features found in the Raman spectra of π -conjugated molecules are:^[17]

- i. High selectivity of some specific transitions, leading to simple spectra (even with no resonance effects);
- ii. An increasing intensity and a wavenumber downshift of the Raman signals when lengthening the π -conjugation.

These characteristics are a consequence of the behaviour of the conjugated systems in the scattering phenomenon. On the one hand, the involved energy states are those forming

the collective π -electron density (the π and π^* molecular orbitals).

To understand the Raman behaviour of π -conjugated molecules, the Effective Conjugation Coordinate (ECC) Theory is employed. Qualitatively, the key point of this theory is that the presence of a large π -electron density gives rise to two strongly active Raman bands, both assigned to collective CC stretching vibration of the conjugated backbone, the double C=C bonds stretch with opposite phase respect the single C—C bonds.^[17, 18] They appears at 1600-1500 cm^{-1} (ν_1) and 1200-1100 cm^{-1} (ν_2).

This collective vibration is named the ECC mode. It accounts for the extension of the π -conjugation, since the wavenumber of this mode depends on the contributions of the single and double bonds. Increasing the π -electron delocalization reduces the CC bond length alternation (or BLA) pattern.^[17-20]

The ECC mode can account for the aromatic \leftrightarrow quinoidal tautomerism. A representative application of the Raman study through the ECC mode of this transformation is given by the quinoidal tetracyano-oligothiophene series, \mathbf{Q}_n .^[20-22] In this systems, the ECC mode is progressively down-shifted as the enlargement of the quinoidal backbone increases the π -electron delocalization ($\mathbf{Q}_2 \rightarrow \mathbf{Q}_4$, from 1466 cm^{-1} to 1322 cm^{-1}). However, the formation of a diradical structure in the longer oligomers provokes the aromatization of the thiophene rings, thus the ECC mode is now up-shifted because of the strengthening of the C=C bonds ($\mathbf{Q}_4 \rightarrow \mathbf{Q}_6$, from 1322 cm^{-1} to 1439

cm^{-1}). The Raman spectra of the \mathbf{Q}_n oligomers and the behaviour of their ECC mode are showed in Figure III.8.

The Experimental Technique

The Raman bands intensities are highly dependent on the power and frequency of the excitation source.^[16] Thus, these two

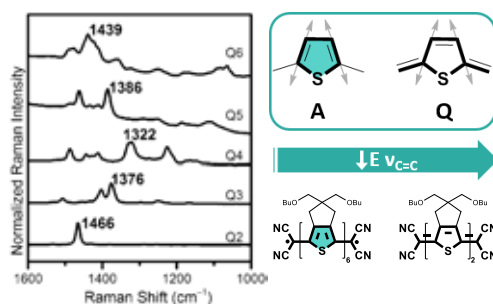


Figure III.8. Raman spectra of \mathbf{Q}_n series in solid state together with the schematic representation of the ECC mode of the thiophene rings.

parameters must be chosen carefully once selected the system under study and the information required. In this sense, higher laser frequencies (in the visible and UV region) and powers result in most intense bands. However, many samples can experiment degradation under these strong conditions. On the other hand, less energy radiation (in the NIR region) avoids electronic absorption and fluorescence processes, leading to “cleaner” Raman spectra.

Other important phenomenon that must be considered when selecting the laser excitation frequency/wavelength, is the resonant Raman effect. When the laser excitation frequency is close to the energy of an electronic transition, the Raman scattering phenomenon can be enhanced

of up to 10^6 .^[16] In addition to the improved sensitivity, the Raman activity of the chromophore responsible of the electronic transition is selectively intensified. In this sense, resonant Raman spectroscopy allows the detection of samples of specific molecules in more complex chemical systems at low concentrations.^[16, 23]

In this Ph. D. thesis, Raman spectra have been measured in both, solid (bulk and pellet, diluted in KBr) and solution (10^{-3} M in CH_2Cl_2). Several laser excitation wavelengths have been employed (described below), indicating in the corresponding spectra if resonant effects are present. In general, the less energy excitation wavelengths were preferred to avoid possible sample degradation. Raman spectra of thin-films were also measured by spin-coating the solution (in CHCl_3) on a glass substrate.

The employed vibrational Raman spectrometers are:

- **Bruker FT-Raman Ram II:** with a Nd:YAG laser that provides an excitation wavelength of 1064nm.
- **Bruker Micro-Raman Senterra:** in this case the Nd:YAG laser offers excitations at 785, 633 and 532 nm.

Both spectrometers allow the variation of the laser power. In general, the lowest power that assure Raman signal was employed to conserve the sample stability. Depending on the signal intensity and fluorescence effects, acquisition times were optimized for each sample to obtain the best signal-to-noise ratio.

III.I. V. Electron Paramagnetic Resonance Spectroscopy

In Electron Paramagnetic Resonance (EPR) spectroscopy (also referred as Electron Spin Resonance, ESR), molecules with unpaired electrons absorb electromagnetic radiation in the microwave. In this spectroscopic technique, an external magnetic field provokes the splitting of the spin energy levels (Figure III.9).^[3, 4] This splitting is known as *Zeeman effect*,^[1, 3, 4] and the resonance absorption process takes place when the frequency of the applied radiation matches the energy difference between the two spin levels. Despite EPR is extensively used in the study of the radical ions and transition metal complexes^[24-26], it is also a valuable tool in the study of the diradical nature of π -conjugated systems.^[27-30]

The spin of an electron is described by \hat{S}^2 and \hat{S}_z operators, as they commute with the Hamiltonian. The corresponding quantum numbers are S and m_s , respectively. For a radical ion species, which only presents one unpaired electron, $S=1/2$ ($2S+1=2$, doublet configuration), thus two degenerate states are possible: $m_s=-1/2$ and $m_s=+1/2$. In presence of an external magnetic field these two states lose their degeneracy, and an EPR signal can be detected (see Figure III.9). In this case, only one signal is observed since only one possible transition can occur.^[3, 4, 30]

For diradical species, two possible configurations must be considered. For singlet open-shell diradicals, which have

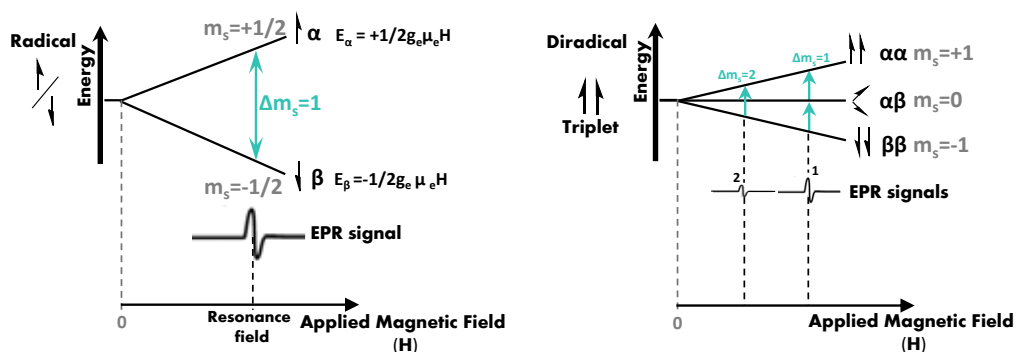


Figure III.9. Representation of the spin energy levels splitting when an external magnetic field interacts with a radical (*left*) and diradical (*right*) molecules, and the resulting EPR spectra.

two opposite spins, $S=0$ ($2S+1=1$) and, hence, $m_S=0$. Since only one orientation of the electron magnetic moment is possible, *i. e.*, only one energy level exist, singlet diradicals are *silent*-EPR species (not active in EPR). Conversely, for triplet open-shell configuration, $S=1$ ($2S+1=3$) and $m_S=-1, 0$ and $+1$, thus triplet diradicals are EPR-active. In these diradicals, the three possible orientations give rise to three possible transitions: two allowed transitions between consecutive levels, according to the selection rules ($\Delta m_S=1$, from $m_S=-1$ to $m_S=0$ and from $m_S=0$ to $m_S=1$) and a less intense forbidden transition ($\Delta m_S=2$) from $m_S=-1$ to $m_S=1$ (see Figure III.9). This forbidden transition is at the half-field of the other two and does not exist in doublets. For this reason, it constitutes a clear evidence of the triplet open-shell configuration. However, it presents a low intensity, which decreases with the distance between the spin centres.^[30] For the two allowed, $\Delta m_S=1$.

In diradical π -conjugated systems due to the Double Spin Polarization mechanism, the ground electronic state usually presents a singlet configuration. However, in some cases the stabilization of

this form respect to the triplet one is not enough to avoid the population of the high-spin state at room temperature (for narrow ΔE_{S-T} values). In consequence, EPR activity in neutral molecules or divalent ions of π -conjugated systems is a proof of the high contribution of the diradical species to the ground electronic state of the chemical structure.^[29, 31-33]

III.I. VI. Combination of the Spectroscopic Techniques with Variable Temperature and Charged and Doped Species Studies

The discussed spectroscopic techniques employed in the present Ph.D. Thesis have been used for the measurement of neutral samples at room temperature, but also for variable temperature (VT) and charged species studies.

Variable temperature electronic absorption spectra were obtained with an **Optistat DN Oxford Instruments cryostat**, which allows sample temperature variations from -196°C to 200°C . For this purpose, the employed solvent was 2-

methyl-tetrahydrofuran (2Me-THF, Sigma-Aldrich/Merck, Anhydrous, $\geq 99\%$), since it provides a transparent frozen matrix at low temperatures. On the other hand, Raman spectra at different temperatures were obtained with a **Linkam FTIR600** accessory for the Senterra spectrometer, operating from -196°C to 600°C . In this case, the VT study can be performed in pellet as well as in solution (2Me-THF).

The study of the charged species of the different systems was performed by electronic absorption and vibrational IR and Raman spectroscopies.

As a previous step, cyclic voltammeteries of the systems under were performed. Cyclic voltammograms were obtained under nitrogen atmosphere at room temperature with concentrations of 10^{-3} M solutions in 0.1M of tetrabutylammonium-hexafluorophosphate in CH_2Cl_2 ($\text{BuN}_4\text{-PF}_6$, Sigma-Aldrich/Merck, 98%), used as supporting electrolyte. These measurements were carried out on a **BASi C3 Epsilon Voltammetry Cell Stand** in a conventional three-electrode cell setup, with glassy-carbon or platinum electrode as the working electrode for reduction or oxidation processes, respectively. A platinum wire was used as the counter electrode, Ag/Ag^+ as the reference electrode and calibrated with ferrocene/ferrocenium (Fc/Fc^+) as an external potential marker. All potentials were corrected against Fc/Fc^+ . CV was measured with a scan rate of 100 mV/s.^[34, 35]

Two different methodologies were followed to obtain the oxidized or reduced species:

- **Electrochemical Processes.** With this procedure the charged species are electrochemically generated and measured *in situ* by UV-Vis-NIR electronic absorption and IR vibrational spectroscopy (for this reason it is referred as spectroelectrochemical process).^[36, 37] In this case, the oxidation or reduction processes take place through the direct removing or injection of electrons.

The corresponding absorption spectra were obtained by using an **optically transparent thin-layer electrochemical (OTTLE) demountable cell** from Specac positioned in the sample compartment of the UV-Vis-NIR or IR spectrometer (described above) to perform *in situ* measurements. This spectroelectrochemical cell consisted of a platinum wire as counter electrode, an Ag gauze as the pseudo-reference electrode, and a Pt gauze as the working electrode. The transparent thin-layer was made of quartz for the UV-Vis-NIR electronic absorption and consisted on a CaF_2 layer for the IR spectroscopy. The potential was controlled with the same potentiostat employed for cyclic voltammetry. The spectra were collected at constant potential electrolysis and the potentials were changed in interval of 15 mV. The sample description is the same employed in cyclic voltammetry.

- **Chemical Processes.** Chemical oxidations and reductions were performed by controlled addition of an appropriate oxidation or reducing agent, respectively, and monitoring the

evolution of the process by UV-Vis-NIR electronic absorption. Once the process was successfully characterized, the Raman spectra of the chemically obtained species were recorded. The samples were solved in CH_2Cl_2 at concentrations suitable for Raman detection. Iron (III) chloride (FeCl_3 , Sigma-Aldrich/Merck, anhydrous powder, $\geq 99.99\%$) was employed as oxidant agent, thanks to the reduction $\text{Fe}^{+3} + 1\text{e}^- \rightarrow \text{Fe}^{+2}$, already employed with π -conjugated systems.^[31, 38, 39] In the case of the reduction processes, triethylamine was used as reductant (Et_3N , Sigma-Aldrich/Merck, $\geq 99.5\%$), which transfers one electron to the conjugated system.^[40-42] In the case of the **2DQoT** series, the chemical reduction was carried out using (2-Cyc-DMBI-Me)₂.^[43]

For the doping treatment of the **2DQoT** series, at the concentration of 5 mg/mL in CHCl_3 solution a molar ratio of 10% of (2-Cyc-DMBI-Me)₂ (N-DMBI) in CHCl_3 was added. The solutions were then spin-coated on glass or KBr substrate, with a rotation rate of 2,000 rpm. (2-Cyc-DMBI-Me)₂ was employed as n-type dopant, synthesized *ad hoc* for the doping of **2DQTT** oligomer by the group of Professor Xiaozhang Zhu.^[43]

III.II. COMPLEMENTARY TECHNIQUES

In this section, other techniques employed in the present Ph.D. Thesis are briefly described. The group in charge of these measurements is indicated in the corresponding chapter.

III.II. I. Single Molecule Conductance

The progressively miniaturization of the organic electronic devices lead to an increasing interest in the molecular electronics field. To achieve a complete control on the performance of these devices, it is of utmost relevance to understand the exact mechanism that controls the charge transport in individual molecules.^[44-46]

In this scenario, single molecule conductance technique provides a useful method to study the charge transport phenomenon in single molecules through the measurement of their conductance (G), *i. e.*, the electrical current (I) per bias voltage ($G= I/V$). To carry out these measurements, the behaviour of the three main components intervening in the charge transport must be controlled.^[47, 48]

- The external electrodes, electronically coupled to the molecule. One of the most used metal electrodes is gold;
- The molecular backbone itself;
- The anchoring groups that matches the molecule to the electrodes, also referred as the contact interface. Depending on the chemical bond, anchoring groups can be covalent bonding groups, as thiol groups (—

SH), or donor-acceptor bonding groups, when an electron transfer from these groups to the electrodes take place (for example, the Nitrogen centre of pyridines).^[48]

Also, the chemical environment surrounding the molecule can affect the conductance value.

Varying the materials and disposition of the interfaces and the external electrodes, different techniques for single molecule conductance measurements can be described.^[47, 48] However, the most widely used is the Mechanically Controllable Break Junctions (MCBJ) method due to its mechanical stability and the finely adjustable inter-electrodes distance.^[46, 49]

Other common technique is the Scanning Tunneling Microscope Break Junction method (STM-BJ), used in this Ph.D. thesis for single molecule conductance measurements by the group of Professor Latha Venkataraman. In this set-up, the molecules are anchored to a stationary, substrate electrode, while the STM tip, performing as the second electrode, can be put in contact and separated from the substrate. In a first step, the STM tip is driven to the surface and anchors to the free anchoring group of the molecules. Then, the STM tip is progressively separated from the substrate, measuring the conductance through the molecule until the elongation is enough to break the junction, *i. e.*, the molecule is disconnected from one of the two electrodes. This process is repeated several times to obtain a statistical

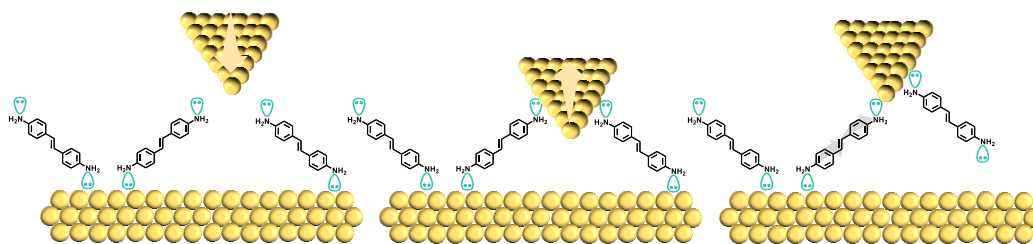


Figure III.10. Representation of a single molecule conductance measurement through Scanning Tunneling Microscope Break Junction (STM-BJ) methodology.

distribution of the conductance values. In a 1D conductance histogram, the conductance values and the times each of this value is obtained is presented.^[47, 49, 50] In a 2D-histogram, each conductance value is assigned to an elongation distance. By this way, the most probable conductance can be related with the corresponding interelectrode distance, which can coincide or not with the elongated molecule.

In Figure III.10 the STM-BJ technique is schematized.

III.II. II. Time-Resolved Spectroscopies

Time-resolved spectroscopies are techniques with high temporal resolution that allow the study of dynamic processes that occur in the picosecond or femtosecond regime.^[51] Since in this time scale the breakdown and formation of chemical bonds take place, excited states can be studied.

Transient spectroscopies are employed for the study of short-lived molecular excited states (or transient states^[1]). In the case of π -conjugated molecules, these transient states differ from the ground

electronic states only in the electronic distribution, but the σ -framework remains unaltered. Consequently, the study of these species leads to a better knowledge of their operational behaviour in the electronic devices.^[31, 29, 32, 52]

In **transient absorption spectroscopy**, the electronic absorption of the generated excited state is measured. The used methodology to characterize the transient species is the “pump-probe” set-up.^[51, 53] First, the *classical* electronic absorption of the sample is recorded. This is the absorption at “pump-off”, in other words, the absorption of the non-excited sample. In a second step, a photoexcitation pulse (“pump” pulse) generates the transient species. After a delay time, that can be tuned, a white light pulse (“probe” pulse) is transmitted through the photoexcited sample. This is the “pump-on” absorption. The transient spectrum is obtained through the difference between the two measured absorptions (see Figure III.11):

$$\Delta A = \frac{A_{ON} - A_{OFF}}{A_{OFF}} \quad \text{III.2.1}$$

The dynamics of the excited state can be study performing the “pump- probe” experiments at different delay times.

As a consequence of the depopulation of the ground electronic state in the

sample photoexcitation, the absorption band corresponding to this state diminishes progressively its intensity. This phenomenon is known as “ground state bleaching”.

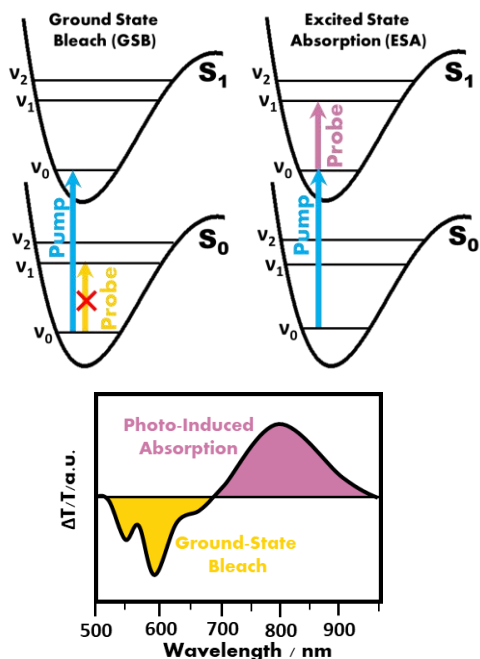


Figure III.11. Top) Scheme of the electronic transitions in a “pump-probe” experiment; Bottom) Representation of a general Transient Absorption spectrum.

The IR vibrational spectra of transient species can be also obtained. In **time-resolved IR spectroscopy** also the “pump-probe” methodology is employed. In this case, the “probe” can be either a continuous wave IR radiation, when the process under study occurs in the nanosecond regime, or a pulsed IR source if a femtosecond timescale is needed.^[53] As in the case of the *conventional* IR vibrational spectroscopy, IR active functional groups are used as indicators of the electronic redistribution.

III.III. QUANTUM CHEMISTRY CALCULATIONS

Theoretical approaches are a useful tool in the search of the structure-properties relationship of chemical systems. In the study of π -conjugated systems with potential applications in electronic devices, it is widely spread the use of theoretical models that allow a better understanding of the chemical and physical behaviours responsible of the optoelectronic properties. In this context, basic theoretical chemical calculations have been performed to assist in the interpretation, and provide a deeper insight, of the experimental results.

III.III.I. Introduction to the Quantum Chemistry Calculations

Theoretical calculations in Chemistry are used to simulate complex molecular structures and predicts their properties and reactivity applying the theoretical principles of the Quantum Chemistry.

The energy, and related properties, of any molecular system can be obtained through the solution of the time-independent Schrödinger equation:

$$H\Psi = E\Psi \quad \text{III.3.1}$$

Solutions of equation III.3.1 in polyatomic systems require sophisticated and complex calculations. Two main approaches are commonly used:

- *Ab initio* methods;
- Semiempirical methods.

While *ab initio* methods use the correct Hamiltonian and the only experimental

values are those of the fundamental physical constants, semiempirical methods employ easier Hamiltonians in which some integrals are replaced by experimental values.^[54]

In this Thesis, quantum chemistry calculations have been carried out with the DFT methodology.

III.III.II. Density Functional Theory

DFT methods calculate the molecular energy through the electronic density.^[54, 55] The success of this theoretical methods is explained by the compromise between its accuracy and the computational efficiency (lower computational costs than other methodologies which present similar accuracy).

According to the Hohenberg-Kohn theorem, for molecules with non-degenerate ground state, the electron density (ρ) determines the Hamiltonian operator and, consequently, the electronic structure of the system. Thus, in the Density Functional Theory, the energy of the ground electronic state and other properties are calculated as a function of the electron density: $E=E[\rho]$. The most employed method to obtain the expression $E[\rho]$ is through the Kohn-Sham equations. This method describes E in a polyatomic molecule of n electrons as a function of the electrons kinetic energy ($T[\rho]$), the electron-nuclei attraction energy ($E_{ne}[\rho]$), the Coulomb repulsion

between two electrons ($J[\rho]$) and the correlation exchange ($E_{XC}[\rho]$):

$$E[\rho] = T[\rho] + E_{ne}[\rho] + J[\rho] + E_{XC}[\rho]$$

III.3.2

$$E[\rho] = -\frac{\eta^2}{2m_e} \sum_{i=1}^n \varphi_i^*(r_1) \nabla_1^2 \varphi_i(r_1) dr_1 - \sum_{i=1}^n \int \frac{Z_i e^2}{4\pi\epsilon_0 r_{i1}} \rho(r_1) dr_1 + \frac{1}{2} \int \frac{\rho(r_1)\rho(r_2)e^2}{4\pi\epsilon_0 r_{12}} dr_1 dr_2 + E_{XC}[\rho]$$

III.3.3

Where φ_i is referred to the Kohn-Sham orbitals and defines ρ through the equation 3.4:

$$\rho(r) = \sum_{i=1}^n |\varphi_i(r)|^2$$

III.3.4

Applying the variational principle, the minimum energy of the molecular electronic state can be found:

$$\left(-\frac{\eta^2}{2m_e} \nabla_1^2 - \sum_{i=1}^n \int \frac{Z_i e^2}{4\pi\epsilon_0 r_{i1}} + \frac{1}{2} \int \frac{\rho(r_2)e^2}{4\pi\epsilon_0 r_2} dr_2 + V_{XC}(r_1) \right) \varphi_i(r_1) = \epsilon_i \varphi_i(r_1)$$

III.3.5

With the exchange-correlation potential:

$$V_{XC}[\rho] = \frac{\delta E_{XC}[\rho]}{\delta \rho}$$

III.3.6

From equation III.3.5 the values of the Kohn-Sham orbitals can be obtained and, then, with the expression III.3.4 the electron density probability.

In DFT methods, the different parameters in equations III.3.3- III.3.6, *i. e.*,

ρ , φ_i and V_{XC} are calculated iteratively, from a fictitious reference system, until it converges to a ρ value.

The correlation exchange energy value is approximated using the Local Density Approximation (LDA), which considers this energy only dependent on the localized electron density (this model is based on the idea of a uniform electron gas). Some improvements to accurate the energy value have been then introduced. With this purpose, several exchange-correlation hybrid functionals have been proposed, that combines calculations through different approximations, as HF, LDA or considering the gradient of the charge density.

DFT calculations in the present Ph.D. Thesis have been carried out with the hybrid functional B3LYP (Becke, 3-parameter, Lee–Yang–Parr functional), which combines the Becke's three parameter (B3) gradient corrected exchange functional with the Lee-Yang-Parr (LYP) non-local correlations.^[56] The mathematical description of the orbitals has been performed with the 6-31G** split valence basis set.^[57] In this basis set, core atomic orbitals are described by a contracted gaussian function resulting from the combination of 6 primitive gaussians. On the other hand, the valence orbitals are described through two basis functions, the first one resulting from the combination of 3 primitive gaussian functions and the second one, from only one primitive function. The double asterisk, also denoted as *d,p*, indicate that polarization functions *d* and *p* are added

on heavier atoms and on the hydrogen atoms, respectively.

Despite DFT calculations have been described for the ground electronic state, some approximations allow their application also for excited states, since the ground state density determines all excited state properties. Time-Dependent DFT methodology (TD-DFT) considers the excitation states as perturbations depending on time. The response of the dipole moment to this perturbation (an electric field with a frequency depending on time) is the dynamic polarizability. Through this parameter, the properties of the excited state can be calculated and, consequently, also the electronic transitions.

Theoretical calculations performed in this Thesis consist on geometry optimizations, minimum energy and vibrational frequency calculations and TD-DFT (allow to obtain UV-Vis-NIR electronic absorption spectra). Calculated vibrational frequencies were scaled down by a factor of 0.96 to correct systematic deviations.^[58] These calculations have been performed at the B3LYP/6-31G** level of theory for closed-shell molecules. However, diradical species have constituted an essential tool in the study of the π -electron delocalization in polyconjugated systems along the present Thesis. Thus, calculations with open-shell configurations are required. For this purpose, the Broken-Symmetry approximation in the unrestricted DFT methodology (BS-UDFT) was employed for the theoretical study of the energies and geometries of singlet open-shell systems.^[59, 60] In this case, 6-

31G** basis set was also used due to the good results described in bibliography^[58, 59] and in order to perform a consistent comparison with the closed-shell systems.

■ REFERENCES

- [1] IUPAC. *Compendium of Chemical Terminology, 2nd ed. (the "Gold Book")*. Compiled by A. D. McNaught and A. Wilkinson. Blackwell Scientific Publications, Oxford (1997). Online version (2019-) created by S. J. Chalk. ISBN 0-9678550-9-8.
<https://doi.org/10.1351/goldbook>.
- [2] *Fundamentals of Analytical Chemistry*, D. A. Skoog, D. M. West, F. J. Holler and S. R. Crouch, Thomson Learning, USA, 2008, 8th ed. (Translation of *Paraninfo S. A.*).
- [3] *Physical Methods for Chemists*, R. S. Drago, Surfside Scientific Publishers, Gainesville: Florida, 1992, 2nd ed.
- [4] *Atkin's Physical Chemistry*, P. Atkins and J. de Paula, Oxford University Press, USA, 2006, 8th ed. (Translation of *Editorial Médica Panamericana*).
- [5] *Modern Spectroscopy*, J. M. Hollas, John Wiley & Sons Ltd, Chichester:England, 2004, 4th ed.
- [6] *Optical Properties of Conducting Polymers*, A. O. Patil, A. J. Heeger and F. Wudl, *Chem. Rev.*, 1988, 88, 183–200.
- [7] *Electronic Materials: The Oligomer Approach*, M. Bürkle, K. Müllen and G. Wegner, Eds.; John Wiley & Sons, LTd: United Kingdom, 2008.
- [8] *Optical Bandgaps of π -Conjugated Organic Materials at the Polymer Limit: Experiment and Theory*, J. Gierschner, J. Cornil and H-J. Egelhaaf, *Adv. Mater.*, 2007, 19, 173–191.
- [9] *Effective Conjugation Length and UV/Vis Spectra of Oligomers*, H. Meier, U. Stalmach and H. Kolshorn, *Acta Polymer.*, 1997, 48, 379–384.
- [10] *Conjugation Oligomers with Terminal Donor-Acceptor Substitution*, H. Meier, *Angew. Chem. Int. Ed.*, 2005, 44, 2482–2506.
- [11] *Monodisperse Dialkoxy-Substituted Oligo(Phenyleneethynylene)s*, U. Stalmach, H. Kolshorn, I. Brehm and H. Meier, *Liebigs Ann.*, 1996, 9, 1449–1456.
- [12] *Effective Conjugation Length and UV/Vis Spectra of Oligomers*, H. Meier, U. Stalmach and H. Kolshorn, *Acta Polymer.*, 1997, 48, 379–384.
- [13] *Polarons, Bipolarons and Solitons in Conducting Polimers*, J. L. Brédas and G. B. Street, *Acc. Chem. Res.*, 1985, 18, 309–315.
- [14] *Polarons, Bipolarons, and Side-By-Side Polarons in Reduction of Oligofluorenes*, L. Zaikowski, P. Kaur, C. Gelfond, E. Selvaggio, S. Asaoka, Q. Wu, H.-C. Chen, N. Takeda, A. R. Cook, A. Yang, J. Rosanelli and J. R. Miller, *J. Am. Chem. Soc.*, 2012, 134, 10852–0863.
- [15] *Electronic Absorption and Vibrational Spectroscopies of Conjugated Conducting Polymers*, Y. Furukawa, *J. Phys. Chem.*, 1996, 100, 15644–15653.
- [16] *Modern Raman Spectroscopy. A Practical Approach*, E. Smith and G. Dent, WILEY-VCH: Weinheim, 2005.
- [17] *Raman Spectroscopy of Polyconjugated Molecules and Materials: Confinement Effect in One and Two Dimensions*, C. Castiglioni, M. Tommasini

- and G. Zerbi, *Phil. Trans. R. Soc. Lond. A*, **2004**, 362, 2425–2459.
- [18] A Simple Interpretation of the Vibrational Spectra of Undoped, Doped and Photoexcited Polyacetylene Amplitude Mode Theory in the GF Formalism, C. Castiglioni, J. T. López Navarrete and G. Zerbi, *Solid State Commun.*, **1988**, 65, 625–630.
- [19] Relation between Effective Conjugation, Vibrational Force Constants and Electronic Properties in Polyconjugated Materials, J. T. López Navarrete, I. B. Tian and G. Zerbi, *Solid State Commun.*, **1990**, 74, 199–202.
- [20] Quinoidal/Aromatic Transformation in π -Conjugated Oligomers: Vibrational Raman Studies on the Limit of Rupture of π -Bonds, P. Mayorga Burrezo, J. L. Zafra, J. T. López Navarrete and J. Casado, *Angew. Chem. Int. Ed.*, **2017**, 56, 2250–2259.
- [21] On the Biradicaloid Nature of Long Quinoidal Oligothiophenes: Experimental Evidence Guided by Theoretical Studies, R. Ponce Ortiz, J. Casado, V. Hernández, J. T. López Navarrete, P. M. Viruela, E. Ortí, K. Takimiya and T. Otsubo, *Angew. Chem. Int. Ed.*, **2007**, 46, 9057–9061.
- [22] Quinoidal Oligothiophenes: Towards Biradical Ground State Species, R. Ponce Ortiz, J. Casado, S. Rodríguez González, V. Hernández, J. T. López Navarrete, P. M. Viruela, E. Ortí, K. Takimiya and T. Otsubo, *Chem. Eur. J.*, **2010**, 16, 470–484.
- [23] Achievements in resonance Raman spectroscopy Review of a technique with a distinct analytical chemistry potential, E. V. Efremov, F. Ariese and C. Gooijer, *Analytica Chimica Acta*, **2008**, 606, 119–134.
- [24] Use of EPR Spectroscopy in Elucidating Electronic Structures of Paramagnetic Transition Metal Complexes, P. Basu, *J. Chem. Ed.*, **2001**, 78, 666–669.
- [25] Chemical Insights from EPR Spectra of Organometallic Radicals and Radical Ions, A. L. Rieger and P. H. Rieger, *Organometallics*, **2004**, 23, 154–162.
- [26] Use of Electron Paramagnetic Resonance to Solve Biochemical Problems, I. D. Sahu, R. M. McCarrick and G. A. Lorigan, *Biochemistry*, **2013**, 52, 5967–5984.
- [27] Interaction of Radical Pairs Through-Bond and Through-Space: Scope and Limitations of the Point-Dipole Approximation in Electron Paramagnetic Resonance Spectroscopy, C. Riplinger, J. P. Y. Kao, G. M. Rosen, V. Kathirvelu, G. R. Eaton, S. S. Eaton, A. Kutateladze and F. Neese, *J. Am. Chem. Soc.*, **2009**, 131, 10092–10106.
- [28] A Stable Non-Kekulé Singlet Biradicaloid from meso-Free 5,10,20,25-Tetrakis(Pentafluorophenyl)-Substituted [26]Hexaphyrin(1.1.1.1.1.1), T. Koide, K. Furukawa, H. Shinokubo, J.-Y. Shin, K. Suk Kim, D. Kim and A. Osuka, *J. Am. Chem. Soc.*, **2010**, 132, 7246–7247.
- [29] Kinetically Blocked Stable Heptazethrene and Octazethrene: Closed Shell or Open-Shell in the Ground State?, Y. Li, W.-K. Heng, B. Sun Lee, N. Aratani, J. L. Zafra, N. Bao, R. Lee, Y. Mo Sung, Z. Sun, K.-W. Huang, R. D. Webster, J. T. López Navarrete, D. Kim, A. Osuka, J.

Casado, J. Ding and J. Wu, *J. Am. Chem. Soc.*, **2012**, *134*, 14913–14922.

[30] *Diradicals*, M. Abe, *Chem. Rev.*, **2013**, *113*, 7011–7088.

[31] *Stable Tetrabenzo-Chichibabin's Hydrocarbons: Tunable Ground State and Unusual Transition between Their Closed-Shell and Open-Shell Resonance Forms*, Z. Zeng, Y. Mo Sung, N. Bao, D. Tan, R. Lee, J. L. Zafra, B. Sun Lee, M. Ishida, J. Ding, J. T. López Navarrete, Y. Li, W. Zeng, D. Kim, K.-W. Huang, R. D. Webster, J. Casado and J. Wu, *J. Am. Chem. Soc.*, **2012**, *134*, 14513–14525.

[32] *Pushing Extended p-Quinodimethanes to the Limit: Stable Tetracyano-oligo(N-annulated-perylene)quinodimethanes with Tunable Ground States*, Z. Zeng, M. Ishida, J. L. Zafra, X. Zhu, Y. Mo Sung, N. Bao, R. D. Webster, B. S. Lee, R.-W. Li, W. Zeng, Y. Li, C. Chi,† J. T. Lopez Navarrete, J. Ding, J. Casado, D. Kim, and J. Wu, *J. Am. Chem. Soc.*, **2013**, *135*, 6363–6371.

[33] *Benzo-Thia-Fused [N]-Thienoacenequinodimethanes with Small to Moderate Diradical Characters: The Role of Pro-Aromaticity versus Anti-Aromaticity*, X. Shi, E. Quintero, S. Lee, L. Jing, T. Seng Heng, B. Zheng, K.-W. Huang, J. T. López Navarrete, J. Ding, D. Kim, J. Casado and C. Chi, *Chem. Sci.*, **2016**, *7*, 3036–3046.

[34] *A Practical Beginner's Guide to Cyclic Voltammetry*, N. Elgrishi, K. J. Rountree, B. D. McCarthy, E. S. Rountree, T. T. Eisenhart and J. L. Dempsey, *J. Chem. Educ.*, **2018**, *95*, 197–206.

[35] *Optical, Redox, and NLO Properties of Tricyanovinyl Oligothiophenes: Comparisons between Symmetric and Asymmetric Substitution Patterns*, J. Casado, M. C. Ruiz Delgado, M. C. Rey Merchán, V. Hernández, J. T. López Navarrete, T. M. Pappenfus, N. Williams, W. J. Stegner, J. C. Johnson, B. A. Edlund, D. E. Janzen, K. R. Mann, J. Orduna and B. Villacampa, *Chem. Eur. J.*, **2006**, *12*, 5458–5470.

[36] *Interplay of α , α - versus α , β -Conjugation in the Excited States and Charged Defects of Branched Oligothiophenes as Models for Dendrimeric Materials*, R. C. González-Cano, G. Saini, Josemon Jacob, J. T. López Navarrete, J. Casado and M. C. Ruiz Delgado, *Chem. Eur. J.*, **2013**, *19*, 17165–17171.

[37] *Antiaromatic Bisindeno-[n]Thienoacenes with Small Singlet Biradical Characters: Syntheses, Structures and Chain Length Dependent Physical Properties*, X. Shi, P. Mayorga Burrezo, S. Lee, W. Zhang, B. Zheng, G. Dai, J. Chang, J. T. López Navarrete, K.-W. Huang, D. Kim, J. Casado and C. Chi, *Chem. Sci.*, **2014**, *5*, 4490–4503.

[38] *Spectroscopic and DFT Studies of Donor–Acceptor Molecules Containing Phenylquinoline and Phenothiazine Moieties in Various Redox States*, R. Ponce Ortiz, R. Malavé Osuna, M. C. Ruiz Delgado, J. Casado, S. A. Jenekhe, V. Hernández and J. T. López Navarrete, *Int. J. Quantum Chem.*, **2005**, *104*, 635–644.

- [39] *Graphenes as Potential Material for Electronics*, J. Wu, W. Pisula and K. Müllen, *Chem. Rev.*, **2007**, *107*, 718–747.
- [40] *Electrochemical Oxidation of Tertiary Amines. The Effect of Structure upon Reversibility*, S. F. Nelsen and P. J. Hintz, *J. Am. Chem. Soc.*, **1972**, *94*, 7114–7117.
- [41] *Chemical Redox Agents for Organometallic Chemistry*, N. G. Connelly and W. E. Geiger, *Chem. Rev.*, **1996**, *96*, 877–910.
- [42] *Synthesis and Doping of a Multifunctional TetrathiafulvaleneSubstituted Poly(isocyanide)*, E. Gomar-Nadal, Laurent Mugica, J. Vidal-Gancedo, J. Casado, J. T. López Navarrete, J. Veciana, C. Rovira and D. B. Amabilino, *Macromolecules*, **2007**, *40*, 7521–7531.
- [43] *Solution Doping of Organic Semiconductors Using Air-Stable n-Dopants*, Y. Qi, S. K. Mohapatra, S. Bok Kim, S. Barlow, S. R. Marder and A. Kahn, *Appl. Phys. Lett.*, **2012**, *100*, 083305.
- [44] *Molecular Electronics. Synthesis and Testing of Components*, J. M. Tour, *Acc. Chem. Res.*, **2000**, *33*, 791–804.
- [45] *Charge Transfer on the Nanoscale: Current Status*, D. M. Adams, L. Brus, C. E. D. Chidsey, S. Creager, C. Creutz, C. R. Kagan, P. V. Kamat, M. Lieberman, S. Lindsay, R. A. Marcus, R. M. Metzger, M. E. Michel-Beyerle, John R. Miller, M. D. Newton, D. R. Rolison, O. Sankey, K. S. Schanze, J. Yardley and X. Zhu, *J. Phys. Chem. B*, **2003**, *107*, 6668–6697.
- [46] *Advance of Mechanically Controllable Break Junction for Molecular Electronics*, L. Wang, L. Wang, L. Zhang and D. Xiang, *Top Curr Chem (Z)*, **2017**, *375*, DOI 10.1007/s41061-017-0149-0.
- [47] *Measurement of Single-Molecule Conductance*, F. Chen, J. Hihath, Z. Huang, X. Li and N. J. Tao, in *Annu. Rev. Phys. Chem.*, **2007**, *58*, 535–564.
- [48] *Concepts in the Design and Engineering of Single-Molecule Electronic Devices*, N. Xin, J. Guan, C. Zhou, X. Chen, C. Gu, Y. Li, M. A. Ratner, A. Nitzan, J. F. Stoddart and X. Guo, *Nat Rev Phys.*, **2019**, *1*, 211–230.
- [49] *Single-Molecule Circuits with Well-Defined Molecular Conductance*, L. Venkataraman, J. E. Klare, I.W. Tam, C. Nuckolls, M. S. Hybertsen, and M. L. Steigerwald, *Nano Lett.*, **2006**, *6*, 458–462.
- [50] *Contact Chemistry and Single-Molecule Conductance: A Comparison of Phosphines, Methyl Sulfides, and Amines*, Y. S. Park, A. C. Whalley, M. Kamenetska, M. L. Steigerwald, M. S. Hybertsen, C. Nuckolls, and L. Venkataraman, *J. Am. Chem. Soc.*, **2007**, *129*, 15768–15769.
- [51] *Introduction to Time-Resolved Spectroscopy: Nanosecond Transient Absorption and Time-Resolved Fluorescence of Eosin B*, E. P. Farr, J. C. Quintana, V. Reynoso, J. D. Ruberry, W. R. Shin and K. R. Swartz, and L. Venkataraman, *J. Chem. Educ.*, **2018**, *95*, 864–871.
- [52] *Two-Electron Transfer Stabilized by Excited-State Aromatization*, J. Kim, J. Oh, S. Park, J. L. Zafra, J. R. DeFrancisco, D. Casanova, M. Lim, J. D. Tovar, J. Casado

and D. Kim, *Nat. Commun.*, **2019**, *10*, 4983–4990.

[53] *Structural Origins of the Electronic Properties of Materials via Time-Resolved Infrared Spectroscopy*, K. T. Munson, E. R. Kennehan and J. B. Asbury, *J. Mater. Chem. C*, **2019**, *7*, 5889–5909.

[54] *Quantum Chemistry*, I. N. Levine, Pearson Education S. A., London: United Kingdom, **2001**, 5th ed.

[55] *Modern Quantum Chemistry: Introduction to Advanced Electronic Structure Theory*, A. Szabo and N. Ostlund, Dover Publications, Inc., Mineola: New York, **1996**, 1st ed.

[56] *How robust is present-day DFT?*, E. R. Davidson, *Int. J. Quantum Chem.*, **1998**, *69*, 241–245.

[57] *A Complete Basis Set Model Chemistry. I. The Total Energies of Closed-Shell Atoms and Hydrides of the First-Row Atoms*, A. Petersson, A. Bennett, T. G. Tensfeldt, M. A. Al-Laham, W. A. Shirley and J. Mantzaris, *J. Chem. Phys.*, **1988**, *89*, 2193–2218.

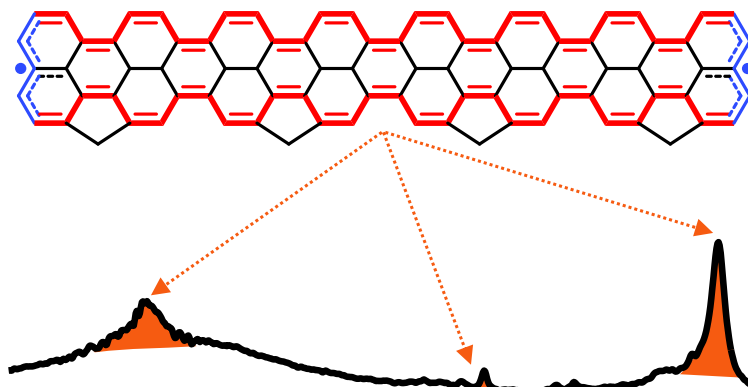
[58] *Harmonic Vibrational Frequencies: An Evaluation of Hartree-Fock, Møller-Plesset, Quadratic Configuration Interaction, Density Functional Theory, and Semiempirical Scale Factors*, A. P. Scott and L. Radom, *J. Phys. Chem.*, **1996**, *41*, 16502–16513.

[59] *Can Unrestricted Density-Functional Theory Describe Open Shell Singlet Biradicals?*, J. Gräfenstein, E. Kraka, M. Filatov and D. Cremer, *Int. J. Mol. Sci.*, **2002**, *3*, 360–394.

[60] *Spin Polarization and Annihilation for Radicals and Diradicals*, J. Gräfenstein, E.R. Davidson and A.E. Clark, *Int. J. Quantum Chem.*, **2005**, *103*, 1–9.

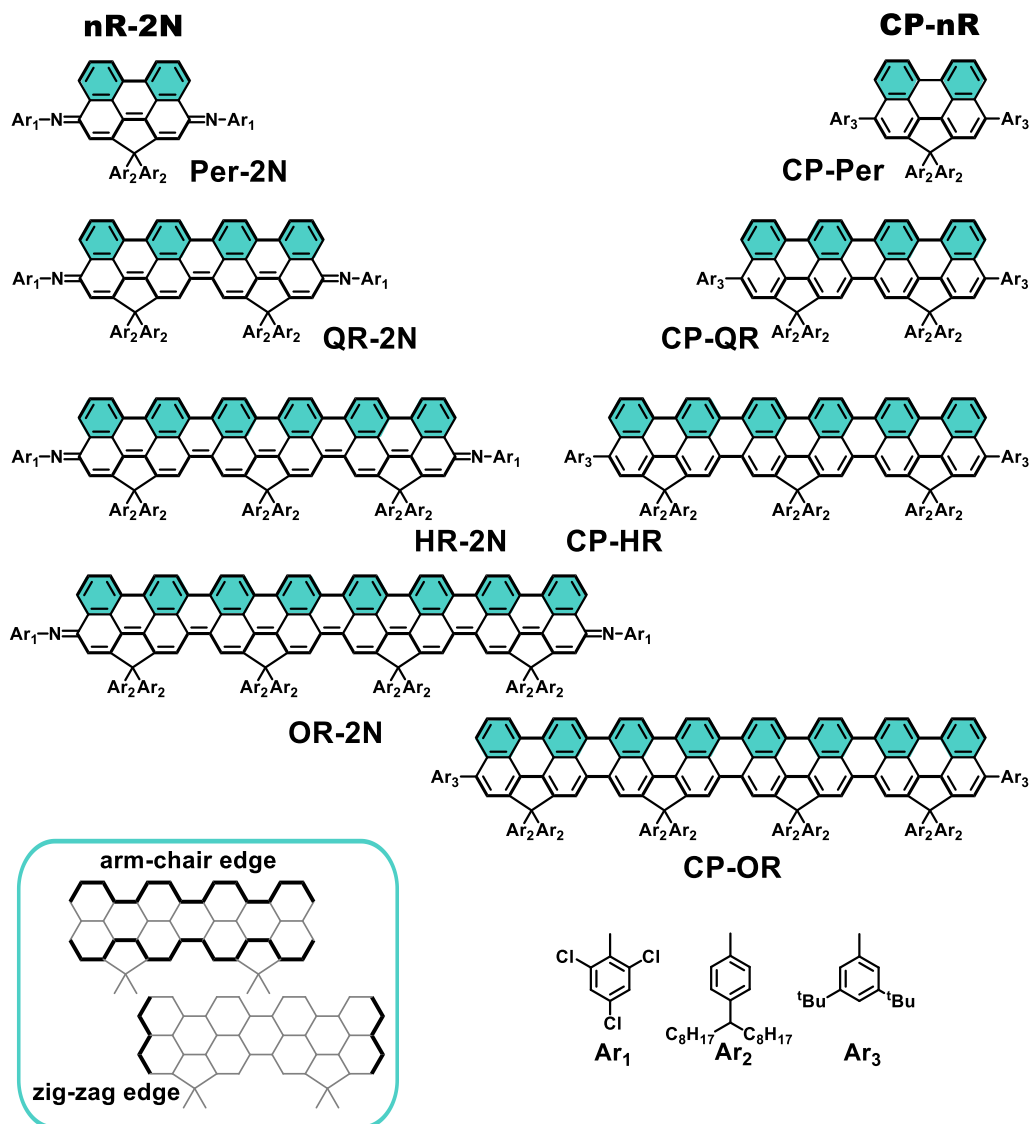
IV. RESULTS AND DISCUSSION

A. LINEARLY π -CONJUGATED DIRADICALS



1. The Case of Aromatic and Quinoidal Oligorylenes

| | |
|--|--------------|
| 1.1 Neutral Species of CP-nR and nR-2N Oligorylenes | 77—94 |
| A. Electronic Structure..... | 77—87 |
| B. Molecular Structure..... | 88—94 |
| 1.2 Conclusions | 95—96 |
| References | 97—99 |



Scheme IV.1.1. Chemical structures of the aromatic (**CP-nR**) and quinoidal (**nR-2N**) oligorylene series. Linearly π conjugated frameworks are highlighted in bold. In the inset, the arm-chair and zig-zag edges present in oligorylene molecules are depicted.

1.1 NEUTRAL SPECIES OF CP-nR and nR-2N OLIGORYLENES

A. Electronic Structure

A. I. Optical Properties

In Figure IV.1.1 the electronic absorption spectra of aromatic and quinoidal rylene families are showed at room temperature in 2Me-THF. Both series present strong absorption from the visible to the near IR spectral region as a consequence of the large extension of the π -conjugated system.^[1, 2] Besides, the absorption bands of both oligorylenes families are progressively redshifted when lengthening the oligomer size.

Absorption maxima wavelength (λ_{\max}) in aromatic oligorylenes evolves from **CP-Per** to **CP-OR**: 471 nm \rightarrow 707 nm \rightarrow 817 nm \rightarrow 983 nm (Figure IV.1.1, top panel). The shift to larger wavelengths with the oligomer size has been already observed in similar rylene systems.^[1, 2] Also, a well-resolved vibronic structure for the electronic absorption bands is observed. The covalent bridge between the perylene units gives rise to a highly planar oligorylenes core, allowing the resolution of the vibronic structure of the electronic absorption bands. Here two different vibronic structures can be differentiated. For the shortest oligomers, **CP-Per** and **CP-QR**, the most intense vibronic transition is redshifted. Conversely, the longest molecules, **CP-HR** and **CP-OR**, display vibronic transitions at larger values than the λ_{\max} wavelength.

In the case of the quinoidal oligorylenes series (Figure IV.1.1, bottom panel), the same λ_{\max} wavelength trend is obtained: 444 nm \rightarrow 660 nm \rightarrow 731 nm \rightarrow 880 nm, from

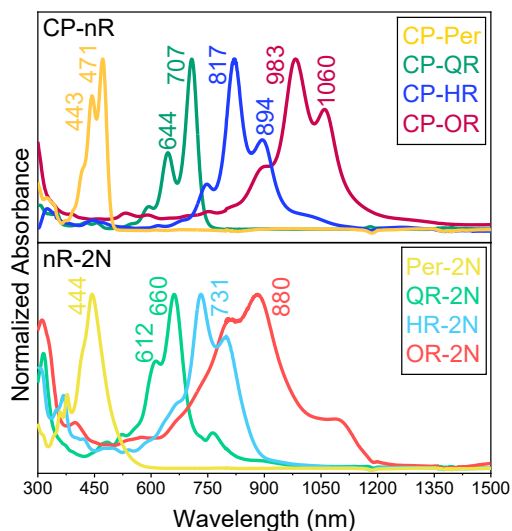


Figure IV.1.1. UV-Vis-NIR electronic absorption spectra of aromatic **CP-nR** (top) and quinoidal **nR-2N** (bottom) oligorylenes in 2Me-THF at room temperature.

Per-2N to **OR-2N**. The quinoidal systems present broader bands than the aromatic molecules (especially when comparing the two longest oligorylenes, **CP-OR** and **OR-2N**). Regarding the vibronic structures, except for **Per-2N**, the quinoidal series presents redshifted vibronic transitions with respect to the λ_{\max} wavelength.

In Table IV.1.1 theoretical TD-DFT electronic transitions at the (U)B3LYP/6-31G** level of theory are presented. Theoretical results nicely reproduce the experimental data. According to these calculations, λ_{\max} wavelengths of **CP-nR** and **nR-2N** series are assigned to $\pi \rightarrow \pi^*$ bands well described by the HOMO \rightarrow LUMO electron transition. For the shortest oligomers of the aromatic **CP-nR** series, the most intense component in the theoretical HOMO \rightarrow LUMO transition (473

Table IV.1.1. Optical data of aromatic CP-nR and quinoidal nR-2N oligorylenes families.

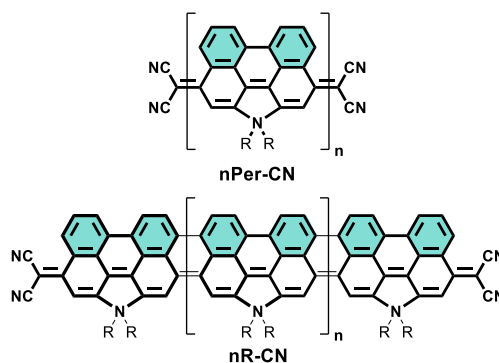
| n | CP-nR | | | nR-2N | | |
|------------------|--------------------------------------|--------------------------------|------------------------------------|--------------------------------------|--------------------------------|------------------------------------|
| | Experimental λ_{\max}^a (nm) | TD-DFT λ_{\max}^b (nm) | Electronic Transition ^b | Experimental λ_{\max}^a (nm) | TD-DFT λ_{\max}^b (nm) | Electronic Transition ^b |
| Per ^c | 443 | 473 | HOMO→LUMO | 420 | 419 | H-2→L |
| | 471 | | | 444 | 532 | HOMO→LUMO |
| QR ^c | 591 | 726 | HOMO→LUMO | 612 | 541 | H-1→L / H→L+1 |
| | 644 | | | 660 | 682 | HOMO→LUMO |
| | 707 | | | 762 | (887) | |
| HR ^d | 747 | 945 | HOMO→LUMO | 668 | 538 | H-1→L+1 |
| | 817 | | | 612 | 598 | H-1→L / H→L+1 |
| | 894 | | | 731 | 817 | HOMO→LUMO |
| | (1007) | | | 796 | | |
| OR ^d | 895 | 922 | H-1→L / H→L+1 | 806 | 654 | H→L+2 |
| | 983 | | | 665 | H-1→L / H→L+1 | |
| | 1060 | 1167 | HOMO→LUMO | 880 | 926 | HOMO→LUMO |
| | (1274) | | | 1092 | | |

^aMeasured in 2Me-THF. ^bTD-DFT calculations at (U)B3LYP/6-31G** level of theory ($f>0.1$). ^cGeometry optimization was performed as closed-shell system (spin restricted B3LYP). ^dGeometry optimization was performed as singlet open-shell system (spin unrestricted B3LYP).

nm and 726 nm, for **CP-Per** and **CP-QR**, respectively), while for **CP-HR** and **CP-OR**, it corresponds to the lowest energy peak (945 nm and 1167 nm, respectively). For quinoidal oligorylenes, the most intense experimental band is attributed to the HOMO→LUMO transition in any case.

The vibronic structure evolution in these families resembles that of the tetracyanorylene molecules (**nPer-CN** and **nR-CN**; see the chemical structures in Scheme IV.1.2), which also present vibronic transitions at higher wavelengths than λ_{\max} for the longest molecules.^[3, 4] For these families, while **Per-CN** and **QR-CN** display quinoidal closed-shell ground states and, hence, their electronic absorption spectra are consistent with these structures; the longer oligomers **2Per-CN**, **3Per-CN**, **4Per-CN** and **HR-CN** are characterized as singlet open-shell molecules. This change in the ground

electronic state is in agreement with the changes observed in the optical transitions, and accounts for the inversion in the intensities ratio in singlet open-shell **nR-2N**. Therefore, comparing these results with those of the two families under study



Scheme IV.1.2. Chemical structures of tetracyanorylenes series from references [3, 4]. Observe that the main difference between the two families is the rigidification of the rylene backbone in **nR-CN**. For **nPer-CN**: **1Per-CN** ($n=1$), **2Per-CN** ($n=2$), **3Per-CN** ($n=3$), **4Per-CN** ($n=4$), **5Per-CN** ($n=5$) and **6Per-CN** ($n=6$). For **nR-CN**: **QR-CN** ($n=0$) and **HR-CN** ($n=1$).

in this chapter, a similar closed-shell to singlet open-shell evolution can explain the optical spectra.

In addition, **HR-CN** oligomer presents a weak absorption band in the NIR region,^[4] similar to those found for **HR-2N** and **OR-2N** (Figure IV.1.1, bottom panel). This absorption is assigned to a HOMO→LUMO double excitation (hereinafter referred as H,H→L,L excitation) in systems with a low-lying excited singlet state, typical of singlet open-shell configurations.^[5-7] By this way, the low-energy feature of both **HR-2N** and **OR-2N** (796 nm and 1092 nm, respectively) is assigned to a H,H→L,L excitation, which takes place because of the singlet open-shell ground state of these molecules. Consequently, the UV-Vis-NIR electronic absorption spectra constitute the first evidence of the relevant contribution of diradical structures to the ground state in the longest quinoidal oligorylenes.

In the aromatic series also a low-energy NIR feature is observed for **CP-HR** and **CP-OR**. Nevertheless, some differences with respect to the quinoidal counterparts can be highlighted. For **CP-HR** and **CP-OR** the most intense band is not the lowest-energy transition. This different optical behaviour reveals that the electronic structures of these molecules must also differ. As indicated above, the lowest-energy component is assigned to the HOMO→LUMO electron transition by TD-DFT calculations, despite it is not the most intense feature.

The complexity of these electronic absorption spectra can be related to the contribution of a thermally populated triplet state due to the open-shell

character of longer oligorylenes.^[8] In order to obtain electronic absorption spectra of pure singlet species, variable temperature experiments were performed. Figure IV.1.2 displays the electronic absorption spectra of both aromatic and quinoidal oligorylenes families recorded at different temperatures.

The shortest oligomers of both series (**CP-Per**, **CP-QR** and **Per-2N**) present a similar behaviour upon cooling: a progressive red-shift and intensification of the optical bands, and enhanced vibrational resolution. The fused structures of these oligorylenes families avoid any rotational freedom and, hence, the redshift of the electronic transitions can be almost exclusively ascribed to the smaller vibrational amplitudes caused by the lower thermal energy. Indeed, any temperature lowering increases the population of the lower energy normal modes. As a consequence, and assuming that this effect involves all the vibrational levels, it will affect especially to the torsion modes of the aromatic systems since they have the lower vibrational energies. On the other hand, torsion modes are out-of-plane skeletal vibrations that noticeably broke the p_z overlapping within the aromatic rings. They have therefore a relevant role in understanding the redshift of the HOMO-LUMO transition upon cooling. In the case of the longer oligomers, different behaviours were found for the two families.

For aromatic oligorylenes, λ_{\max} wavelengths of electronic absorption spectra at 80K coincide with the less energy bands: 476 nm → 720 nm → 902 nm → 1067 nm, from **CP-Per** to **CP-OR**,

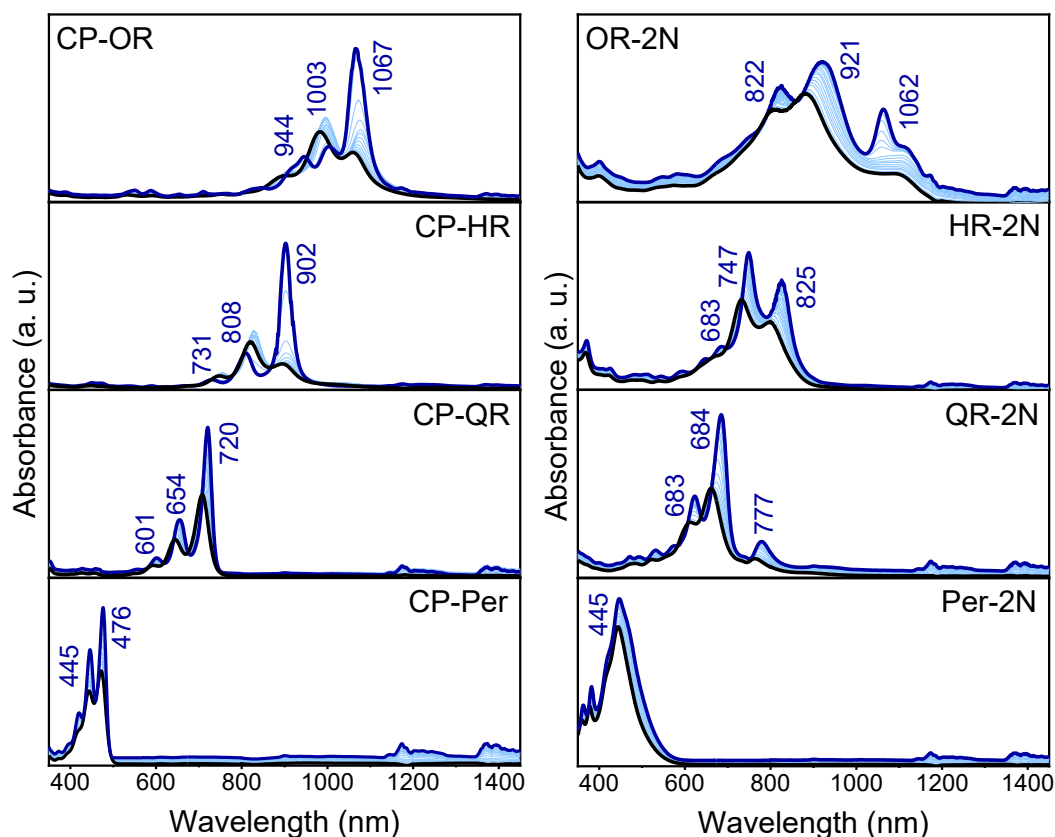


Figure IV.1.2. Variable temperature electronic absorption spectra of aromatic **CP-nR** (left) and quinoidal **nR-2N** (right) oligorylenes in 2Me-THF from room temperature (black lines) to 80 K (dark blue lines). Light blue lines correspond to absorption spectra at intermediate temperatures.

assigned to the HOMO→LUMO electron transition.

In the case of the quinoidal oligorylenes, λ_{max} wavelength at 80 K evolves: 445 nm → 684 nm → 747 nm → 921 nm, from **Per-2N** to **OR-2N**, and the H,H→L,L excitation band is also detected in longer molecules.

The evolution of λ_{max} wavelengths when enlarging the oligomer length in linearly π -conjugated systems can be studied through the Meier's equations: [9-11]

$$E(n) = E_{\infty} + (E_1 - E_{\infty})e^{-a(n-1)}$$

Eq. IV.1.1

$$\lambda(n) = \lambda_{\infty} + (\lambda_1 - \lambda_{\infty})e^{-b(n-1)}$$

Eq. IV.1.2

Equation IV.1.1 corresponds to the Meier's expression in terms of energy, while equation IV.1.2 is expressed in terms of wavelength. These equations relate the number of monomeric units (n) with the transition energy or wavelength of the infinite chain (E_{∞} and λ_{∞} , respectively). E_1 and λ_1 correspond to the data of the first oligomer of the series, and parameters a and b indicate how fast the limit of convergence is reached. [9, 10] By fitting the experimental optical data to these exponential equations, the values of E_{∞} , λ_{∞}

and n can be obtained. The minimum number of monomeric units (n) at which the limit of convergence is reached is called *effective conjugation length* (n_{ECL}). In other words, the n_{ECL} is defined as the oligomer length at which the wavelength of the absorption maxima is equal or less than 1 nm larger than that of the previous oligomer.^[9, 10, 12] In this context, all the properties derived from the π -electron delocalization can be considered unaltered for any oligomer with $n \geq n_{\text{ECL}}$.

Figure IV.1.3 displays the Meier's fitting of λ_{max} wavelengths of both oligorylenes families according to equation IV.1.2. In Table IV.1.2 the fitting parameters, including n_{ECL} and λ_{∞} wavelengths, are indicated. The values of n_{ECL} and λ_{∞} strongly differ between both oligorylenes families, despite their similar chemical structures. The aromatic **CP-nR** series presents larger values than those of the quinoidal family: $n_{\text{ECL}}=45$ and $n_{\text{ECL}}=28$ for **CP-nR** and **nR-2N**, respectively. The high effective conjugation length of **nR-2N** oligorylenes is explained by the synergistic effect of the quinoidal shape together with the planar structure^[13] afforded by the covalent bridging of the perylene moieties. However, the aromatic series presents a larger n_{ECL} value than **nR-2N** molecules. Consequently, in addition to the planarity of the rylene backbone, another factor that reduces the aromaticity of the benzene rings and favours the π -electron delocalization through the carbon-based skeleton must come into play.

The optical behaviour observed for both oligorylene families can be explained considering their diradical properties. Regarding the quinoidal **nR-2N** series,

when enlarging the oligomer length, the diradical character is increased. The driving force for this transformation is of enthalpic nature: the gain of aromatic stabilization energy. Consequently, the extension of the π -electron density in shorter, closed-shell **nR-2N** molecules is reduced when increasing the contribution of the aromatic diradical structure. Then, saturation of the Meier's fitting is reached faster as the number of monomeric units is increased.

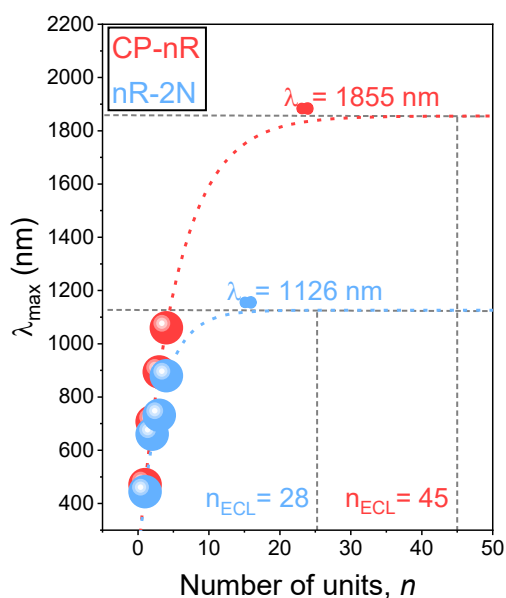


Figure IV.1.3. Meier's plot fitting of aromatic **CP-nR** (red circles) and quinoidal **nR-2N** (blue circles) oligorylenes, together with their effective conjugation length (n_{ECL}) and their corresponding absorption maximum of the infinite chain (λ_{∞}).

Table IV.1.2. Meier's plot fitting parameters for **CP-nR** and **nR-2N** oligorylenes series.

| | CP-nR | nR-2N |
|--------------------|---------|---------|
| λ_{∞} | 1855 nm | 1126 nm |
| n_{ECL} | 45 | 28 |
| b | 0.1842 | 0.3206 |
| R^2 | 0.9998 | 0.9763 |

On the other hand, aromatic **CP-nR** display the opposite behaviour: as the

diradical character rises when enlarging the oligomer size, the contribution of the quinoidal structure is larger. Now, the driving force for the stabilization of the open-shell configuration is not an enthalpic phenomenon. In these cases, the origin of the diradical character is a small HOMO-LUMO gap. The progressive narrowing of the optical band gap implies a decrease in the singlet-triplet gap (ΔE_{S-T}). In this scenario, the entropy must be considered, and this term is larger for the triplet configuration than for the singlet one (higher number of states). Therefore, the population of the triplet state in the open-shell structure in longer **CP-nR** molecules is entropically favoured.^[14]

Returning to the Meier's fitting, for the aromatic **CP-nR**, as the oligorylene is enlarged, the aromatic character is decreased, and the π -electron density is more spread over the carbon-based backbone. In other words, as the diradical contribution increases the effective conjugation is also larger, explaining the higher n_{ECL} of **CP-nR** than that of the quinoidal **nR-2N** systems.

Considering the λ_{max} wavelengths discussion, the contribution of the diradical form to the ground electronic states can be evaluated through the singlet-triplet gap (ΔE_{S-T}). In Figure IV.1.4 the energy differences between the optimized geometries as closed-shell and singlet and triplet open-shell configurations calculated at the (U)B3LYP/6-31G** level of theory are shown.

In agreement with the optical behaviour observed through UV-Vis-NIR

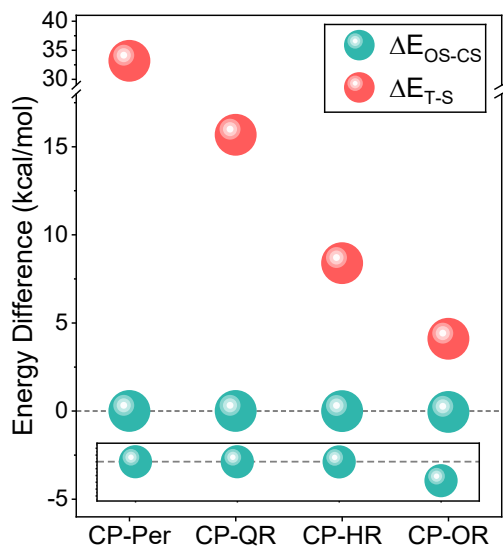


Figure IV.1.4. Formation energy differences (kcal/mol) between the singlet open-shell (OS) and the closed-shell (CS) configurations (green circles) and the triplet state respect to the corresponding ground state (red circles) of aromatic **CP-nR** oligorylenes calculated at the (U)B3LYP/6-31G** level of theory. The singlet-triplet gap was calculated taking **CP-Per** and **CP-QR** as closed shell systems, and **CP-HR** and **CP-OR** with singlet open-shell ground state.

electronic absorption, the shortest molecules of the aromatic family, **CP-Per** and **CP-QR**, display a closed-shell configuration of the ground electronic state, while the longer ones, **CP-HR** and **CP-OR**, are singlet open-shell systems. Accordingly, ΔE_{S-T} is progressively narrowed as the diradical contribution to the ground electronic state increases. The open-shell character of the longer **CP-nR** supports the discussion of the Meier's fitting and the higher n_{ECL} of this family respect to the quinoidal one. However, the ground state does not present in any case a triplet configuration, which is actually the case of **5Per-CN** and **6Per-CN**.^[3] The triplet ground electronic state in the oligorylenes families studied in the present chapter is

avoided through the planarization of the rylene backbone by the fusion of the perylene units. This molecular structure allows the chemical connection between the radical centres, providing the singlet character.

In the case of the quinoidal **nR-2N**, the formation energies of the three possible configurations of the ground electronic states were also calculated. However, despite the evident diradical contribution observed through the optical experiments for **HR-2N** and **OR-2N** molecules, no energy differences between the closed and singlet open-shell forms were found. The thermally-accessible triplet state in **HR-2N** and **OR-2N** oligorylenes and, hence, the considerable contribution of a diradical form to the ground electronic state, was experimentally demonstrated by Electron Paramagnetic Resonance. EPR measurements were performed by the group of Professor Jishan Wu and the obtained spectra are presented in Appendix VII.V.

A. II. Energy of the Frontier Molecular Orbitals

Since the HOMO and LUMO levels in π -conjugated molecules are of π -nature and the HOMO \rightarrow LUMO electron transition largely describes the absorption maxima band, the energy of these frontier molecular orbitals (FMO) in π -systems is very influenced by the electronic structure.

Figure IV.1.5 presents the FMO energies calculated at the (U)B3LYP/6-31G** level of theory for both oligorylenes

families.

The evolution of the energies of the FMO and, hence, that of the optical bandgap (E_g), can be explained by three main structural factors:^[12, 15, 16]

1. The aromaticity or resonance stabilization energy. In aromatic molecules, the π -electrons confinement within the rings results in a gain of a stabilization energy, the aromatic or resonance energy. As the contribution of the quinoidal form to the chemical structure increases, HOMO/LUMO levels are destabilized/stabilized, respectively, narrowing the optical bandgap.

However, this is not the case of the studied oligorylenes families, in which the aromatic oligomers display shorter E_g values than their quinoidal counterparts (except in the case of the smallest molecule of the series). This fact can be explained with the increasing diradical character when lengthening the oligorylene size for both families. For **CP-nR** the aromatic structure is kept along the series and, hence, a continuous diminution of the optical bandgap as a consequence of the increasing effective conjugation length is observed. Conversely, **nR-2N** molecules adopt a more aromatic pattern as the open-shell contribution increases. From this point, the HOMO-LUMO gap reduction due to the quinoidal structure does not prevail, and E_g increases as a consequence of the contribution of the aromatic form.

2. The planarity or rigidity of the system. Both **CP-nR** and **nR-2N** oligorylenes present a completely planar carbon-based backbone with an in-plane bending angle between the molecule centre and the end-

capped positions. The covalent bridge between perylene units assures the oligomers rigidity, in contrast with the non-planar **nPer-CN** series (see Scheme IV.1.2). On the other hand, the sp^3 carbon bridging the two naphthalene moieties in each perylene unit provokes the bending of the rylene skeleton. The strain induced by the cyclopenta ring-fused perylene moieties can be diminished through the decrease of the bond length alternation (BLA) pattern. Therefore, the aromaticity of the benzene rings in **CP-nR** family is also reduced by this structural factor, contributing to reduce their HOMO-LUMO gap together with the entropy gain.

For oligomers with more than one cyclopenta ring-fused perylene units, the E_g values are even shorter in the aromatic series than in the quinoidal one.

In Figure IV.1.6 the variation of the bending angle (θ) with the oligomer size is depicted for both oligorylenes families. The bending angle is defined as the angle between the central benzene ring and between the central benzene ring and the two end carbon atoms (see red arrows in Figure IV.1.6).^[17] In Table IV.1.3 the calculated bending angles are indicated together with those obtained through X-ray crystallographic analysis by the group of Professor Jishan Wu.^[17]

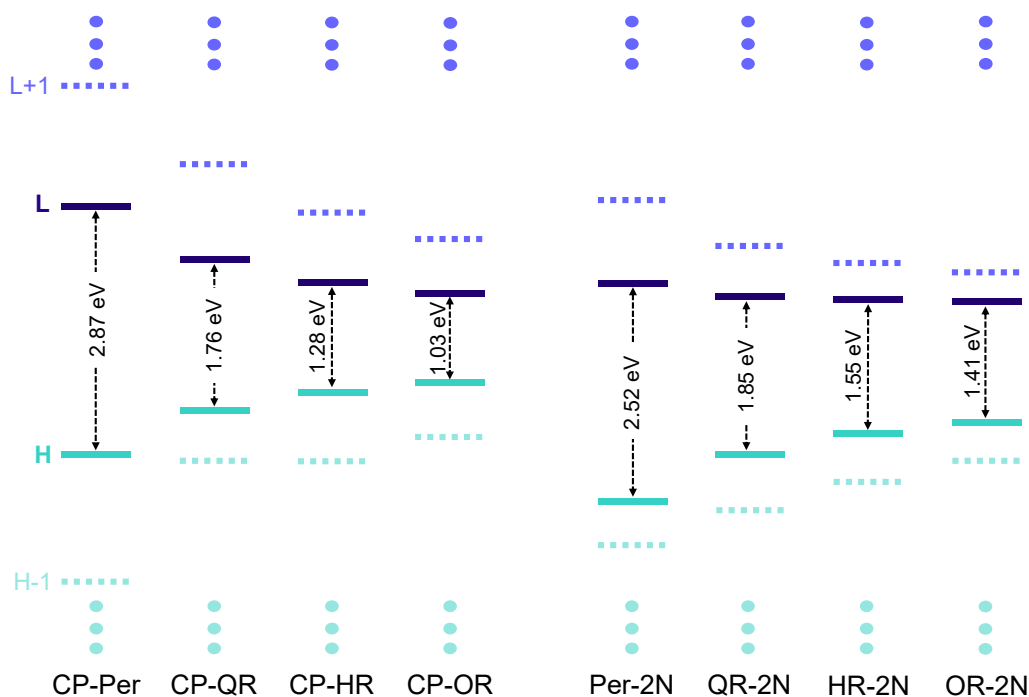


Figure IV.1.5. Energy level diagram of the frontier molecular orbitals of aromatic **CP-nR** (left) and quinoidal **nR-2N** (right) oligorylenes. **CP-Per**, **CP-QR**, **Per-2N** and **QR-2N** molecules were optimized as closed-systems while **CP-HR**, **CP-OR**, **HR-2N** and **OR-2N** were calculated with singlet open-shell configuration at the (U)B3LYP/6-31G** level of theory. Green lines correspond to the HOMOs; blue lines correspond to the LUMOs; dashed lines correspond to the HOMO-1 and LUMO+1 levels.

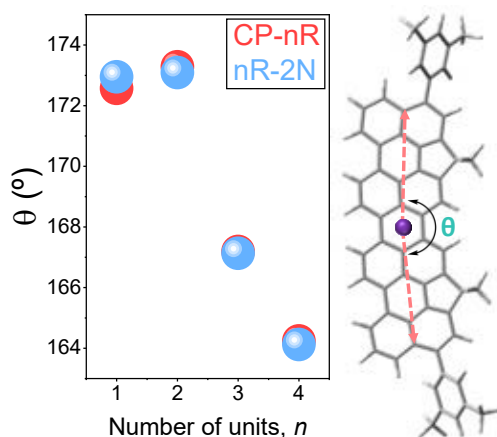


Figure IV.1.6. Bending angle evolution with the number of perylene units for **CP-nR** (red circles) and quinoidal **nR-2N** (blue circles) oligorylenes, together with an schematization of the bending angle in **CP-QR**.

Table IV.1.3. Bending angles values for **CP-nR** and **nR-2N** oligorylenes series.

| | CP-nR | | nR-2N | |
|------------------------|--------------------|-------------------|--------------------|-------------------|
| | Calc. ^b | Exp. ^a | Calc. ^b | Exp. ^a |
| Per^c | 172.57 | 173.26 | 172.95 | 174.09 |
| QR^c | 173.28 | 173.35 | 173.09 | 172.92 |
| HR^d | 167.19 | 167.73 | 167.13 | 166.48 |
| OR^d | 164.24 | — | 164.12 | — |

^aSingle crystal X-Ray analysis. ^bObtained from the optimized geometries at (U)B3LYP/6-31G** level of theory.

^cGeometry optimization was performed for closed-shell systems (spin restricted B3LYP). ^dGeometry optimization was performed for singlet open-shell systems (spin unrestricted B3LYP).

From the quarter-rylenes to the octa-rylenes oligomers of both series, the bending angles progressively diminishes and, hence, the backbone strain is increased. All θ values are shorter for the quinoidal oligorylenes than for the aromatic ones with the same length, except for **CP-Per** and **Per-2N**, which is also the trend found for the HOMO-LUMO gap. The larger diminution of the bending angle is found on going from the quarter-rylenes to the hexa-rylenes in both families. That

is, molecules which present a singlet open-shell ground state are those with the most strained structure.

3. The substituent groups. While aromatic **CP-nR** oligorylenes are end-capped with 3,5-di(*tert*-butyl)phenyl groups, the quinoidal forms in **nR-2N** are bearing (2,4,6-trichlorophenyl) imine groups. The larger electron-withdrawing character of the 2,4,6-trichlorophenyl groups respect to the 3,5-di(*tert*-butyl)phenyl moieties accounts for the LUMO stabilization in the quinoidal oligorylenes.

A. III. Topologies of the Frontier Molecular Orbitals

The delocalization of the π -electron density in linearly π -conjugated system can be analysed through the topologies of the FMO. In Figures IV.1.7 and IV.1.8 the HOMO and LUMO topologies of the optimized **CP-nR** and **nR-2N** structures, respectively, at the (U)B3LYP/6-31G** level of theory are displayed. In both series, the frontier molecular orbitals are spread over the rylene backbone. In

contrast, for the open shell systems, α and β SOMO electronic densities are placed in the molecule centre. This behaviour is more noticeable in the longest oligorylenes, **CP-OR** and **OR-2N**.

In the case of **CP-nR** molecules, the HOMO presents an aromatic shape, while in the LUMO the wavefunction is of quinoidal form. These structures are inverted in the **nR-2N** oligorylenes. However, in both series the frontier

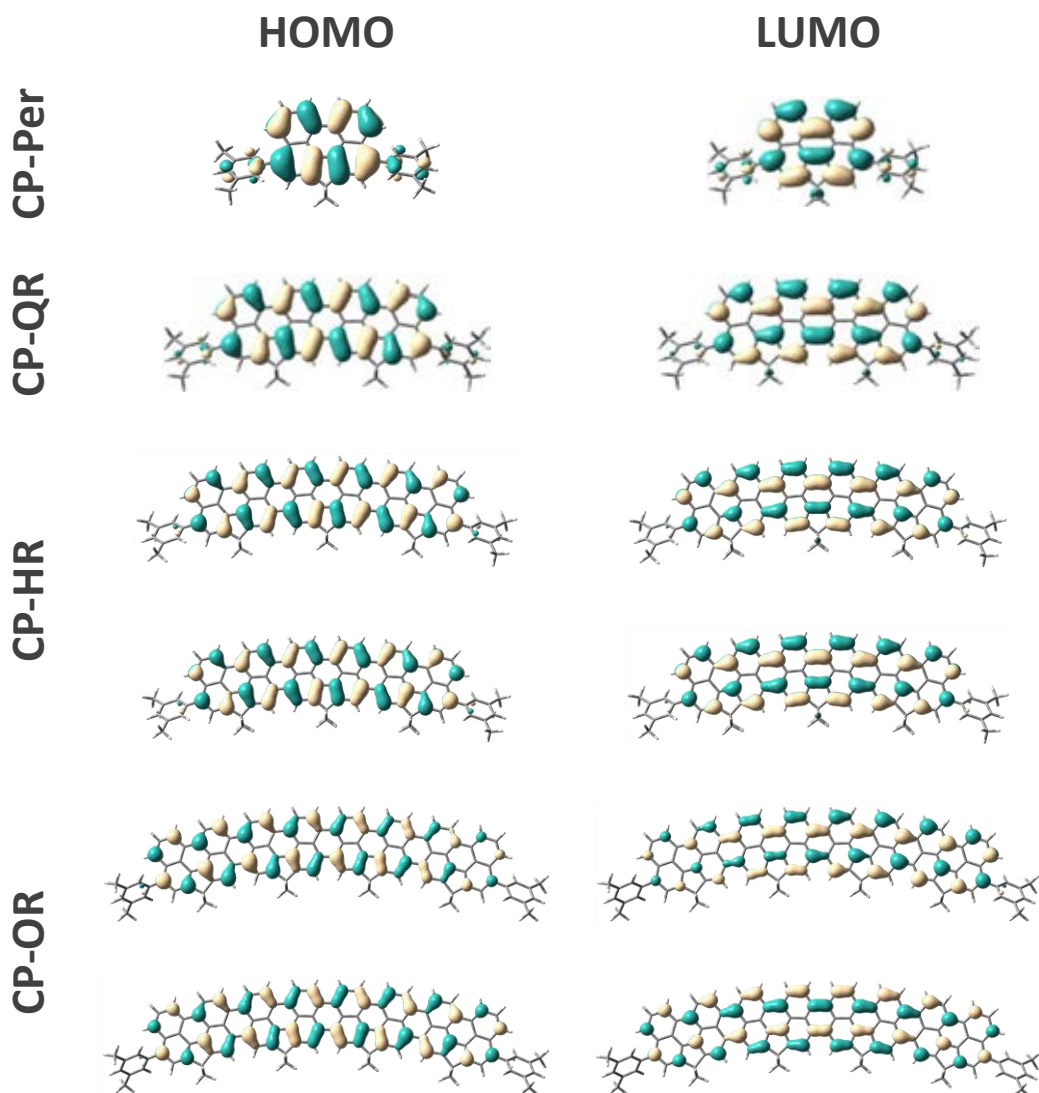


Figure IV.1.7. Topologies of the frontier molecular orbitals of aromatic **CP-nR** molecules calculated at the (U)B3LYP/6-31G** level of theory. **CP-Per** and **CP-QR** were calculated as closed-shell systems while **CP-HR** and **CP-OR** were optimized as singlet open-shell molecules (top: α -spins, and bottom: β -spins).

molecular orbitals are mainly located in the arm-chair edges, and in aromatic-like FMOs the π -electrons are not delocalized within the benzene rings.

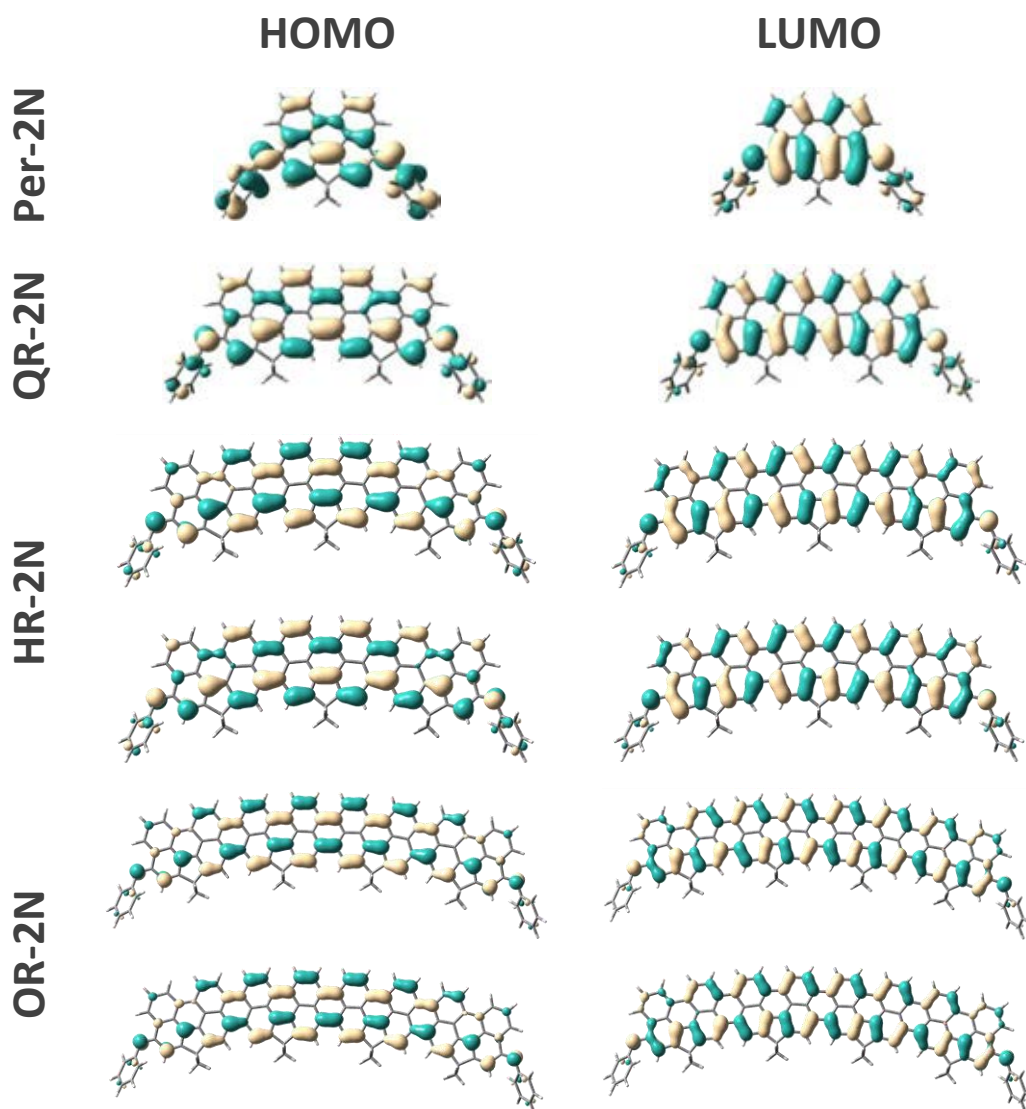


Figure IV.1.9. Topologies of the frontier molecular orbitals of quinoidal **nR-2N** molecules calculated at the (U)B3LYP/6-31G** level of theory. **Per-2N** and **QR-2N** were calculated as closed-shell systems while **HR-2N** and **OR-2N** were optimized as singlet open-shell molecules (top: α -spins, and bottom: β -spins).

B. Molecular Structure

B. I. Vibrational IR Spectroscopic Properties

For π -conjugated systems, vibrational IR spectroscopy is usually employed in the study of functional groups with large dipole moment that are included in the π -delocalization framework or are affected by it. In this context, terminal imino groups in quinoidal oligorylenes bring the possibility of performing an IR study. However, this is not the case of the aromatic **CP-nR**.

In Figure IV.1.9 vibrational IR spectra of **nR-2N** molecules in solid state at room

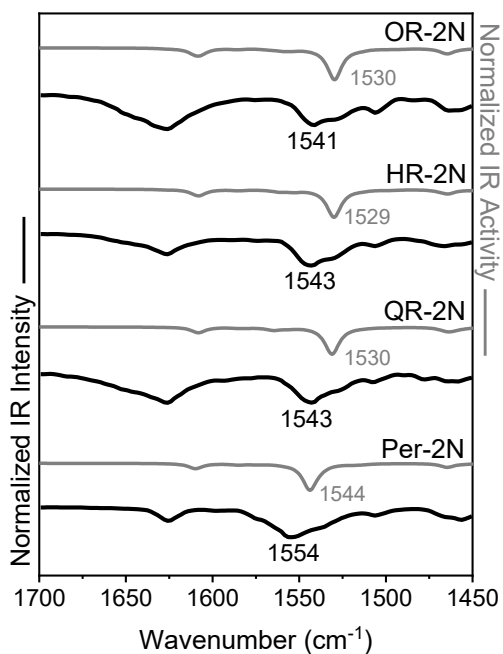
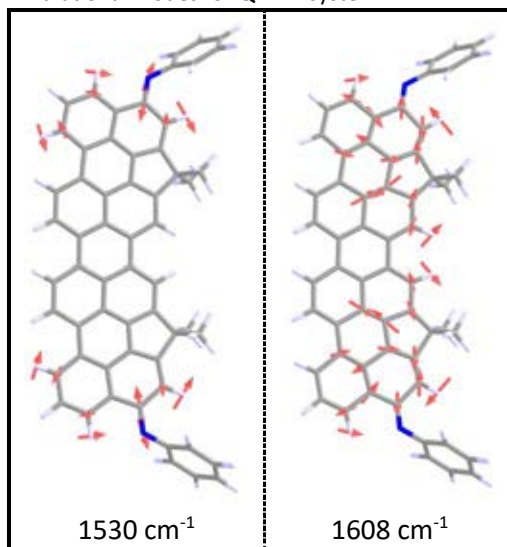


Figure IV.1.9. $\nu_{N=C}$ region of FT-IR spectra of **nR-2N** oligorylenes in solid state at room temperature. From bottom to top: **Per-2N**, **QR-2N**, **HR-2N** and **OR-2N**. Black lines correspond to the experimental IR spectra while grey lines correspond to the theoretical IR spectra calculated at the (U)B3LYP/6-31G** level of theory and scaled down uniformly by a factor of 0.96.

Table IV.1.4. Eigenvectors of the discussed IR vibrational modes for **QR-2N** system.



temperature are showed (black solid lines). Additionally, calculated spectra performed at the (U)B3LYP/6-31G** level of theory are also displayed (grey lines). Discussed eigenvectors corresponding to the imino vibrational mode are presented in Table IV.1.4 for **QR-2N** molecule as model of **nR-2N** series.

According to the experimental calculations, imino stretching vibration ($\nu_{N=C}$) of **nR-2N** molecules evolves: $1554\text{ cm}^{-1} \rightarrow 1543\text{ cm}^{-1} \rightarrow 1543\text{ cm}^{-1} \rightarrow 1541\text{ cm}^{-1}$ from **Per-2N** to **OR-2N**. Imino groups usually present their stretching vibration at $1630\text{--}1690\text{ cm}^{-1}$.^[18] The considerably lower wavenumber values of $\nu_{N=C}$ for the quinoidal oligorylenes are explained by the synergistic effect of the large effective conjugation length observed by electronic absorption and the bending angle of the chemical structure. On the other hand, the progressive decreasing of the bond length

alternation when enlarging the oligomer size is a direct consequence of the increasing diradical character, *i. e.*, the larger π -electron delocalization in open-shell structures is responsible of the $\nu_{N=C}$ shift to lower wavenumbers. As the BLA is reduced, N=C bond in the imino moiety becomes weaker, diminishing its stretching force constant and, consequently, the vibrational wavenumber. Observe that the most important change is experimented from **Per-2N** to **QR-2N** (11 cm^{-1}), while for the other molecules of the series the wavenumber shift is of only 2 cm^{-1} . As the number of cyclopenta ring-fused perylene units is increased, the π -electron delocalization is less spread towards the extremes of the molecule, thus the final imino groups are less affected by the enlargement of the oligomer.

B. II. Vibrational Raman Spectroscopic Properties

Raman spectroscopy is widely used in the study of π -conjugated systems due to the large activity of the collective C—C/C=C alternation pattern vibration of the carbon-based backbone.^[19] Since this Raman vibration is very sensitive to the bond length alternation pattern, its variation through the oligomeric series can be used to determine the extension of the π -electron delocalization.

In Figure IV.1.10 FT-Raman spectra of both oligorylene families in solid state at room temperature are presented, together with the corresponding

theoretical spectra. In both cases, the Raman spectra are dominated by two sets of bands: i) the more energy group, located at $1670\text{--}1500\text{ cm}^{-1}$ (highlighted in grey), correspond to the CC stretching vibration of the benzene rings (hereinafter referred as benzenoid bands, see the eigenvectors in Table IV.1.5); and ii) a more down-shifted bands, between $1331\text{ and }1070\text{ cm}^{-1}$ (highlighted in green), corresponding to a mixed CC skeletal stretching and CH deformation vibrations, that is, dominated by the vibrations of the arm-chair edge collective vibration and, for this reason, referred as polyacetylene-like bands. Observe that as the oligorylene size is enlarged, the polyacetylene-like bands increase their relative intensity respect to the benzenoid ones. These groups of signals resemble those of the graphene systems, the characteristic G and D bands, and has been also observed in other polycyclic aromatic hydrocarbons (PAHs) that can be described as nanographene systems.^[20]

As can be seen in Figure IV.1.10, left panel, the most intense feature of the benzenoid set in the aromatic **CP-nR** family evolves as follows: $1584\text{ cm}^{-1}\rightarrow 1528\text{ cm}^{-1}\rightarrow 1517\text{ cm}^{-1}\rightarrow 1510\text{ cm}^{-1}$, from **CP-Per** to **CP-OR**. The progressive down-shift of this collective vibration is ascribed to a gradual enlargement of the double C=C bonds and shortening of the single C—C bonds. In other words, to the larger extension of the π -electron delocalization when the number of perylene units is increased. The largest shift was found from **CP-Per** to **CP-QR** (56 cm^{-1}), as a consequence of the addition of the second perylene unit, while the two diradicaloid molecules, **CP-HR** and

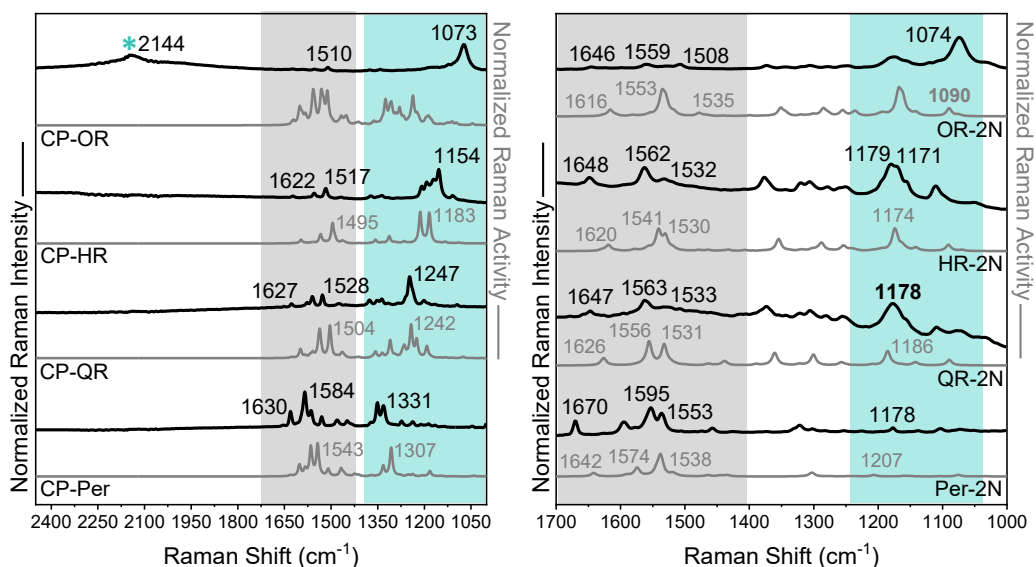


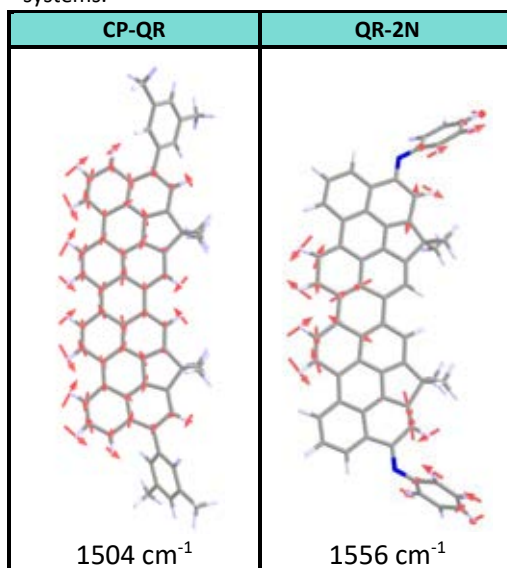
Figure VI.1.10. FT-Raman spectra of aromatic **CP-nR** (left) and quinoidal **nR-2N** (right) oligorylenes in solid state at room temperature. From bottom to top: **CP-Per** and **Per-2N**, **CP-QR** and **QR-2N**, **CP-HR** and **HR-2N** and **CP-OR** and **OR-2N**. Black lines correspond to the experimental Raman spectra while grey lines correspond to the theoretical Raman spectra calculated at the (U)B3LYP/6-31G** level of theory and scaled down uniformly by a factor of 0.96. Benzenoid CC stretching spectral region is highlighted in grey, while the polyacetylene-like region is highlighted in green.

CP-OR, only differ in 7 cm^{-1} . In the case of the polyacetylene-like bands, the same behaviour was observed along the aromatic oligorylene series: $1331\text{ cm}^{-1} \rightarrow 1247\text{ cm}^{-1} \rightarrow 1154\text{ cm}^{-1} \rightarrow 1073\text{ cm}^{-1}$, from **CP-Per** to **CP-OR**. As the oligomer length is increased, the weight of the polyacetylene-like bands rises in a way that, while for **CP-Per** the benzenoid bands dominate the spectrum, in **CP-OR** constitute the most intense vibration. This change in the dominant vibrational mode in the Raman spectra coincides with the transformation of the ground electronic state from closed-shell to singlet open-shell.

The difference between the Raman spectra of **CP-OR** molecule and the rest of the aromatic oligorylenes is not only evidenced by the dominance of the

polyacetylene-like feature at 1073 cm^{-1} , but also for the emerging of a new band at 2144 cm^{-1} , only observed for this molecule

Table IV.1.5. Eigenvectors of the discussed benzenoid vibrational modes for quarter-rylene systems.



(indicated with an asterisk in Figure IV.1.10). This Raman band is located at almost twice the value of the polyacetylene-like one ($2 \times 1073 \text{ cm}^{-1} = 2146 \text{ cm}^{-1}$) and is assigned to an overtone of the fundamental vibrational Raman band. Overtones arise from the promotion from the lowest vibrational state ($v=0$) to excited vibrational states different from the first one ($v=2, 3\dots$). Since transitions with $\Delta v > 1$ are theoretically forbidden in Raman spectroscopy, overtones can be detected as weaker bands only in special circumstances.^[21] However, overtones have been already observed in nanographene-like PAHs by M. Tommasini *et al.*^[22]

The three-band pattern of the Raman spectrum of **CP-OR** is similar to that found for neutral polyacetylene (PA).^[23-25] PA presents two intense Raman bands around 1100 and 1500 cm^{-1} (1073 and 1510 cm^{-1} in **CP-OR**) and a weak feature at 2100-2200 cm^{-1} corresponding to the overtone of the less energy vibration (2144 cm^{-1} for **CP-OR**). Oligoene molecules also display this PA-like behaviour, with Raman vibrations at 1600 and 1200 cm^{-1} .^[25] The down-shift of these bands with the extension of the π -electron delocalization is explained by the relaxation of the bond length alternation pattern, which is the same phenomenon that governs the PA Raman behaviour. In PA, the two Raman bands present lower values than those of the oligoene systems and correspond to two different domains with noticeable BLA. These molecular domains, which present inverse C—C/C=C patterns, are confined between soliton defects, thus a radicaloid structure is obtained.^[26, 27] In this scenario, Raman

spectrum of aromatic **CP-OR** molecule is closer to the PA pattern, with large π -electron delocalization and contribution of the diradical structure, than to the benzenoid pattern of the shortest **CP-nR** oligomers.

In the case of the quinoidal oligorylenes, also two sets of Raman bands are distinguished, corresponding to the benzenoid and the polyacetylene-like modes. As in the case of the aromatic molecules, the more energy bands vanish with the number of perylene units, while the arm-chair edge features are the predominant domain in the longest **OR-2N** molecule. The most intense band of the benzenoid-like vibrations evolves as follows: 1595 $\text{cm}^{-1} \rightarrow 1563 \text{ cm}^{-1} \rightarrow 1562 \text{ cm}^{-1} \rightarrow 1559 \text{ cm}^{-1}$, from **Per-2N** to **OR-2N**. This trend agrees with the extension of the effective conjugation length found by electronic absorption spectroscopy, also followed by the aromatic molecules. This down-shift is likewise found for the polyacetylene-like features: 1178 $\text{cm}^{-1} \rightarrow 1178 \text{ cm}^{-1} \rightarrow 1179/1171 \text{ cm}^{-1} \rightarrow 1074 \text{ cm}^{-1}$, from **Per-2N** to **OR-2N**. The largest shift found from **HR-2N** to **OR-2N**, together with the similar spectrum shape of **OR-2N** to that of the aromatic **CP-OR**, suggest that the Raman activity of the longest **OR-2N** is governed by the arm-chair edge. The rest of the molecules of the quinoidal series present a benzenoid behaviour. However, different from **CP-OR**, **OR-2N** does not display the overtone of the fundamental vibrational Raman band.

In addition, in quinoidal **nR-2N** oligorylenes a new Raman feature corresponding to the C=N stretching vibration of the imino group ($\nu_{N=C}$)

emerges. From **Per-2N** to **OR-2N**, $\nu_{N=C}$ is progressively down-shifted, as it was already observed by vibrational IR spectroscopy: $1553\text{ cm}^{-1} \rightarrow 1533\text{ cm}^{-1} \rightarrow 1532\text{ cm}^{-1} \rightarrow 1508\text{ cm}^{-1}$. The continuous shortening of the $\nu_{N=C}$ wavenumber is another evidence of the BLA diminution with the oligorylene length towards the diradical structure.

The variation of the discussed Raman bands with the oligorylene length are represented in Figure IV.1.11. The linear fit was performed assigning the upper limit (100% of aromatic/quinoidal character) to the shortest oligomers (**CP-Per** and **Per-2N**) and the lower limit (BLA $\rightarrow 0$) value to the longest ones (**CP-OR** and **OR-2N**).

According to this fitting, while the benzenoid bands (empty circles) display a similar trend, with localized single and double CC bonds only for **CP-Per** and **Per-2N** molecules, polyacetylene-like features (fulfilled circles) evolve in a different way for each oligorylene series. In **CP-nR** family, this vibrational mode experiments a continuous down-shift along the series, thus the aromatic oligorylenes are progressively transformed from benzenoid to arm-chair edge-like behaviour.

However, in **nR-2N**, the change between the two regimes takes place drastically from the shorter oligomers to **OR-2N**. These different transition ways can be ascribed to the structural changes imposed by the contribution of the diradical form. In the aromatic series, both closed-shell and singlet open-shell configurations are of aromatic nature.

However, for **nR-2N** molecules, this transformation implies the

tautomerization from the quinoidal to the aromatic shape. This structural change explains the large wavenumber shift in the polyacetylene-like bands of **OR-2N** respect to the shorter oligomers. Regarding the benzenoid bands, also two well differentiated regimes are obtained, with not intermediate values.

In the case of the imino groups, $\nu_{N=C}$ down-shifts gradually with the enlargement of the oligorylene backbone (light blue triangles in Figure IV.1.11).

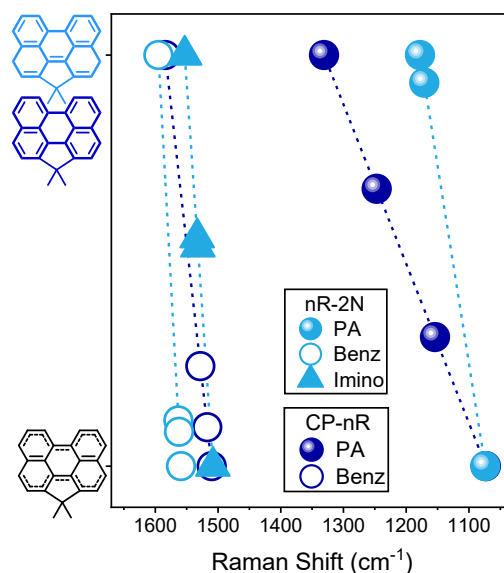


Figure IV.1.11. Linear fit of polyacetylene-like (fulfilled circles), benzenoid (empty circles) and imino (triangles) Raman bands of the aromatic **CP-nR** (dark blue) and quinoidal **nR-2N** (light blue) oligorylenes.

B. III. Bond Length Alternation (BLA) Analysis

Bond length alternation (or BLA) parameter is defined as the difference between the averaged lengths of the single

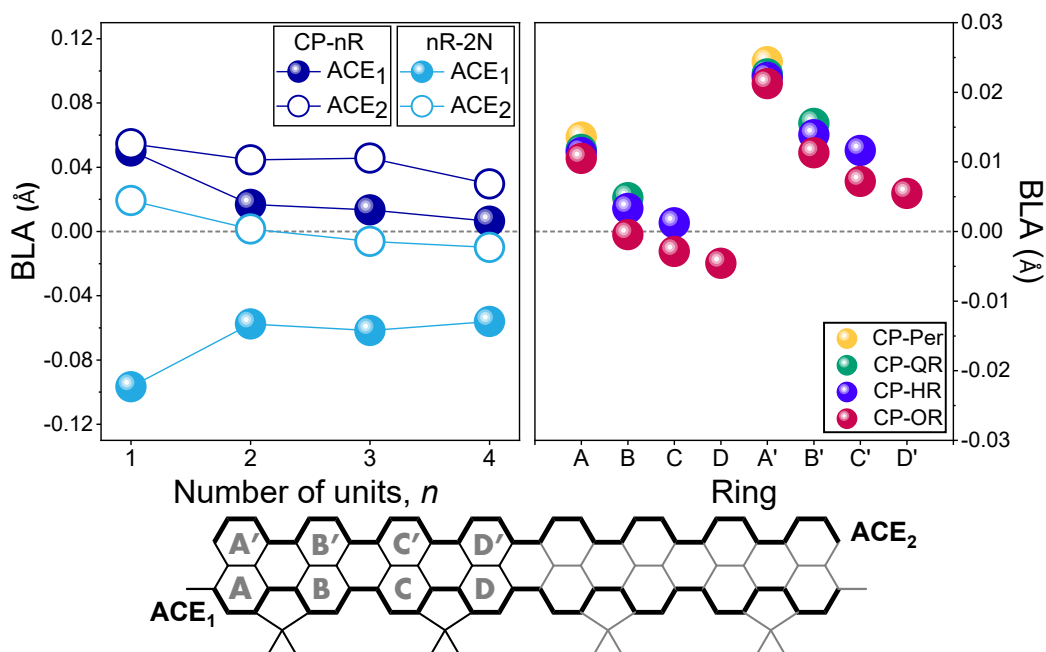


Figure IV.1.12. Bond length alternation (BLA) values (Å) in the arm-chair edges (ACE) for **CP-nR** and **nR-2N** series (*left*), and within the benzene rings of **CP-nR** oligorylenes (*right*) for the optimized molecular structures of oligorylene series calculated at the (U)B3LYP/6-31G**. **CP-Per**, **Per-2N**, **CP-QR** and **QR-2N** were optimized with a closed-shell configuration while longer oligorylenes were optimized as singlet open-shell systems.

and double bonds in a π -conjugated system.^[28, 29] Consequently, BLA is directly related to the extension of the effective conjugation length. BLA values closer to zero indicate larger π -electron delocalization.

In Figure IV.1.12 BLA values for the aromatic and quinoidal oligorylene families obtained from the optimized geometries are presented. This parameter was calculated for both arm-chair edges (denoted as ACE) of each molecule (Figure IV.1.12, left panel) and for the benzene rings for the **CP-nR** series (right panel).

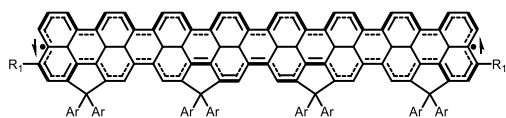
For the arm-chair edges, while values of **CP-nR** family are positive for the whole series, *i. e.*, the bond length alternation pattern is kept with the oligomer length, in the case of **nR-2N** molecules, ACE₂ changes

from positive to negative BLA values when increasing the number of perylene moieties. This behaviour implicates that the single CC bonds get double character, and the opposite for the double CC bonds. In the case of **CP-nR** oligorylenes, ACE₂ retains the positive value along the series, although the BLA slightly diminishes with the oligomer length. This reduction is accentuated in the arm-chair edge attached to the terminal groups (ACE₁) in a way that in **CP-Per** both polyacetylene-like edges have similar BLA values, while in **CP-OR** ACE₁ the single and double CC bond lengths are almost equalized (BLA \rightarrow 0).

In the case of the quinoidal oligorylenes, ACE₂ experiments a BLA diminution for the longer oligomers. In ACE₁ BLA values are also reduced along the series, but no change of sign is observed.

According to the electronic and vibrational spectroscopy studies, **HR-2N** and **OR-2N** present large diradical character, and the driving force that accounts for the closed to open-shell transformation is the aromatization of the quinoidal benzene rings. Therefore, ACE_1 BLA values of these molecules shift to the positive region. However, as it was explained in *Optical Properties* section, theoretical calculations at the (U)B3LYP/6-31G** level of theory were not able to reproduce properly this open-shell character.

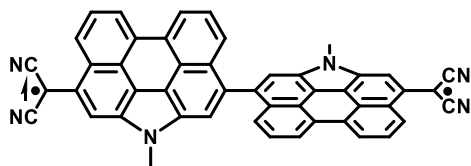
BLA values of the benzenoid rings (Figure IV.1.12, right panel) indicate that the larger π -electron delocalization in aromatic oligorylenes take place in the internal rings. For **CP-OR**, BLA is relaxed in rings B and C, while A and D present a more differentiated C=C/C—C pattern. This scenario suggests that the radical centres are delocalized in the zig-zag edges of **CP-OR** oligorylene, and two different aromatic and quinoidal domains are present in ACE_1 on going from ring A to D, respectively, according to Scheme IV.1.3.



Scheme IV.1.3. Chemical structure of the diradical form of **CP-OR** oligorylene. The larger aromatic or quinoidal shape of each benzenoid ring is indicated in bold.

The linear π -conjugation through the arm-chair edges provides the connection between the radical centres to account for the singlet character. The conjugation of both unpaired, opposite spins with the π -conjugated bridge (the oligorylene core) represents an extra stabilization of the

singlet open-shell configuration *versus* the triplet one (in which only one of the two radicals can conjugate with the bridge due to their parallel spin). This phenomenon is known as the *Double Spin Polarization* (DSP) mechanism and justifies the stabilization of the singlet state respect to the triplet one in Kekulé diradicals, violating the Hund's rule.^[27, 30, 31] Any interruption of the π -electron conjugation through the bridge avoids this stabilization and, hence, rises the energy of the singlet state. This is indeed the case of **nPer-CN** oligorylene series, in which the longest **5Per-CN** and **6Per-CN** present a triplet diradical ground state.^[3] For these molecules, the aromatization of the quinoidal non-fused oligorylene backbone allows the free rotation through the interperylene C—C bonds, interrupting the π -electron conjugation:



Scheme IV.1.4. Schematization of the interruption of the π -electron delocalization in long **nPer-CN** molecules through the rotation of the interperylene CC bond, explaining the triplet ground state.

However, the conformational interruption of the DSP mechanism is not the only way to destabilize the singlet open-shell state. In the next chapters of this thesis the affection of the DSP mechanism with the presence of alternative π -conjugated frameworks, competitive to the linear one, will be studied.

1.2 CONCLUSIONS

The study of **CP-nR** and **nR-2N** oligorylene series as models of linearly π -conjugated aromatic and quinoidal systems, respectively, brings the following conclusions:

- **CP-nR** and **nR-2N** oligorylenes have been studied through UV-Vis-NIR electronic absorption and spectra of both families present characteristic features of diradical species. In quinoidal **nR-2N** the singlet open-shell character is evidenced in the presence of a low-lying singlet excited state, giving rise to a double $H,H \rightarrow L,L$ electronic transition.
 - The driving force for the diradical formation when lengthening the oligorylene size in **nR-2N** is the aromatization of the quinoidal backbone. In the case of the aromatic **CP-nR**, the small HOMO-LUMO gap in longer molecules is responsible of their diradical character, and the population of the triplet state is driven by entropy gain. The behaviour of these diradical species explain the larger effective conjugation length of the aromatic oligorylenes respect to the quinoidal series.
 - The cyclopenta-fused perylene moieties, and these, in turn, covalently fused between them, impose a bending angle on the rigid oligorylene backbone. This angle is reduced with the enlargement of the oligorylene length. The bending angle diminishes the benzene ring aromaticity, and, together with the diradical character,
- explain the great extension of the effective conjugation length found for both families.
- The aromatization of **nR-2N** with the contribution of the open-shell species and the diradical character of longer aromatic **CP-nR** are traduced in similar HOMO-LUMO gaps.
 - Vibrational IR and Raman studies confirm the diradical character of the longest oligomers of both series. The progressive down-shift of the Raman bands when increasing the number of perylene units is representative of the larger linear π -electron delocalization, also supported by the calculated BLA values.
 - Interestingly, different Raman behaviour was observed for **CP-OR** and **OR-2N** and the other oligorylenes. While Raman spectra of shorter molecules present a clear benzenoid regime, those of **CP-OR** and **OR-2N** are governed by a polyacetylene-like behaviour. Consequently, π -electron delocalization mainly takes place through the benzenoid rings in shorter oligorylenes, while for the longest ones, it occurs through the arm-chair edges. This phenomenon is also manifested in the emerging of an overtone band in the Raman spectrum of **CP-OR**.
 - The obtained results suggest a large contribution of a diradical form to the chemical structure in longer oligorylenes of both families (**CP-HR**,

CP-OR, HR-2N and OR-2Nn). In **CP-nR**, these forms are characterized by the stabilization of the two radical centres in opposite zig-zag edges.

- The highly planar structure of these oligorylenes assures the activation of the DSP mechanism in the diradical molecules and, hence, their ground electronic states present a singlet open-shell configuration.

REFERENCES

- [1] *Pentarylene- and Hexarylenebis(dicarboximide)s: Near-Infrared-Absorbing Polyaromatic Dyes*, N. G. Pschirer, C. Kohl, F. Nolde, J. Qu and K. Müllen, *Angew. Chem. Int. Ed. Engl.*, **2006**, *45*, 1401–1404.
- [2] *The Rylene Colorant Family—Tailored Nanoemitters for Photonics Research and Applications* T. Weil, T. Vosch, J. Hofkens, K. Peneva and K. Müllen, *Angew. Chem. Int. Ed.*, **2010**, *49*, 9068–9093.
- [3] *Pushing Extended p-Quinodimethanes to the Limit: Stable Tetracyano-oligo(N-annulated perylene)quinodimethanes with Tunable Ground States*, Z. Zeng, M. Ishida, J. L. Zafra, X. Zhu, Y. Mo Sung, N. Bao, R. D. Webster, B. S. Lee, R-W. Li, W. Zeng, Y. Li, C. Chi,† J. T. Lopez Navarrete, J. Ding, J. Casado, D. Kim, and J. Wu, *J. Am. Chem. Soc.*, **2013**, *135*, 6363–6371.
- [4] *Tetracyanoquaterrylene and Tetracyanohexarylenequinodimethanes with Tunable Ground States and Strong Near-Infrared Absorption*, Z. Zeng, S. Lee, J. L. Zafra, M. Ishida, X. Zhu, Z. Sun, Y. Ni, R. D. Webster, R-W. Li, J. T. López Navarrete, C. Chi, J. Ding, J. Casado, D. Kim and J. Wu, *Angew. Chem. Int. Ed.*, **2013**, *52*, 8561–8565.
- [5] *Zethrenes, Extended p-Quinodimethanes, and Periacenes with a Singlet Biradical Ground State*, Z. Sun, Z. Zeng, and J. Wu, *Acc. Chem. Res.*, **2014**, *47*, 2582–2591.
- [6] *Pro-aromatic and Anti-aromatic π -Conjugated Molecules: An Irresistible Wish to Be Diradicals*, Z. Zeng, X. Shi, C. Chi, J. T. López Navarrete, J. Casado and J. Wu, *Chem. Soc. Rev.*, **2015**, *44*, 6578–6596.
- [7] *Biradicaloid and Polyenic Character of Quinoidal Oligothiophenes Revealed by the Presence of a Low-Lying Double-Exciton State*, S. Di Motta, F. Negri, D. Fazzi, C. Castiglioni, and E. Valeria Caneis, *J. Phys. Chem. Lett.*, **2010**, *1*, 3334–3339.
- [8] *Synthesis and Characterization of Quarteranthenes: Elucidating the Characteristics of the Edge State of Graphene Nanoribbons at the Molecular Level*, A. Konishi, Y. Hirao, K. Matsumoto, H. Kurata, R. Kishi, Y. Shigeta, M. Nakano, K. Tokunaga, K. Kamada and T. Kubo, *J. Am. Chem. Soc.*, **2013**, *135*, 1430–1437.
- [9] *Monodisperse Dialkoxy-Substituted Oligo(Phenyleneethynylene)s*, U. Stalmach, H. Kolshorn, I. Brehm and H. Meier, *Liebigs Ann.*, **1996**, *9*, 1449–1456.
- [10] *Effective Conjugation Length and UV/Vis Spectra of Oligomers*, H. Meier, U. Stalmach and H. Kolshorn, *Acta Polymer.*, **1997**, *48*, 379–384.
- [11] *Conjugation Oligomers with Terminal Donor-Acceptor Substitution*, H. Meier, *Angew. Chem. Int. Ed.*, **2005**, *44*, 2482–2506.
- [12] *Optical Bandgaps of π -Conjugated Organic Materials at the Polymer Limit: Experiment and Theory*, J. Gierschner, J. Cornil and H-J. Egelhaaf, *Adv. Mater.*, **2007**, *19*, 173–191.
- [13] *Multifaceted Regioregular Oligo(thieno[3,4-b]thiophene)s Enabled by Tunable Quinoidization and Reduced*

- Energy Band Gap, F. Liu, G. L. Espejo, S. Qiu, M. Moreno Oliva, J. Pina, J. S. Seixas de Melo, J. Casado, X. Zhu, *J. Am. Chem. Soc.*, **2015**, *137*, 10357–10366.
- [14] *The Energy Barrier in Singlet Fission Can Be Overcome Through Coherent Coupling and Entropic Gain*, W. Chan, M. Ligges and X. Zhu, *Nature Chem.*, **2012**, *4*, 840–845.
- [15] *Synthetic Principles for Bandgap Control in Linear π -Conjugated Systems*, J. Roncali, *Chem. Rev.*, **1997**, *97*, 173–205.
- [16] *Molecular Engineering of the Band Gap of π -Conjugated Systems: Facing Technological Applications*, J. Roncali, *Macromol. Rapid Commun.*, **2007**, *28*, 1761–1765.
- [17] *Rylene Ribbons with Unusual Diradical Character*, H. Saeki, W. Zeng, H. Phan, T. Seng Herng, T. Y. Gopalakrishna, N. Aratani, Z. Zeng, H. Yamada, J. Ding and J. Wu, *Chem*, **2017**, *2*, 81–92.
- [18] *General Outline for IR and Raman Spectral Interpretation*, P. J. Larkin in *Infrared and Raman Spectroscopy*, Elsevier Inc., Amsterdam: Netherlands, **2018**, 2nd ed., 135–151.
- [19] *Raman Spectroscopy of Polyconjugated Molecules and Materials: Confinement Effect in One and Two Dimensions*, C. Castiglioni, M. Tommasini and G. Zerbi, *Phil. Trans. R. Soc. Lond. A*, **2004**, *362*, 2425–2459.
- [20] *A Computational Study of the Raman Spectra of Large Polycyclic Aromatic Hydrocarbons: Toward Molecularly Defined Subunits of Graphite*, F. Negri, C. Castiglioni, M. Tommasini and G. Zerbi, *J. Phys. Chem. A*, **2002**, *106*, 3306–3317.
- [21] *Modern Raman Spectroscopy. A Practical Approach*, E. Smith and G. Dent, WILEY-VCH: Weinheim, **2005**.
- [22] *Overtone and Combination Features of G and D Peaks in Resonance Raman Spectroscopy of the C₇₈H₂₆ Polycyclic Aromatic Hydrocarbon*, A. Maghsoumi, L. Brambilla, C. Castiglioni, K. Müllen and M. Tommasini, *J. Raman Spectrosc.*, **2015**, *46*, 757–764.
- [23] *Raman Spectra of trans- and cis-Polyacetylenes Excited with Nd:Yag Laser 1064- and 532-nm Pulses*, M. Tasumi, H. Yoshida, M. Fujiwara, H. Hamaguchi and H. Shirakawa, *Synth. Met.*, **1987**, *17*, 319–324.
- [24] *Resonant Raman Scattering from cis and trans-Polyacetylene*, E. Mulazzi in *Electronic Properties of Polymers and Related Compounds*, Springer Series in Solid-State Sciences, vol 63, H. Kuzmany, M. Mehring and S. Roth, Eds.; Springer, Heidelberg:Berlin, **1985**.
- [25] *Conjugation Length Dependence of Raman Scattering in a Series of Linear Polyenes: Implications for Polyacetylene*, H. E. Schaffer, R. R. Chance, R. J. Silbey, K. Knoll and R. R. Schrock, *J. Chem. Phys.*, **1991**, *94*, 4161–4170.
- [26] *Polarons, Bipolarons and Solitons in Conducting Polimers*, J. L. Brédas and G. B. Street, *Acc. Chem. Res.*, **1985**, *18*, 309–315.
- [27] *Quinoidal/Aromatic Transformation in π -Conjugated Oligomers: Vibrational Raman Studies on the Limit of Rupture of π -Bonds*, P. Mayorga Burrezo, J. L. Zafra, J.

T. López Navarrete and J. Casado, *Angew. Chem. Int. Ed.*, **2017**, *56*, 2250–2259.

[28] *The Alternation of Bond Lengths in Long Conjugated Chain Molecules*, H. C. Longuet-Higgins and L. Salem, *Proc. R. Soc. Lond. A*, **1959**, *251*, 172–185.

[29] *Synthetic Principles for Bandgap Control in Linear π -Conjugated Systems*, J. Roncali, *Chem. Rev.*, **1997**, *97*, 173–205.

[30] *Pro-aromatic and Anti-aromatic π -Conjugated Molecules: An Irresistible Wish to Be Diradicals*, Z. Zeng, X. Shi, C. Chi, J. T. López Navarrete, J. Casado and J. Wu, *Chem. Soc. Rev.*, **2015**, *44*, 6578–6596.

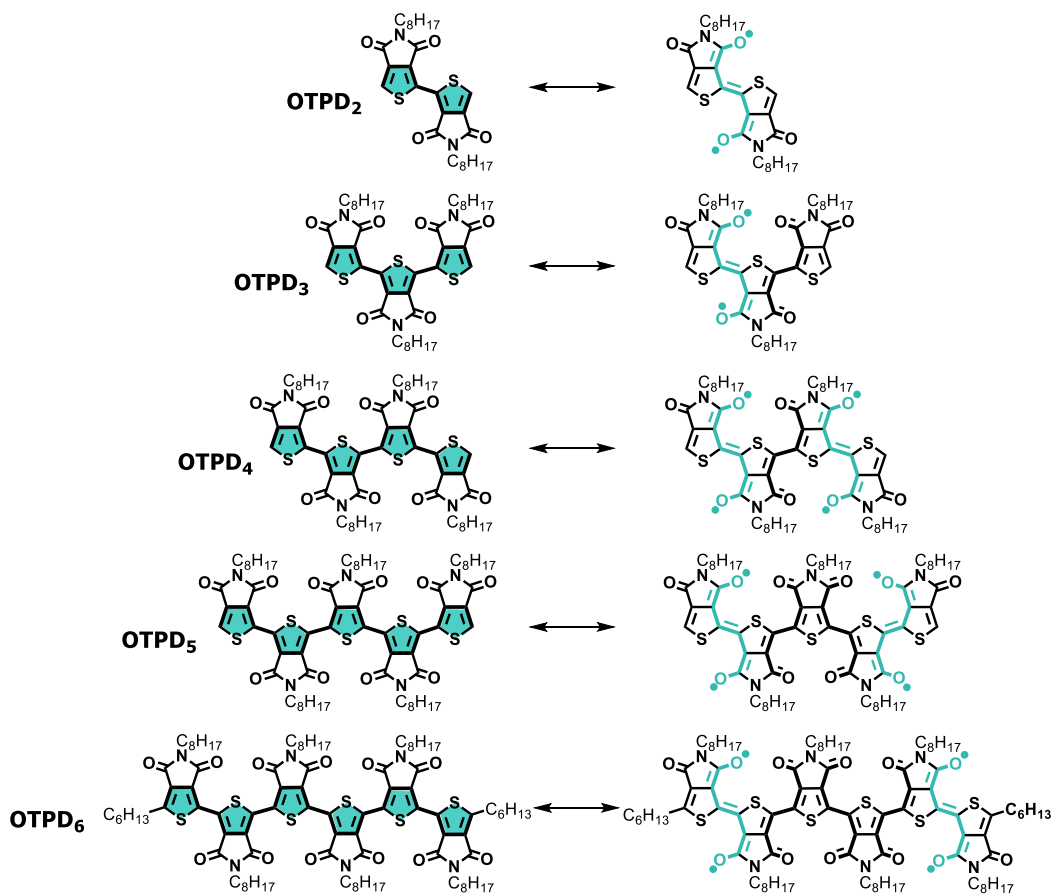
[31] *Para-Quinodimethanes: A Unified Review of the Quinoidal-Versus-Aromatic Competition and its Implications*, J. Casado, *Top Curr Chem (Z)*, **2017**, *375*, doi:10.1007/s41061-017-0163-2.

B. CROSS-CONJUGATED DIRADICALS



2. The case of Aromatic Oligothiopyrrolediones: Cross-Conjugated Dianions

| | |
|---|----------------|
| 2.1 Neutral Species of OTPD_n Oligomers..... | 103—115 |
| A. Electronic Structure..... | 103—109 |
| B. Molecular Structure..... | 110—115 |
| 2.2 Charged Species of OTPD_n Oligomers..... | 116—125 |
| A. Electronic Structure..... | 116—120 |
| B. Molecular Structure..... | 121—125 |
| 2.3 Conclusions..... | 126—127 |
| References..... | 128—130 |



Scheme IV.2.1. Resonant chemical structures of the molecules forming the OTPD_n series studied in this chapter. The two alternative, orthogonal π -conjugated paths are highlighted in bold.

2.1 NEUTRAL SPECIES OF OTPD_n OLIGOMERS

A. Electronic Structure

A. I. Optical Properties

Figure IV.2.1 shows the UV-Vis-NIR electronic absorption spectra of neutral OTPD_n molecules in CH₂Cl₂ at room temperature:

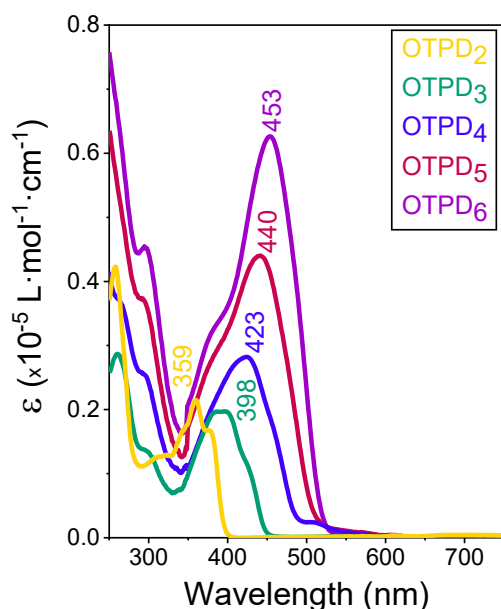


Figure IV.2.1. Electronic absorption spectra of OTPD_n molecules in CH₂Cl₂ at room temperature.

Regarding the absorption maxima (λ_{\max}), a progressive red-shift is observed upon increasing the number of TPD units: from OTPD₂ to OTPD₆, 359 nm \rightarrow 453 nm, respectively (see Table IV.2.1 for optical data). The intensity of the bands also increases with the oligomers length.

Table IV.2.1 shows the main electronic transitions calculated at the (U)B3LYP/6-31G** level of theory, which correctly correlate with the experimental data. The absorption maxima of π -conjugated organic molecules correspond to $\pi \rightarrow \pi^*$ bands assigned to the HOMO \rightarrow LUMO electron transition. This is indeed the case of the OTPD_n series. As a consequence of this assignment, the fact that λ_{\max} successively shifts to larger wavelengths (in consequence to lower energies) is traduced in a progressive narrowing of the HOMO-LUMO gap.

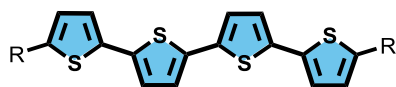
When comparing the transition energies of the target molecules with those of the non-substituted α -oligothiophenes (α -OT_n)^[2, 3] (see Scheme

Table IV.2.1. Optical data of OTPD_n and α -OT_n series.

| n | OTPD _n ^a | | | | | α -OT _n ^{[1] b} | |
|---|--------------------------------|---|--------------------------|-----------------------------------|-------------------------|--|---|
| | Experimental | | TD-DFT ^c | | | λ_{\max} (nm) | ϵ ($\times 10^{-5}$ L·mol ⁻¹ ·cm ⁻¹) |
| | λ_{\max} (nm) | ϵ ($\times 10^{-5}$ L·mol ⁻¹ ·cm ⁻¹) | λ_{\max} (nm) | Oscillator Strength (a. u.) | Electronic Transition | | |
| 2 | 359 (375) | 0.17 | 355 | 0.40 | HOMO \rightarrow LUMO | 303 | 0.12 |
| 3 | 385/398 | 0.20 | 415 | 0.56 | HOMO \rightarrow LUMO | 354 | 0.22 |
| 4 | 423 | 0.29 | 452 | 0.84 | HOMO \rightarrow LUMO | 391 | 0.32 |
| 5 | 440 | 0.46 | 482 | 1.30 | HOMO \rightarrow LUMO | 417 | 0.43 |
| 6 | 453 | 0.64 | 508 | 1.47 | HOMO \rightarrow LUMO | 436 | 0.48 |

^a Measured in CH₂Cl₂. ^b Measured in dioxane. ^c TD-DFT calculations at (U)B3LYP/6-31G** level of theory ($f > 0.1$).

IV.2.2 for chemical structures), in both cases the λ_{\max} wavelength increases with the oligomers size.



Scheme IV.2.2. Chemical structures of $\alpha\text{-OT}_4$ molecule, belonging to the $\alpha\text{-OT}_n$ family used as reference of linear conjugation.

However, for the same number of units, the λ_{\max} wavelengths of $\alpha\text{-OT}_n$ are blue-shifted compared to those of the OTPD_n molecules (see Table IV.2.1).

Hence, the effect of the oligomer length on the absorption maxima can be explored by means of the Meier's equations: [3-5]

$$E(n) = E_{\infty} + (E_1 - E_{\infty})e^{-a(n-1)}$$

IV.2.1

$$\lambda(n) = \lambda_{\infty} + (\lambda_1 - \lambda_{\infty})e^{-b(n-1)}$$

IV.2.2

In Figure IV.2.2 and Table IV.2.2 absorption maxima wavelengths of OTPD_n and $\alpha\text{-OT}_n$ series are represented versus the number of units (n).

Despite the structural differences, Meier's behaviour of the target series is close to that of the unsubstituted oligothiophenes, $\alpha\text{-OT}_n$. However, although λ_{∞} are similar for both series, n_{ECL} of $\alpha\text{-OT}_n$ family is 18 units while for OTPD_n is only 14. In consequence, the effective π -electron conjugation is shorter in this family. This fact is related with the presence of the inter-dione cross-conjugated frameworks, that tend to confine the π -electron density in the centre of the molecule. However, the rotational freedom between the thiophene rings in $\alpha\text{-OT}_n$ molecules also

plays a crucial role in the π -overlapping of the frontier molecular orbitals. The β , β' -disubstitution in OTPD_n diminishes this conformational freedom between monomeric units.

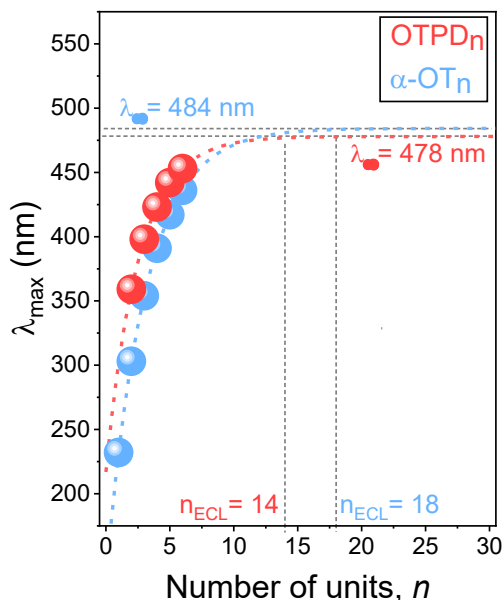


Figure IV.2.2. Meier's plot fitting of OTPD_n (red circles) and $\alpha\text{-OT}_n$ (blue circles) series, together with their effective conjugation length (n_{ECL}) and their corresponding absorption maxima of the infinite chain (λ_{∞}).

Table IV.2.2. Meier's plot fitting parameters for OTPD_n and $\alpha\text{-OT}_n$ series.

| | OTPD_n | OT_n |
|--------------------|-----------------|---------------|
| λ_{∞} | 478 nm | 484 nm |
| n_{ECL} | 14 | 18 |
| b | 0.3931 | 0.3309 |
| R^2 | 0.9997 | 1 |

With the aim of having a better understanding of the conformational freedom of OTPD_n oligomers, variable temperature UV-Vis-NIR spectra of these molecules were performed (Figure IV.2.3). The temperature lowering allows to obtain the vibronic structure of the electronic

absorption bands. For **OTPD_n** series, by decreasing the temperature, the λ_{max} wavelength is progressively red-shifted and the vibronic structure is resolved, especially for **OTPD₆**. For the longest oligomer also a new feature at 536 nm was found at 80 K. The planarization of the molecular structure as the temperature diminishes can explain this behaviour, observed also for α -**OT_n** oligomers.^[1] As mentioned above, the π -overlapping improves with the planarity, explaining the displacement of the electronic transition to lower energies. Also the temperature decrease favours the more stable

conformers and it is responsible of the narrower and more intense bands. However, for α -**OT_n** series this planarization effect on cooling is not noticeable for all oligomers,^[1] which is actually the case of **OTPD_n**. This fact highlights the presence of another different factor that contributes to the planarization, and accounts for the vibronic peak of **OTPD₆** at 536 nm at 80 K.

A. II. Energy of the Frontier Molecular Orbitals

In addition to the absorption maxima of the optical spectra and the effective conjugation length, another feature that can be directly related with the electronic structure of π -conjugated organic oligomers is the energy of the frontier molecular orbitals and, in consequence, the optical bandgap (E_g).

Figure IV.2.4 shows the comparison of the FMO energies of both, the linear and cross-conjugated series of aromatic oligothiophenes, and their corresponding E_g . For the shortest oligomers, the optical bandgap is narrower for **OTPD_n** compounds than for the α -**OT_n** counterparts. However, regarding the longest molecules, this behaviour is reversed: the linear oligothiophenes present smaller E_g values. The intermediate members of both series, **OTPD₄** and α -**OT₄**, present similar optical bandgaps.

The differences of the HOMO-LUMO gap between these two series can be

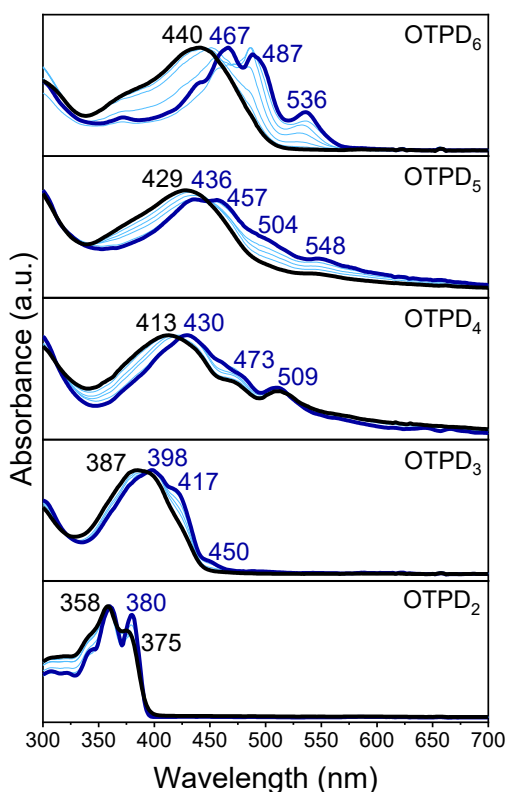


Figure IV.2.3. Variable temperature electronic absorption spectra of **OTPD_n** oligomers in 2Me-THF from room temperature (black lines) to 80 K (dark blue lines). Light blue lines correspond to absorption spectra at intermediate temperatures.

mainly described by four contributions:^[6,7]

1. The aromaticity or resonance stabilization energy. In $\alpha\text{-OT}_n$ molecules the π -electrons are mainly confined within the aromatic rings, resulting in a higher resonance stabilization energy than that of the OTPD_n compounds. In consequence, larger optical band gaps are obtained for $\alpha\text{-OT}_n$. The extension of the π -overlapping of the frontier molecular orbitals explains the reduction of the HOMO-LUMO gap when increasing the number of thiophene units.

2. The planarity or rigidity of the system. As explained in the *Optical Properties* section, the TPD moieties constitute an

extra source of planarization in OTPD_n , while $\alpha\text{-OT}_n$ molecules present a higher rotational freedom around the exocyclic C—C single bond between thiophene rings.

3. The substituent groups. Two main structural features of TPD substituents must be taken into account to compare OTPD_n and $\alpha\text{-OT}_n$ series:

- i) The electron-withdrawing character of the TPD moiety. This electron-withdrawing inductive effect provokes the stabilization of LUMO levels in OTPD_n in comparison with those of the $\alpha\text{-OT}_n$ (see Figure IV.2.4).
- ii) The existence of a second, competitive π -conjugated framework in OTPD_n , which

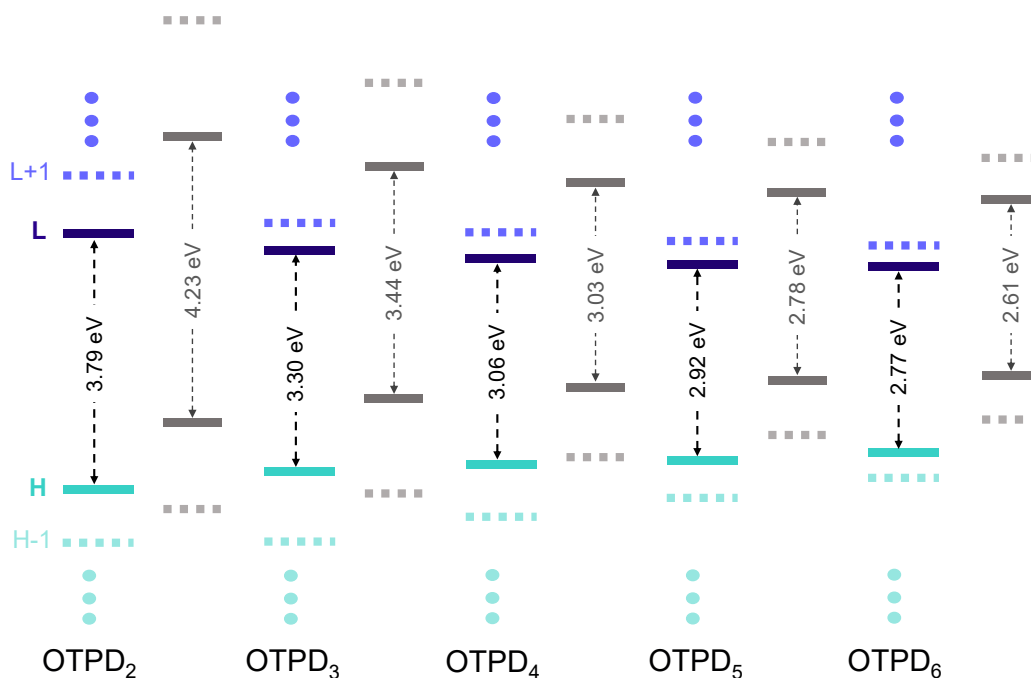


Figure IV.2.4. Energies of the frontier molecular orbitals and E_g values of OTPD_n series together with those of the $\alpha\text{-OT}_n$ molecules (lines in grey) used as reference, both calculated at the B3LYP/6-31G** level of theory. Green lines correspond to the HOMO levels; blue lines correspond to the LUMO levels; dashed lines correspond to the HOMO-1 and LUMO+1 levels.

interrupts the linear electron delocalization through the oligothiophene backbone (see resonant structures in Scheme IV.2.1). Despite in cross-conjugated molecules π electrons have two dimensions for their delocalization (the two orthogonal conjugated frameworks), they only can delocalize through one of them at the expense of the other (competitive π -conjugated paths). In longer **OTPD_n** molecules, the presence of more cross-conjugated sequences increases this competition between the two orthogonal paths, pushing the electron density to the innermost part of the molecule. As a consequence, E_g values of α -**OT₅** and α -**OT₆** are shorter than those of the corresponding **OTPD_n** oligomers.

Regarding the non-substituted oligothiophene family α -**OT_n**, the values of their optical bandgaps are not affected by any substitution pattern, and the planarity and resonance energy are exclusively due to the oligothiophene structure. For these reasons, these molecules establish a perfect reference to study the mentioned contributions in the **OTPD_n** series.

In the case of the **OTPD_n** molecules, the balance between the discussed factors provokes that the gap narrowing trend to be considerably less significant than for the α -**OT_n** family. The optical bandgap variation from $n=2$ to $n=6$ for α -**OT_n** is 1.62 eV, while for **OTPD_n** is 1.02 eV.

The variations between the HOMO/LUMO energies in the two aromatic oligothiophenes series also explain the fact that **OTPD_n** systems reach the λ_∞ value at shorter oligothiophene lengths than α -**OT_n**, i. e., n_{ECL} of the second

one is larger than that of the target family.

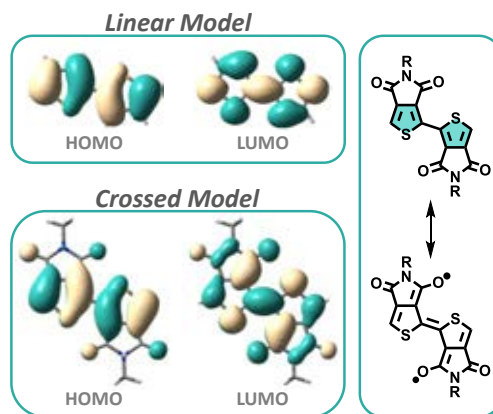
A. III. Topologies of the Frontier Molecular Orbitals

In order to obtain a straightforward image of the electronic structure when *cross-conjugative* effects are involved, frontier molecular orbitals topologies of **OTPD_n** were studied. Figure IV.2.5 shows the HOMO and LUMO topologies corresponding to the optimized structures of **OTPD_n** molecules at the B3LYP/6-31G** level of theory.

Both the HOMO and LUMO are of π nature and spread along the oligothiophene backbone. HOMO levels preserve the *intra-ring* aromaticity for the thiophene units, while the LUMO topologies are of quinoidal shape, with exocyclic bonding coupling. As can be seen in the topologies of the unoccupied molecular orbitals in Figure IV.2.4, the π -cross-conjugated path is revealed in the bonding character between the carbons of the carbonyl groups and the C_β of the thiophene units.

In addition to the three contributions mentioned in the *Section A. II*, the HOMO destabilization when increasing the number of units is also affected by the quinoidal-aromatic tautomerism. For non-degenerate ground state systems (in which the aromatic form is more stable than the corresponding quinoidal one), this destabilization effect is attributed to the higher contribution of the quinoidal form to the aromatic ground electronic state.

For **OTPD_n** family, the changes in the HOMO energies with the oligomer size are smaller than those for the **α-OT_n**, since for the former a less *complete* quinoidal structure contributes to the ground electronic states. The participation of the dione groups in the LUMO topologies diminishes the quinoidization of the thiophene units. In consequence, the quinoidal character of the ground electronic state is smaller than in the case of the **α-OT**. The extension of the LUMO levels to the carbonyl groups as a consequence of the contribution of the inter-dione cross-conjugated framework in the chemical structure of the **OTPD_n** family is presented in Scheme IV.2.3. These differences between the topologies of the frontier molecular orbitals of **OTPD_n** and **α-OT_n** also explain the shorter effective conjugation length (n_{ECL}) of the β , β' -disubstituted oligothiophenes.



Scheme IV.2.3. Left) Topologies of the frontier molecular orbitals of $\alpha\text{-OT}_2$ (top) and **OTPD₂** (bottom) as models of linear and cross-conjugated π -systems; Right) Linear and cross-conjugated resonance structures that mainly contribute to the ground electronic state of **OTPD₂**.

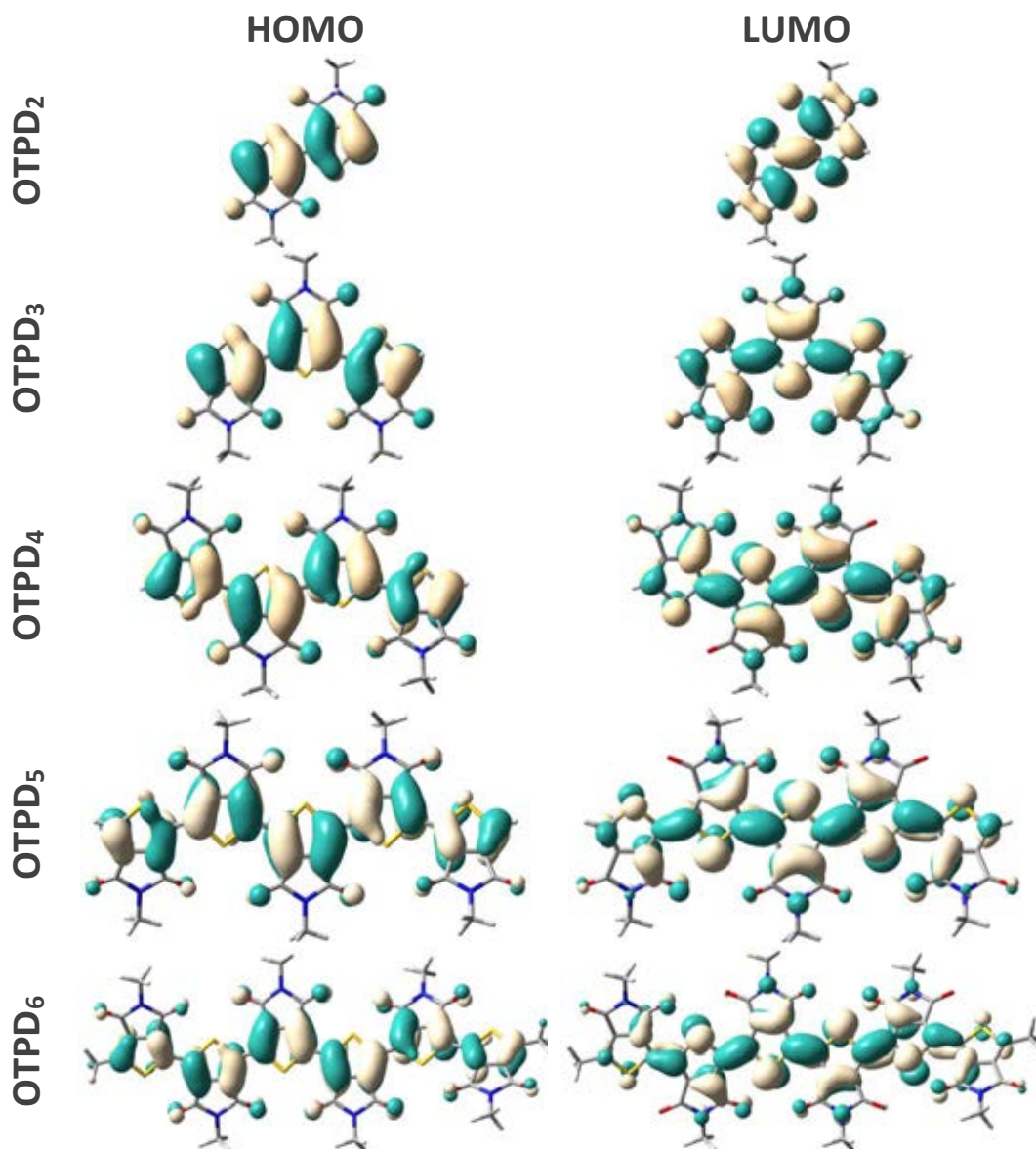


Figure IV.2.5. Topologies of the frontier molecular orbitals of **OTPD_n** oligomers calculated at the B3LYP/6-31G** level of theory.

B. Molecular Structure

B. I. Vibrational IR Spectroscopic Properties

The large IR intensity of the carbonyl group and the fact that its characteristic absorption frequency appears in a relatively clean spectral region make molecules with this group suitable candidates for vibrational IR spectroscopic studies. This is actually the case of **OTPD_n** oligomers, in which the dione groups are of critical importance since they represent the basis of the cross-conjugation properties of these molecules.

Vibrational IR spectra in pellet (KBr) of **OTPD_n** molecules are showed in Figure IV.2.6 (black lines), together with the corresponding calculated spectra at B3LYP/6-31G** level of theory (grey lines). Table IV.2.3 displays the eigenvectors corresponding to the carbonyl group stretching vibration ($\nu_{C=O}$).

The evolution of the $\nu_{C=O}$ in the IR spectra of **OTPD_n** series is as follows: 1759, 1691 cm^{-1} \rightarrow 1760, 1691 cm^{-1} \rightarrow 1760, 1689 cm^{-1} \rightarrow 1762, 1693 cm^{-1} \rightarrow 1763, 1689 cm^{-1} , from **OTPD₂** to **OTPD₆**, respectively. In general, no significant variations with the oligomer length were found, with a maximum shift of 4 cm^{-1} . Since these groups do not participate in the main π -electron delocalization path, they are not affected by the oligomer size, that is, by the linear π -conjugation. Consequently, it is expected that $\nu_{C=O}$ does not experiment larger shifts when only the number of monomeric units is changed.

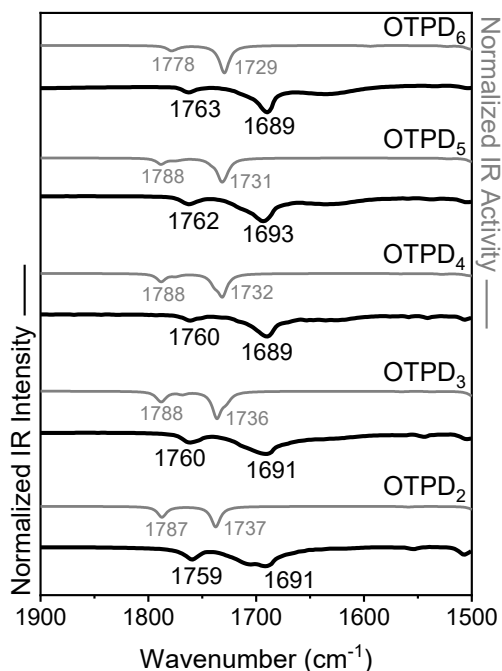
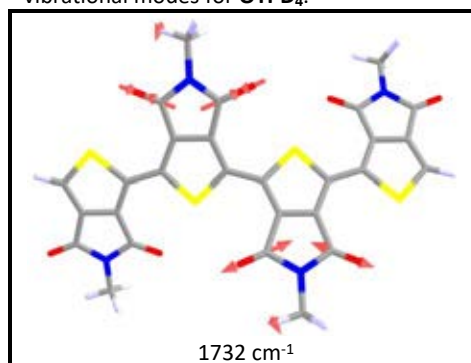


Figure IV.2.6. $\nu_{C=O}$ region of FT-IR spectra of **OTPD_n** oligomers in solid state at room temperature (black lines), together with the calculated spectra at the B3LYP/6-31G** level of theory (grey lines). From bottom to top: **OTPD₂**, **OTPD₃**, **OTPD₄**, **OTPD₅** and **OTPD₆**.

Table IV.2.3. Eigenvectors of the discussed IR vibrational modes for **OTPD₄**.



B. II. Vibrational Raman Spectroscopic Properties

Vibrational Raman spectroscopy is a reference tool to study the π -electron delocalization due to its high sensitivity to the variations of the C=C/C–C pattern in π -conjugated organic molecules.

Figure IV.2.7 displays the FT-Raman spectra of the **OTPD_n** oligomers in solid state (black solid lines), together with the theoretical spectra (grey lines). The strongest Raman band corresponds to the C=C stretching vibration of the thiophene units ($\nu_{\text{C=C/C-C}}$) (eigenvectors of this band for **OTPD₄** are showed in Table IV.2.4). This band down-shifts progressively as the oligomer size increases: $1533\text{ cm}^{-1} \rightarrow 1526\text{ cm}^{-1} \rightarrow 1524\text{ cm}^{-1} \rightarrow 1518\text{ cm}^{-1} \rightarrow 1512\text{ cm}^{-1}$, from **OTPD₂** to **OTPD₆**, respectively.

This is the classical behaviour of π -

conjugated oligomers in which the delocalization of π -electrons increases with the oligomer size. The diminution of the bond length alternation pattern, that is, the equalization of the bond lengths of the alternated C=C/C–C bonds, moves the vibrations to lower energies as the thiophene C=C bonds are weakening.^[8] These results are in agreement with the electronic structure discussion in the former point. Theoretical Raman spectra follow the same trend that the experimental data, but underestimate the values of $\nu_{\text{C=C/C-C}}$ due to the well-known overestimation of π -electron delocalization in DFT calculations.^[9]

FT-Raman spectra also show the C=O stretching vibration of the pyrrole-dione units ($\nu_{\text{C=O}}$) (Figure IV.2.7, left, and Table IV.2.4). This band remains almost invariable when lengthening the oligomer

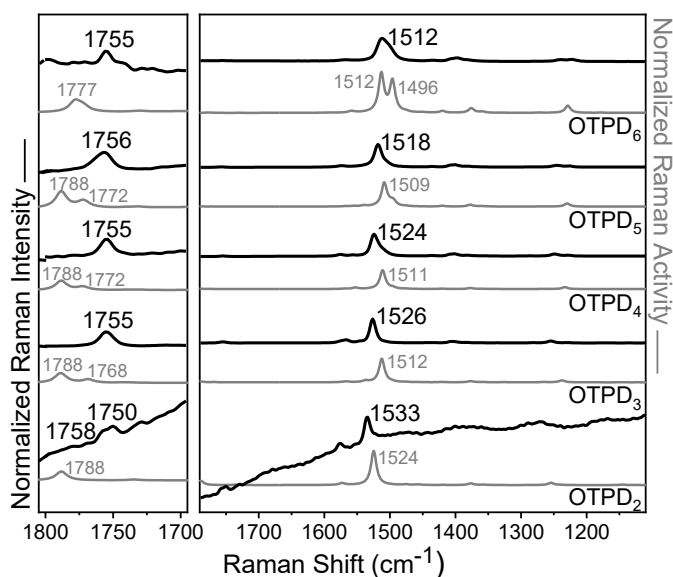


Table IV.2.4. Eigenvectors of the discussed Raman vibrational modes for **OTPD₄**.

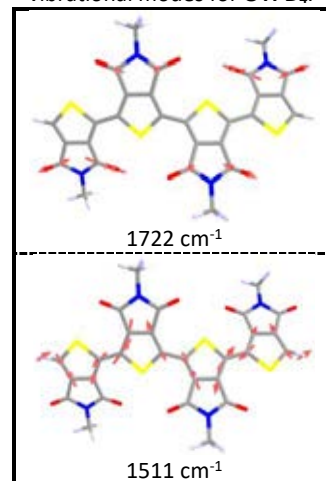


Figure IV.2.7. FT-Raman spectra of **OTPD_n** oligomers in solid state at room temperature in the $\nu_{\text{C=O}}$ (left) and $\nu_{\text{C=C/C-C}}$ (right) spectral region (black lines), together with the calculated spectra at the B3LYP/6-31G** level of theory (grey lines). From bottom to top: **OTPD₂**, **OTPD₃**, **OTPD₄**, **OTPD₅** and **OTPD₆**.

size, indicating that is decoupled from the oligothiophene backbone. These results are in agreement with the vibrational IR spectra.

In order to study the frozen species observed in the variable temperature electronic absorption experiments, Raman spectra were measured at room temperature and at 80 K in 2Me-THF solution (Figure IV.2.8). Unfortunately, sample signals were only obtained for the compound **OTPD₆**, since this is the unique oligomer that presents resonant Raman effect.^[10, 11] In this case, λ_{exc} at 532 nm is resonant with the vibronic peak at 537 nm of **OTPD₆** at 80 K (see Figures IV.2.3 and IV.2.8, top). The resonant Raman effect is revealed in the absence of signals at room temperature (black Raman spectrum in Figure IV.2.8, bottom), and the presence of clear Raman signals upon cooling to 80 K (blue Raman spectrum).

Upon cooling, the $\nu_{\text{C=O}}$ is largely downshifted: $1755 \text{ cm}^{-1} \rightarrow 1633/1613 \text{ cm}^{-1}$ from room temperature (in bulk) to 80 K (in 2Me-THF solution), respectively. The great downshift experimented by the $\nu_{\text{C=O}}$ is classical of systems in which the carbonyl group is involved in hydrogen bonding.^[12, 13] In this case, the oxygen atom of the carbonyl groups of the pyrrole-dione moieties can behave as a donor with the sulphur atom of the adjacent thiophene unit, which acts as an acceptor in a dative bond interaction. The establishment of this $\text{O} \rightarrow \text{S}$ non-covalent bond through the formation of a six-member ring enhances the structure planarization upon cooling. This could explain the electronic

absorption spectra obtained at 80 K in Figures IV.2.3 and IV.2.8.

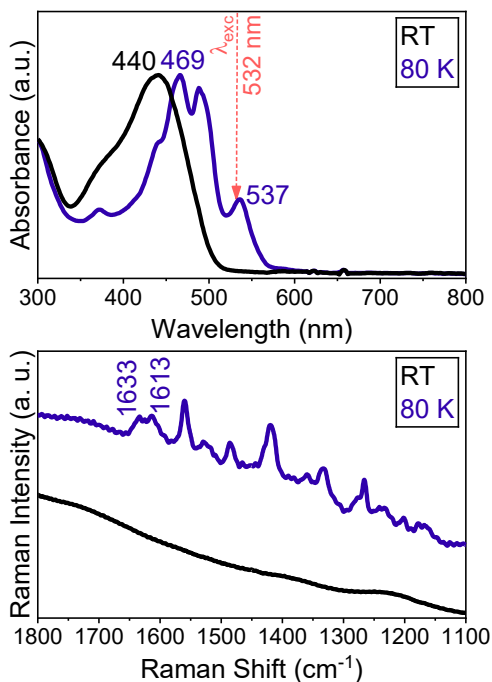


Figure IV.2.8. *Top*) Variable temperature electronic absorption spectra of **OTPD₆** in 2Me-THF, together with the Raman laser excitation wavelength at 532 nm; *Bottom*) Variable temperature Raman spectra at 532 nm of **OTPD₆** in 2Me-THF. Black lines correspond to room temperature spectra and blue lines, to spectra at 80 K.

In order to corroborate the hypothesis of the formation of $\text{O} \rightarrow \text{S}$ dative bond as an *extra* source of planarization on cooling only present in **OTPD_n** oligomers, the rotation energies between two monomeric units of the two mentioned systems (**OTPD₂** and **OT₂**) were calculated.^[14] To account for the effect of the β, β' -disubstitution of the thiophene rings in **OTPD₂**, a thieno-thiophene dimer without carbonyl groups (**OTbT₂**)^[15] has been also considered. In Figure IV.2.9 the rotation energy differences between the most stable conformation (a dihedral angle

of $\sim 180^\circ$ between the two successive units (or *anti*-planar conformation) with the rest of possible dihedral angles for this bond are shown. The *anti*-planar conformer is the most stable structure since the steric hindrance between two successive thiophene rings is minimized (especially for β , β' -disubstituted oligothiophenes) and the complete planarization guarantees the maximum π -overlapping.

For the three systems almost the same behaviour is observed, being the **OTPD₂** oligomer the one with higher energy differences. The maximum energy barrier corresponds to the dihedral angle of 0° in the two β , β' -disubstituted oligothiophenes, being especially unstable the conformer of **OTPD₂** due to the steric hindrance and electrostatic repulsion between the two carbonyl groups. **OTPD₂**, **OTbT₂** and **OT₂** show a local minimum at 50° , 40° and 30° , respectively, which

correspond to a decrease of the steric congestion but still enough planarity to assure an efficient π -overlapping.

The local maximum for **OTPD₂** and **OTbT₂** at 90° is explained by the interruption of π -electron delocalization between the two orthogonal units. In the case of **OT₂**, which is not β , β' -disubstituted, i.e., the steric hindrance is lower than for the other two dimers, the 90° dihedral angle constitutes the absolute maximum.

The energy decrease to the 180° structures is more pronounced for **OTPD₂**, pointing out a higher stabilization of this structure than in the other two systems. This *extra* stabilization energy in this system could be explained through the formation of the O \rightarrow S dative bond, as mentioned above. Upon cooling, the rotation energy barrier is decreased and

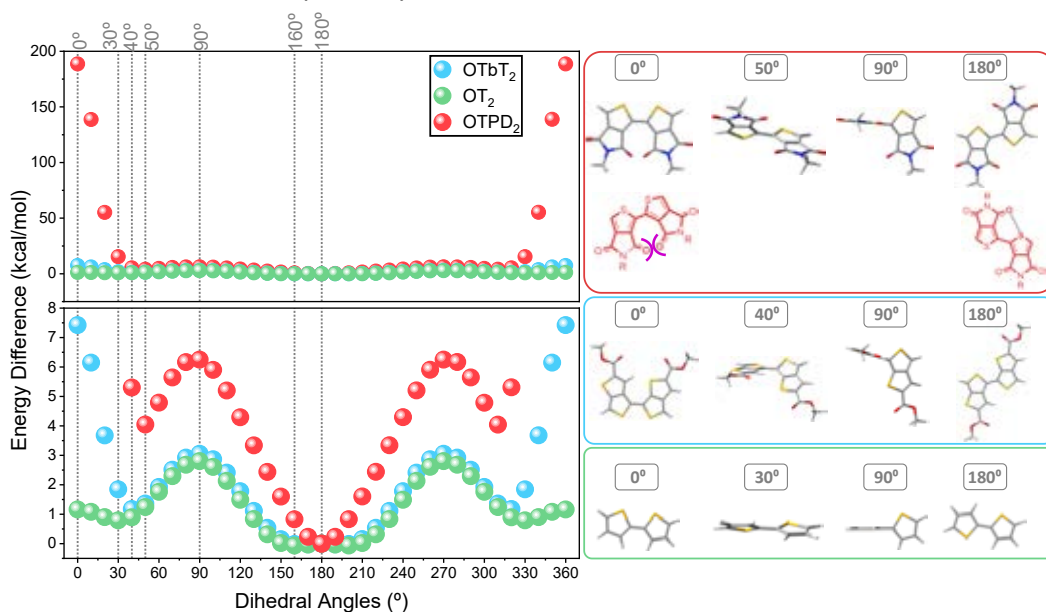
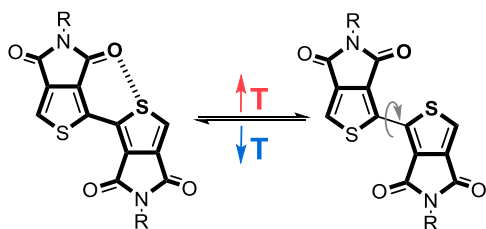


Figure IV.2.9. *Left*) Energy rotation barriers of **OTPD₂** (red circles), **OTbT₂** (blue circles) and **OT₂** (green circles) calculated at B3LYP/6-31G** level of theory. *Right*) Chemical structures of the three systems at the highlighted dihedral angles, corresponding to local and absolute minima and maxima.

the dihedral angle between the repeating units is placed around 180° . This allows the formation of the dative bond which helps to the rigidification and planarization of the molecular structure. In this sense, a thermal equilibrium between different conformers is established:



Scheme IV.2.4. Thermal equilibrium between the two OTPD_n conformers through the formation/rupture of the $\text{O}\rightarrow\text{S}$ dative bond (represented in dashed line).

The *anti*-planar conformer of OTPD_6 at 80 K is responsible of the electronic transition at 537 nm, thus the Raman spectrum in Figure IV.2.8, right (blue line) corresponds to the $\text{O}\rightarrow\text{S}$ dative bond system.

B. III. Bond Length Alternation (BLA) Analysis

The degree of quinoidization /aromatization of the π -conjugated backbone can be easily deduced through the bond length alternation (BLA) between single and double C–C bonds.^[7, 16, 17] In Figure IV.2.10 calculated BLA values of OTPD_n and $\alpha\text{-OT}_n$ from the optimized closed-shell geometries are displayed. The evaluated π -conjugated frameworks are indicated in Scheme IV.2.5.

According to Figure IV.2.10 (left panel),

BLA parameter decreases with the number of monomeric units when the linearly π -conjugated framework (BLA_L , green circles) is evaluated for both series. Smaller values of BLA means that the π -electron delocalization is larger, since single and double C–C bonds are equalized. This bond equalization is in agreement with the previous optical band gap, λ_{max} wavelengths and Raman spectra discussion. Similar values of BLA_L are found for OTPD_n and $\alpha\text{-OT}_n$ families from $n=3$ to $n=6$. However, for $\alpha\text{-OT}_2$ the value of this parameter is considerably higher than that of the corresponding cross-conjugated counterpart. The planarity distortion through the exocyclic C–C single bond in $\alpha\text{-OT}_2$ with confines the π -electron within the thiophene rings and, in consequence, provokes the localization of the single and double C–C bonds.

When the BLA values for the cross-conjugated paths are calculated (BLA_{ID}), three different inter-diones connections must be taken into account, all of them with values higher than the corresponding *linear* BLA in the neutral molecules. ID_1 (pink filled circles in Figure IV.2.10) corresponds to the *external* interdione paths, which is the only orthogonal sequence in OTPD_2 and OTPD_3 . ID_2 and ID_3 (blue and orange filled circles, respectively) are assigned to the *inner* cross-conjugated patterns, being ID_3 the *innermost* path, only presents in OTPD_6 . For these conjugated sequences, BLA does not display any evolution with the number of monomeric units since the inter-dione paths remain unaltered whatever the oligomer length. The only remarkable result is the smaller values for the inter-

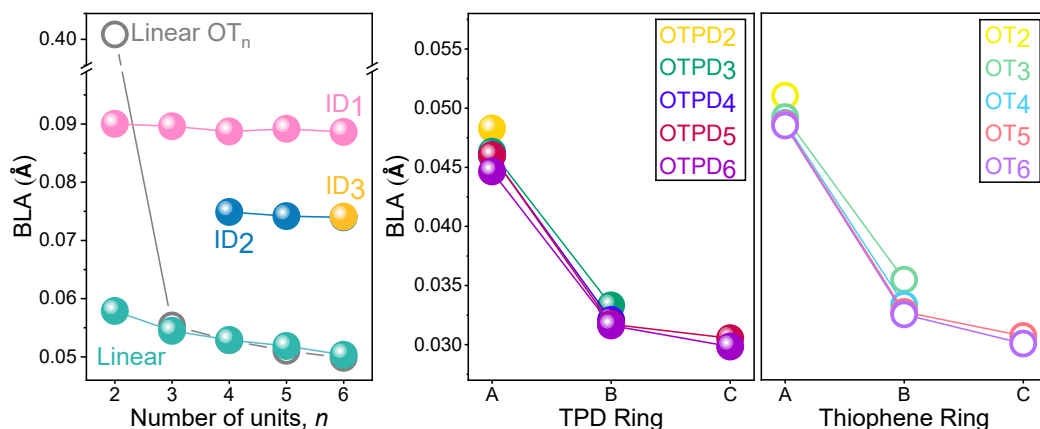
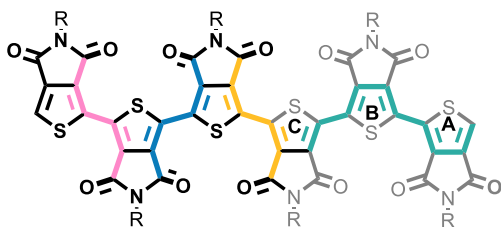


Figure IV.2.10. Calculated Bond Length Alternation (BLA) values (Å) for π -conjugated paths (*left*) and for thiophene rings (*middle and right*) for the optimized molecular structures of **OTPD_n** (filled circles) and α -**OT_n** (empty circles) at the B3LYP/6-31G** level of theory, together with the scheme of the evaluated π -conjugated sequences. ID corresponds to the inter-dione paths.



Scheme IV.2.5. Scheme of the evaluated π -conjugated sequences and thiophene rings of **OTPD_n** in the BLA analysis.

dione paths 2 and 3, revealing a larger equalization of the C–C bonds lengths through the *inner* inter-dione paths than through the *external* ones.

BLA values can be also evaluated within the thiophene rings (Figure IV.2.10, *middle and right* panels).^[16, 17] In this case, values of **OTPD_n** are slightly shorter than those of the corresponding α -**OT_n** molecules, also in agreement with the *Electronic Structure* discussion. Nonetheless, the trend with the thiophene rings is kept between both series.

The competition between the linear and ID frameworks can also explain the

shorter n_{ECL} value of **OTPD_n** than that of the **OT_n** series despite the similar λ_{∞} values (see Meier's plot fitting in Figure IV.2.2). In the case of the cross-conjugated oligothiophenes, the π -conjugated *area* is confined to the molecule centre but constitutes a 2D delocalization region, as demonstrated with the HOMO-LUMO topologies in *Section A.III*.

2.2 CHARGED SPECIES OF OTPD_n OLIGOMERS

A. Electronic Structure

A. I. Electrochemical Properties

Figure IV.2.11 and Table IV.2.5 show the cyclic voltammograms and electrochemical data of OTPD_n oligomers carried out in dichloromethane solutions at room temperature by the group of the Professor Xiaozhang Zhu.

All molecules present two reduction processes corresponding to the consecutive formation of the radical anion and dianion species. Reduction potentials slightly change with the oligomer size, indicating that the extra electrons are located in the inter-dione cross-conjugated framework.

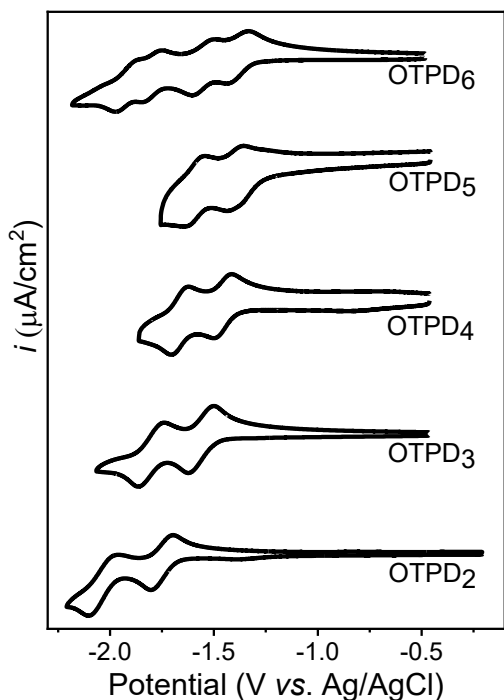


Figure IV.2.11. Cyclic voltammetry curves of OTPD_n oligomers in 0.1M Bu₄NClO₄ in CH₂Cl₂ at room temperature (vs. Fc/Fc⁺). From bottom to top: OTPD₂, OTPD₃, OTPD₄, OTPD₅ and OTPD₆.

Table IV.2.5. Electrochemical data of OTPD_n oligomers.

| | E _{red-1} ^{1/2 a} (V) | E _{red-2} ^{1/2 a} (V) |
|-------------------|--|--|
| OTPD ₂ | -1.70 | - |
| OTPD ₃ | -1.65 | -1.85 |
| OTPD ₄ | -1.45 | -1.70 |
| OTPD ₅ | -1.40 | -1.60 |
| OTPD ₆ | -1.38 | -1.55 |

^aMeasured in 0.1M Bu₄NClO₄ in CH₂Cl₂ at room temperature (vs. Fc/Fc⁺).

A. II. Optical Properties: UV-Vis-NIR Spectroelectrochemical Reduction

The UV-Vis-NIR spectroelectrochemical reduction processes of OTPD_n oligomers are shown in Figure IV.2.12, and the main optical data are summarized in Table IV.2.6.

For [OTPD₂]^{•-}, the radical anion species presents only one band at 487 nm (with two components at 542 nm and 620 nm). However, reduction of the neutral species in the longest oligomers gives rise to the typical two bands pattern of polaronic radical anions (pink lines in Figure IV.2.12): 552/2191 nm for [OTPD₃]^{•-}; 639/2191 nm for [OTPD₄]^{•-}; 670/2343 nm for [OTPD₅]^{•-}; and 688/2416 nm for [OTPD₆]^{•-}. Radical cations and anions of linearly π-conjugated oligomers are doublets which usually presents two bands in their electronic absorption spectra: the polaron structure (see Scheme IV.2.6). The most intense band correspond to the excitation from

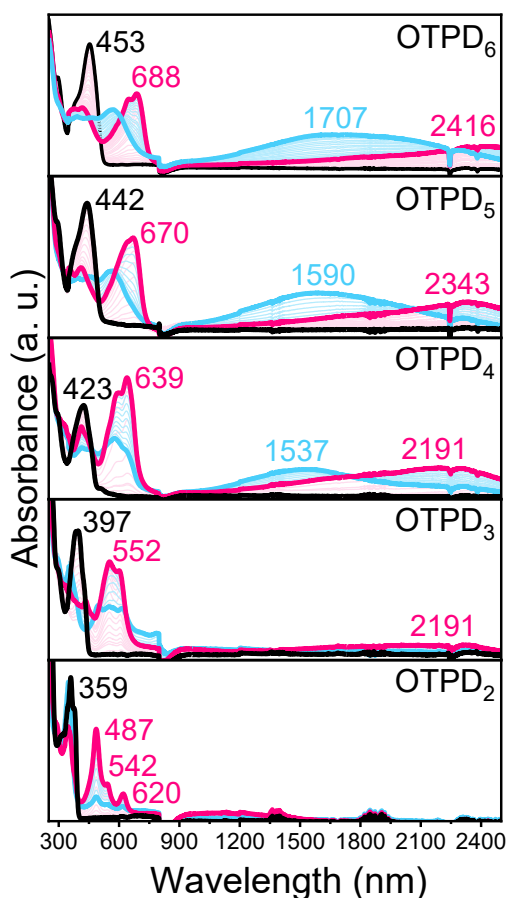
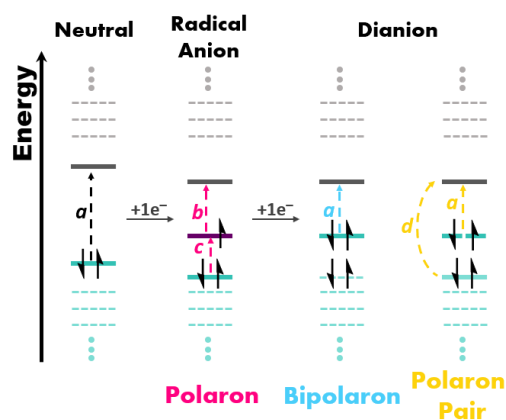


Figure IV.2.12. UV-Vis-NIR spectroelectrochemical reduction of **OTPD_n** oligomers in Bu₄N-PF₆ 0.1 M in CH₂Cl₂ at room temperature. Black lines correspond to the spectra of neutral molecules; pink lines correspond to the spectra of the completely formed radical anions; and blue lines corresponds to the spectra of the completely formed dianion species. Light color lines correspond to the intermediate spectra between the former species in the reduction process.

Table IV.2.6. Optical data of UV-Vis-NIR spectroelectrochemical reduction of **OTPD_n** oligomers in Bu₄N-PF₆ 0.1 M in CH₂Cl₂ at room temperature.

| | OTPD ₂ | OTPD ₃ | OTPD ₄ | OTPD ₅ | OTPD ₆ |
|----------------------|-------------------|-------------------|-------------------|-------------------|-------------------|
| Neutral | 359, 378 | 397 | 423 | 442 | 453 |
| Radical Anion | 487 (542) 620 | 552 (599) 2191 | 639 2191 | 670 2343 | 688 2416 |
| Dianion | — | — | 580 1537 | 569 1590 | 568 1707 |

the semi-occupied to the empty frontier molecular orbitals (SOMO→LUMO), while the second band, placed at lower energies (frequently a broad band in the near IR region), is assigned to the doubly-occupied to the semi-occupied frontier molecular orbitals transition (HOMO→SOMO).^[18-20] This pair of bands are progressively red-shifted when increasing the oligomer size as a consequence of the larger π- electron delocalization.



Scheme IV.2.6. Energy levels and transitions of neutral, polaron radical anion, bipolaron and polaron pair dianion species. HOMO levels are in green; LUMO levels are in grey; SOMO level is in purple; light green and light grey dashed lines correspond to HOMO-*n* and LUMO+*n*, respectively. Designated electronic transitions are: *a*: HOMO→LUMO; *b*: SOMO→LUMO; *c*: HOMO→SOMO; *d*: HOMO-1→LUMO.

For the dianionic species a similar two bands motif is obtained for $[\text{OTPD}_4]^{2-}$, $[\text{OTPD}_5]^{2-}$ and $[\text{OTPD}_6]^{2-}$ (blue lines in Figure IV.2.12): 580/1537 nm, 569/1590nm and 568/1707 nm, respectively. However, classical closed-shell dianions present a single, intense absorption band in their optical spectra caused by the HOMO \rightarrow LUMO transition (see Scheme IV.2.6). Thus, the $[\text{OTPD}_n]^{2-}$ absorption spectra are assigned to segregated polarons or side-by-side polarons,^[18, 19] where the two extra charges are localized in different parts of the molecule, such as two symmetrical polarons (or two isolated radical anions). For this reason, this open-shell polaron pair structure is very similar to that of the radical anions (polaron structure), revealing a diradical character in the dianion species.

Considering the dianion species as two segregated polarons, the electrostatic repulsion between these two negative charges pushes them to locate as far as possible. In consequence, polaron pair structure is favoured when the spatial overlap of the spin orbitals is diminished, that is, in disjoint orbitals. Accordingly to this information, $[\text{OTPD}_2]^{2-}$ is a closed-shell system, in consequence with a bipolaron-type electronic absorption spectra. However, in longer oligomers the open-shell character allows the two charges to locate in different parts of the molecules. In the case of $[\text{OTPD}_3]^{2-}$ the *two radical anions* that conform the polaron pair shares the central TPD unit.

In order to establish the electronic structure of the dianions, the difference

between the formation energies of the closed-shell (green circles) and triplet (red circles) systems respect to the open-shell are represented in Figure IV.2.13. In agreement with the discussion of the optical data, for $[\text{OTPD}_2]^{2-}$ the closed-shell bipolaron configuration is the most stable situation, while the longer oligomers are singlet open-shell systems (infringing the Hund's rule), explaining their polaron pair-type electronic absorption. Again $[\text{OTPD}_3]^{2-}$ presents an intermediate behaviour between these two states. As the length of the oligomer increases, the triplet state becomes more stable in energy, but even for the longest one, $[\text{OTPD}_6]^{2-}$, the ground electronic state is a singlet open-shell diradical. However, for $[\text{OTPD}_5]^{2-}$ and $[\text{OTPD}_6]^{2-}$, the singlet-triplet gap is shorter enough to allow the thermal population of the triplet state, demonstrated by EPR experiments performed for the group of the professor Xiaozhang Zhu and showed in *Appendix V*.

In this sense, despite the two polarons are *spatially* separated in $[\text{OTPD}_n]^{2-}$ species, they are not *chemically* isolated: the singlet configuration of these diradicals means that some extent of chemical bond or interaction exists between the two radical centres. By this manner, the double spin polarization (DSP) mechanism comes into play. According to the DSP mechanism, for diradical systems where the two radical centres are appropriately connected through the molecular bridge (Kekulé-type diradicals), the singlet state becomes energetically favoured violating the Hund's rule, which establishes the high spin systems as the most stable configurations. This effect can

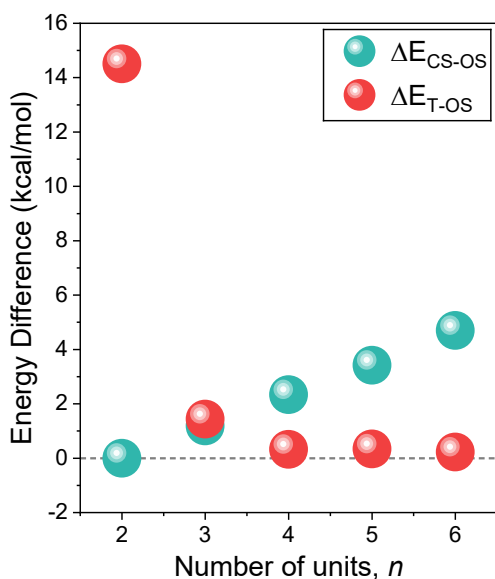
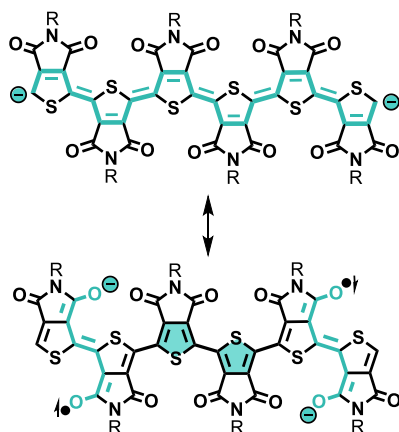


Figure IV.2.13. Formation energy differences (kcal/mol) between the closed-shell (CS) (green circles) and the triplet (red circles) states respect to the singlet open-shell (OS) configuration of $[\text{OTPD}_n]^{2-}$ species calculated at the (U)B3LYP/6-31G** level of theory.

be easily understood taking into account the tautomerism between the closed and open-shell configurations in Kekulé diradicals (Scheme IV.2.7).^[21, 22]

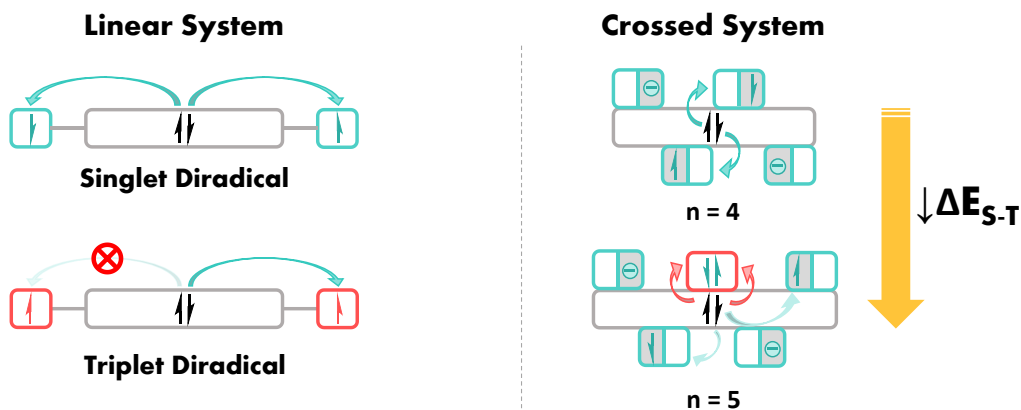


Scheme IV.2.7. Closed-shell (top) and singlet open-shell (bottom) resonant structures of OTPD_5 dianion.

With this information, the uncommon structure of the $[\text{OTPD}_n]^{2-}$ species in longer

oligomers constitutes an interesting situation where the cross-conjugation seems to play an important role. The electronic structure study of the charged species suggests a polaron pair pattern for the dianions, conferring diradical properties on them. Despite the two radical anions centres are confined to different parts of the molecules, the singlet open-shell configuration of the ground state establishes that a chemical interaction must exist between them by the DSP mechanism: they are connected through the π -conjugated structure (Scheme IV.2.8). In this scenario, two possible dispositions for the dianions can be proposed. On the one hand, the position of the two radical anions in the extremes of the oligothiophene backbone implies the complete loss of aromaticity by forming a quinoidal pattern. Thus, the diradical configuration for the dianion species would not be favoured respect to the closed-shell. On the other hand, locating the two radical anions in two cross-conjugated inter-dione paths, establishes a spatial separation between them but allows the chemical connection of the two centres through the linearly π -conjugated sequence, explaining the singlet character of the ground state.

Nevertheless, longer OTPD_n do not lose their planarity respect to the shorter molecules. In this series, when increasing the number of monomeric units, also the number of cross-conjugated paths is raised. From $[\text{OTPD}_4]^{2-}$, neutral TPD moieties exist between the two external segregated polarons. The carbonyl groups of these *neutral* units can also conjugate with the π -electrons of the oligothiophene



Scheme IV.2.8. Left) Double Spin Polarization mechanism in linearly π -conjugated diradicals with singlet and triplet ground electronic states; Right) Double Spin Polarization mechanism in cross-conjugated systems with different oligomer size, like **OTPD_n** molecules for **OTPD₄** ($n=4$) and **OTPD₅** (5 units), and the interaction of the bridge with the polaron pair spins (green arrows) and the neutral **TPD** moieties (red arrows). The π -conjugated bridge is represented in grey and their π -electrons, in black. Antiparallel spins (singlet) are in green, and parallel spins (triplet) in red.

bridge, interrupting the chemical connection between the two radical centres (Scheme IV.2.8, bottom). Thus, in longer **OTPD_n** the conjugative effect of the bridge is not as effective as in the shortest molecules, and in consequence the stabilization of the singlet state is lower. Therefore, the cross-conjugation properties of the **OTPD_n** systems explain the narrowing of their ΔE_{S-T} when lengthening the oligomer size.

The validity of these hypothesis is tested in the molecular structure study.

B. Molecular Structure

B. I. IR Spectroelectrochemical Reduction

The electrochemical reduction process was monitored through IR vibrational spectroscopy (Figure IV.2.14) in order to examine the structure of the carbonyl groups.

In agreement with the data obtained for the pellet samples, for neutral species

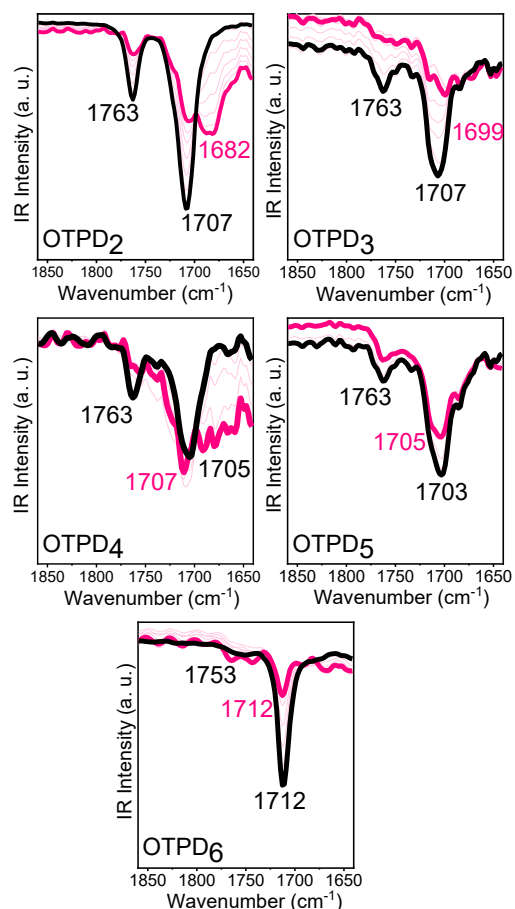


Figure IV.2.14. IR spectroelectrochemical reduction of OTPD_n oligomers in $\text{Bu}_4\text{N-PF}_6$ 0.1 M in CH_2Cl_2 at room temperature. Black lines correspond to the spectra of neutral molecules; pink lines correspond to the spectra of the completely formed reduced species. Light color lines correspond to the intermediate spectra between the former species in the reduction process.

the two stretching bands ($\nu_{\text{C=O}}$) (black spectra in Figure IV.2.14) experiment little changes with the oligomer size since they are decoupled from the linearly π -conjugated path (from OTPD_2 to OTPD_6 : $1707/1763 \rightarrow 1707/1763 \rightarrow 1705/1763 \rightarrow 1703, 1763 \rightarrow 1712, 1753 \text{ cm}^{-1}$). Alteration of these bands upon the reduction process indicates that the extra charge interacts in some way with the carbonyl groups. In the IR spectra of the reduced species (red lines in Figure IV.2.14), $\nu_{\text{C=O}}$ are generally unresolved, indicating that the identity of this group is lost due to the weakening of the double bond. In the case of the reduced OTPD_2 and OTPD_3 , the most intense band down-shifts to 1682 and 1699 cm^{-1} , respectively. The weakening of the C=O bond due to the reduction to C–O[−] can explain this displacement to lower wavenumbers. However, for longer oligomers this effect is not so clear, probably because some of the carbonyl groups keep their neutral character.

It is noteworthy that only one reduced species was obtained for each oligomer, despite the same potential window as in the case of the UV-Vis-NIR spectroelectrochemical experiments was employed. This fact can be a clear indication that both the radical anion and the dianion species present similar configurations for the dione groups of the TPD moieties.

B. II. Vibrational Raman Study of Charged Species

Electronic absorption spectra of the reduced species of the longest **OTPD_n** molecules (i. e., **OTPD₄**, **OTPD₅** and **OTPD₆**) show that it is possible to obtain the Resonant Raman spectra, particularly with the 633 nm excitation wavelength. The resonant effect can be clearly identified in Figure IV.2.15 for the different species of **OTPD₆**. Since for the non-resonant neutral molecule the most intense bands of the Raman spectra correspond to the solvent (**CH₂Cl₂**), in the reduced species the sample bands are almost of the same intensity than those of the **CH₂Cl₂**, a direct consequence of the selective enhancement of the Raman bands of the *optically active* species in the resonant effect.

For the three longest oligomers, the 633 nm Raman excitation wavelength is resonant with both radical anion and dianion species (see Figure IV.2.12), making possible to obtain the Raman spectra of them.

In linearly π -conjugated oligothiophenes, upon oxidation of the neutral molecules, the aromatic backbone suffers a quinoidization that weakens the double C=C bonds and strengthens the single C-C bonds ($\text{BLA} \rightarrow 0$). As a consequence, the thiophene $\nu_{\text{C=C/C-C}}$ is largely down-shifted ($\sim 40 \text{ cm}^{-1}$). [23, 24] However, in the reduction of **OTPD_n** oligomers, the $\nu_{\text{C=C/C-C}}$ Raman band experiments a slight up-shift (5-10 cm^{-1}). From neutral to radical anion species, the evolution of the $\nu_{\text{C=C/C-C}}$ is: 1524 \rightarrow 1530,

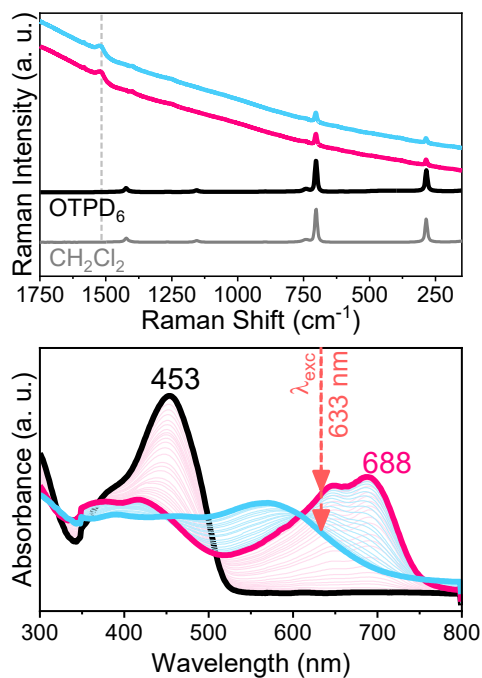


Figure IV.2.15. Top) 633 nm Raman spectra of neutral, radical anion and dianion species of **OTPD₆** in **CH₂Cl₂** at room temperature, together with the Raman spectra of **CH₂Cl₂** as reference (grey line); Bottom) UV-Vis-NIR electronic absorption spectra of **OTPD₆** during the electrochemical reduction process, together with the Raman excitation wavelength at 633 nm used for the Raman experiments (arrows in red). Black lines correspond to the neutral molecule, pink lines correspond to the radical anion and blue lines correspond to the dianion.

1518 \rightarrow 1523 and 1512 \rightarrow 1521 for **[OTPD₄]^{•-}**, **[OTPD₅]^{•-}** and **[OTPD₆]^{•-}**, respectively (Figure IV.2.16, top).

An increase in the value of $\nu_{\text{C=C/C-C}}$ indicates a decrease of the π -electron delocalization through the oligothiophene backbone, that is, the double and single character of the C-C bonds are more pronounced. This fact can be explained placing the extra negative charge in the carbonyl groups of the **TPD** units. When one extra electron is added to this group,

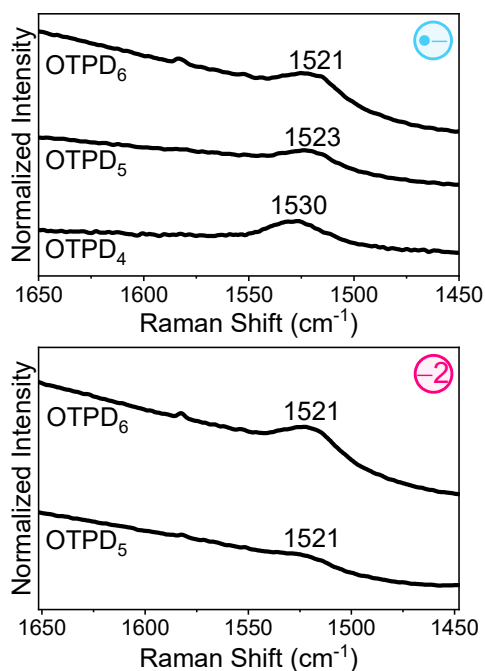
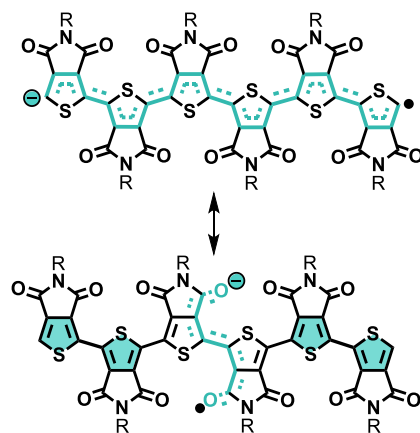


Figure IV.2.16. 633 nm resonant Raman spectra of **OTPD_n** radical anion (*top*) and dianion (*bottom*) species in CH_2Cl_2 at room temperature. From bottom to top: **OTPD₄**, **OTPD₅** and **OTPD₆**.

it can delocalize to the carbonyl of the vicinal **TPD** unit (inter-dione cross-conjugated path), interrupting the π -conjugation through the oligothiophene (see Scheme IV.2.9). This interference in the linear conjugation not only provokes the up-shift of the $\text{V}_{\text{C}=\text{C}/\text{C}-\text{C}}$ Raman band, but also is a clear evidence of the cross-conjugation effect in the **OTPD_n** radical anions.

Upon a second reduction step, no significant variations in the Raman bands were found for the dianion species: $1523 \rightarrow 1521$ and $1521 \rightarrow 1521$ for $[\text{OTPD}_5]^{-2}$ and $[\text{OTPD}_6]^{-2}$, respectively (Figure IV.2.16, bottom). Similar Raman spectra for both radical anions and dianions suggests similar distributions of the π -electrons.



Scheme IV.2.9. Representation of the linear (*top*) and crossed (*bottom*) π -conjugated frameworks in **OTPD₅** radical anion species. Linearly and crossed π -conjugated sequences are highlighted in green.

B. III. Bond Length Alternation (BLA) Analysis

As in the case of the neutral species, the study of the BLA parameter, complementing the Raman spectra, provides a more accuracy picture of the chemical structure in radical anion and dianion species. Again, three different inter-dione paths can be described ($\text{BLA}_{\text{ID}1}$, $\text{BLA}_{\text{ID}2}$ and $\text{BLA}_{\text{ID}3}$), all of them cross-conjugated to the *linearly* π -conjugated backbone (BLA_L). BLA values of dianions were calculated for the singlet open-shell optimized geometry. In the case of the **OTPD₂** molecule, singlet open-shell and closed-shell configurations converge.

According to the calculated BLA values, for the radical anion species (Figure IV.2.17, *left*) the π -electron delocalization of the extra charge can take place in the linear interthiophene path or between two carbonyl groups of vicinal moieties in the

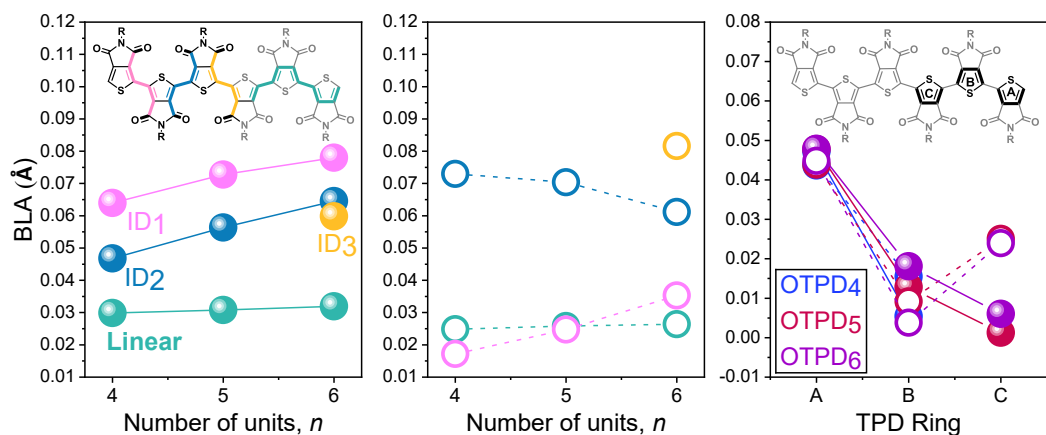


Figure IV.2.17. Calculated Bond Length Alternation (BLA) values (Å) for π -conjugated paths in $[\text{OTPD}_n]^+$ (left) and $[\text{OTPD}_n]^{2-}$ (middle), and for thiophene rings (right) for the optimized open-shell structures at (U)B3LYP/6-31G** level of theory, together with the schemes of the evaluated π -conjugated sequences (insets). ID corresponds to the inter-dione paths.

innermost part of the molecule (interdione paths 2 for $[\text{OTPD}_4]^+$ and $[\text{OTPD}_5]^+$, and interdione path 3 for $[\text{OTPD}_6]^+$) (see Scheme IV.2.9). The mediation of this second path in the radical anion delocalization is in agreement with the Raman up-shift of the $\nu_{\text{C}=\text{C}/\text{C}-\text{C}}$ band upon reduction since it provokes an interruption in the π -electron conjugation through the linear oligothiophene.

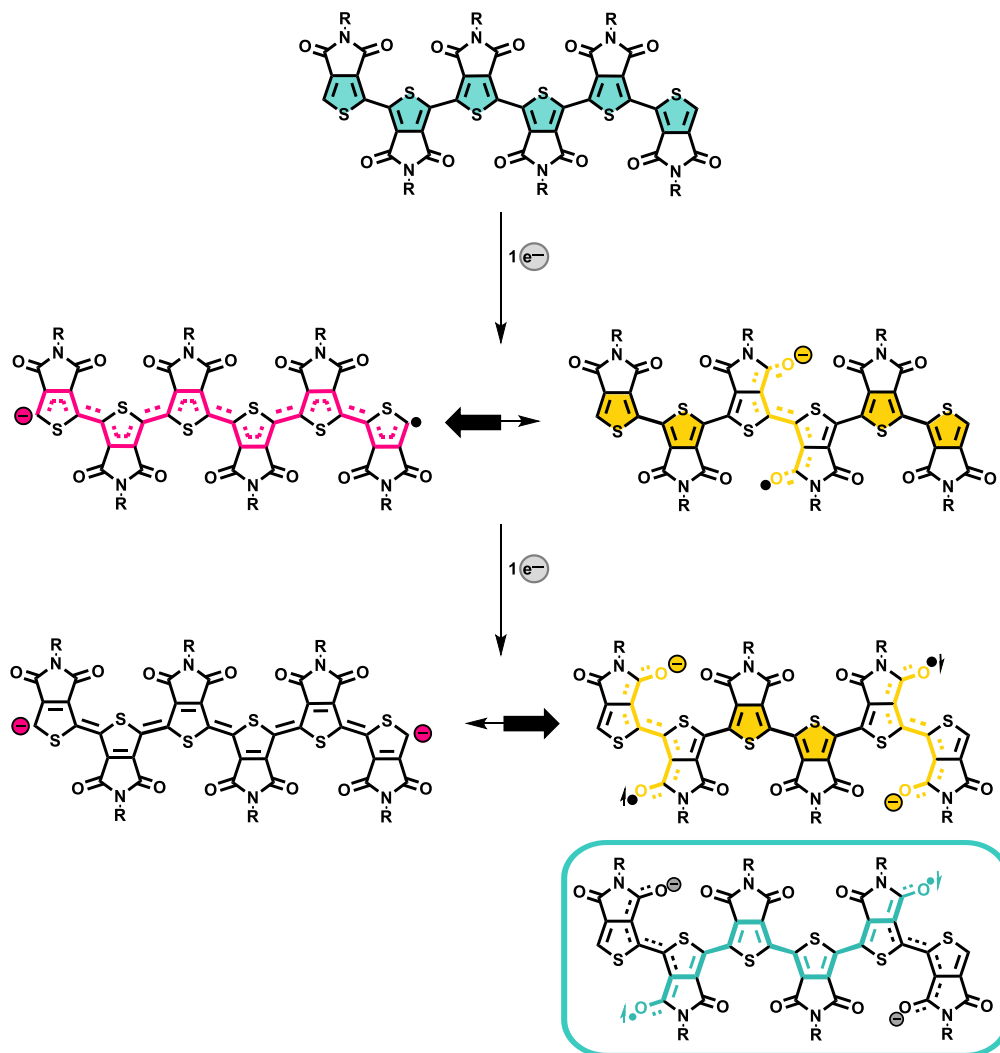
Regarding the values for the dianion species (middle panel in Figure IV.2.17), the delocalization of the two extra electrons arises with almost the same probability in both the linear and the cross-conjugated path ID₁ (smaller BLA values). In this case, the electrostatic repulsion between the two electrons pushes them to the opposite parts of the molecule, making the *external* interdione paths (ID₁) the preferred to accommodate the negative charges (lower value of BLA).

BLA values for the thiophene rings were also calculated (Figure IV.2.17, right). For the radical anion species (filled circles) the

higher conjugation was found for the innermost ring (ring C), thus the delocalization of the radical anion must take place through it. Despite the BLA values of the radical anions follow the same trend as in the case of the neutrals (Figure IV.2.10), for the charged species BLAs in rings C are closer to zero, that is, the π -conjugation is larger than for the neutral molecules.

In the case of the dianion species (empty circles), the shorter BLA values are those of the thiophene rings B. The non-affected rings between the two radical anions, placed in the ID₁ paths (which affect rings A and B) in $[\text{OTPD}_5]^{2-}$ and $[\text{OTPD}_6]^{2-}$, provide a connection for the two radicals. These centres can interact through a sequence of conjugated bonds explaining the singlet configuration of the ground electronic state, and supporting the DSP mechanism.

Scheme IV.2.10 shows the proposed structures of the **OTPD_n** species after the discussion of the present chapter.



Scheme IV.2.10. Proposed structures for **OTPD₆** neutral, radical anion and dianion species (applicable to the rest of the oligomers of the series). The linearly inter-thiophene and cross-conjugated inter-dione π -conjugated pathways are highlighted in pink and yellow, respectively. In the inset and highlighted in green, the connection of the two radical centres through the π -conjugated oligothiophene bridge is depicted, supporting the DSP mechanism for the singlet open-shell ground state in the dianions.

2.3 CONCLUSIONS

According to the results obtained in the study of the optical and vibrational properties of the **OTPD_n** oligomers in their neutral and charged species, and in agreement with the performed theoretical calculations, the following conclusions can be extracted:

- The linear π -conjugation of **OTPD_n** oligomers is altered by the presence of the inter-dione cross-conjugated sequences between vicinal **TPD** moieties. The existence of these orthogonal paths provokes the confinement of the π -electron density in the centre of the molecules, diminishing the overall π -conjugation of the series and counteracting the substituents effects on the HOMO-LUMO gap reduction.
- In addition to constitute an alternative π -conjugation sequence to the linear oligothiophene, the dione groups have been demonstrated to be responsible of an *extra* source of planarization upon cooling. This property is explained by the formation of an O→S dative bond between the oxygen atom of the **TPD** moiety and the sulphur atom of the vicinity thiophene ring. The conformer at low temperature was characterized by Raman spectroscopy thanks to resonant effects.
- Reduced species of **OTPD_n** oligomers were characterized through UV-Vis-NIR electronic absorption and IR and Raman vibrational spectroscopies. In all cases the first reduction step gives rise to the formation of a radical anion species with the classical polaron pattern in the optical experiments. Raman spectra and the calculated values of the bond length alternation suggest that the inter-dione paths provokes the *extra* charge to mainly delocalize in the molecule centre, as in the case of the neutral molecules.
- Dianion species were characterized for the longer oligomers, [**OTPD₅**]²⁻ and [**OTPD₆**]²⁻, and their electronic absorption spectra display a polaron pair or segregated polarons structure, with a singlet open-shell diradical character in their ground electronic state.
- According to the obtained results by the different employed spectroscopies and through the theoretical calculations, the unique chemical structures that explain these properties are those were the *two radical anion* centres of the polaron pair are delocalized over two carbonyl groups of vicinal **TPD** moieties, that is, over the inter-dione cross-conjugated path. These radical centres are *chemically* connected through the linearly π -conjugated oligothiophene bridge, according to the DSP mechanism and explaining the singlet character of these diradicals.
- Also the singlet-triplet gap of the dianions is affected by the cross-conjugation properties. The presence of interfering cross-conjugated

sequences reduces the effect of the DSP mechanism and, hence, diminishes the singlet-triplet gap.

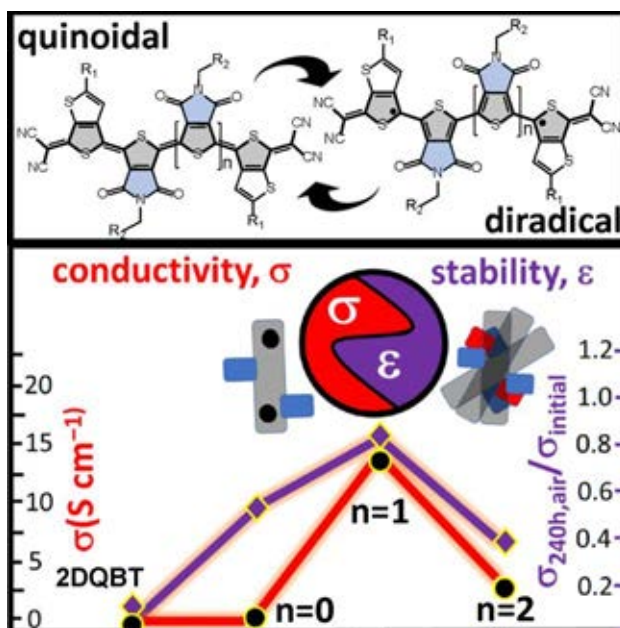
- The cross-conjugation property has been demonstrated to have a direct impact in the HOMO-LUMO gap of the π -conjugated organic materials, as well as in the singlet-triplet gap and diradical character, properties which are of critical interest in organic electronic applications. Taking into account the results obtained in the study of the **OTPD_n** family, the next step is to take advantage of the modulation effect of the cross-conjugation on all these properties not only in the dianion species but also in *less reduced* molecules, feasible at doping levels. The critical point to achieve this goal seems to be the diradical character of the molecule, since it goes together with the cross-conjugation properties.

REFERENCE

- [1] *Comprehensive Evaluation of the Absorption, Photophysical, Energy Transfer, Structural, and Theoretical Properties of π -Oligothiophenes with One to Seven Rings*, R. S. Becker, J. Seixas de Melo, A. L. Maçanita, F. Elisei, *J. Phys. Chem.*, **1996**, *100*, 18683–18695.
- [2] *From Oligomers to Polymer: Convergence in the HOMO–LUMO Gaps of Conjugated Oligomers*, S. S. Zade and M. Bendikov, *Org. Lett.*, **2006**, *8*, 5243–5246.
- [3] *Monodisperse Dialkoxy-Substituted Oligo(Phenyleneethynylene)s*, U. Stalmach, H. Kolshorn, I. Brehm and H. Meier, *Liebigs Ann.*, **1996**, *9*, 1449–1456.
- [4] *Effective Conjugation Length and UV/Vis Spectra of Oligomers*, H. Meier, U. Stalmach and H. Kolshorn, *Acta Polymer.*, **1997**, *48*, 379–384.
- [5] *Conjugation Oligomers with Terminal Donor-Acceptor Substitution*, H. Meier, *Angew. Chem. Int. Ed.*, **2005**, *44*, 2482–2506.
- [6] *Handbook of Thiophene-Based Materials*, I. F. Perepichka and D. F. Perepichka, Eds.; John Wiley & Sons, Ltd: United Kingdom, **2009**.
- [7] *Molecular Engineering of the Band Gap of π -Conjugated Systems: Facing Technological Applications*, J. Roncali, *Macromol. Rapid Commun.*, **2007**, *28*, 1761–1765.
- [8] *Quinoidal/Aromatic Transformation in π -Conjugated Oligomers: Vibrational Raman Studies on the Limit of Rupture of π -Bonds*, P. Mayorga Burrezo, J. L. Zafra, J. T. López Navarrete and J. Casado, *Angew. Chem. Int. Ed.*, **2017**, *56*, 2250–2259.
- [9] *Insights into Current Limitations of Density Functional Theory*, A. J. Cohen, P. Mori-Sánchez and W. Yang, *Science*, **2008**, *321*, 792–794.
- [10] *Achievements in resonance Raman spectroscopy Review of a technique with a distinct analytical chemistry potential*, E. V. Efremov, F. Ariese and C. Gooijer, *Analytica Chimica Acta*, **2008**, *606*, 119–134.
- [11] *Modern Raman Spectroscopy – A Practical Approach*, E. Smith and G. Dent; John Wiley & Sons, Ltd: United Kingdom, **2004**.
- [12] *Hydrogen Bonding Effects on Infrared and Raman Spectra of Drug Molecules*, L. Bondesson, K. V. Mikkelsen, Y. Luo, P. Garberg and H. Agren, *Spectrochimica Acta A*, **2007**, *66*, 213–224.
- [13] *Structural and Electronic Contributions to Hyperpolarizability in Methyl *p*-Hydroxy Benzoate*, D. Sajan, H. Joe, V. S. Jayakumar and J. Zaleski, *J. Mol. Struct.*, **2006**, *785*, 43–53.
- [14] *Robust Ethylenedioxythiophene-Vinylene Oligomers from Fragile Thiophene-Vinylene Cores: Synthesis and Optical, Chemical and Electrochemical Properties of Multicharged Shapes*, P. Mayorga Burrezo, B. Pelado, R. Ponce Ortíz, P. De la Cruz, J. T. López Navarrete, F. Langa and J. Casado, *Chem. Eur. J.*, **2015**, *21*, 1713–1725.

- [15] *Multifaceted Regioregular Oligo(thieno[3,4-b]thiophene)s Enabled by Tunable Quinoidization and Reduced Energy Band Gap*, F. Liu, G. L. Espejo, S. Qiu, M. Moreno Oliva, J. Pina, J. S. Seixas de Melo, J. Casado, X. Zhu, *J. Am. Chem. Soc.*, **2015**, *137*, 10357–10366.
- [16] *On the Biradicaloid Nature of Long Quinoidal Oligothiophenes: Experimental Evidence Guided by Theoretical Studies*, R. Ponce Ortiz, J. Casado, V. Hernández, J. T. López Navarrete, P. M. Viruela, E. Ortí, K. Takimiya and T. Otsubo, *Angew. Chem. Int. Ed.*, **2007**, *46*, 9057–9061.
- [17] *Quinoidal Oligothiophenes: Towards Biradical Ground State Species*, R. Ponce Ortiz, J. Casado, S. Rodríguez González, V. Hernández, J. T. López Navarrete, P. M. Viruela, E. Ortí, K. Takimiya and T. Otsubo, *Chem. Eur. J.*, **2010**, *16*, 470–484.
- [18] *Polarons, Bipolarons and Solitons in Conducting Polymers*, J. L. Brédas and G. B. Street, *Acc. Chem. Res.*, **1985**, *18*, 309–315.
- [19] *Polarons, Bipolarons, and Side-By-Side Polarons in Reduction of Oligofluorenes*, L. Zaikowski, P. Kaur, C. Gelfond, E. Selvaggio, S. Asaoka, Q. Wu, H.-C. Chen, N. Takeda, A. R. Cook, A. Yang, J. Rosanelli and J. R. Miller, *J. Am. Chem. Soc.*, **2012**, *134*, 10852–0863.
- [20] *Electronic Absorption and Vibrational Spectroscopies of Conjugated Conducting Polymers*, Y. Furukawa, *J. Phys. Chem.*, **1996**, *100*, 15644–15653.
- [21] *Pushing Extended p-Quinodimethanes to the Limit: Stable Tetracyano-oligo(N-annulated perylene)quinodimethanes with Tunable Ground States*, Z. Zeng, M. Ishida, J. L. Zafra, X. Zhu, Y. Mo Sung, N. Bao, R. D. Webster, B. S. Lee, R.-W. Li, W. Zeng, Y. Li, C. Chi,† J. T. Lopez Navarrete, J. Ding, J. Casado, D. Kim, and J. Wu, *J. Am. Chem. Soc.*, **2013**, *135*, 6363–6371.
- [22] J. L. Zafra. *Birradicales Kekulé. Espectroscopía Raman en la Transición Singlete-Triplete*. Ph. D. Dissertation, University of Málaga, 2014. Retrieved from <http://hdl.handle.net/10630/8632>.
- [23] *FT-Raman Studies of Charged Defects Created on Methyl End-Capped Oligothiophenes by Doping with NOBF₄*, J. Casado, V. Hernández, S. Hotta and J. T. López Navarrete, *Adv. Mater.*, **1998**, *10*, 1458–1461.
- [24] *Spectroelectrochemical Raman Study of Two End-Capped Sexithiophenes with Applications as Electroactive Molecular Materials*, J. Casado, H. E. Katz, V. Hernández and J. T. López Navarrete, *J. Phys. Chem. B.*, **2002**, *106*, 2488–2496.

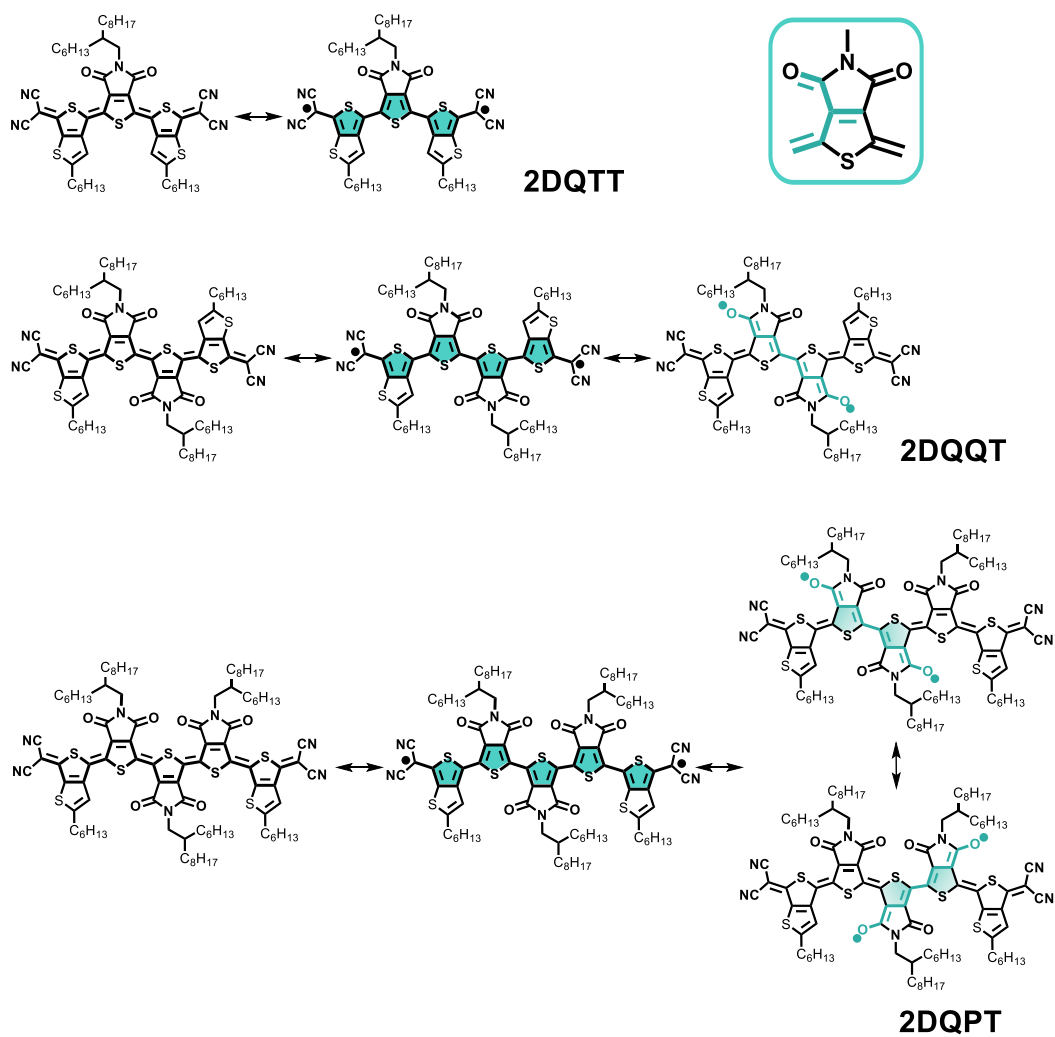
B. CROSS-CONJUGATED DIRADICALS



3. The case of Quinoidal Oligothienopyrrolediones: The Effect of Size

| | |
|--|----------------|
| 3.1 Neutral Species of 2DQoT Oligomers..... | 133—146 |
| A. Electronic Structure..... | 133—139 |
| B. Molecular Structure..... | 140—146 |
| 3.2 Charged Species of 2DQoT Oligomers. N-Doping..... | 147—165 |
| A. Electronic Structure..... | 147—152 |
| B. Molecular Structure..... | 153—158 |
| C. 2DQoT as Stable N-Doped Conductors..... | 159—165 |
| 3.3 Cross-Conjugation in Closed-Shell Molecules. Single Molecule Conductance..... | 166—173 |
| A. Electronic Structure of Neutral and Charged Species..... | 166—170 |
| B. Single Molecule Conductance Measurements..... | 171—173 |
| 3.4 Conclusions..... | 174—175 |
| References..... | 176—180 |

3. The Case of Quinoidal Oligothiopyrrolediones: The Effect of Size



Scheme IV.3.1. Resonant chemical structures of the molecules forming the **2DQoT** series studied in this chapter. The two alternative, orthogonal π -conjugated paths are highlighted in bold. The inset shows the cross-conjugated motif in **2DQoT** molecules.

3.1 NEUTRAL SPECIES OF 2DQoT OLIGOMERS

A. Electronic Structure

A. I. Optical Properties

Figure IV.3.1 shows the electronic absorption spectra of **2DQoT** molecules in CH_2Cl_2 at room temperature. These oligomers present considerably red-shifted absorption bands regarding the aromatic **OTPD_n** series (see Table IV.3.1), and also differ in the band structure. For **2DQoT**, the electronic absorption spectra comprise from the visible to the NIR spectral region, while for **OTPD_n** is restricted between 340-440 nm.

The absorption maxima wavelengths (λ_{max}) are displaced when lengthening the oligomer size as follows: 749 nm \rightarrow 876 nm \rightarrow 523 nm, from **2DQTT** to **2DQPT**. The longest oligomer also present an important electronic absorption at 900 nm.

TD-DFT calculations were performed for **2DQoT** oligomers, and the main

electronic transitions are presented in Table IV.3.1. As the oligomer length is enlarged, the theoretical data deviate from the experimental spectra. However,

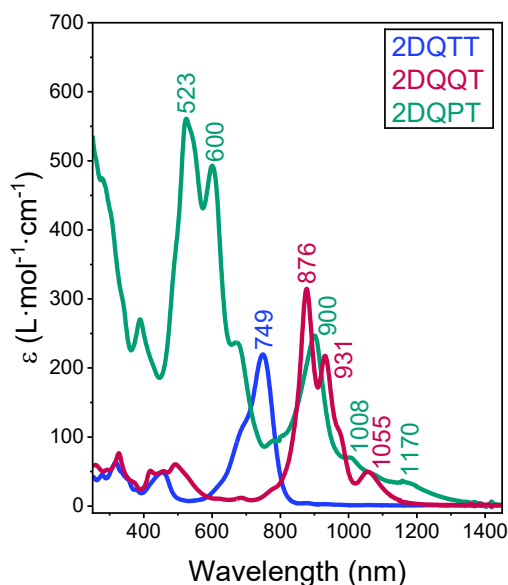


Figure IV.3.1. UV-Vis-NIR electronic absorption spectra of **2DQoT** molecules in CH_2Cl_2 at room temperature.

Table IV.3.1. Optical data of **2DQoT** and **OTPD_n** series

| n | 2DQoT ^a | | | | | OTPD _n ^a | |
|---|---------------------------------------|---|-----------------------------|-----------------------------|--------------------------------|--------------------------------|---|
| | Experimental | | TD-DFT ^b | | | λ_{max} (nm) | ϵ ($\times 10^{-5}$ L·mol ⁻¹ ·cm ⁻¹) |
| | λ_{max} (nm) | ϵ ($\times 10^{-5}$ L·mol ⁻¹ ·cm ⁻¹) | λ_{max} (nm) | Oscillator Strength (a. u.) | Electronic Transition | | |
| 2 | — | — | — | — | — | 359 (375) | 0.17 |
| 3 | 749 (690) | 219.57 | 745 | 1.02 | HOMO→LUMO | 385/398 | 0.20 |
| 4 | 876 (931) 1055 | 314.59 | 978 | 0.63 | HOMO→LUMO (α/β) | 423 | 0.29 |
| 5 | 523 (600) 900 (1006) 1008, 1170 | 560.77 247.02 | 666 | 0.75 | HOMO→LUMO (α/β) | 440 | 0.46 |
| 6 | — | — | 1041 | 0.39 | HOMO→LUMO+1 (α/β) | 453 | 0.64 |

^aMeasured in CH_2Cl_2 at room temperature. ^bTD-DFT calculations at (U)B3LYP/6-31G** level of theory ($f > 0.1$). Geometry optimization of **2DQTT** was performed as closed-shell system (spin restricted B3LYP), while **2DQQT** and **2DQPT** were optimized as singlet open-shell systems (spin unrestricted B3LYP).

the general trend is correctly reproduced: 745 nm → 978 nm → 666 nm, from **2DQTT** to **2DQPT**.

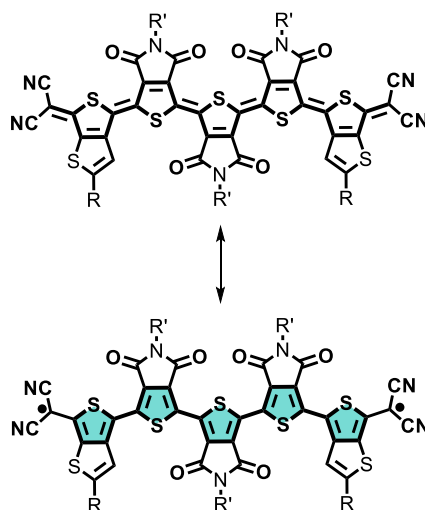
As in the case of the **OTPD_n** family, the electronic absorption maxima correspond to the HOMO→LUMO electron transition.

In addition to the main electronic absorption, **2DQQT** and **2DQPT** also show a broader feature in the near IR region. These bands are characteristic of diradicaloid systems. The presence of a low-lying excited singlet state originates a doubly excited electronic transition (H, H→L, L) responsible of a low energy electronic absorption band.^[1-3]

The classical λ_{\max} wavelengths red-shift with the oligomer size in π -conjugated molecules is clearly interrupted by the longest oligomer of **2DQoT**. The most intense band of **2DQPT** is placed at 523 nm, in the same spectral region as the **OTPD_n** molecules. This transition arises as a consequence of the large contribution of a diradical shape to the ground electronic state.^[3, 4] The main driving force for the formation of this diradical structure is the gain of aromaticity of the quinoidal thiophene rings. In Scheme IV.3.2 the resonant structures that explain this property are showed.

In this way, the electronic absorption experiments constitute the first evidence of the diradical character of the ground electronic state in the longest oligomers of the **2DQoT** family.

The relation of the different electronic transitions of **2DQoT** with their quinoidal/aromatic character is clearly observed in Figure IV.3.2. In this figure, the



Scheme IV.3.2. Quinoidal closed-shell (top) and aromatic diradical (bottom) resonant structures of **2DQPT**.

λ_{\max} wavelengths of **2DQoT** are plotted versus the number of monomeric units (n).

Also the λ_{\max} wavelengths of **OTPD_n** and a family of linearly, π -conjugated quinoidal oligothiophenes^[4] (**Q_n**) are presented (see Scheme IV.3.3 for the chemical structure of **Q_n** series). Due to the small number of compounds of this series, the Meier's plot fitting cannot be obtained for **2DQoT** family.

As can be seen in Figure IV.3.2, for both quinoidal **Q_n** and aromatic **OTPD_n** oligothiophene series λ_{\max} wavelengths successively increase with the number of monomeric units. The quinoidal family **Q_n** is red-shifted compared to the aromatic **OTPD_n**. Regarding the **2DQoT** family, λ_{\max} wavelengths of **2DQTT** and **2DQQT** are close to the values of the **Q_n** series, with a similar dependence on the number of units. However, λ_{\max} wavelength of **2DQPT** is drastically blue-shifted to a value closer to that of **OTPD₅** than to the corresponding **Q₅**.

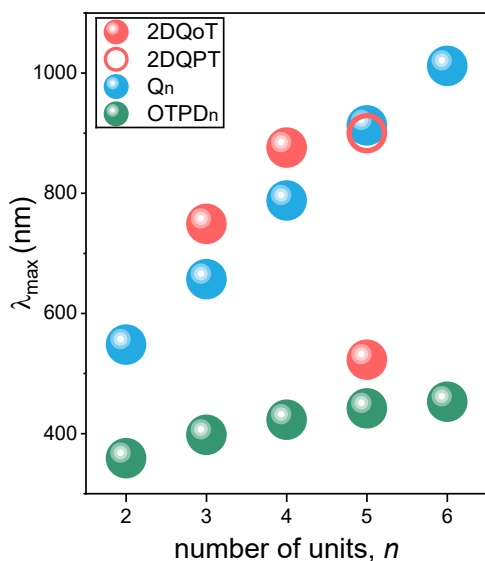
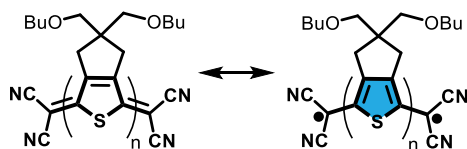


Figure IV.3.2. Plot of the λ_{\max} (nm) versus the number of monomeric units (n) of **2DQoT** (red filled circles), **Q $_n$** (blue circles) and **OTPD $_n$** (green circles) series. Red empty circle correspond to the **2DQPT** electronic absorption at 900 nm.



Scheme IV.3.3. Quinoidal closed-shell (left) and aromatic diradical (right) resonant structures of **Q $_n$** molecules (with $n = 1 - 6$).

This change indicates that **2DQPT** presents a behaviour more similar to the aromatic counterpart than to the quinoidal one. Therefore, the open-shell resonant structure in Scheme IV.3.2 displays an important contribution to the ground electronic state of **2DQPT**.

However, when the electronic transition of **2DQPT** at 900 nm is taken into account (empty red circle in Figure IV.3.2), the λ_{\max} wavelength dependence on n is kept. In this case, despite it is not

possible to perform the Meier's fitting, λ_{\max} wavelengths of **2DQoT** seem to converge to a value close to 900 nm.

The thermal activation/deactivation of the different electronic transitions present in **2DQoT** oligomers were studied through variable temperature electronic absorption (Figure IV.3.3). **2DQTT** presents the classical red-shift of the λ_{\max} due to the smaller vibrational amplitudes at low temperatures. For **2DQQT** and **2DQPT** the more remarkable result on cooling is the loss of the doubly excited electronic transition (H, H \rightarrow L, L) in the NIR region.

The contribution of the diradical character to the ground electronic state of **2DQoT** can be explored theoretically through the singlet-triplet gap. The three molecules were optimized as closed-shell

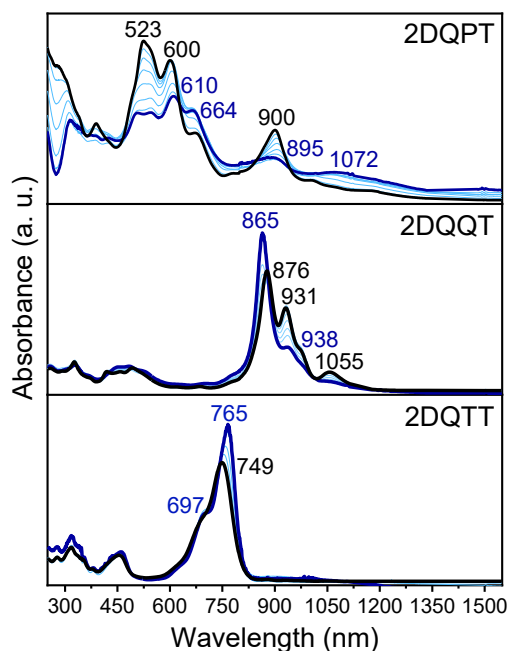


Figure IV.3.3. Variable temperature UV-Vis-NIR electronic absorption spectra of **2DQoT** oligomers in CH_2Cl_2 from room temperature (black lines) to 80 K (dark blue lines). Light blue lines correspond to absorption spectra at intermediate temperatures.

and singlet and triplet open-shell systems at the (U)B3LYP/6-31G** level of theory. The smallest formation energy was that of the singlet open-shell (S-OS) geometry for the longer oligomers, while **2DQTT** displays a closed-shell configuration. Figure IV.3.4 displays the formation energy differences between the closed-shell and the two open-shell configurations. Note that the energy differences trend with the oligomer size for **2DQoT** is similar to that found for the dianion species of **OTPD_n** systems, which were characterized as singlet open-shell structures.

While for **2DQTT** the closed-shell configuration is the most stable situation, longer oligomers have a clear singlet open-shell ground electronic states (energy differences with respect to the closed-shell structure are negative for both S-OS and T states) as a consequence of the increasing diradical character with the oligomer length. [5, 6] The *chemical* connection between the two radical centers through the oligothiophene bridge explains the stabilization of the singlet configuration instead of the triplet one, violating the Hund's rule (DSP effect).

Also, the narrowing of the singlet-triplet gap (ΔE_{S-T}) when increasing the oligomer size can be observed in Figure IV.3.4. As in the case of the **[OTPD_n]⁻²** systems, no significant variations in the planarity of these molecules occur from **2DQQT** to **2DQPT**. In consequence, the presence of a second cross-conjugated framework in **2DQPT** must be responsible of the destabilization of the singlet open-shell configuration respect to the triplet. The orthogonal π -conjugated path

interrupts the *chemical* connection between the two radical centers. The existence of a thermally populated triplet state as a consequence of the ΔE_{S-T} narrowing was experimentally demonstrated for **2DQQT** by the group of Professor Xiaozhang Zhu through EPR and SQUID measurements in solid state (see Appendix V).

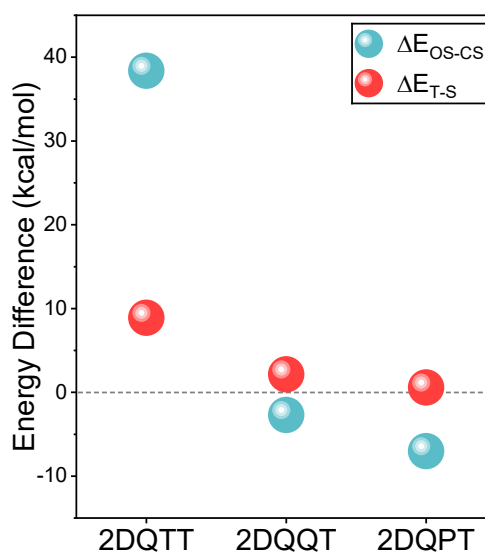


Figure IV.3.4. Formation energy differences (kcal/mol) between the singlet open-shell (OS) and the closed-shell (CS) configuration (green circles) and the triplet state respect to the corresponding ground state (red circles) of **2DQoT** molecules calculated at the (U)B3LYP/6-31G** level of theory. The singlet-triplet gap was calculated considering **2DQTT** as a closed-shell system, and **2DQQT** and **2DQPT** as singlet open-shell configurations.

A. II. Energy of the Frontier Molecular Orbitals

Since the λ_{max} wavelengths observed in the electronic absorption spectra of **2DQoT** correspond to the HOMO→LUMO

electron transitions, the energy levels of the frontier molecular orbitals were calculated (Figure IV.3.5). As for **OTPD_n**, the energy of the optical bandgap of the **2DQoT** family is also narrowed as the oligomer length is enlarged.

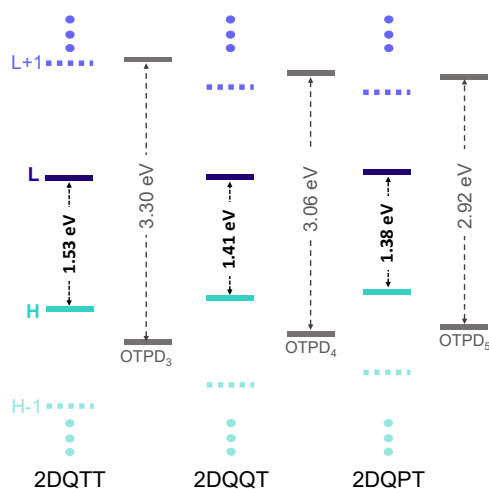
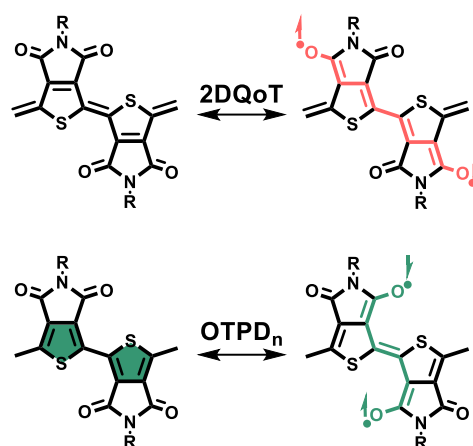


Figure IV.3.5. Energy of the frontier molecular orbitals of the **2DQoT** oligomers calculated at the (U)B3LYP/6-31G** level of theory, together with those calculated for the **OTPD_n** counterparts (grey levels). Green lines correspond to the HOMO levels; blue lines correspond to the LUMOs; dashed lines correspond to the HOMO-1 and LUMO+1 levels.

The destabilization/stabilization of the HOMO/LUMO levels when the oligothiophene backbone is *quinoidized* can be observed comparing with the frontier molecular orbitals of **OTPD_n** family in Figure IV.3.5 (grey levels). Regarding both β , β' -disubstituted oligothiophene families, not only the quinoidization of the linear backbone must be taken into account, but also the different cross-conjugated structures. While for **OTPD_n** the number of cross-conjugated paths is $n-1$, being n the number of monomeric units (**OTPD₂** \rightarrow 1 inter-dione path; **OTPD₃** \rightarrow 2 inter-dione path, etc.), for the **2DQoT**

oligomers the quinoidal structure and the outmost thieno[3,4-b]thiophene (TbT) units restraint this number. For **2DQoT**, the cross-conjugated framework is not established between the two closest carbonyl groups of vicinal TPD moieties, as in **OTPD_n** (see Scheme IV.3.4). The quinoidal pattern forces the π -cross-conjugated sequence through the distal carbonyl groups of adjacent TPD units, according to Schemes IV.3.1 and IV.3.4:



Scheme IV.3.4. Closed-shell (left) and cross-conjugated singlet open-shell (right) resonant structures of **2DQoT** (top) and **OTPD_n** (bottom) series. π -Cross-conjugated framework between nearby carbonyl groups is highlighted in green, while the one between distal carbonyl groups is highlighted in red.

With this structural changes in mind, **2DQTT** has not cross-conjugation properties, **2DQQT** presents only one cross-conjugated path and **2DQPT** has two equivalent inter-dione frameworks (see Scheme IV.3.1 for the corresponding resonant structures of the complete **2DQoT** family). The shorter number of TPD moieties in **2DQoT** molecules regarding their **OTPD_n** counterparts confines the 2D conjugation in the centre of the molecule

(the external TbT units do not participate in this 2D π -delocalization).

In analogy with the frontier molecular orbitals energy levels discussion for **OTPD_n** oligomers, the main contributions to the HOMO-LUMO gap differences between the two oligothiophene series are the following:

1. The aromaticity or resonance stabilization energy. According to the contribution of the ring aromaticity to the HOMO-LUMO gap, quinoidal molecules will present narrower gaps since π -electrons are not confined within the rings.^[7, 8] As explained above, this is the main reason for the red-shift of the λ_{max} wavelengths of the **2DQoT** family respect to those of the **OTPD_n** series.

2. The planarity or rigidity of the system. The exocyclic $C_{\alpha}=C_{\alpha}$ double bond in quinoidal oligothiophenes avoids the rotation between two consecutive monomeric units. This rigidification of the conjugated structure reduces the E_g value because of the enhancing of the π -overlapping between successive monomeric units.

3. The substituent groups. The most important difference between **2DQoT** and **OTPD_n** families regarding the substituent groups are the dicyanomethylene moieties in the former. The presence of these highly electron-withdrawing groups stabilizes the LUMO levels, and consequently narrows the HOMO-LUMO gap. Another important property of quinoidal systems derived from the low-lying LUMO level is the possibility of perform n-doping processes

to obtain n-type organic semiconducting molecules.^[9-11]

A. III. Topologies of the Frontier Molecular Orbitals

Figure IV.3.6 discloses the topologies of the frontier molecular orbitals of **2DQoT** family. For the shortest oligomer of the series, with a closed-shell configuration of its ground electronic state, HOMO and LUMO levels are reversed to those of the **OTPD₃** analogue.^[6]

However, for longer oligomers the quinoidal/aromatic nature of the HOMO/LUMO are not as clear as in the case of **2DQTT**, especially for the central TPD moieties. In these units, the wave function is spread towards the carbonyl groups, highlighting their participation in the electronic structure of these molecules. In addition, the bonding nature of the exocyclic $C_{\alpha}=C_{\alpha}$ double bonds is less marked than in the case of the quinoidal *tert*-thiophene.

This distribution of the π -electron density supports the idea of a high contribution of a diradical cross-conjugated form to the molecular structure in longer molecules. Observing the central thienopyrrole-dione moieties, the π -overlapping between the C_{β} of the thiophene units and the C of the carbonyl group accounts for the cross-conjugation property.

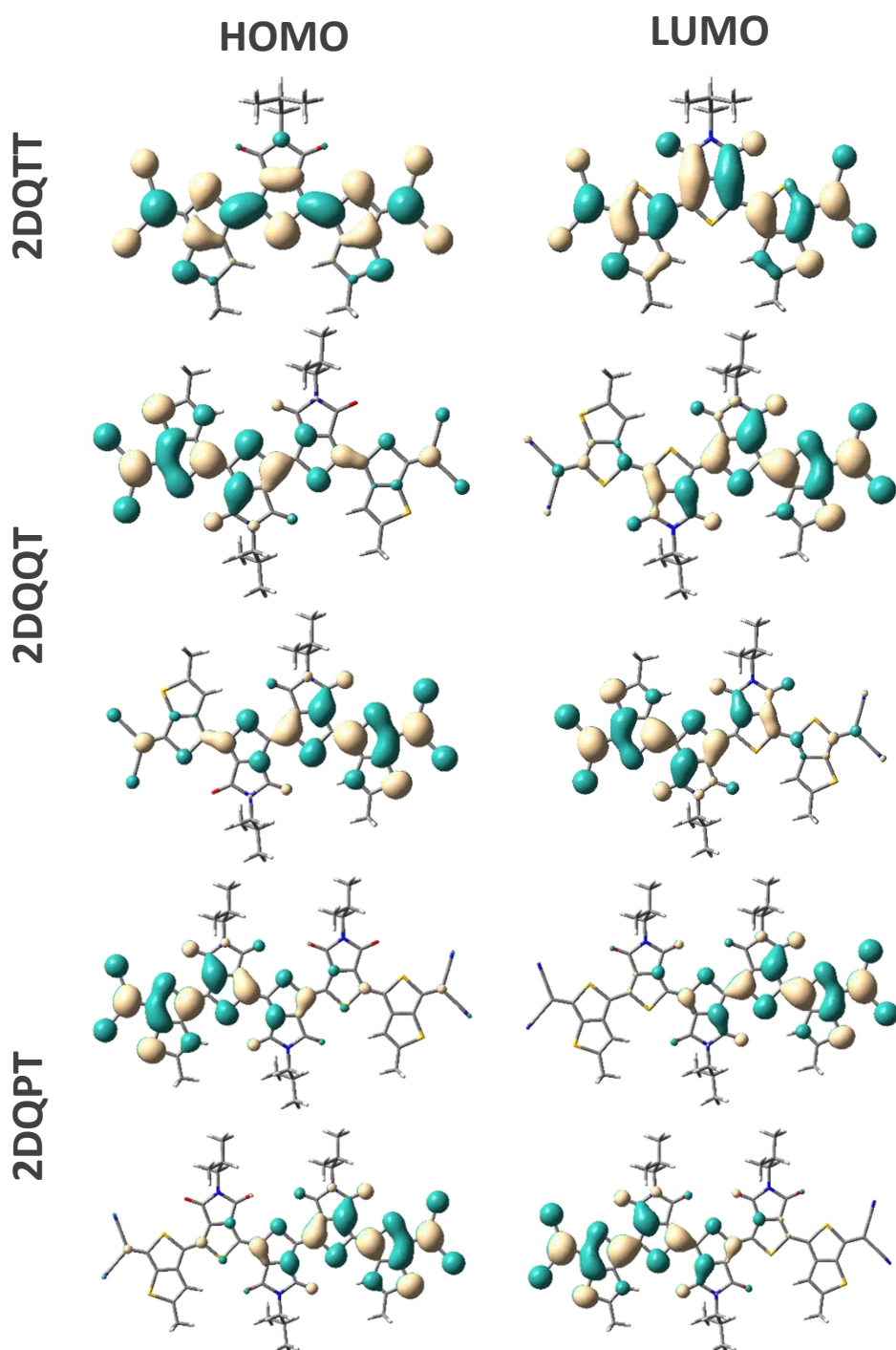


Figure IV.3.6. Topologies of the frontier molecular orbitals of **2DQoT** oligomers calculated at the (U)B3LYP/6-31G** level of theory as singlet open-shell systems for **2DQQT** and **2DQPT**, and **2DQTT** with a closed-shell configuration. For singlet open-shell configurations: α -spins (top) and β -spins (bottom) are shown.

B. Molecular Structure

B. I. Vibrational IR Spectroscopic Properties

The carbonyl and cyano groups of **2DQoT** molecules were studied through vibrational IR spectroscopy thanks to their large IR intensity. Figure IV.3.7 displays the experimental (black lines) and theoretical (grey lines) IR spectra of these samples at room temperature. According to the eigenvectors of **2DQQT** in Table IV.4.2, signals around 2190-2210 cm^{-1} correspond to the stretching vibration of the $\text{C}\equiv\text{N}$ groups (ν_{CN}), while bands at 1770-1690 cm^{-1} are due to the stretching vibration of the $\text{C}=\text{O}$ groups (ν_{CO}).

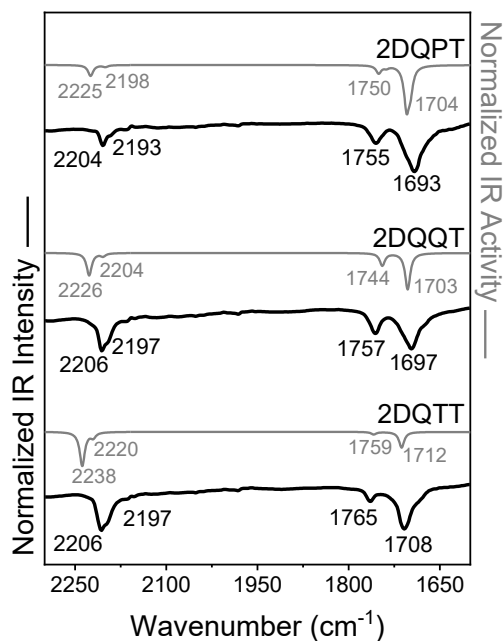
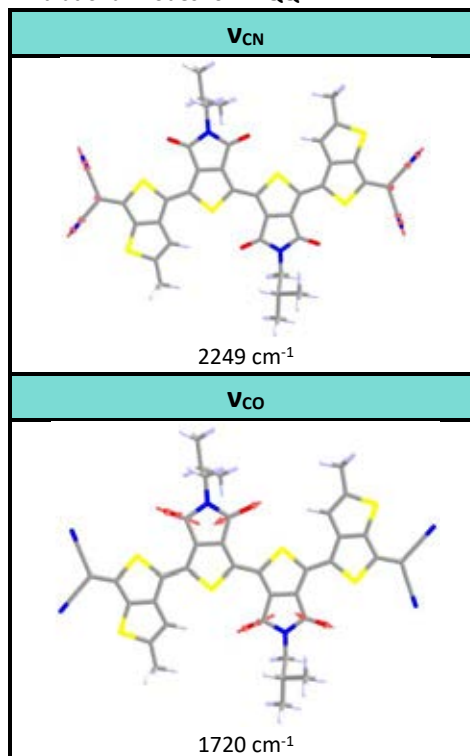


Figure IV.3.7. $\nu_{\text{C}=\text{O}}$ and $\nu_{\text{C}\equiv\text{N}}$ region of FT-IR spectra of **2DQoT** oligomers in solid state at room temperature; From bottom to top: **2DQTT**, **2DQQT** and **2DQPT**. Black lines correspond to the experimental IR spectra while grey lines correspond to the theoretical IR spectra calculated at the (U)B3LYP/6-31G** level of theory and scaled down uniformly by a factor of 0.96.

Table IV.3.2. Eigenvectors of the discussed IR vibrational modes for **2DQQT**.



The evolution of the ν_{CN} in Figure IV.3.7 is: 2206/2197 cm^{-1} \rightarrow 2206/2197 cm^{-1} \rightarrow 2204/2193 cm^{-1} , from **2DQTT** to **2DQPT**. The characteristic wavenumber of α , β -unsaturated cyanides systems is 2240-2215 cm^{-1} .^[12] The down-shifted ν_{CN} bands of **2DQoT**, specially for **2DQPT**, are due to the mesomeric effect caused by the contribution of the diradical. This trend was also observed in the IR vibrational spectra of Q_n oligomers.^[5, 6]

Regarding the carbonyl groups, from **2DQTT** to **2DQPT**: 1708/1765 cm^{-1} \rightarrow 1697/1757 cm^{-1} \rightarrow 1693/1755 cm^{-1} . $\nu_{\text{C}=\text{O}}$ bands progressively down-shift when increasing the number of TPD moieties, that is, with the number of cross-

conjugated paths. In **2DQTT** the carbonyl groups are decoupled from the π -delocalization framework, presenting the larger wavenumber values. Upon adding one TPD moiety, in **2DQQT**, $\nu_{C=O}$ downshifts by 8-11 cm^{-1} , due to the conjugation effect between the carbonyl groups of the two vicinal TPD units (inter-dione paths). From **2DQQT** to **2DQPT** this displacement is not as dramatic as for the shortest oligomer.

B. II. Vibrational Raman Spectroscopic Properties

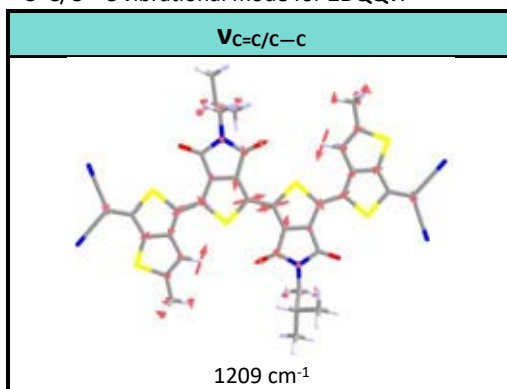
Vibrational Raman spectra of solid **2DQoT** oligomers at room temperature are showed in Figure IV.3.8.

According to the eigenvectors showed in Table IV.3.3, Raman bands at 2200 - 2215 cm^{-1} are assigned to the stretching vibration of the $C\equiv N$ groups (ν_{CN}). This vibration mode evolves from 2213 cm^{-1} in **2DQTT** to 2206 cm^{-1} in **2DQPT** (ν_{CN} was not detected for **2DQQT**). The formation of a diradical **2DQPT** species weakens the $C=C$ double bond between the dicyanomethylene moieties and the pentathiophene backbone and, as a consequence, provokes the debilitation of the $C\equiv N$ bond (diminishes the stretching force constant), and subsequently downshifts the ν_{CN} Raman band.

The stretching vibration of carbonyl groups ($\nu_{C=O}$), predicted to be located at 1750-1770 cm^{-1} , changes with the oligomer size as follows: 1764 cm^{-1} \rightarrow 1755 cm^{-1} \rightarrow 1761/1758 cm^{-1} , from **2DQTT** to

2DQPT. The largest down-shift of 9 cm^{-1} from **2DQTT** to **2DQQT** is due to the addition of a second TPD unit, which introduces the possibility of π -electron delocalization through the orthogonal, inter-dione framework in the tetramer. The contribution of the cross-conjugated structure (see Schemes IV.3.1 and IV.3.4) weakens the $C=O$ bonds, diminishing the $\nu_{C=O}$ wavenumber. $\nu_{C=O}$ of **2DQQT** and **2DQPT** are similar to those found for **OTPD₃₋₅** ($\nu_{C=O} = 1755\text{-}1756 \text{ cm}^{-1}$).

Table IV.3.3. Eigenvectors of the conjugated $C=C/C-C$ vibrational mode for **2DQQT**.



The more dramatic changes in the Raman spectra of **2DQoT** systems are found in the conjugated $C-C/C=C$ spectral region ($\nu_{C=C/C-C}$ bands) due to a collective ring $C=C$ stretching vibration mode,^[13-15] thus their frequencies are extremely affected by the aromatic \leftrightarrow quinoidal tautomerism. According to Scheme IV.3.5, where the $\nu_{C=C/C-C}$ mode of oligothiophenes is depicted, the increase of the quinoidal tautomer contribution to the electronic structure provokes a weakening of this mode. In consequence, the $\nu_{C=C/C-C}$ bands experiment a wavenumber down-shift.^[5, 6, 16-18]

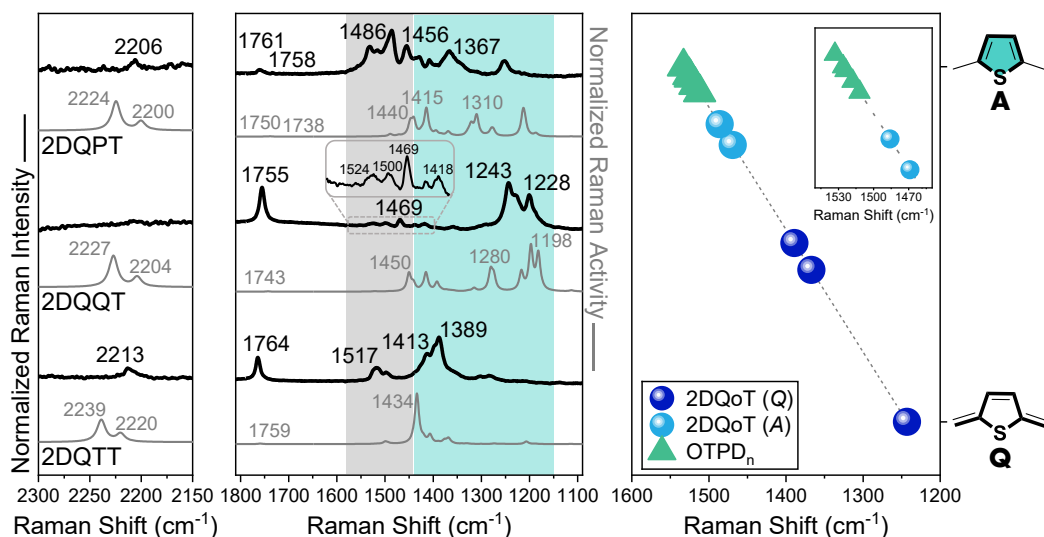
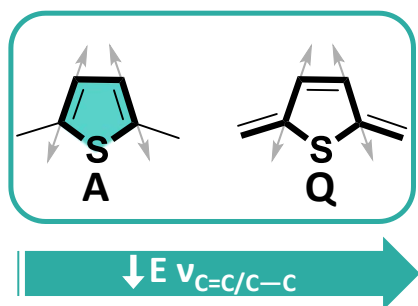


Figure IV.3.8. Left) 633 nm Raman spectra of **2DQoT** oligomers in solid state at room temperature in the $\nu_{C=N}$ (left) and $\nu_{C=O}$ and $\nu_{C=C-C}$ (right) spectral region. From bottom to top: **2DQTT**, **2DQQT** and **2DQPT**. Black lines correspond to the experimental Raman spectra while grey lines correspond to the theoretical Raman spectra calculated at the (U)B3LYP/6-31G** level of theory and scaled down uniformly by a factor of 0.96. $\nu_{C=C-C}$ mode aromatic spectral region is highlighted in grey, while the quinoidal region is highlighted in blue.; Right) Linear fit of $\nu_{C=C-C}$ Raman bands of **2DQoT** (dark blue circles for the quinoidal bands and light blue circles for the aromatic ones), and **OTPD_n** (green triangles).



Scheme IV.3.5. Representation of the $\nu_{C=C-C}$ mode in aromatic (A) and Quinoidal (Q) thiophenes. $\nu_{C=C-C}$ Raman band down-shifts with quinoidization as a consequence of the less energy vibration mode.

The evolution of the most representative Raman bands of **2DQoT** molecules in the $\nu_{C=C-C}$ mode region is: $1389 \text{ cm}^{-1} \rightarrow 1243/1469 \text{ cm}^{-1} \rightarrow 1486 \text{ cm}^{-1}$, from **2DQTT** to **2DQPT**. When comparing with the **OTPD_n** systems ($1533 \text{ cm}^{-1} \rightarrow 1512 \text{ cm}^{-1}$, from **OTPD₂** to **OTPD₆**), $\nu_{C=C-C}$ bands of **2DQoT** are considerably down-shifted

as a consequence of their quinoidal chemical structure. In addition, different from the progressive down-shift of $\nu_{C=C-C}$ with the oligomer size in **OTPD_n** molecules, for **2DQoT** systems two different regimes are observed. In Figure IV.3.8, middle, the linear fit of the $\nu_{C=C-C}$ bands of aromatic **OTPD_n** and quinoidal **2DQoT** is presented, establishing the Raman shift of **OTPD₂** as the 100% aromatic limit and **2DQTT** as the 100% quinoidal one. As discussed above, **OTPD_n** molecules are placed closer to the aromatic limit (more than 92% aromatic, according to the linear fit). However, **2DQoT** present both aromatic and quinoidal signals.

For **2DQTT** and **2DQQT** oligomers, the most important $\nu_{C=C-C}$ Raman bands are placed in the quinoidal wavenumber region (region highlighted in blue and dark blue circles in Figure IV.3.8). However,

Raman spectrum of **2DQQT** also presents a set of bands in the aromatic region (grey region and light blue circles). From **2DQTT** to **2DQQT**, $\nu_{C=C/C-C}$ evolves from 1389 cm^{-1} to 1243 cm^{-1} , according to the increase in the effective conjugation length with the oligomer size.^[5, 6, 18]

On the other hand, for the two longest oligomers important Raman bands are found in the $\nu_{C=C/C-C}$ aromatic region (note that **2DQTT** Raman band at 1517 cm^{-1} correspond to the C-H in-plane bending,^[12] on the basis of theoretical calculations). For **2DQQT**, despite the most intense band is placed at 1243 cm^{-1} , also aromatic $\nu_{C=C/C-C}$ vibrations are detected ($1500, 1649, 1418\text{ cm}^{-1}$). In the case of the longest oligomer **2DQPT**, the *aromatic* signals are even more intense than the quinoidal ones. From **2DQQT** to **2DQPT**, the most intense aromatic feature up-shifts from 1469 cm^{-1} to 1486 cm^{-1} . This enlargement in the $\nu_{C=C/C-C}$ mode indicates a higher aromatic character in the oligothiophene backbone of **2DQPT**, explained by the tautomerization of the quinoidal to the aromatic diradical form. This trend is evidenced in Figure IV.3.8, middle, where these two Raman bands (light blue circles) are closer to the **OTPD_n** region than to the other **2DQoT** wavenumbers (dark blue circles). In fact, these $\nu_{C=C/C-C}$ bands are calculated to be 74% and 84% aromatic for **2DQQT** and **2DQPT**, respectively.

The evolution of the $\nu_{C=C/C-C}$ modes in the Raman spectra are in complete agreement with the results obtained in the electronic structure studies (*Section A*), and closely reproduce the behavior of the **Q_n** series.^[5, 6] In both quinoidal

oligothiophene families, the shortest oligomers (**2DQTT** and **Q₂₋₃**) present a predominantly quinoidal electronic structure (closed-shell systems, as discussed in *Section A*). On the contrary, for the longest members (**2DQPT** and **Q₅₋₆**) the contribution of the diradical structure provokes an important aromatization of the oligothiophene framework.

Finally, for both series, **2DQQT** and **Q₄** molecules disclose an intermediate behavior between these two regimes. In this case, the inter-dione cross-conjugated resonant structure of **2DQQT** perfectly accounts for the Raman spectrum. The partial aromatization of the central TPD units when the diradical structure is formed explains the aromatic $\nu_{C=C/C-C}$ features. In contrast, the external Tbt moieties conserve their quinoidal shape.

B. III. Bond Length Alternation (BLA) Analysis

In order to determine the extension of the aromatization in **2DQoT** family and as a complementary study to the Raman spectra, the bond length alternation values (BLA) were calculated from the optimized geometries. BLA values closer to zero indicate an equalization of the C–C/C=C bonds and, in consequence, a higher degree of π -electron delocalization. As in the case of the **OTPD_n** oligomers, the linear and inter-dione paths were evaluated, as well as the BLA values within the thiophene rings (Figure IV.3.9).

Note that for quinoidal oligothiophenes

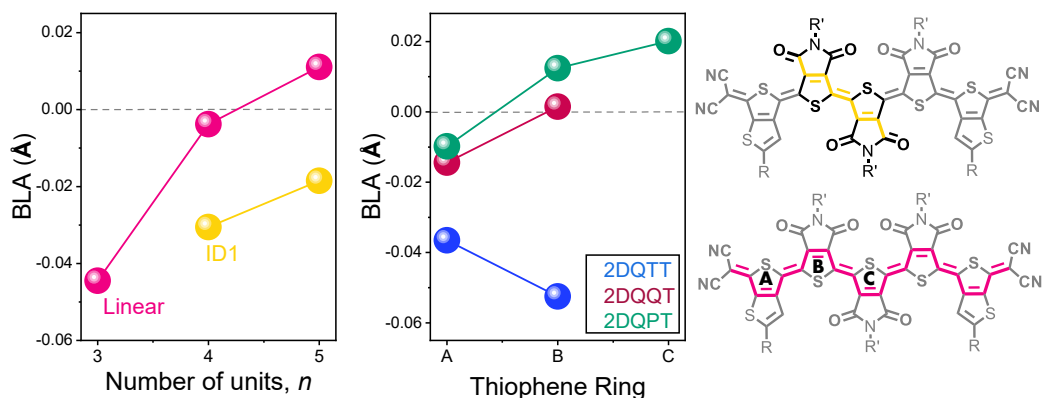


Figure IV.3.9. Bond length alternation (BLA) values (Å) for the π -conjugated paths (*left*) and for the thiophene rings (*right*) for the optimized molecular structures of **2DQoT** calculated at the (U)B3LYP/6-31G**. **2DQTT** was optimized with a closed-shell configuration while **2DQQT** and **2DQPT** were optimized as singlet open-shell systems. ID corresponds to the inter-dione paths.

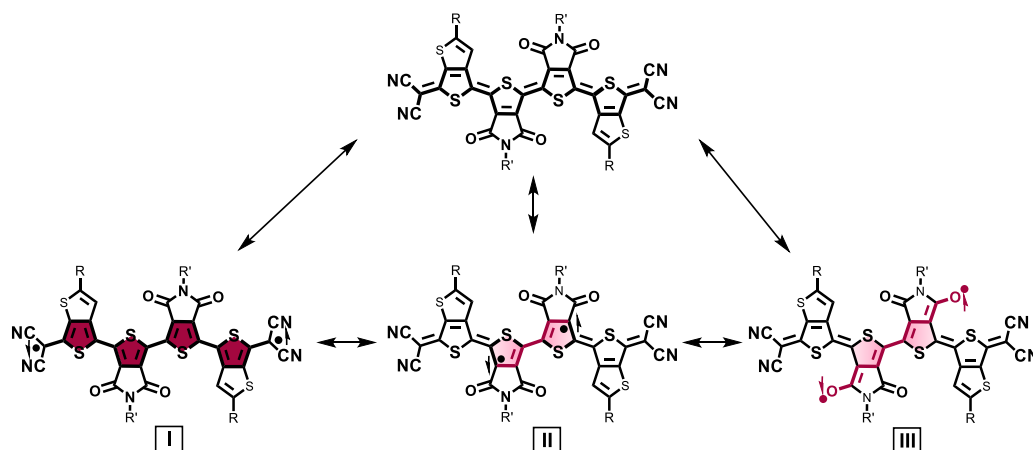
BLA values are negative since the C=C and C–C bonds are inverted respect to the aromatic counterparts.

Regarding the BLA values of the π -conjugated frameworks, both linear and inter-dione BLA values approach to zero when lengthening the oligomer size (Figure IV.3.9, *left*). Also, linear BLAs are closer to 0 than the corresponding inter-dione values. Nevertheless, in contrast with the constant value of ID paths for **OTPD_n**, for the quinoidal molecules ID absolute value diminishes from **2DQQT** to **2DQPT**. The higher diradical character of the longest oligothiophene can explain this trend, since the aromatic contribution to the molecular structure helps to equalize the C–C/C=C pattern (see the resonant structures that describe the **2DQPT** molecule in Scheme IV.3.1). However, the most remarkable result obtained for **2DQoT** molecules is the change in the sign of linear BLA values from **2DQQT** to **2DQPT**. This trend means that double and single C–C bonds are inverted, i.e., an aromatic \leftrightarrow quinoidal tautomerism

exists.^[5-7, 19, 20] According to Figure IV.3.9, in **2DQPT** the aromatic canonical form is preferred than the quinoidal one, while **2DQQT** structure is in the limit between both behaviors.

In the case of the BLA values within the thiophene rings (Figure IV.3.9, *right*), all oligomers present negative values for ring A. In the case of **2DQQT** and **2DQPT**, rings B present BLA values closer to zero, indicating a large π -electron delocalization in these central TPD moieties. The innermost thiophene unit in **2DQPT** (ring C) has the highest BLA value. In Scheme IV.3.6 the three possible resonant diradical structures of **2DQQT** are showed. Only structure II explains the electronic and molecular properties deduced from the obtained results.

However, in the case of the **2DQPT**, the two central thiophene rings (B and C) are predominantly aromatic. The presence of two cross-conjugated sequences competing for the π -electron delocalization through the innermost TPD unit cancel each other (see Scheme IV.3.7),



Scheme IV.3.6. Closed shell (left) and open-shell (right) linear (I) and cross-conjugated (II and III) resonant structures of **2DQQT** molecule.

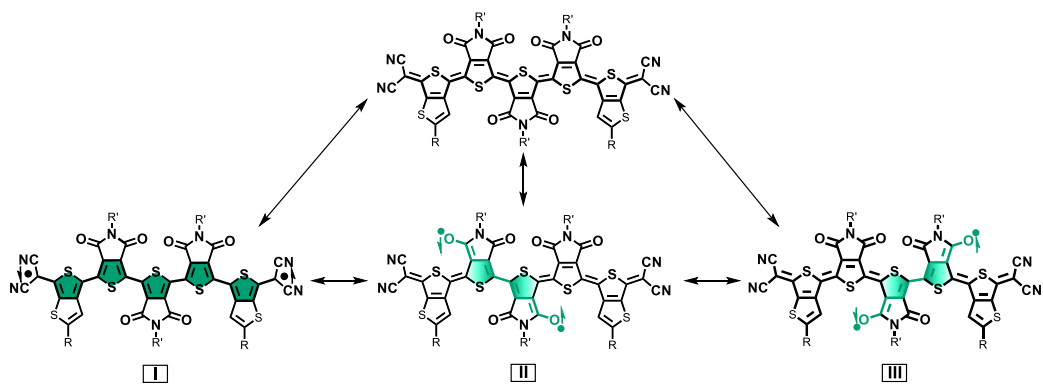
avoiding the structure presented for **2DQQT**. In consequence, the aromatic shape is spread over the most part of the oligothiophene backbone in **2DQPT** (structure I in Figure IV.3.7), in agreement with its high diradical character and accounting for the $\nu_{C=C-C}$ Raman shifts.

The radical centers of the open-shell forms of **2DQQT** and **2DQPT** (resonant structures II and III in Schemes IV.3.6 and IV.3.7) are depicted as singlets since a chemical connection can be established between them through the conjugated carbon-based backbone. In other words, **2DQQT** and **2DQPT** are presented as singlet diradicals due to the Double Spin Polarization mechanism (see *Section A. I*).

On the other hand, the behavior of the shortest molecule is completely different. The two different thiophene rings of **2DQTT** are of quinoidal nature, and the C–C/C=C pattern is less discernible in the extremes of the molecules than in the central ring B ($BLA_A > BLA_B$). This fact can be explained thanks to the effect of the

electron-withdrawing dicyanomethylene terminal groups, which attract the electron density of the oligothiophene backbone. In **2DQQT** and **2DQPT**, the larger number of units and the presence of the cross-conjugated inter-dione paths reduce the impact of the dicyanomethylene groups in the oligothiophene backbone.

3. The Case of Quinoidal Oligothiopyrrolediones: The Effect of Size



Scheme IV.3.7. Closed shell (left) and open-shell (right) linear (I) and cross-conjugated (II and III) resonant structures of **2DQPT** molecule.

3.2. CHARGED SPECIES OF 2DQoT OLIGOMERS. N-DOPING

A. Electronic Structure

A. I. Electrochemical Properties

The electrochemical processes of **2DQoT** have been studied by cyclic voltammetry in CH_2Cl_2 at room temperature (see Figure IV.3.10 and Table IV.3.4) by the group of Professor Xiaozhang Zhu.

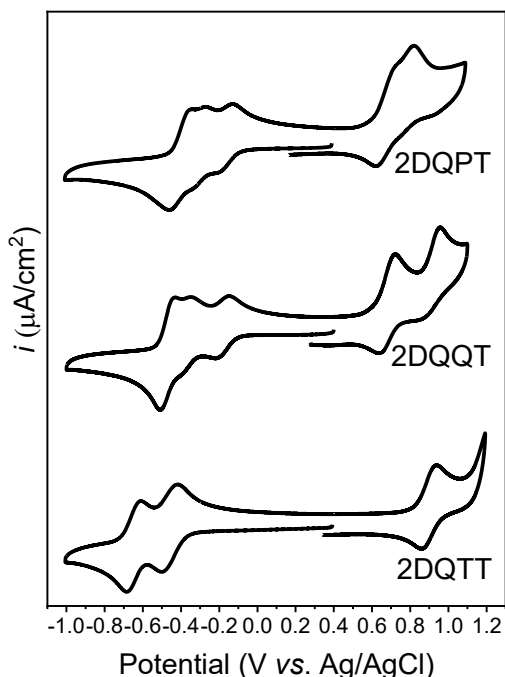


Figure IV.3.10. Cyclic voltammetry curves of **2DQoT** oligomers in 0.1M Bu_4NPF_6 in CH_2Cl_2 at room temperature (vs. Fc/Fc^+). From bottom to top: **2DQTT**, **2DQQT** and **2DQPT**.

Table IV.3.4. Electrochemical data of **2DQoT** oligomers.

| | $E_{\text{red-1}^{1/2a}}$ (V) | $E_{\text{red-2}^{1/2a}}$ (V) | $E_{\text{red-3}^{1/2a}}$ (V) |
|--------------|----------------------------------|----------------------------------|----------------------------------|
| 2DQTT | -0.46 | -0.65 | — |
| 2DQQT | -0.18 | -0.37 | -0.47 |
| 2DQPT | -0.17 | -0.30 | -0.41 |

^a Measured in 0.1M Bu_4NClO_4 in CH_2Cl_2 at room temperature (vs. Fc/Fc^+).

Figure IV.3.10 shows that **2DQQT** and **2DQPT** are characterized by three cathodic processes, while **2DQTT** only shows two separated reduction waves. Reduction potentials do not change significantly between the two longest oligomers.

A. II. Optical Properties: UV-Vis-NIR Reduction Processes

UV-Vis-NIR spectroelectrochemical reduction processes of **2DQoT** oligomers are disclosed in Figure IV.3.11 (see Table IV.3.5 for optical data). Two regimes can be identified attending to the presence of cross-conjugated inter-dione paths: one for the shortest oligomer, and another one for **2DQQT** and **2DQPT** molecules.

For **2DQTT**, addition of one electron gives rise to a two-bands pattern at 841/1557 nm (pink spectrum), classical of polaronic radical anion species.^[21, 22] This structure is similar to that found for the aromatic **OTPD_n** radical anions, in which the extra negative charge is delocalized in the linear oligothiophene backbone. In this case, the extra electron density moves between the two external dicyanomethylene groups, provoking the partial aromatization of the thiophene rings. According to the TD-DFT calculations, the most intense blue-shifted band correspond to the SOMO→LUMO electron transition, while the broader feature in the NIR region is due to the HOMO→SOMO transition.^[21, 22]

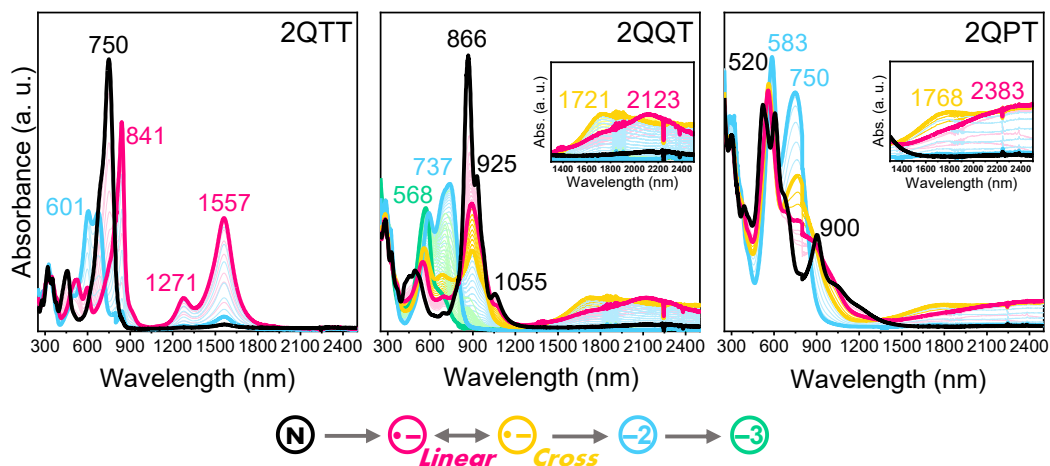
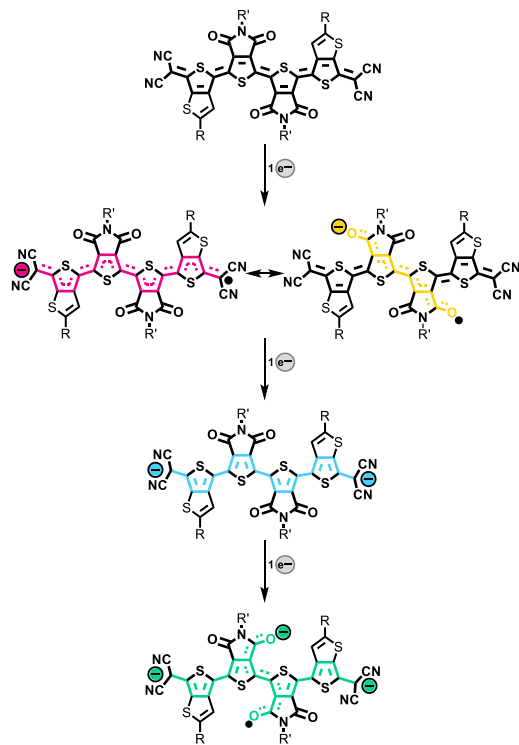


Figure IV.3.11. UV-Vis-NIR spectroelectrochemical reduction of **2DQoT** molecules in $\text{Bu}_4\text{N-PF}_6$ 0.1 M in CH_2Cl_2 at room temperature. From left to right: **2DQTT**, **2DQQT** and **2DQPT**. Black lines correspond to the spectra of neutral molecules; pink lines correspond to the spectra of the completely formed linearly conjugated radical anions, yellow lines correspond to the spectra of the completely formed cross-conjugated radical anions, blue lines correspond to the spectra of the completely formed dianions and green lines correspond to the spectra of the completely formed radical trianion species. Light color lines correspond to the intermediate spectra between the former species in the reduction process.



Scheme IV.3.8. Chemical structures of **2DQQT** upon reduction as a model of **2DQoT** family.

Neutral **2DQQT** and **2DQPT** oligomers present a similar behaviour upon addition of one electron (pink spectra in Figure IV.3.11). However, in the same potential range (before the second electrochemical wave), a new reduced species is found for **2DQQT** and **2DQPT** with a similar two bands profile: 895/1721 nm and 562/1768 nm, respectively (yellow spectra in Figure IV.3.11). The HOMO→SOMO transition of these second species are blue-shifted regarding the same bands of the first ones: 2123 nm→1721 nm and 2383 nm→1768 nm for **2DQQT** and **2DQPT**, respectively.

The fact that the second reduced species of **2DQQT** and **2DQPT** are formed in the same potential window and with a similar bands pattern than the radical anion, suggest that its nature must be similar.

Table IV.3.5. Optical data of UV-Vis-NIR spectroelectrochemical reduction of **2DQoT** oligomers in Bu₄N-PF₆ 0.1 M in CH₂Cl₂ at room temperature, together with their calculated electronic transitions at the B3LYP/6-31G** level of theory.

| 2DQoT | 2DQTT | | 2DQQT | | 2DQPT | | TD-DFT |
|-----------------------|-------------------|----------------------|-------------------|----------------------|-------------------|----------------------|------------------------------------|
| | Exp. ^a | TD-DFT. ^b | Exp. ^a | TD-DFT. ^b | Exp. ^a | TD-DFT. ^b | Electronic Transition ^b |
| Neutral | 750 (690) | 745 | 866 (925) | 978 | 900 520, 606 | — 666 | HOMO→LUMO |
| Linear Radical Anion | 841 1557/1271 | 716 1289 | 892 2123 | 840 1873 | 557 2383 | 802 2511 | SOMO→LUMO HOMO→SOMO |
| Crossed Radical Anion | — | — | 895 1721 | — | 562, 765 1768 | — | — |
| Dianion | 601/678 | 611 | 737, 590 | 791, 519 | 750, 583 | 863, 526 | HOMO→LUMO H-1→L+2 |
| Radical Trianion | 675 (626) | — | 568 | — | — | — | — |

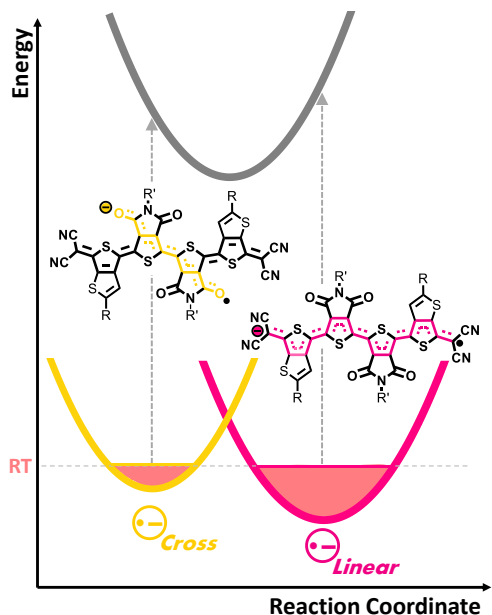
^aMeasured in Bu₄N-PF₆ 0.1 M in CH₂Cl₂ at room temperature. ^bTD-DFT calculations at (U)B3LYP/6-31G** level of theory.

Therefore, they should constitute electronic isomers or electromers, which are molecules that only differs in their electronic distribution.^[23, 24] Thus, the formation of a second radical anion in which the extra electron density is located in a different region of the molecule is proposed. Since the main structural difference between the shortest oligomer and **2DQQT** and **2DQPT** is the presence of the cross-conjugated sequences in the last two, it is evident that the second radical anion formed in the tetramer and pentamer has to be located in the interdione framework (see Scheme IV.3.8). Then, hereafter the first radical anion will be referred as *linear* radical anion (pink spectra in Figure IV.3.11), while the second one will be called *crossed* radical anion (yellow spectra) to avoid confusions between the two species. These two competing electromers constitute a local

and absolute minima in the potential energy surface of the electronic ground state of [**2DQQT**]^{•-} and [**2DQPT**]^{•-} radical anions, represented in Scheme IV.3.9.

Linear radical anion evolution with the oligomer size is: 841/1557 nm → 892/2123 nm → 557/2383 nm, from **2DQTT** to **2DQPT**. The progressive red-shift of the linear radical anion bands is in agreement with the enlargement of the linear inter-dicyanomethylenes π-conjugated path when increasing the number of monomeric units. Regarding the crossed radical anions, a considerably shorter red-shift is also found (from **2DQQT** to **2DQPT**, 0.0637 eV for the *linear* radical anion and 0.0191 eV for the *crossed* radical anion). This displacement cannot be explained by the lengthening of the oligomer size, since the cross-conjugated frameworks are independent of the extension of the linear π-conjugated backbone. In this case, the

3. The Case of Quinoidal Oligothiopyrrolediones: The Effect of Size



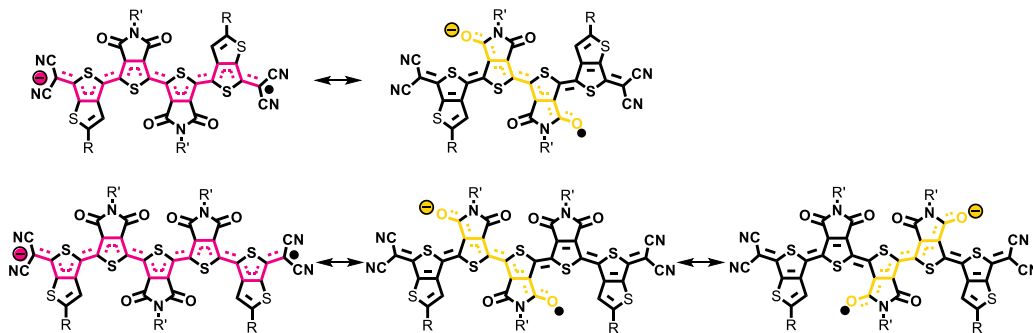
Scheme IV.3.9. Representation of the potential energy surface of the ground electronic state of the radical anion of **2DQQT** as deduced from the electronic absorption spectra.

slight changes in the crossed radical anion wavelengths on going from **2DQQT** to **2DQPT** are due to the presence of a second inter-dione framework in the pentamer, which provides a second orthogonal path for the extra electron delocalization (see Scheme IV.3.10).

The degree of aromatization when forming the radical anion species is larger

in the case of the *linear* one, which takes place in the total extension of the oligothiophene backbone. In the case of the cross-conjugated radical anions, only a partial aromatization of the thiophene rings of central TPD moieties occurs. Thus, the aromatic gain (or stabilization) for the *linear* electronic isomer is higher than that of the *crossed* one.

Upon addition of a second extra electron, for the three oligomers a similar dianion species is obtained at 678/601 nm \rightarrow 737 (590) nm \rightarrow 750 (583) nm, from **2DQTT** to **2DQPT**. Electronic absorption spectra of dianion species of π -conjugated oligomers usually present only one absorption band corresponding to the HOMO \rightarrow LUMO electron transition, forming a bipolaron structure^[21, 22] (see the electronic band assignment in Table IV.3.3). Quinoidal **2DQoT** molecules form bipolaronic dianions upon reduction, where the two extra electrons are spread along the inter-dicyanomethylene framework and causing the extensive aromatization of the oligothiophene backbone (blue structure in Scheme IV.3.8). This aromatic character of $[\mathbf{2DQoT}]^{-2}$ dianion explains the significant



Scheme IV.3.10. Resonant structures of the linear (pink lines) and cross-conjugated (yellow lines) electronic isomers of the radical anion species of **2DQQT** (left) and **2DQPT** (right).

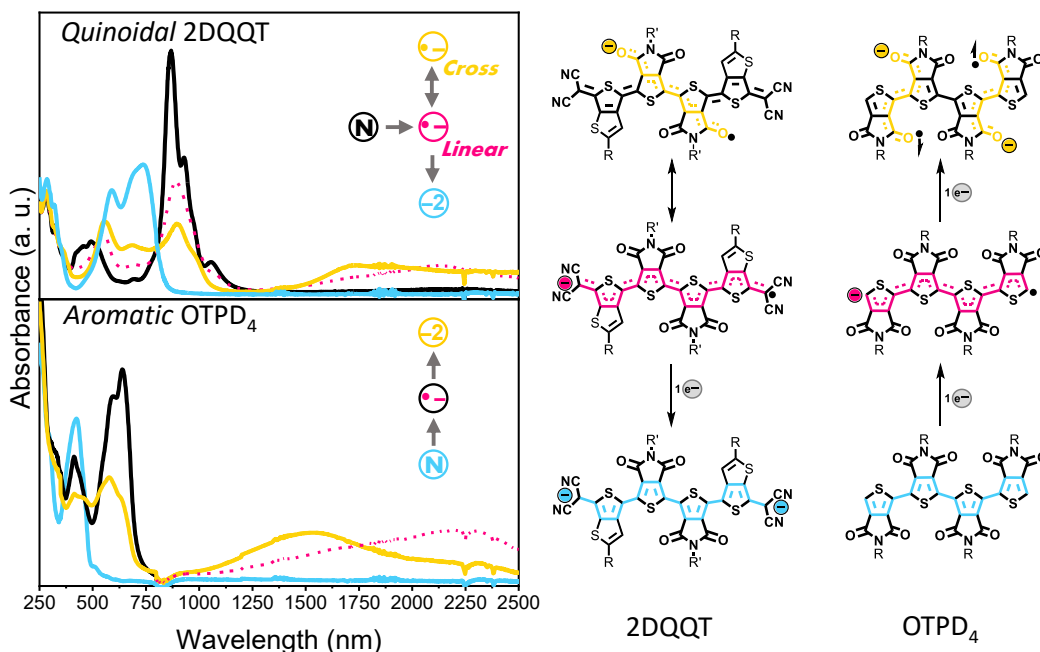


Figure IV.3.12. Left) Comparison of the neutral, radical anion and dianion UV-Vis-NIR electronic absorption spectra of the quinoidal **2DQQT** (top) and the aromatic **OTPD₄** molecules as models of their corresponding families ; Right) Comparison of the chemical structures of **2DQQT** and **OTPD₄** oligomers according to their aromatic/quinoidal patterns. Neutral and linear radical anion **2DQQT** present a quinoidal profile comparable to that of the **OTPD₄** radical anion; cross-conjugated radical anion of **2DQQT** can be related with the **OTPD₄** dianion specie; **2DQQT** dianion present the same aromatic structure as the neutral **OTPD₄**.

blue-shift of the dianion bands, with λ_{\max} wavelengths even shorter than those of the corresponding neutral specie.

When comparing with the aromatic cross-conjugated counterparts, aromatic **OTPD_n** dianions present a polaron pair pattern, locating the two extra electrons in the cross-conjugated inter-dione paths. In this sense, the polaronic radical anion species of **OTPD_n** are directly compared to the *linear* radical anions of **2DQoT**. However, the *crossed* radical anions of the quinoidal series are those that can be related with the polaron pair dianions of **OTPD_n** molecules. Figure IV.3.12 displays this relation for the tetramers of both series attending to the aromatic/quinoidal shapes of their reduced species.

Finally, a third reduced species is formed in **2DQoT** molecules upon a third reduction step (green spectra in Figure IV.3.11; not detected for **2DQPT**). The third extra electron in the radical trianion is located in the inter-dione sequence of the TPD units, orthogonal to the inter-dicyanomethylene dianion.

As mentioned in the *Energy of the Frontier Molecular Orbitals* Section, organic semiconducting molecules with low LUMO energy levels and electron-withdrawing substituents are easy to reduce chemically, making them suitable candidates for n-doping processes.^[25-27] This is actually the case of **2DQoT** oligomers, which can be conveniently

reduced with the appropriate reducing agent.

Figure IV.3.13 shows the UV-Vis-NIR titrations of **2DQoT** molecules with (2-Cyc-DMBI-Me)₂ at room temperature. This reducing agent was successfully tailored by the group of Professor Xiaozhang Zhu in 2017 for the efficient n-doping of **2DQTT** molecule,^[28] and belongs to the N-DMBI well-known family of n-doping organic agents.^[29, 30]

In contrast to the electrochemical process, only the first reduced species were found in this case. The successful reduction of neutral **2DQoT** to their corresponding radical anion species brings to light the possibility of n-doping with (2-Cyc-DMBI-Me)₂ to obtain n-type doped organic semiconductors from **2DQoT** family.

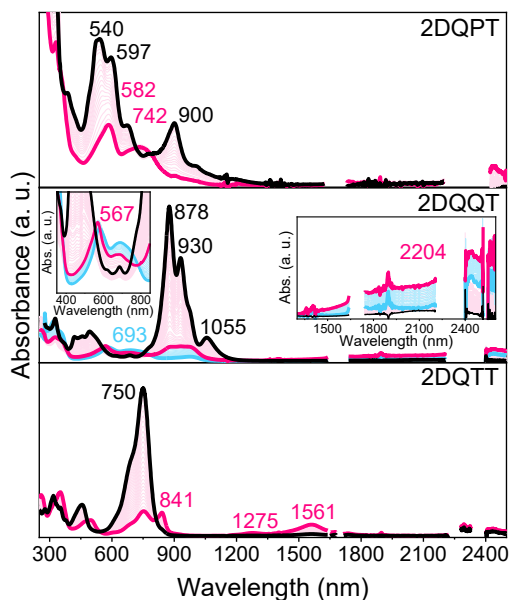


Figure IV.3.13. UV-Vis-NIR chemical reduction of **2DQoT** molecules with (2-Cyc-DMBI-Me)₂ as reducing agent in CH₂Cl₂ at room temperature. From bottom to top: **2DQTT**, **2DQQT** and **2DQPT**. Black lines correspond to the spectra of neutral molecules; pink lines correspond to the spectra of the completely formed radical anions. Light color lines correspond to the intermediate spectra between the former species in the reduction process.

Table IV.3.6. Optical data of UV-Vis-NIR chemical reduction of **2DQoT** oligomers in CH₂Cl₂ at room temperature with (2-Cyc-DMBI-Me)₂ as reducing agent.

| 2DQoT | 2DQTT | 2DQQT | 2DQPT |
|----------------------|------------------------|-------------------|-----------------|
| Neutral | 750 | 878, 930, 1055 | 900 540, 597 |
| Radical Anion | 751, 841 1561, 1275 | 567, 883 2204 | 582, 742 |

B. Molecular Structure

B. I. IR Spectroelectrochemical Reduction

To investigate the affectation of the dicyanomethylene and dione groups in the reduced species of **2DQoT**, the spectroelectrochemical reductions were also monitored by IR spectroscopy (Figure IV.3.14 and Table IV.3.7).

Upon reduction of neutral **2DQoT**, the stretching band of CN groups (ν_{CN}) moves to lower wavenumbers because of the weakening of the C \equiv N triple bond (pink spectra in Figure IV.3.14, left). The evolution of ν_{CN} with the oligomer length is: $2186 \text{ cm}^{-1} \rightarrow 2183 \text{ cm}^{-1} \rightarrow 2192/2175 \text{ cm}^{-1}$, from **2DQTT** to **2DQQT**. The antibonding character of the LUMO established when the extra electron charge is added (causing the partial aromatization of the thiophene rings) is responsible of this down-shift. Note that the radical anion ν_{CN} band in **2DQQT** and **2DQPT** is broader, denoting the presence of several species, likely the two discussed electronic isomers: the linear and the crossed radical anion species. However, since the CN groups are only affected when the extra electron is delocalized in the linear oligothiophene backbone, only one reduced species is distinguished by IR spectroscopy.

Addition of a second extra electron to the radical anion species causes the following displacement of the ν_{CN} band from **2DQTT** to **2DQPT**: $2186 \text{ cm}^{-1} \rightarrow 2170 \text{ cm}^{-1}$; $2183 \text{ cm}^{-1} \rightarrow 2173 \text{ cm}^{-1}$; $2192/2175 \text{ cm}^{-1} \rightarrow 2175 \text{ cm}^{-1}$ (blue spectra in Figure IV.3.14, left). This second electron provokes the complete aromatization of

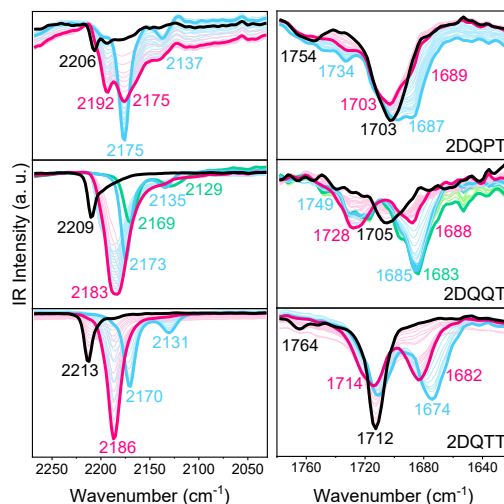


Figure IV.3.14. ν_{CN} (left) and $\nu_{\text{C=O}}$ (right) spectral region of IR spectroelectrochemical reduction of **2DQoT** molecules in $\text{Bu}_4\text{N-PF}_6$ 0.1 M in CH_2Cl_2 at room temperature. From bottom to top: **2DQTT**, **2DQQT** and **2DQPT**. Black lines correspond to the spectra of neutral molecules; pink lines correspond to the spectra of the completely formed radical anion electromers, blue lines correspond to the spectra of the completely formed dianions and green lines corresponds to the spectra of the completely formed radical trianion species. Light color lines correspond to the intermediate spectra between the former species in the reduction processes.

the thiophene backbone, explaining the ν_{CN} down-shift and the appearance of sharp bands due to the localization of the extra electrons in the dicyanomethylene units.

For **2DQPT** the radical trianion ν_{CN} band was also detected (green spectrum in Figure IV.3.14, left). In this case, the wavenumber down-shift is considerably smaller than for the other two reduction steps, denoting a lower affectation of the CN groups, since the extra electron goes to the TPD moieties.

Table IV.3.7. Optical data of IR spectroelectrochemical reduction of **2DQoT** oligomers in Bu₄N-PF₆ 0.1 M in CH₂Cl₂ at room temperature.

| 2DQoT | V _{CN} | | | V _{C=O} | | |
|------------------|-----------------|----------------|----------------------|-------------------------|---------------------------------------|-------------------------|
| | 2DQTT | 2DQQT | 2DQPT | 2DQTT | 2DQQT | 2DQPT |
| Neutral | 2213, 2188 | 2209 (2197) | 2206, 2193 (2179) | 1712, 1764 | 1705 | 1703, 1754 |
| Radical Anion | 2186 | 2183 | 2192, 2175 | 1714 (1720), 1682 | 1728 (1724), 1688 | 1703 (1689), 1731 |
| Dianion | 2170, 2131 | 2173, 2135 | 2175, 2137 | 1711, 1674 | 1685, 1730/1718, 1749 | 1697, 1687, 1734 |
| Radical Trianion | — | 2169, 2129 | — | — | 1683 (1696), 1731/1716, 1748 | — |

Figure IV.3.14, right, also displays the IR spectroelectrochemical reduction processes for the stretching band of carbonyl groups ($\nu_{C=O}$) of the of **2DQoT** molecules. Since these groups possess also an electron-withdrawing character, they constitute not only a second orthogonal π -electron delocalization path but also another region different from the CN groups for the charge injection. This is why, despite **2DQTT** does not present a cross-conjugated framework, its carbonyl groups are affected in the reduction process.

B. II. Raman Spectra of Charged Species

Resonant Raman spectra of the chemically reduced species of **2DQoT** (pink electronic absorption spectra in Figure IV.3.13) were obtained at room temperature in CHCl₃. In Figure IV.3.15 Raman spectra of **2DQoT** radical anions (black lines) are compared to those of the neutral species (grey lines).

In general, an up-shift of the main Raman bands corresponding to the $\nu_{C=C/C-C}$ modes can be observed. This is caused by a partial aromatization of the quinoidal oligothiophene backbone upon reduction.

For **2DQTT**, $\nu_{C=C/C-C}$ bands move 1390, 1416 cm⁻¹ → 1398, 1439 cm⁻¹ from neutral to radical anion. The strengthening of the C_α-C_β single bond in thiophene rings when the contribution of the aromatic structure increases is responsible of this wavenumber up-shift.

The quinoidal *quarter*-thiophene is the **2DQoT** member that presents the biggest changes in the Raman spectra upon titration. Reduction of neutral **2DQQT** provokes a clear loss of intensity of the quinoidal features and a displacement of the $\nu_{C=C/C-C}$ mode to higher wavenumbers (1415/1495 cm⁻¹ → 1527/1551 cm⁻¹, from neutral to radical anion). Aromatic $\nu_{C=C/C-C}$ feature of [**2DQQT**]^{•-} is broader than that of the linear [**2DQTT**]^{•-} (1514 cm⁻¹) due to the contribution of the two different electronic isomers.

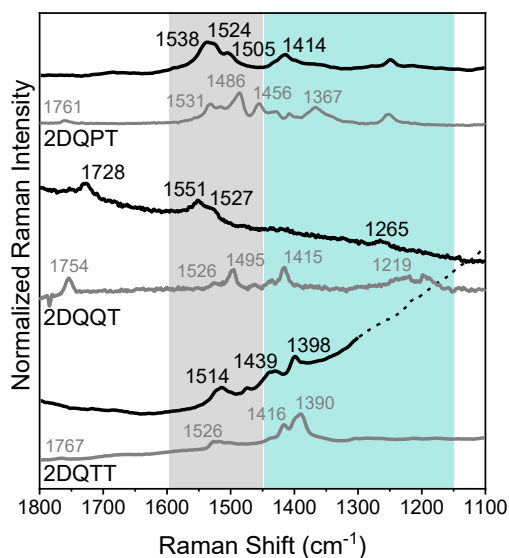


Figure IV.3.15. Resonant Raman spectra of neutral (grey lines) and radical anion (black lines) species of **2DQoT** oligomers in CHCl_3 at room temperature. Reduced species were obtained chemically through titration using N-DMBI as reductant agent. Neutral **2DQPT** corresponds to the solid 633 nm Raman spectrum, since no signal was obtained in CHCl_3 with any Raman excitation wavelength. From bottom to top: **2DQTT**, **2DQQT** and **2DQPT**. $\nu_{\text{C}=\text{C}/\text{C}-\text{C}}$ aromatic spectral region is highlighted in grey, while the quinoidal region is highlighted in blue.

Upon addition of one extra electron, aromatic $\nu_{\text{C}=\text{C}/\text{C}-\text{C}}$ Raman bands of **2DQPT** experiments an intensification respect to the quinoidal ones. The main bands evolve: $1367 \text{ cm}^{-1} \rightarrow 1414 \text{ cm}^{-1}$, $1486 \text{ cm}^{-1} \rightarrow 1524/1528 \text{ cm}^{-1}$ from neutral to radical anion species.

When including the Raman wavenumbers of the $\nu_{\text{C}=\text{C}/\text{C}-\text{C}}$ mode of **[2DQQT]^{•-}** in the **OTPD_n** and **2DQoT** fit, the values perfectly adjust to the linear trend (Figure IV.3.16). According to the discussion above, **[2DQTT]^{•-}** presents the more quinoidal character of the radical anion species, but slightly more aromatic than the corresponding neutral species (from 50% to 53% aromatic upon

reduction). Since the superior limit of the linear fit was established with the $\nu_{\text{C}=\text{C}/\text{C}-\text{C}}$ of **OTPD₂**, these results indicate that the aromatic contribution in **2DQTT** and **2DQPT** radical anions is of the same extension as in the neutral aromatic **OTPD_n**.

On the other hand, the stretching vibration of the carbonyl groups ($\nu_{\text{C}=\text{O}}$) was only detected for **2DQQT**, and experiments a significant down-shift (26 cm^{-1}) upon reduction: $1754 \text{ cm}^{-1} \rightarrow 1728 \text{ cm}^{-1}$. This displacement implies that the carbonyl groups are highly involved in the π -electron delocalization in the reduced species. The $\text{C}=\text{O}$ double bond is weakened when the extra electron charge is delocalized through the inter-dione framework.

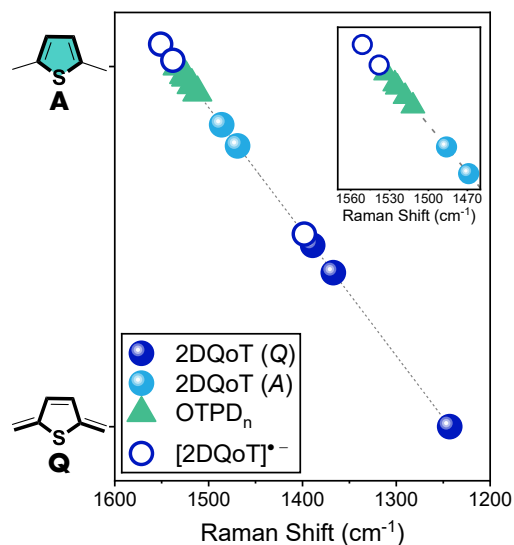


Figure IV.3.16. Linear fit of $\nu_{\text{C}=\text{C}/\text{C}-\text{C}}$ Raman bands of neutral **2DQoT** (dark blue filled circles for the quinoidal bands and light blue filled circles for the aromatic ones), **2DQoT** radical anions (empty dark blue circles) and **OTPD_n** (green triangles).

B. III. Bond Length Alternation (BLA) Analysis

In order to complete the study of the molecular structure of the anion species of **2DQoT** family, the BLA values of radical anions and dianions were calculated from their optimized geometries (Figure IV.3.17).

Regarding the radical anion species (Figure IV.3.17, left panel), despite their BLA values are closer to zero, they display the same trend when lengthening the oligomer size as in the case of the neutral molecules. Between the three oligomers, **2DQQT** presents the larger equalization of the C–C/C=C bonds pattern (pink filled circles), while **2DQTT** and **2DQPT** present a slight quinoidal/aromatic shape, respectively. These results can be directly related with the quinoidal/aromatic Raman bands of the $\nu_{C=C-C}$ mode in Figure IV.3.15. In the case of the inter-dione framework (yellow filled circles), for both **[2DQTT]^{•-}** and **[2DQPT]^{•-}** BLA values are placed in the quinoidal regime (BLA<0). It must be noted that theoretical calculations do not differentiate the two radical anion electromers. To explain the linear and ID BLA values, the C–C/C=C bonds alternation pattern within the thiophene rings must be analysed (Figure IV.3.17-right, filled circles). In all the **2DQoT** oligomers, rings B (corresponding to a central TPD moiety) display an almost equalization of their single and double C–C bonds, while rings A are slightly quinoidal. For **2DQPT**, the central thiophene ring (ring C) presents an aromatic BLA value. With these results, the main conclusion that can be extracted from the BLA analysis

of radical anion species is the larger delocalization of the electron density in the middle of the molecules due to the effect of the carbonyl groups, especially for **2DQQT** and **2DQPT**. In fact, in the pentamer even the tautomerization to the aromatic form is observed for ring C.

On the other hand, dianion species showed a different behaviour (Figure IV.3.17, empty circles in the middle and right panels). In this case, linear BLA values are clearly aromatic, while those of the inter-dione framework of the longest oligomers are around 0. Also values for the thiophene rings correspond to an aromatic profile, except for the TbT moiety in **[2DQQT]²⁻** (BLA<0), denoting the influence of the cross-conjugated inter-dione sequence in the linear π -electron delocalization framework.

According to the *Charged Species* Section discussion, Scheme IV.3.11 and IV.3.12 show the proposed structures for the **2DQQT** and **2DQPT** reduction processes.

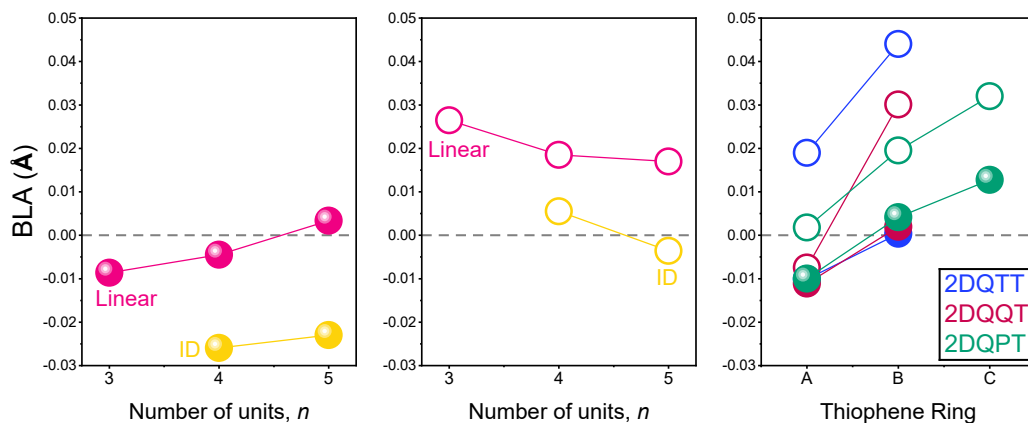
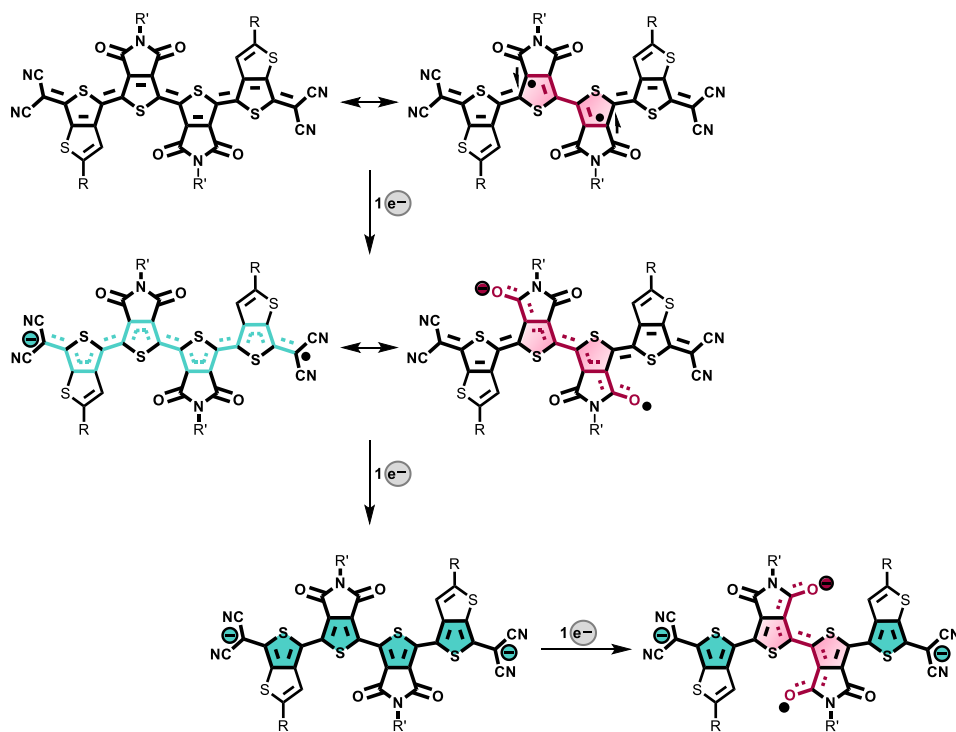
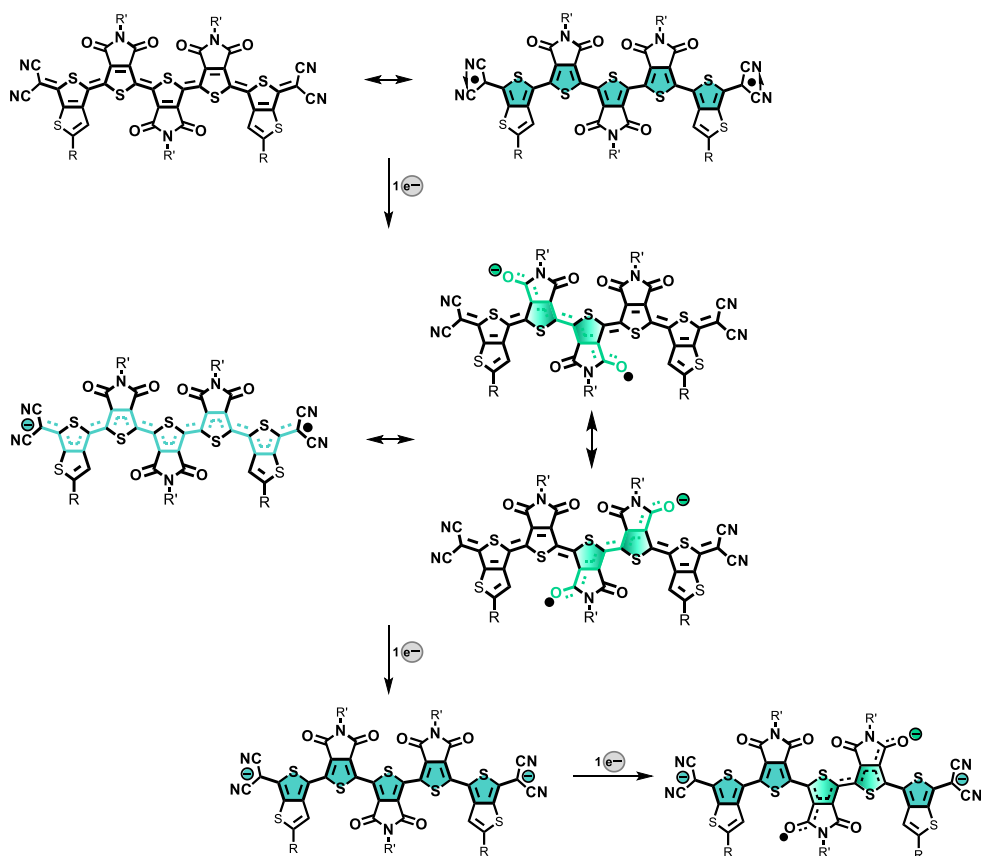


Figure IV.3.17. Calculated Bond Length Alternation (BLA) values (Å) for π -conjugated paths in radical anions (*left*, filled circles) and dianions (*middle*, empty circles) of **2DQoT** molecules, and for their thiophene rings (*right*) for the optimized geometries at (U)B3LYP/6-31G** level of theory, together with the schemes of the evaluated π -conjugated sequences (inset). ID corresponds to the inter-dione paths.



Scheme IV.3.11. Proposed structures for **2DQQT** neutral, radical anion and dianion species. The linearly interthiophene and cross-conjugated inter-dione π -conjugated paths are highlighted in blue and red, respectively.

3. The Case of Quinoidal Oligothiopyrrolediones: The Effect of Size



Scheme IV.3.12. Proposed structures for 2DQPT neutral, radical anion and dianion species. The linearly inter-thiophene and cross-conjugated inter-dione π -conjugated paths are highlighted in blue and green, respectively.

C. 2DQoT as Stable n-Doped Conductors

C. I. Electrical Conductivity and n-Doping Stability

Dicyanomethylene end-capped quinoidal oligothiophenes have been extensively studied as n-type semiconductors thanks to their low-lying LUMO energy level and their electron-deficient character. [9-11] In fact, some isomers of **2DQTT** and even **2DQTT** itself have been successfully proved as n-type semiconductor materials for ambient-stable n-channel organic thin-film transistors. [28, 31, 32] With the aim of testing the n-type semiconducting properties of the longer oligomers of the **2DQoT** family, the optical and spectroscopic characterization of the n-doped thin-films was performed.

Figure IV.3.18 displays the results of the electrical conductivity and n-doping stability experiments of **2DQoT** performed by the group of Professor Xiaozhang Zhu. (2-Cyc-DMBI-Me)₂ was employed as n-type dopant, synthesized *ad hoc* for the doping of **2DQTT** oligomer. [28]

Electrical conductivities of n-doped films of **2DQoT** measured by the four-point probe method are showed in Figure IV.3.18, left. In general, high conductivities are found for these materials, especially for the longer ones. At the optimized dopant ratio (10% molar), the best electrical conductivity (σ) was found for **2DQQT** oligomer: 14.0 S/cm. For **2DQTT** and **2DQPT**, at the same dopant ratio the electrical conductivities were 0.21 S/cm and 2.85 S/cm, respectively.

n-Doped thin-films of **2DQoT** molecules

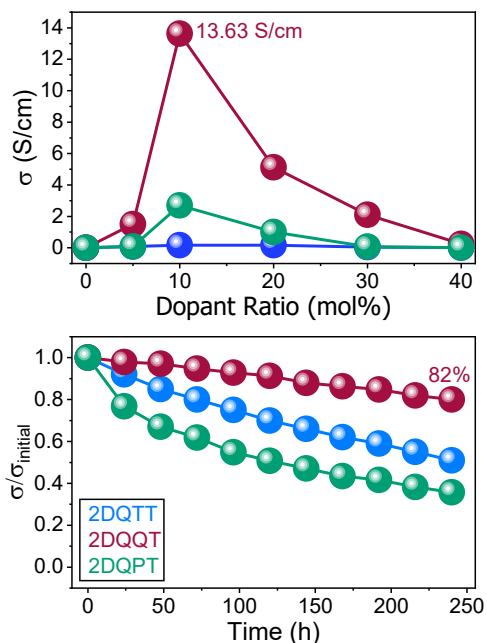


Figure IV.3.18. Left) Variation of the electrical conductivity, σ (in S/cm), of **2DQoT** oligomers when increasing the dopant ratio; Right) Attenuation ratio of electrical conductivity ($\sigma/\sigma_{\text{initial}}$) in air of **2DQoT** doped in 10% molar ratio thin-films with the exposure time. Dopant agent: (2-Cyc-DMBI-Me)₂. Blue lines correspond to **2DQTT**, red and green lines correspond to **2DQQT** and **2DQPT**, respectively.

were placed in ambient conditions monitoring their electrical conductivity over time (Figure IV.3.18, right) in order to study the stability of these materials. After 240 hours, doped **2DQQT** conserved the 82% of its initial conductivity value. **2DQTT** and **2DQPT** retained the 52% and 39% of their initial values, respectively. Conforming to these results, doped **2DQQT** presents the best ambient stability reported until now, according with the consulted bibliography. [33, 34]

Once the optimal dopant ratio was found, doped thin films characterization through optical and spectroscopic techniques was performed at the dopant

ratio of 10% in order to establish the relation between the material structure and the outstanding electrical conductivity properties of **2DQoT**, especially in the case of the quinoidal quaterthiophene.

C. II. Electronic Structure

Figure IV.3.19 and Table IV.3.8 show the UV-Vis-NIR electronic absorption spectra and λ_{\max} wavelengths of pristine and doped thin films of **2DQoT**.

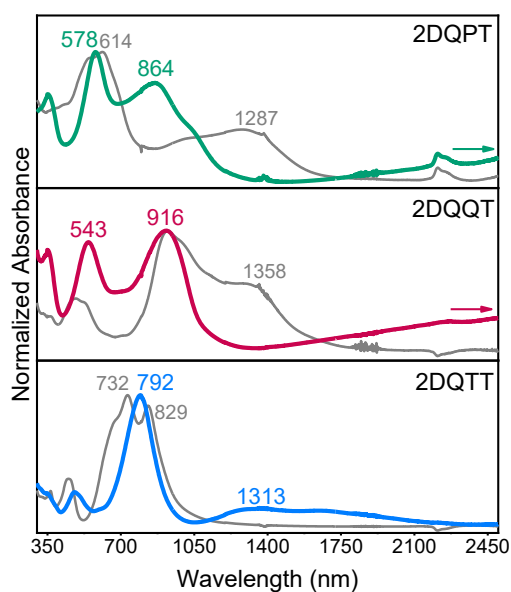


Figure IV.3.19. UV-Vis-NIR electronic absorption spectra of pristine (grey lines) and 10% mol doped (blue, red and green lines) thin films of **2DQoT** at room temperature.

Electronic absorption spectra of pristine **2DQTT** thin film (grey line in Figure IV.3.19, bottom) presents two electronic transitions at 732 nm and 829 nm that are displaced to 792 nm upon doping. Also a new, wide band at 1313 nm appears in the doped thin film. This spectrum is similar to

Table IV.3.8. Optical data of pristine and doped thin films of **2DQoT** oligomers.

| 2DQoT | λ_{\max} (nm) | |
|-------|-----------------------|--------------------|
| | Pristine | Doped ^a |
| 2DQTT | 451 | 476 |
| | 732, 829 | 792 1313 (1667) |
| 2DQQT | 485 | 543 |
| | 925, 1358 | 916 NIR |
| 2DQPT | 614, 547 | 578 |
| | 1287 (1019) | 864 NIR |

^aDopant molar ratio of 10%.

2DQTT (Figure IV.3.13) and is indicative of the formation of the radical anion species. Spectra of both thin films are broader and red-shifted compared to that obtained in solution ($\lambda_{\max} = 749$ nm), a clear indication of the formation of aggregates.^[35]

In the case of the longer quinoidal oligothiophenes, changes in the electronic absorption spectra upon doping are more pronounced. n-Doped **2DQQT** thin film shows two bands at 916 nm and 543 nm, both also present in the pristine film (925 nm, 485 nm). However, the more energy electronic absorption, related with the aromatic features of **2DQQT** molecule (Section A.1 in *Neutral Species*), is intensified after the doping process. For **2DQPT**, is the quinoidal component of the electronic spectrum that changes to 864 nm upon doping. Therefore, for both doped oligomers a certain aromatic character is revealed due to the formation of the radical anion species, in agreement with the discussion in Section A.1 of *Charged Species* and with the resonant structures in Schemes IV.3.11 and IV.3.12. In **2DQQT**, the quinoidal band and, in

consequence, the quinoidal character, is kept upon doping.

In addition, for both doped **2DQQT** and **2DQPT** thin films a new, broad band extending from 1400 nm and 1640 nm, respectively, to the middle-IR spectral region is obtained.

The formation of the radical anion species of **2DQoT** upon doping with (2-Cyc-DMBI-Me)₂ was investigated through EPR measurements, performed by the group of Professor Xiaozhang Zhu. Figure IV.3.20 displays the EPR spectra of pristine and doped thin films of **2DQoT** oligomers.

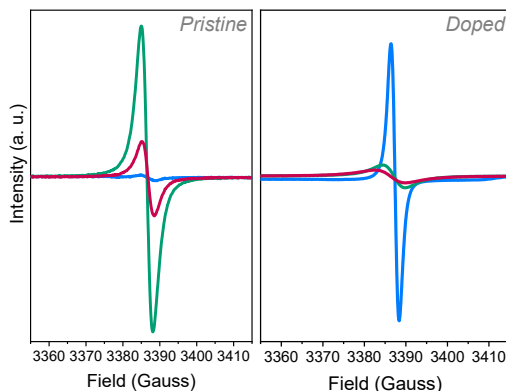


Figure IV.3.20. EPR spectra of pristine (left) and 10% mol doped (right) thin films of **2DQoT** at room temperature. Blue lines correspond to **2DQTT**, red and green lines correspond to **2DQQT** and **2DQPT**, respectively.

Figure IV.3.20 (left panel) displays the EPR spectra of pristine **2DQoT** thin films. The increasing diradical character of **2DQoT** series when lengthening the oligomer size is followed by the growing EPR signal in pristine thin films on going from **2DQTT** to **2DQPT** (CS→OS systems, see Figure IV.3.2).

Upon n-doping (Figure IV.3.20, right), the formation of [**2DQTT**]^{•-} provokes the

rise of the EPR signal for this oligomer because of the presence of the radical centre. However, in the case of **2DQPT** the inverse behaviour is observed. This evolution in the EPR signal of **2DQPT** is explained by the loss of spin concentration when going from the thermally populated triplet state in the pristine thin film to the doublet state in the doped one.

For **2DQQT** oligomer, the loss of EPR signal is not as dramatic as for the pentamer, presenting an intermediate behaviour between the other two members of the series.

C. III. Molecular Structure

Figure IV.3.21 shows the IR spectra of pristine and doped thin films of **2DQoT** molecules.

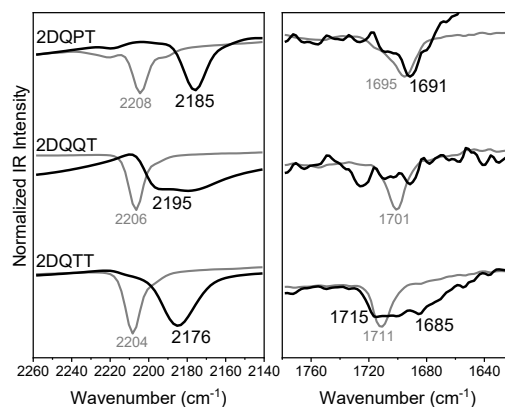


Figure IV.3.21. ν_{CN} (left) and $\nu_{\text{C=O}}$ (right) region of FT-IR spectra of thin films of **2DQoT** oligomers at room temperature. From bottom to top: **2DQTT**, **2DQQT** and **2DQPT**. Black lines correspond to the 10%-doped thin films while grey lines correspond to the IR spectra of pristine thin films.

For the three oligomers, the stretching vibration of CN groups is displaced to lower wavenumbers upon doping. This downshift is explained by the weakening of the $C\equiv N$ triple bond when the radical anion species is formed and coincides with the data obtained by the electrochemical reduction (Figure IV.3.14).

ν_{CN} evolution with the oligomer size in doped thin films is: $2176\text{ cm}^{-1} \rightarrow 2195\text{ cm}^{-1} \rightarrow 2185\text{ cm}^{-1}$, from **2DQTT** to **2DQPT**. The larger wavenumber value of doped **2DQQT** indicates that the extra electron density is not completely injected in the dicyanomethylene moieties, but it is shared among several molecules. [36, 37] In addition, the broader IR band for **2DQQT** in comparison with the other two oligomers of the series is a clear indication of the contribution of different species, i. e., the presence of the previously discussed electronic isomers.

n-Doping of **2DQoT** thin films was also investigated through Raman spectroscopy (Figure IV.3.22).

In line with the Raman spectra of the chemically reduced species (Figure IV.3.15), the $\nu_{C=C-C}$ mode of the oligothiophene backbone of **2DQoT** molecules undergoes a general upshift upon doping as a consequence of the partial aromatization of the thiophene units. As can be seen in Figure IV.3.22, the aromatic contribution to the Raman spectra increases when lengthening the oligomer size, being doped **2DQPT** predominantly aromatic. Doped **2DQQT** presents again an intermediate behaviour, with both aromatic and quinoidal contributions to its Raman spectra.

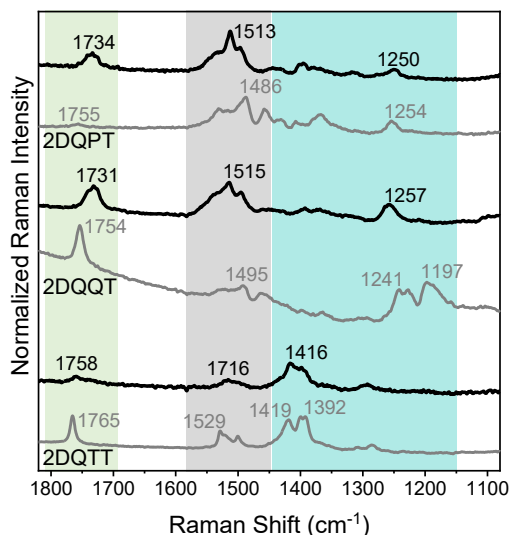


Figure IV.3.22. 633 nm Raman spectra of thin films of **2DQoT** oligomers at room temperature. From bottom to top: **2DQTT**, **2DQQT** and **2DQPT**. Black lines correspond to the 10%-doped thin films while grey lines correspond to the IR spectra of pristine thin films. $\nu_{C=C-C}$ mode aromatic spectral region is highlighted in grey, while the quinoidal region is highlighted in blue. $\nu_{C=O}$ spectral region is in green.

However, the most important changes with the doping process are found for the stretching vibrations of the carbonyl groups, $\nu_{C=O}$. This band downshifts by more than 20-cm^{-1} for doped **2DQQT** and **2DQPT** oligomers. This behaviour can be explained by the injection of the extra electron in the inter-dione framework available in the longer oligomers of **2DQoT** family (cross-conjugated electromer of the radical anion species, Schemes IV.3.10 and IV.3.11).

On the contrary, $\nu_{C=O}$ of doped **2DQTT** only suffers a displacement of 7 cm^{-1} ($1765\text{ cm}^{-1} \rightarrow 1758\text{ cm}^{-1}$ upon doping) and present the highest value among the doped **2DQoT** thin films.

The vibrational spectroscopy study allows to establish the preferential aggregation mode (observed by UV-Vis-NIR electronic absorption) for each doped

2DQoT system.

The spectroscopic data obtained for doped **2DQTT** suggest that each molecule hosts one extra charge, and the carbonyl groups are not significantly affected upon doping. Thus, the extra negative charge is injected in the dicyanomethylene moieties, promoting a slipped π - π stacking due to the intermolecular interactions between the planar radical anion species. This aggregation mode assures the maximal π -overlapping surface to also maximize the intermolecular charge transfer. The single-crystal structure of **2DQQT**^[31] confirmed these results, which are in line with other supramolecular aggregates formed in similar quinoidal trithiophene-based systems.^[9] Unfortunately, for the two longer oligomers of **2DQoT** family, single crystals could not be obtained for X-ray diffraction studies.

In the case of the **2DQPT**, the high diradical character of the neutral molecule drives the formation of σ -polymers, already observed for similar quinoidal systems with a marked diradical character.^[38] Neutral **2DQPT** presents an open-shell configuration, where the two radical centers are located in the dicyanomethylene moieties. The interaction between radical centers of vicinal **2DQPT** molecules promotes the formation of long C–C single bonds among the terminal methylene carbons. The injection of an extra electron to these σ -polymers on the doping process gives rise to its localization in the extremes of the polymer. This charge trapping prevents the appropriate electron transfer between molecules.

2DQQT must be understood as an intermediate state between the other two oligomers of the family, as the optical and spectroscopic results have shown over this chapter. The combination of its incipient diradical character and the presence of the cross-conjugated inter-dione framework provokes the confinement of the diradical centers in the two TPD moieties, in the molecular center (Scheme IV.3.6, resonant structure II). In the case of the pentamer, the higher diradical character and the competition between the two existing cross-conjugated paths prevent the stabilization of the diradical in the molecular center, extending it towards the external dicyanomethylene groups.

The location of the diradical in **2DQQT** promotes the formation of π - π stacking arrangements, driven by the overlapping between the innermost parts of the molecules. Aggregation of radical π -conjugated organic molecules has been proved to be responsible of the formation of multicenter π - π bonding structures.^[39, 40] In these arrangements, the SOMO orbitals of one molecule overlap with those of the neighboring molecule, provoking a SOMO-SOMO stabilization as a consequence of the doubly occupancy of the highest occupied molecular orbital of the dimer. These systems present a strong interaction and short intermolecular distances between the π - π stacked molecules. Considering the chemical structure of **2DQQT**, the shorter distances between molecules in this kind of arrangements imply the presence of important steric hindrance effects between the carbonyl groups of different molecules, and also between the lateral

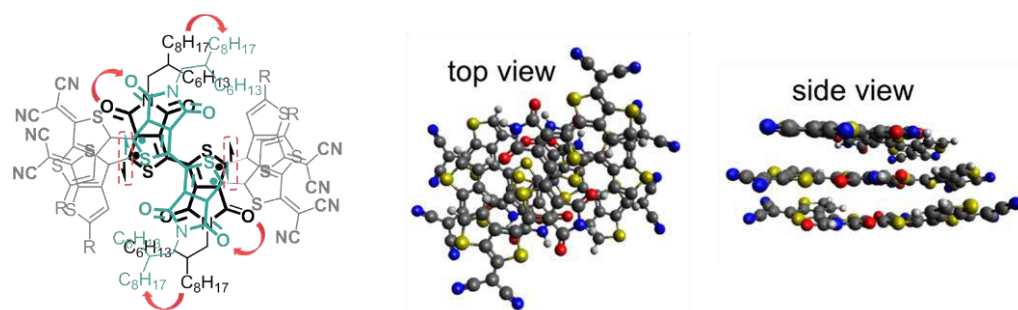


Figure IV.3.23. Left) Chemical structure of a **2DQQT** dimer in a cholesteric-like π - π stacking. Red arrows indicate the rotation displacement while dashed red squares highlight the multicentre radical bonding; Middle-Right) Optimized structure of the cholesteric-like mode of aggregation of a **2DQQT** trimer calculated at the DFT/(U) ω B97X-D/6-31G** level of theory.

branched alkyl chains. This repulsive effect pushes the molecules to rotate a certain angle respect to the previous stacked unit. This kind of aggregation mode is known as cholesteric-like π - π stacking arrangement (or helicoidal aggregation mode), and has been also observed in perylene- and naphthalene-diiimides.^[41] In Figure IV.3.23 the chemical structures of the cholesteric-like arrangement are depicted, together with the optimized structure of a trimer conformation of **2DQQT** performed by the group of Professor David Casanova.

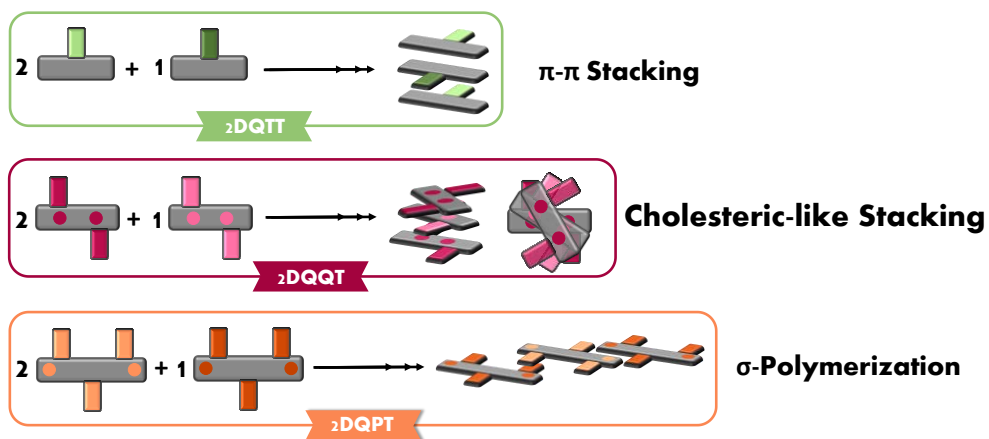
Upon n-doping of the **2DQQT** cholesteric-like π - π stacking system, the extra electron can easily delocalize through the helicoidal structure thanks to the intermolecular short distances and the limited overlapping area. This enhancement in the charge transport with respect to the classical π - π stacking and the σ -polymerization in **2DQTT** and **2DQPT**, respectively, is finally translated in the best electrical conductivity of the **2DQoT** series.

But not only its high electrical conductivity but also its outstanding ambient stability characterize **2DQQT** from

the others **2DQoT** oligothiophenes. To explain this exceptional property, two different factors must be considered:

- i) Doped **2DQQT** keeps partially its quinoidal shape due to its small diradical character and the confinement of the radical centers in the central TPD moieties. Consequently, the doped system preserves the low-lying LUMO levels of the neutral molecule. For **2DQPT**, the complete aromatization of the pentathiophene backbone provokes the rise of the LUMO energy, making the system less stable against O_2 .
- ii) The fact that the radical centers, which constitute the most chemically reactive part of the molecule, are located in the innermost area of the molecule. This disposition protects the radical centers, and the charge carriers upon doping, from external agents.

In Scheme IV.3.13, the three different aggregation modes proposed for the **2DQoT** molecules are displayed.



Scheme IV.4.13. Representation of the aggregation modes for the three oligomers of the 2DQoT family.

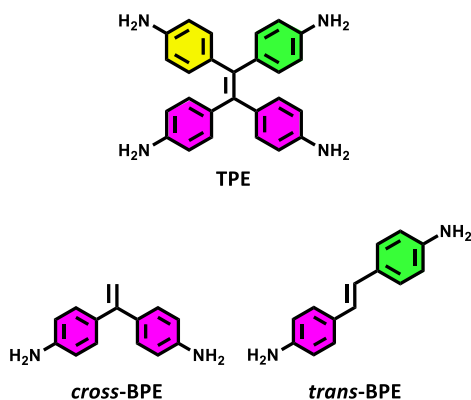
3.3. CROSS-CONJUGATION IN CLOSED-SHELL MOLECULES. SINGLE MOLECULE CONDUCTANCE

A. Electronic Structure of Neutral and Charged Species

The diradical character of **2DQoT** molecules has been proved as a determining factor in the development of the cross-conjugation properties in this family. The combination of these two features in **2DQoT** systems lead to three aggregates with different conductivities and ambient stabilities.

In the case of the aromatic counterparts **OTPD_n**, the contribution of the π -cross-conjugated framework was revealed for the dianion species, described as singlet open-shell systems.

In this context, it is reasonable to wonder about the role of cross-conjugation in closed-shell systems. With this purpose, a tetraphenyl-substituted ethene (**TPE**) has been study, together with its linear (**trans-BPE**) and cross-conjugated (**cross-BPE**) bisphenyl-substituted models. In Scheme IV.3.14 the chemical structures of these molecules are



Scheme IV.3.14. Chemical structures of **nPE** molecules.

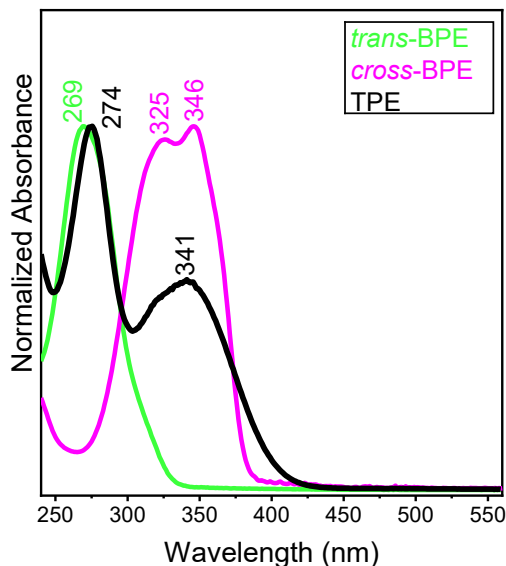


Figure IV.3.24. UV-Vis electronic absorption spectra of **nPE** molecules in CH_2Cl_2 at room temperature.

depicted. It is observed that in **TPE**, linear *trans*- and *cis*- and cross-conjugated sequences are present.

Figure IV.3.24 and Table IV.3.9 presents the UV-Vis electronic absorbance spectra and optical data of the **nPE** family in CH_2Cl_2 at room temperature.

According to the number of π -conjugated pathways, from 1 in **trans-BPE** to 3 in **TPE** molecule, the changes of the absorption maxima wavelengths (λ_{max}) are 346/325 nm \rightarrow 269 nm \rightarrow 274, 341 nm, respectively. From the mono-conjugated linear **trans-BPE** to the **cross-BPE**, the presence of a second, orthogonal π -conjugated framework provokes a downshift of the λ_{max} wavelength. It is noted that

Table IV.3.9. Optical data of nPE series.

| nPE ^a | Experimental | TD-DFT ^c | | |
|-------------------|--------------------------|--------------------------|--------------------------------|-----------------------|
| | λ_{\max} (nm) | λ_{\max} (nm) | Oscillator Strength (a. u.) | Electronic Transition |
| <i>trans</i> -BPE | 346, | 339 | 1.17 | HOMO→LUMO |
| | 325 | 293 | 0.15 | HOMO→LUMO+1 |
| <i>cross</i> -BPE | 269 | 246 | 0.45 | HOMO→LUMO+3 |
| | (280) | 274 | 0.17 | HOMO-1→LUMO |
| | | 284 | 0.11 | HOMO→LUMO |
| TPE | 274, | 278 | 0.47 | H→L+6 / H→L+4 |
| | 341 | 380 | 0.44 | HOMO→LUMO |

^a Measured in CH₂Cl₂. ^b TD-DFT calculations at B3LYP/6-31G** level of theory.

the *p*-aminophenylene moieties in **cross-BPE** are disconnected from each other. On the other hand, the electronic absorbance spectrum of the multi-conjugated **TPE** seems to be a sum of the two mono-conjugated molecules, with λ_{\max} wavelengths at 274, 341 nm.

In Table IV.3.7 also the main electronic transitions calculated at the B3LYP/6-31G** level of theory are shown. The theoretical calculations properly reproduce the experimental data. While for **trans-BPE** and in **TPE** molecules, the λ_{\max} wavelengths correspond to the HOMO→LUMO transition, in the case of **cross-BPE** it is due to a HOMO→LUMO+3 transition. In fact, the second contribution to the electronic spectrum of **TPE** (341 nm) correspond to a HOMO→LUMO+6 electronic transition.

Since **nPE** family does not constitute an oligomeric series, the study of the evolution of λ_{\max} wavelengths with the number of units (or Meier's fitting) is not applicable.

Figure IV.3.25 presents the FMO levels involved in the electronic transitions

observed in Figure IV.3.24, and their topologies.

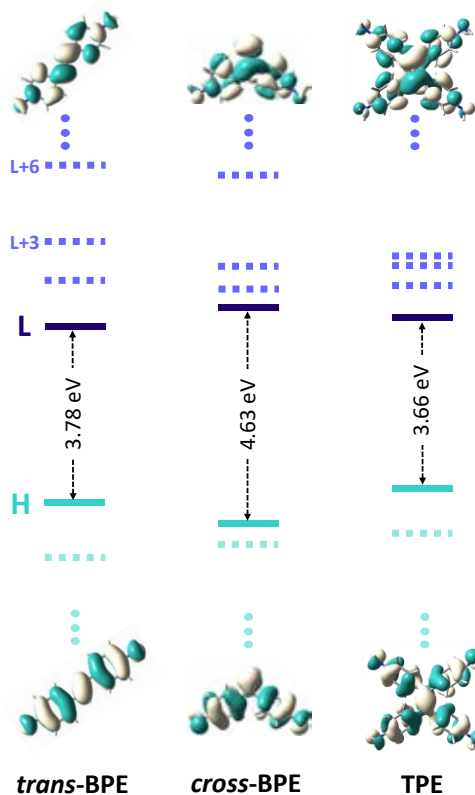


Figure IV.3.25. Energy and topologies of the frontier molecular orbitals of the **nPE** family calculated at the B3LYP/6-31G** level of theory. Green lines correspond to the HOMO levels; blue lines correspond to the LUMOs; dashed lines correspond to the HOMO-1 and LUMO+1 levels. Also, LUMO+3 and LUMO+6 are showed.

The larger value of the HOMO-LUMO gap is found for **cross-BPE** in which both HOMO and LUMO energy levels are stabilized and destabilized, respectively, regarding the other two members of the family. The competition between two orthogonal π -conjugated sequences limits the extension of the effective conjugation length, explaining this larger value of E_g . This effect was already observed in **OTPD_n** oligomers, in which the narrowing of the HOMO-LUMO gap when lengthening the oligomer size was mainly due to the molecular planarization.

For the other two molecules, they present similar optical bandgap values, with that of the **TPE** molecule slightly shorter than that of the **trans-BPE**.

Since the amino groups are susceptible to protonation, chemical titration with trifluoroacetic acid (TFA) of **nPE** molecules was carried out (Figure IV.3.26 and Tables IV.3.10 and 11). Titration processes can be compared with the electrochemical oxidation spectra consulting *Appendix VI*.

In the case of **trans-BPE**, upon titration the neutral band is blue-shifted from 344, 323 nm to 295, 308 nm. Also, new bands at 445 and 553 nm appears. For **cross-BPE**, titration gives rise to a new intense band at 550 nm. A second feature at 363 nm is also detected. These spectra are similar to those found for the first electrochemically oxidized species of **trans-** and **cross-BPE**.

However, protonation of neutral **TPE** gives rise to a different spectrum from that obtained through electrochemical oxidation. The titration process generates a red-shifted band at 436 nm, together with the growing of a couple of bands at

310-317 nm.

In order to study the species formed upon titration, TD-DFT/B3LYP/6-31G** theoretical calculations of the mono- and bisprotonated species of **nPE** molecules were performed (Tables IV.3.10 and IV.3.11). Since **TPE** has four different amino groups which can be protonated, TD-DFT of the bisprotonated species were calculated for the three different conformations. *cis-*, *trans-* (for the distal *p*-aminophenylene groups) and *cross-*

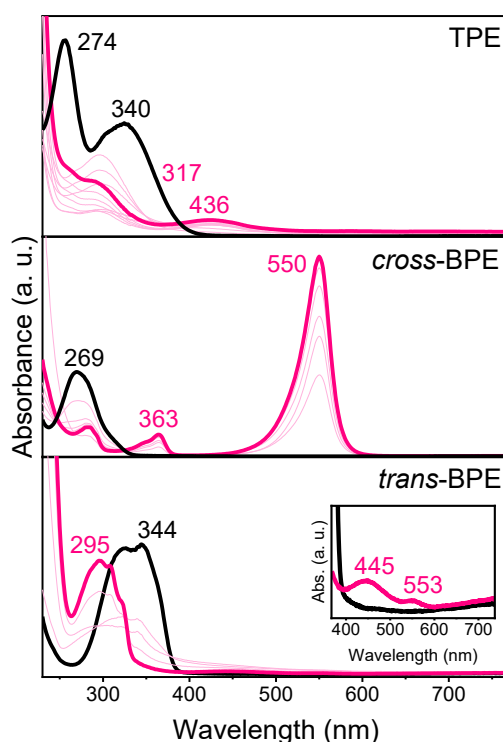


Figure IV.3.26. UV-Vis-NIR spectroelectrochemical titration of **nPE** molecules in CH_2Cl_2 with trifluoroacetic acid (TFA) at room temperature. From bottom to top: **trans-BPE**, **cross-BPE** and **TPE**. Black lines correspond to the spectra of neutral molecules and pink lines correspond to the spectra of the completely formed bisprotonated species. Light color lines correspond to the intermediate spectra between the former species in the titration process.

bisprotonated dication, for the two vicinal *p*-aminophenylene moieties (Table IV.3.11).

According to the theoretical calculations, titration of **trans-BPE** and **cross-BPE** provokes directly the formation of the bisprotonated species (see Table IV.3.8). The observed UV-Vis bands correspond to the HOMO→LUMO transition for both systems.

In the case of **TPE** (Table IV.3.11), TD-

DFT of bis-protonation occupying the two distal positions of the linear *trans*-conjugated path gives rise to a main band at 307 nm accompanied by another transition at 557 nm in very nice agreement with the two bands observed experimentally (top panel in Figure Figure IV.3.26). Alternatively, if bis-protonation of **TPE** is occupying the *cross*-conjugation positions, two theoretical excitations at 421 and 489 nm are predicted, while if the dication is occupying the *cis*-disposition,

Table iv.3.10. Optical data of UV-Vis-NIR titration of **trans-BPE** and **cross-BPE** molecules with trifluoroacetic acid in CH₂Cl₂ at room temperature, together with their calculated electronic transitions at the B3LYP/6-31G** level of theory.

| nPE | <i>trans</i> -BPE | | | <i>cross</i> -BPE | | | TD-DFT |
|------------------------|--------------------------|---------------------|----------------------|--------------------------|---------------------|-----------------------------------|------------------------------------|
| | Exp. ^a | TD-DFT ^b | Osc. Strength (a.u.) | Exp. ^a | TD-DFT ^b | Osc. Strength (a.u.) ^b | Electronic Transition ^b |
| Neutral | 323 344 | 339 293 | 1.17 0.15 | 269 | 246 274 284 | 0.45 0.17 0.11 | See Table 1 |
| Mono-protonated | — | 283 421 | 0.24 0.95 | — | 283 | 0.32 | H-2→LUMO/H→L+3 HOMO→LUMO |
| Bis-protonated | 295 445 | 313 — | 1.07 — | 363 550 | 264 — | 0.12 — | HOMO→LUMO |

^aMeasured in CH₂Cl₂ at room temperature. ^bTD-DFT calculations at (U)B3LYP/6-31G** level.

Table iv.3.11. Optical data of UV-Vis-NIR titration of **TPE** molecule with trifluoroacetic acid in CH₂Cl₂ at room temperature, together with the calculated electronic transitions at the B3LYP/6-31G** level of theory for the *cis*-, *trans*- and *cross*-bisprotonated configurations.

| TPE | | Experimental ^a | TD-DFT ^b | | |
|------------------------|----------------|---------------------------|-----------------------|----------------------|--------------------------|
| | | λ _{max} (nm) | λ _{max} (nm) | Osc. Strength (a.u.) | Electronic Transition |
| Neutral | | 274 340 | 278 380 | 0.47 0.44 | See Table 1 |
| Mono-protonated | | — | 528 963 | 0.16 0.15 | H-1→L/H→L+3 HOMO→LUMO |
| Bis-protonated | <i>cis</i> - | — | 484 | 0.23 | HOMO→LUMO+1 |
| | | — | 691 | 0.14 | HOMO→LUMO |
| | <i>trans</i> - | 317 | 307 | 0.62 | HOMO→LUMO+6 |
| | | 436 | 557 | 0.16 | HOMO→LUMO |
| <i>cross</i> - | — | 421 | 0.23 | HOMO→LUMO+2 | |
| | — | 489 | 0.36 | HOMO→LUMO | |

^aMeasured in CH₂Cl₂ at room temperature. ^bTD-DFT calculations at (U)B3LYP/6-31G** level.

two transitions at 484 and 691 nm are revealed.

Regarding these results, also the relative stability of the three bis-protonated forms of **TPE** has been explored by DFT calculations. The formation energy differences of these isomers are shown in Figure IV.3.27.

The most stable isomer is the *trans*-conjugated one, which presents the larger distance between the two protonated amino groups and therefore largest mitigation of the electronic repulsion. Energy difference between the former and the *cross*-isomer is less than 2 kcal/mol, while *cis*-bisprotonated **TPE** is the less stable isomer, at 7.09 kcal/mol respect to the *trans*- disposition.

Regarding the FMO depicted in Figure IV.3.27, for the *cis*- and *trans*- isomers their topologies reveal smaller atomic contributions along the paths between the protonated *p*-aminophenylene groups. Contrarily, the *cross*-conjugated dication displays larger atomic contribution along its path. However, for the LUMOs of the three isomers the main atomic contributions come from those atoms in the inter-protonated paths.

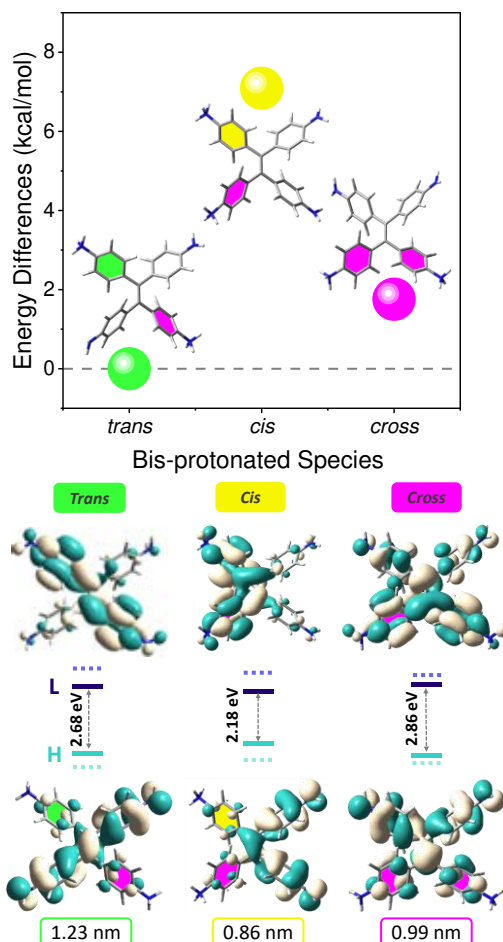


Figure IV.3.27. *Top*) Formation energy differences (in kcal/mol) of the *cis*- (yellow circle) and *cross*-configuration (pink circle) respect to the *trans*-isomer (green circle) of **TPE** bisprotonated species calculated at the B3LYP/6-31G** level of theory; *Bottom*) The corresponding HOMO and LUMO energy levels and topologies calculated at the B3LYP/6-31G** level of theory, together with the protonated N-N distances obtained from the optimized geometries.

B. Single Molecule Conductance Measurements

The presence of the amino groups in **nPE** molecules not only allows the protonation of these groups but also the ability of coordination to metals. With this property in mind, single molecular conductance measurements can be carried out forming gold-molecule junction thanks to the lone pair on the nitrogen atoms in **nPE** systems.^[42, 43]

As has been discussed in *Electronic Structure of Neutrals and Charged Species* Section, **TPE** presents three different bisprotonated isomers (linear *cis*- and *trans*- and *cross*-configurations), in which the distances between the two protonated nitrogen atoms also differ (see Figure IV.3.27). In consequence, these three coordination positions for molecular conductance measurements offer three different inter-electrode distances. Thus, the π -electron delocalization pathways in **TPE** will modulate the conductance value.

Single molecular conductance of **TPE** has been measured using the Scanning Tunneling Microscope Break Junction method (STM-BJ) by the group of Professor Latha Venkataraman, and the obtained results are shown in Figure IV.3.28.

According to the 1D histogram of **TPE** (Figure IV.3.28, left), the most common transport configurations are those corresponding to the conductance values of $7 \times 10^{-4} G_0$ and $2.5 \times 10^{-5} G_0$. When the measured conductance values are assigned to their corresponding junction elongation in a 2D histogram (Figure IV.3.28, right), both molecular configurations of the high conductance

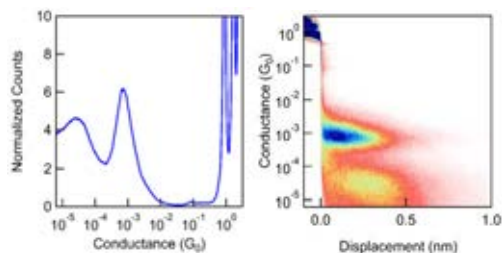


Figure IV.3.28. Left) 1D conductance histogram compiled from 10,000 traces for **TPE** at 100 mV bias; Right) 2D conductance histogram compiled from 10,000 traces for **TPE** at 100 mV bias. The reported conductance values are calculated from the peak positions in the 1D histograms.

($7 \times 10^{-4} G_0$) and the low conductance ($2.5 \times 10^{-5} G_0$) features present a conductance *plateau* length of approximately 0.5 nm. The *plateau* distance is the elongation during which the corresponding configuration presents conductance, but this distance does not correspond to the total length of the molecule (the *plateau* length will always be an underestimate of the true molecule length due to the elastic relaxation of the electrodes upon rupture of the gold-gold point contact^[44]).

Regarding the appearance of two *plateaus* with different conductance values, **TPE** molecule coordinates to gold electrodes adopting two different configurations. *Cross*-conjugated compounds are known to present a very low and poorly defined conductance,^[45] then the high conductance feature in Figure IV.4.28 is ascribed to both *cis*- and *trans*- isomers (with a similar conductance value to analogue linearly conjugated stilbenes^[46]). On the other hand, the smaller conductance value is attributed to

the *cross*-conjugated geometry, which is clearly detected and associated with a very well-defined conduction process. This result constitutes a rare example among the previous attempts to detect single molecular conductance in *cross*-conjugated systems.^[46] It has to be noted that the model molecule **cross-BPE** does not show a measurable conductance in the same conditions as **TPE** was measured. Consequently, *cross*-conjugation alone blocks conduction in the mono-conjugated compound, but, when *cross*-conjugation is implemented together with *linear*-conjugation, such as in **TPE**, an overall transmission is turned on.

In order to corroborate which isomers are involved in the conduction mechanisms, the transmission spectra and the local current maps for the three different anchoring dispositions (the three isomers) were calculated by the group of Professor Mercedes Alonso (Figures IV.3.29 and IV.3.30).

The transmission spectra show that both linear configurations presents similar conductance values around the Fermi level (grey dotted line), while the *cross*-isomer discloses a lower conductance feature. According to that, the high conductance observed in the 2D-histogram of **TPE** must correspond to the linear transport configurations (*trans*- and *cis*- isomers), while the low conductance is originated by the *crossed* state. As mentioned above, the lower conductance values in *cross*-conjugated molecules have been already studied and are ascribed to destructive quantum interference effects (DQI).^[45, 47, 48] As can be observed in the transmission spectra, only the *cross* isomer presents

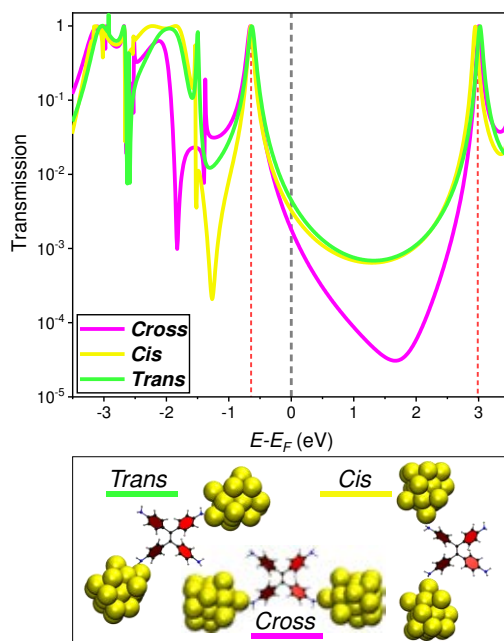


Figure VI.3.29. Top) Transmission spectra for the *cross*-, *cis*- and *trans*-anchoring configurations of **TPE** on gold electrodes. The Fermi level is indicated with a grey dotted line, while the HOMO and LUMO transmission peaks are indicated with dashed red lines; Bottom) Structures of the molecular junctions for the three anchoring modes.

quantum interference (the only configuration with a pronounced transmission minimum between the HOMO and LUMO peaks).

With these results in mind, it can be established that at the initial distances, the higher conductance value is assigned to the conduction channels between the two linearly π -conjugated frameworks. According to the calculated protonated N-N distances (Figure VI.3.27), the *cis*-anchoring mode, due to the smaller value, could better fit the junction volume displaying the dominant contribution. However, the most probable situation is that both linear channels might jointly act. Enlargement of the junction distance leaves only the *cross*-conjugation channel

active which is the species with the next larger N-N distance, displaying a smaller conductance peak. After this second measured conductance, the heterojunction is broken. Then, a conduction channel through the larger linear N-N distance, *i. e.*, the *trans*-bisprotonated sequence, is not detected.

Regarding the local current maps through the three possible anchoring configurations of **TPE** (Figure VI.3.30), for the linear dispositions the main transmission takes place through the central C=C bond, through a C—C/C=C alternating bonds sequence. However, this pathway is partially avoided in the *cross*-conjugation case, but, from the current map and the LUMO topology, a complementary transmission circuit is detected: a through-space channel exists between the two non-connected carbon atoms.

By this way, two phenomena contributes to the detection of a well-measurable conductance through the *cross*-conjugation configuration in **TPE** despite the destructive interference: i) the larger atomic contribution of the protonated N-N framework to the HOMO; and ii) the existence of a second through-space transmission channel in the LUMO.

The observed conjugation-dependent conductance and its control to obtain the desirable properties is of uttermost importance in single molecule functional devices. Polyconjugated systems similar to the studied **TPE** molecule can be use as switching or ON/OFF charge transport materials.^[48]

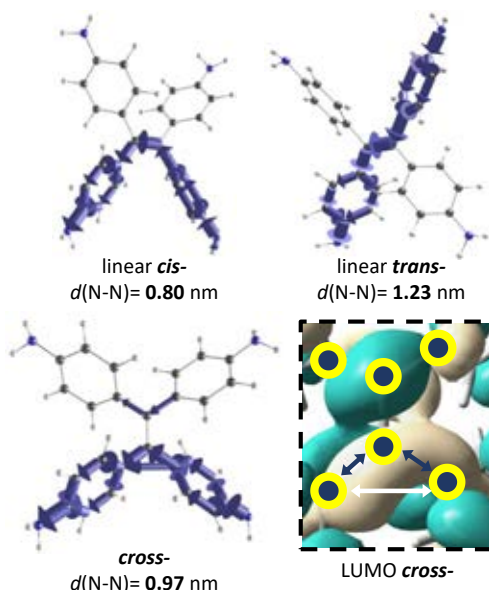


Figure VI.3.30. Local transmission plots at the Fermi level for the three anchoring modes. Inset: LUMO topology of the central molecular part of the *cross*-conjugated geometry with yellow circles showing the atoms, the white arrow showing the delocalization path between non-connected atoms and blue arrows displaying delocalization between connected atoms.

In addition to the detection of conductance through a *cross*-conjugated channel, the study of **TPE** also highlights the relevance of through-space interactions in organic electronics.

3.4. CONCLUSIONS

Joining together the obtained results in the optical and spectroscopic study of **2DQoT** oligomers and their reduced species, the following conclusions are established:

- Neutral species of **2DQoT** family have been successfully characterized by electronic absorption and vibrational spectroscopy. The contribution of their diradical canonical forms have been evaluated and found to increase when lengthening the oligomer size. By this way, **2DQTT** presents a closed-shell ground state, while **2DQPT** constitutes a singlet open-shell system. **2DQQT** possesses an intermediate diradical character between the two other members of the family.
- The presence of a second π -delocalization framework, orthogonal to the linear oligothiophene has been demonstrated. This sequence is established between distal carbonyl groups of vicinal TPD moieties, and provokes the two dimensional extension of the π -electron density.
- **2DQQT** and **2DQPT** diradicals are characterized as singlet open-shell systems due to the Double Spin Polarization mechanism. However, the presence of π -cross-conjugated frameworks (and the number of them) disturb the π -electron delocalization through the linear oligothiophenes bridge, narrowing the singlet-triplet gap on going from **2DQQT** to **2DQPT**.
- Also the presence of the cross-conjugated inter-dione sequences drives the location of the radical centers in the case of **2DQQT** oligomer. The competition between the linear oligothiophene backbone and the inter-dione paths pushes the diradical to the innermost thiophene rings. For **2DQPT**, the two orthogonal frameworks cancel each other and, together with its large diradical character, provoke the location of the radical centers in the dicyanomethylene moieties. This form is stabilized by the aromatization of the quinoidal pentathiophene backbone.
- The reduction processes of **2DQoT** have been studied by UV-Vis-NIR electronic absorption and IR spectroscopy, and the radical anion species have been characterized through vibrational spectroscopy and theoretical calculations. For **2DQQT** and **2DQPT**, the cross-conjugated sequences are responsible of the existence of two different radical anions. These species constitute electronic isomers since they only differ in the radical anion delocalization framework: through the linear inter-dicyanomethylene one or through the cross-conjugated inter-dione sequence.

- While **2DQTT** suffers only two reduction steps, the longer oligomers can also give rise to the formation of a radical trianion species that can be accommodated in the inter-dione framework.
- **2DQoT** molecules have been also evaluated as n-type semiconducting materials, showing outstanding electrical conductivity values and exceptional stability at room temperature and ambient pressure conditions, particularly **2DQQT**. These results are intimately related with the combination of the diradical character and the cross-conjugation properties.
- In the case of **2DQTT** and **2DQPT**, the two extreme configurations (closed-shell and highly diradical) provokes the formation of slipped π - π stacking arrangements and σ -polymers in thin film, respectively.
- In **2DQQT**, the incipient diradical character together with the properties conferred by the presence of the inter-dione cross-conjugated framework, give rise to a cholesteric-like π - π arrangement. This aggregation mode has been shown to present the more desirable characteristics to obtain stable n-type semiconducting materials.
- The influence of a second, orthogonal π -conjugated framework has been also evaluated in closed-shell systems. The competition between cross-conjugated sequences has been demonstrated to influence the conductance measurements, thus it is also expected to alter other electronic properties.
- **TPE** has been demonstrated to present well-defined conductance through the *cross-conjugated* channel. The combination of atomic orbitals contribution to the HOMO along the N-N transmission framework and the existence of a through-space channel makes possible to overcome the destructive interference ascribed to the *cross-conjugated* sequence.
- Regarding these results, the role of through-space interactions in the electronic properties of π -conjugated systems seems to be a relevant phenomenon to be addressed.

REFERENCES

- [1] *Biradicaloid and Polyenic Character of Quinoidal Oligothiophenes Revealed by the Presence of a Low-Lying Double-Exciton State*, S. Di Motta, F. Negri, D. Fazzi, C. Castiglioni, and E. Valeria caneis, *J. Phys. Chem. Lett.*, **2010**, *1*, 3334–3339.
- [2] *Pushing Extended p-Quinodimethanes to the Limit: Stable Tetracyano-oligo(N-annulated perylene)quinodimethanes with Tunable Ground States*, Z. Zeng, M. Ishida, J. L. Zafra, X. Zhu, Y. Mo Sung, N. Bao, R. D. Webster, B. S. Lee, R-W.Li, W. Zeng, Y. Li, C. Chi, J. T. Lopez Navarrete, J. Ding, J. Casado, D. Kim, and J. Wu, *J. Am. Chem. Soc.*, **2013**, *135*, 6363–6371.
- [3] *Zethrenes, Extended p-Quinodimethanes, and Periacenes with a Singlet Biradical Ground State*, Z. Sun, Z. Zeng, and J. Wu, *Acc. Chem. Res.*, **2014**, *47*, 2582–2591.
- [4] *Extensive Quinoidal Oligothiophenes with Dicyanomethylene Groups at the Terminal Positions as Highly Amphoteric Redox Molecules*, T. takahashi, K. Matsuoka, K. takimiya, T. Otsubo and Y. Aso, *J. Am. Chem. Soc.*, **2005**, *127*, 8928–8929.
- [5] *On the Biradicaloid Nature of Long Quinoidal Oligothiophenes: Experimental Evidence Guided by Theoretical Studies*, R. Ponce Ortiz, J. Casado, V. Hernández, J. T. López Navarrete, P. M. Viruela, E. Ortí, K. Takimiya and T. Otsubo, *Angew. Chem. Int. Ed.*, **2007**, *46*, 9057–9061.
- [6] *Quinoidal Oligothiophenes: Towards Biradical Ground State Species*, R. Ponce Ortiz, J. Casado, S. Rodríguez González, V. Hernández, J. T. López Navarrete, P. M. Viruela, E. Ortí, K. Takimiya and T. Otsubo, *Chem. Eur. J.*, **2010**, *16*, 470–484.
- [7] *Handbook of Thiophene-Based Materials*, I. F. Perepichka and D. F. Perepichka, Eds.; John Wiley & Sons, LTd: United Kingdom, **2009**.
- [8] *Molecular Engineering of the Band Gap of π -Conjugated Systems: Facing Technological Applications*, J. Roncali, *Macromol. Rapid Commun.*, **2007**, *28*, 1761–1765.
- [9] *A π -Stacking Terthiophene-Based Quinodimethane Is an n-Channel Conductor in a Thin Film Transistor*, T. M. Pappenfus, R. J. Chesterfield, C. D. Frisbie, K. R. Mann, J. Casado, J. D. Raff and L. L. Miller, *J. Am. Chem. Soc.*, **2002**, *124*, 4184–4185.
- [10] *Organic Semiconducting Oligomers for Use in Thin Film Transistors*, A. R. Murphy and J. M. J. Fréchet, *Chem. Rev.*, **2007**, *107*, 1066–1096.
- [11] *Quinoidal Oligothiophenes: New Properties Behind an Unconventional Electronic Structure*, J. Casado, R. Ponce Ortíz and J. T. López Navarrete, *Chem. Soc. Rev.*, **2012**, *41*, 5672–5686.
- [12] *Structural Identification of Organic Compounds with Spectroscopic Techniques*, Y.-C. Ning, WILEY-VCH: Weinheim, **2005**.
- [13] *Relation between Effective Conjugation, Vibrational Force Constants and Electronic Properties in*

- Polyconjugated Materials*, J.T. López-Navarrete, B. Tian and G. Zerbi, *Solid State Commun.*, **1988**, 65, 625–630.
- [14] *Confinement Potential and N-Electron Delocalization in Polyconjugated Organic Materials*, V. Hernández, C. Castiglioni, M. del Zoppo and G. Zerbi, *Phys.Rev. B*, **1994**, 50, 9815–9823.
- [15] *Structure and Optical Properties of Conjugated Oligomers from their Vibrational Spectra*, G. Zerbi, C. Castiglioni and M. Del Zoppo in *Electronic Materials: The Oligomer Approach* K. Müllen and G. Wegner, Eds.; Wiley-VCH: Weinheim, **1998**, 345–402.
- [16] *Spectroscopic and Theoretical Study of the Molecular and Electronic Structures of a Terthiophene-Based Quinodimethane*, J. Casado, T. M. Pappenfus, K. R. Mann, E. Ortí, P. M. Viruela, B. Milián, V. Hernández and J. T. López Navarrete, *ChemPhysChem*, **2004**, 5, 529–539.
- [17] *The Longest Quinoidal Oligothiophene: A Raman Story*, J. Casado and J. T. López Navarrete, *The Chemical Record*, **2011**, 11, 45–53.
- [18] *Quinoidal/Aromatic Transformation in π -Conjugated Oligomers: Vibrational Raman Studies on the Limit of Rupture of π -Bonds*, P. Mayorga Burrezo, J. L. Zafra, J. T. López Navarrete and J. Casado, *Angew. Chem. Int. Ed.*, **2017**, 56, 2250–2259.
- [19] *Molecular Engineering of the Band Gap of π -Conjugated Systems: Facing Technological Applications*, J. Roncali, *Macromol. Rapid Commun.*, **2007**, 28, 1761–1765.
- [20] *Relationship between Band Gap and Bond Length Alternation in Organic Conjugated Polymers*, J. L. Brédas, *J. Chem. Phys.*, **1985**, 82, 3808–3811.
- [21] *Polarons, Bipolarons and Solitons in Conducting Polymers*, J. L. Brédas and G. B. Street, *Acc. Chem. Res.*, **1985**, 18, 309–315.
- [22] *Electronic Absorption and Vibrational Spectroscopies of Conjugated Conducting Polymers*, Y. Furukawa, *J. Phys. Chem.*, **1996**, 100, 15644–15653.
- [23] “Electromers” of the Tetramethyleneethane Radical Cation and Their Nonexistence in the Octamethyl Derivative: Interplay of Experiment and Theory, B. Müller, T. Bally, F. Gerson, A. de Meijere, and M. von Seebach, *J. Am. Chem. Soc.*, **2003**, 125, 13776–13783.
- [24] *Isomerism: The Same but Different*, T. Bally, *Nat. Chem.*, **2010**, 2, 165–166.
- [25] *Molecular Engineering of the Band Gap of π -Conjugated Systems: Facing Technological Applications*, J. Roncali, *Macromol. Rapid Commun.*, **2007**, 28, 1761–1765.
- [26] *Organic Semiconducting Oligomers for Use in Thin Film Transistors*, A. R. Murphy and J. M. J. Fréchet, *Chem. Rev.*, **2007**, 107, 1066–1096.
- [27] *n-Type Organic Semiconductors in Organic Electronics*, J. E. Anthony, A. Facchetti, M. Heeney, S. R. Marder and X. Zhang, *Adv. Mater.*, **2010**, 22, 3876–3892.
- [28] *Efficient Solution-Processed n-Type Small-Molecule Thermoelectric Materials Achieved by Precisely Regulating Energy Level of Organic Dopants*, D. Yuan, D.

Huang, C. Zhang, Y. Zou, C.Di, X. Zhu and D. Zhu, *ACS Appl. Mater. Interfaces*, **2017**, 9, 28795–28801.

[29] *Solution Doping of Organic Semiconductors Using Air-Stable n-Dopants*, Y. Qi, S. K. Mohapatra, S. Bok Kim, S. Barlow, S. R. Marder and A. Kahn, *Appl. Phys. Lett.*, **2012**, 100, 083305.

[30] *Solubility-Limited Extrinsic n-Type Doping of a High Electron Mobility Polymer for Thermoelectric Applications*, R. A. Schlitz, F.G. Brunetti, A. M. Glaudell, P. L. Miller, M. A. Brady, C. J. Takacs, C. J. Hawker and M. L. Chabiny, *Adv. Mater.*, **2014**, 26, 2825–2830.

[31] *Two-Dimensional π -Expanded Quinoidal Terthiophenes Terminated with Dicyanomethylenes as n-Type Semiconductors for High-Performance Organic Thin-Film Transistors*, C. Zhang, Y. Zang, E. Gann, C. R. McNeill, X. Zhu, C.Di and D. Zhu, *J. Am. Chem. Soc.*, **2014**, 136, 16176–16184.

[32] *Pursuing High-Mobility n-Type Organic Semiconductors by Combination of “Molecule-Framework” and “Side-Chain” Engineering*, C. Zhang, Y. Zang, F. Zhang, Y. Diao, C. R. McNeill, C.Di, X. Zhu and D. Zhu, *Adv. Mater.*, **2016**, 28, 8456–8462.

[33] *Passivation of Molecular n-Doping: Exploring the Limits of Air Stability*, M.L. Tietze, B.D. Rose, M. Schwarze, A. Fischer, S. Runge, J. Blochwitz-Nimoth, B. Lüssem, K. Leo and J.-L. Brédas, *Adv. Funct. Mater.*, **2016**, 26, 3730–3737.

[34] *High Conductivity and Electron - Transfer Validation in an n - Type Fluoride - Anion - Doped Polymer for*

Thermoelectrics in Air, X. Zhao, D. Madan, Y. Cheng, J. Zhou, H. Li, M. Thon Susanna, E. Bragg Arthur, E. DeCoster Mallory, E. Hopkins Patrick, and E. Katz Howard, *Adv. Mater.*, **2017**, 29, 1606928.

[35] *Role of Intermolecular Coupling in the Photophysics of Disordered Organic Semiconductors: Aggregate Emission in Regioregular Polythiophene*, J. Clark, C. Silva, R. H. Friend, and F. C. Spano, *PRL*, **2007**, 98, 206406.

[36] *The Vibrational and Electronic Spectra of the Mono-, Di-, and Trianion Salts of TCNQ*, M. S. Khatkale and J. P.I Devlin, *J. Chem. Phys.*, **1979**, 70, 1851–1859.

[37] *Tetracyanoethylene (TCNE): The Characteristic Geometries and Vibrational Absorptions of Its Numerous Structures*, J. S. Miller, *Angew. Chem. Int. Ed.*, **2006**, 45, 2508–2525.

[38] *Reversible Dimerization and Polymerization of a Janus Diradical to Produce Labile C-C Bonds and Large Chromic Effects*, J. L. Zafra, L. Qiu, N. Yanai, T. Mori, M. Nakano, M. P. Álvarez, J. T. L. Navarrete, C. J. Gómez-García, M. Kertesz, K. Takimiya and J. Casado, *Angew. Chem. Int. Ed.*, **2016**, 55, 14563–14568.

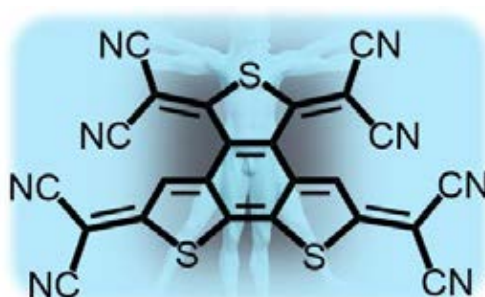
[39] *Double Pancake Bonds: Pushing the Limits of Strong π - π Stacking Interactions*, Z. Cui, H. Lischka, H. Z. Beneberu and M. Kertesz, *J. Am. Chem. Soc.*, **2014**, 136, 12958–12965.

[40] *Rotational Barrier in Phenalenyl Neutral Radical Dimer: Separating Pancake and van der Waals Interactions*, Z. Cui, H. Lischka, H. Z. Beneberu and M. Kertesz, *J. Am. Chem. Soc.*, **2014**, 136, 5539–5542.

- [41] *Perylene Bisimide Dye Assemblies as Archetype Functional Supramolecular Materials*, F. Würthner, C. R. Saha-Möllner, B. Fimmel, S. Ogi, P. Leowanawat and D. Schmidt, *Chem. Rev.*, **2016**, *116*, 962–1052.
- [42] *Single-Molecule Circuits with Well-Defined Molecular Conductance*, L. Venkataraman, J. E. Klare, I.W. Tam, C. Nuckolls, M. S. Hybertsen, and M. L. Steigerwald, *Nano Lett.*, **2006**, *6*, 458–462.
- [43] *Contact Chemistry and Single-Molecule Conductance: A Comparison of Phosphines, Methyl Sulfides, and Amines*, Y. S. Park, A. C. Whalley, M. Kamenetska, M. L. Steigerwald, M. S. Hybertsen, C. Nuckolls, and L. Venkataraman, *J. Am. Chem. Soc.*, **2007**, *129*, 15768–15769.
- [44] *Formation and Evolution of Single-Molecule Junctions*, M. Kamenetska, M. Koentopp, A. C. Whalley, Y. S. Park, M. L. Steigerwald, C. Nuckolls, M. S. Hybertsen and L. Venkataraman, *Phys. Rev. Lett.*, **2009**, *102*, 126803–126806.
- [45] *Chemical principles of single-molecule electronics*, T. A. Su, M. Neupane, M. L. Steigerwald, L. Venkataraman and C. Nuckolls, *Nat. Rev. Mater.*, **2016**, *1*, 16002.
- [46] *Dissecting Contact Mechanics from Quantum Interference in Single-Molecule Junctions of Stilbene Derivatives*, S. V. Aradhya, J.S. Meisner, M. Krikorian, S. Ahn, R. Parameswaran, M.L. Steigerwald, C. Nuckolls and L. Venkataraman, *Nano Lett.*, **2012**, *12*, 1643–1647.
- [47] *The Orbital Selection Rule for Molecular Conductance as Manifested in Tetraphenyl-Based Molecular Junctions*, M. Bürkle, L. Xiang, G. Li, A. Rostamian, T. Hines, S. Guo, G. Zhou, N. Tao, and Y. Asai, *J. Am. Chem. Soc.*, **2017**, *139*, 2989–2993.
- [48] *Quantum Interference Effects in Charge Transport through Single-Molecule Junctions: Detection, Manipulation, and Application*, J. Liu, X. Huang, F. Wang, and W. Hong, *Acc. Chem. Res.*, **2019**, *52*, 151–160.

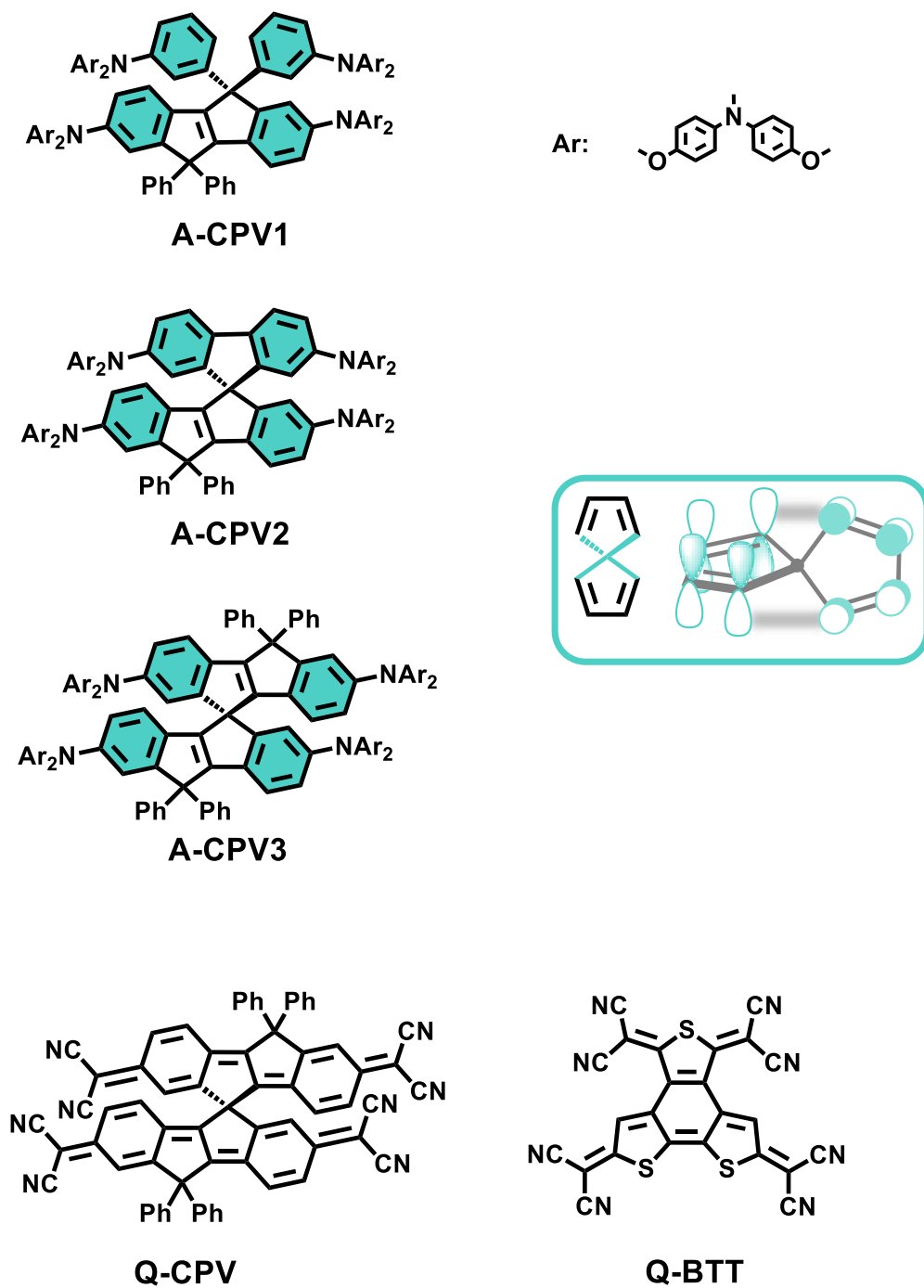


C. SPIRO-CONJUGATED DIRADICALS



4. The Case of Octacyano Diradicals: Spiro *versus* Parallel π -Conjugation

| | |
|---|----------------|
| 4.1 Neutral Species of CPV Family..... | 183—201 |
| A. Electronic Structure..... | 183—193 |
| B. Molecular Structure..... | 194—201 |
| 4.2 Charged Species of CPV Family..... | 202—221 |
| A. Electronic Structure..... | 202—213 |
| B. Molecular Structure..... | 214—221 |
| 4.3 Conclusions..... | 222—224 |
| References..... | 225—228 |



Scheme IV.4.1. Chemical structures of the molecules forming the CPV family studied in this chapter. The spiro-conjugated motif is schematized in the inset.

4.1 NEUTRAL SPECIES OF CPV FAMILY

A. Electronic Structure

A. I. Optical Properties

Figure IV.4.1 shows the electronic absorption spectra of **CPV** molecules in CH_2Cl_2 at room temperature. While the absorption maxima wavelengths (λ_{max}) of the aromatic **CPVs** are placed between 300-440 nm (see Table IV.4.1), the value corresponding to the quinoidal **CPV** is considerably red-shifted (λ_{max} at 618 nm).

Theoretical calculations of the electronic transitions of neutral **CPV** molecules were carried out and results nicely reproduce the experimental data (see Table IV.4.1). According to the TD-DFT calculations, λ_{max} wavelengths of **CPV** molecules are assigned to the HOMO→LUMO electron transitions.

Since **CPV** molecules do not constitute an oligomeric series, the evolution of their λ_{max} wavelengths must be discussed in

terms of their spiro-conjugation properties, and not as a consequence of the increasing number of monomeric

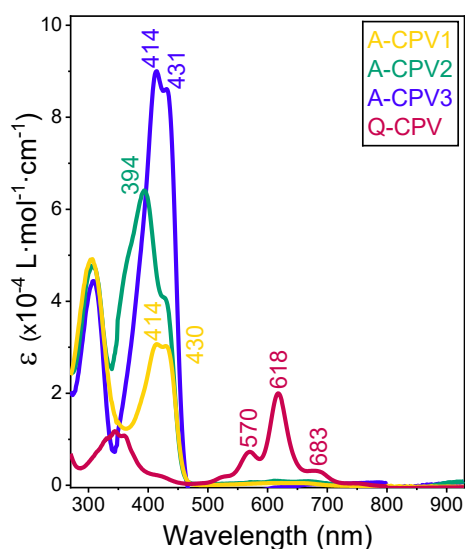


Figure IV.4.1. UV-Vis-NIR electronic absorption spectra of **CPV** molecules in CH_2Cl_2 at room temperature.

Table IV.4.1. Optical data of **CPV** family.

| CPVs | Experimental ^a | | TD-DFT ^b | | |
|--------|-----------------------------|---|-----------------------------|-----------------------------|----------------------------------|
| | λ_{max} (nm) | ϵ ($\times 10^{-4}$ L·mol ⁻¹ ·cm ⁻¹) | λ_{max} (nm) | Oscillator Strength (a. u.) | Electronic Transition |
| A-CPV1 | 304 | | 325 | 0.106 | HOMO→LUMO+6 |
| | 414/430 | 4.7 | 443 | 0.919 | HOMO→LUMO |
| | | | 309 | 0.14 | H-1→L+9/H-1→L+10 |
| A-CPV2 | 307 | | 397 | 0.79 | HOMO-1→LUMO+1 |
| | 394 (428, 365) | 6.4 | 443 | 0.88 | HOMO→LUMO |
| | | | 322 | 0.34 | H→L+6/H-1→L+7 |
| A-CPV3 | 309 | | 434 | 0.99 | H-1→L/H→L+1 |
| | 414/431 | 9.0 | 452 | 0.25 | HOMO→LUMO |
| | | | | | |
| Q-CPV | 344 (330/360) | | 416 | 0.35 | HOMO-1→LUMO+3 (α/β) |
| | 570 (524) | | 583 | 0.22 | HOMO-1→LUMO+1 (α/β) |
| | 618 | 2.0 | 596 | 1.66 | HOMO→LUMO (α/β) |
| | 683 | | 652 | 0.89 | HOMO-1→LUMO+1 (α/β) |

^aMeasured in CH_2Cl_2 at room temperature. ^bTD-DFT calculations at (U)B3LYP/6-31G** level of theory ($f > 0.1$). Geometry optimization of **A-CPV** molecules was performed as closed-shell system (spin restricted B3LYP), while **Q-CPV** was optimized as singlet open-shell system (spin unrestricted B3LYP).

units. This is why the Meier fitting is not applicable for this family.

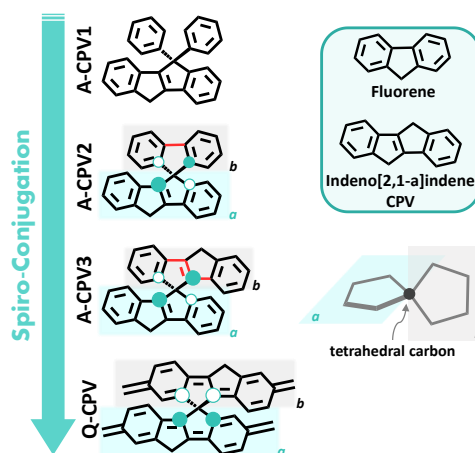
The spiro-conjugation of the π -electron density in **CPV** molecules is managed by their chemical structures. The main difference between the aromatic **CPV** systems **1** and **2** is the formation of a bond between the two phenylene rings linked to the tetrahedral carbon (see Scheme IV.4.2, new bond highlighted in red). Now, **A-CPV2** is formed by a planar moiety (or **CPV** unit, placed in the green plane in Scheme IV.4.2) and a planar fluorene moiety (grey plane). Thus, the new bond provokes the rigidification of the chemical structure, which can be described now by two orthogonal planes. As a consequence, **A-CPV2** is able to experiment the spiro-conjugation phenomenon, while in **A-CPV1** the flexibility of the two aryl groups attached to the tetrahedral carbon prevent this delocalization mechanism.

In the case of the **A-CPV3**, the phenylene rings are linked through a rigidified vinylic bridge, thus these molecules are defined by two indeno[2,1-a]indene moieties (or **CPV** units) in two different planes. This new carbon-bridged phenylenevinylene unit provokes the extension of the π -conjugated backbone respect to the fluorene moiety in **CPV2**. In the symmetric **A-CPV3** system, the π -electron density over the two spiro-conjugated carbon atoms involved in the vinylic bridge is larger than in the other two carbons, which belong to benzene rings. Thus, spiro-conjugation is facilitated in **A-CPV3** respect to **A-CPV2**.

Finally, the quinoidization of **CPV3** results in the **Q-CPV** system. This

quinoidization increases the π -electron density over the spiro-conjugated carbons in both **CPV** units, enhancing the spiro effect in **Q-CPV** respect to its aromatic counterpart **A-CPV3**.

In agreement with these structural differences, the spiro-conjugation phenomenon is favoured according to Scheme IV.4.2:



Scheme IV.4.2. Spiro-conjugation enhancement in the **CPV** family. The different bridges between the phenylene rings are highlighted in red, and the two orthogonal planes *a* and *b* are in green and grey, respectively. Individual atomic coefficient contributing to the HOMO orbitals (top view) are schematized with the white and green circles. In the inset the chemical structure of the two planar carbon-based cores forming the **CPV** molecules are showed.

Once the structural differences between the **CPV** molecules are established, changes in the electronic absorption spectra can be discussed. Regarding the absorption bands of aromatic **CPVs** (see Figure IV.4.1), while **A-CPV1** and **A-CPV3** present similar shapes, **A-CPV2** differs. As showed in Scheme IV.4.2, **A-CPV2** is formed by a carbon-bridged phenylene vinylene unit (**CPV**),

which λ_{\max} wavelength is at 428 nm (according to the theoretical calculations), and a fluorene moiety, with a λ_{\max} wavelength at 394 nm.^[1] The contribution of the **CPV** unit to the absorption spectrum is in line with the λ_{\max} wavelengths of the other two aromatic systems, while the absorption of the fluorene chromophore is responsible of the differences between **A-CPV2** and **A-CPV1** and **3**.

From **A-CPV1** to **A-CPV3**, the rigidification and extension of the phenylene rings takes place through a vinylenic bridge, forming a spiro-linked dimer between two **CPV** units. Since λ_{\max} wavelength of **A-CPV1** is mainly due to the absorption of the **CPV** core, it is not unexpected that that of the **A-CPV3** presents the same value (414/430 nm and 414/431 nm, respectively), since it is constituted by two identical **CPV** moieties. In the case of the two rigidified molecules, the slight redshift of λ_{\max} wavelength from **A-CPV2** to **A-CPV3** (428/394 nm \rightarrow 431/414 nm, respectively) is explained by the extension of the effective conjugation length when the fluorene moiety is substituted by the longer **CPV** one.

As observed in previously studied quinoidal systems, λ_{\max} wavelengths of **Q-CPV** are considerably red-shifted in comparison with those of the aromatic molecules due to the quinoidization of the carbon-based backbone. This molecule presents two groups of absorption bands: the main group at 618 nm (524, 570, 683 nm), with a well-resolved vibronic structure due to the planar **CPV** quinoidal cores; and the second one at 344 nm (330, 360 nm). When comparing **Q-CPV** with the non-spiro **QM1CN** (see blue spectrum in

Figure IV.4.2),^[2, 3] similar λ_{\max} wavelengths are found: 616 nm (526, 567, 682 nm). In addition, the second set of bands of **Q-CPV** at 344 nm coincides with the electronic absorption features of aromatized **CPV** cores, such as those of the **QM1CN** σ -dimer formed upon cooling (yellow spectrum).^[3]

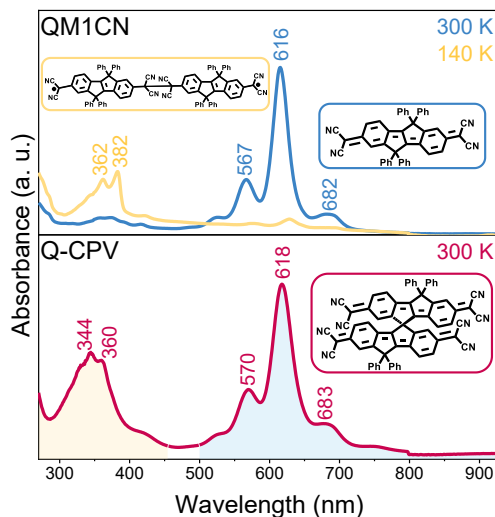


Figure IV.4.2. Comparison between the UV-Vis-NIR electronic absorption spectra of **QM1CN** at room temperature (blue line) and its σ -dimer (formed at 140 K; yellow line) (*top*) with that of the **Q-CPV** system at room temperature (*bottom*). Quinoidal features are highlighted in blue, while the aromatic bands are in yellow.

The driving force for the dimerization process in **QM1CN** is the gain of aromaticity of the benzene rings in the **CPV** core in the dimerized form. Thus, the blue-shifted bands of the σ -dimer are related with an aromatic contribution. The presence of these same features around 344 nm in the optical spectrum of **Q-CPV** at room temperature reveals its open-shell character, in contrast with the closed-shell quinoidal **QM1CN**.^[2, 3] This optical behaviour of a molecule with an incipient diradical character was already observed

in **2DQQT** and **2DQPT** oligomers, in the former chapter.

To evaluate the viability of the open-shell configuration of the spiro systems, the formation energies of the ground electronic states were calculated at the B3LYP/6-31G** level of theory. In Figure IV.4.3, the energy difference between the corresponding ground electronic state and the triplet state for the **CPV** molecules is depicted (red circles), that is, the singlet-triplet gap (ΔE_{S-T}). For this purpose, aromatic **CPV** molecules were considered with a closed-shell configuration of their ground electronic state, while the quinoidal one is described as a singlet open-shell system. While the aromatic **CPV** systems present a singlet-triplet gap (ΔE_{S-T}) around 40 kcal/mol, in the case of the **Q-CPV**, ΔE_{S-T} is considerably narrowed as a consequence of its open-shell character, as it was already observed in **2DQOT** oligomers.

According to theoretical calculations, despite **Q-CPV** is formed by two **QM1CN** units, while the spiro molecule presents an open-shell character, **QM1CN** is a closed-shell system. As explained above, this non-spiro **QM1CN** counterpart is able to form singlet open-shell σ -dimers upon cooling, while the next oligomer of the series, **QM2CN**, is a diradical species *per se* (see Scheme IV.4.3).^[2, 3] Therefore, the aromatization of two **CPV** π -systems accounts for the energy required to break one π -bond and forming the diradical species. In other words, the formation of at least three Clar's sextets is enough to stabilize the diradical configuration.

However, as can be seen in Scheme

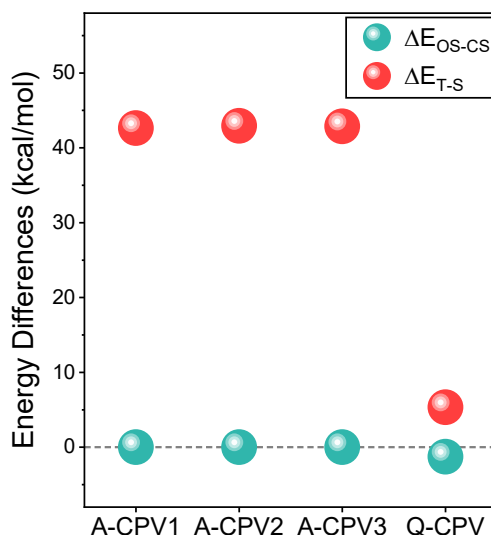
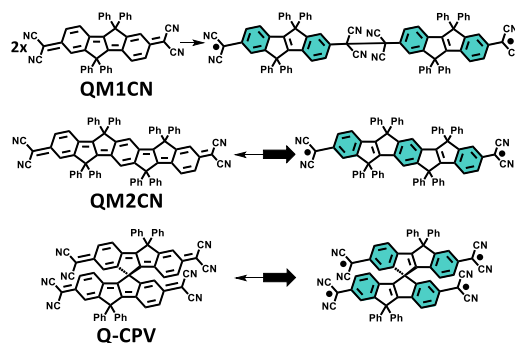


Figure IV.4.3. Formation energy differences (kcal/mol) between the singlet open shell and the closed shell (green circles) and between the triplet and the ground electronic state of **CPVs** (red circles) family calculated at the at the (U)B3LYP/6-31G** level of theory.

IV.4.3, the *fully* open-shell form of **Q-CPV** is a tetraradical system (quintet state). Thus, two π -bonds must be broken. According to the results obtained for the non-spiro **QM1CN** and **QM2CN** molecules, four Clar's sextets do not represent enough driving force to justify the *fully* open-shell



Scheme IV.4.3. Resonance structures of quinoidal closed-shell (*left*) and aromatic open-shell (*right*) forms of **CPV** derivatives. Clar's sextets are highlighted in green.

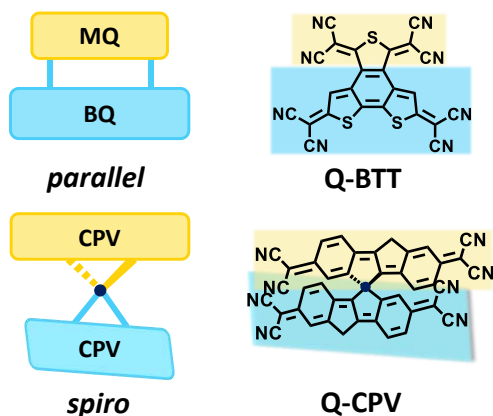
structure of **Q-CPV**. Consequently, not only the aromaticity gain but also another different factor must be responsible of the formation of an open-shell **Q-CPV** system. The differences between the σ -dimer of **QM1CN** and the molecule **Q-CPV** are evident:

- The spiro-conjugation between the two CPV units in **Q-CPV**. In the case of the **QM1CN** σ -dimer, the two moieties remain isolated from each other, *i. e.*, no conjugation exists between them;
- The rigidity imposed by the spiro bridge and the steric hindrance in **Q-CPV**, while **QM1CN** is a more relaxed structure.

In some way, the synergy between these three factors (aromaticity, spiro-conjugation and rigidity) provokes the stabilization of the tetradical form of **Q-CPV**. Also, a dimerization process between two **Q-CPV** molecules can be considered, forming a *partial* singlet open-shell system: only one of the two CPV units possesses diradical character). In that case, a σ -dimer similar to that found for **QM1CN** is formed.

In order to have a deeper insight into the open-shell character of **Q-CPV** molecule, another octacyano substituted quinoidal system, denoted as **Q-BTT**, is studied. In **Q-BTT**, the two chromophores (the monothiophene and the bithiophene moieties, hereinafter referred as **MQ** and **BQ**, respectively) are parallelly-linked while in **Q-CPV** the two **CPV** cores are linked through a tetrahedral carbon atom.

As in the case of spiro **Q-CPV**, **Q-BTT** is



Scheme IV.4.4. Chemical structure of **Q-BTT** molecule (top, right) together with that of **Q-CPV** (bottom, right). A scheme of the linkage between the π -conjugated moieties in both systems is also showed (left).

susceptible to form a *fully* open-shell tetradical species in its four dicyanomethylene groups.

Figure IV.4.4 displays the UV-Vis-NIR electronic spectra of the two quinoidal systems studied in this chapter, and the main optical transitions are indicated in Table IV.4.2. In general, the optical spectrum of **Q-BTT** is blue-shifted in comparison with that of the **Q-CPV**, a direct consequence of the less planar and shorter π -conjugation surface in **Q-BTT** (see optimized geometries of both molecules in *Appendix VII.IV*).

According to the TD-DFT calculations, λ_{\max} wavelength of **Q-BTT** at 425 nm corresponds to the HOMO-1 \rightarrow LUMO+1 electron transition (theoretically at 397 nm) involving the **MQ** moiety, while the feature at 538 nm (calculated at 493 nm) is ascribed to the HOMO \rightarrow LUMO+1 transition related to the **BQ** unit. The HOMO-1 \rightarrow LUMO+1 transition is also observed for **Q-CPV** at 570/683 nm.

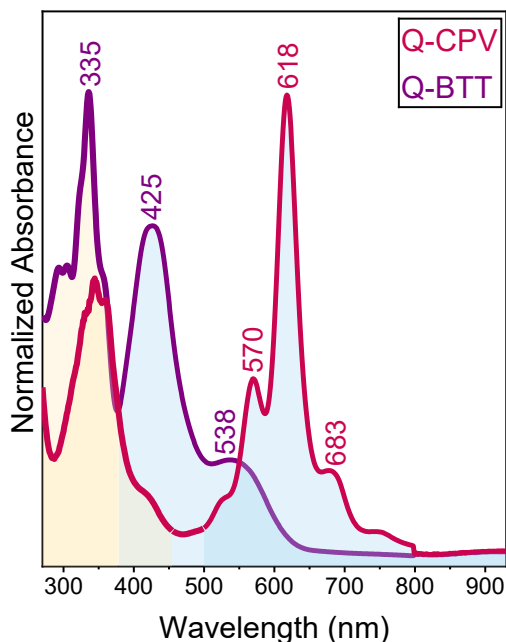


Figure IV.4.4. UV-Vis-NIR electronic absorption spectra of **Q-CPV** and **Q-BTT** molecules in CH_2Cl_2 at room temperature. Quinoidal bands are highlighted in blue while the aromatic ones are in yellow.

Both octacyano systems present two sets of bands, and in agreement with the already discussed optical spectrum of **Q-CPV**, the highest wavelengths correspond to the quinoidal shape (highlighted in blue in Figure IV.4.4).

The configuration of the ground electronic state of **Q-BTT** was explored through DFT calculations (Figure IV.4.5) and, similar to the case of the quinoidal spiro molecule, the singlet open-shell form was the most stable situation for this system. Since diradical molecules present low-lying triplet states, the singlet-triplet gap of **Q-CPV** and **Q-BTT** were also evaluated (red circles). As can be seen in Figure IV.4.5, both quinoidal molecules present similar ΔE_{S-T} values: 5.33 kcal/mol and 5.57 kcal/mol for **Q-CPV** and **Q-BTT**, respectively, considerably smaller than those of the aromatic **CPV** molecules. However, the stabilization of the quintet state observed in **Q-CPV** does not take place in parallel **Q-BTT** (9.59 kcal/mol and 32.11 kcal/mol, respectively; purple circles in Figure IV.4.5). Therefore, it must be the spiro-conjugation phenomenon the effect that accounts for this stabilization in **Q-CPV**.

The open-shell character of **Q-BTT** was compared with those of the **MQ** and **BQ** moieties treated as individual molecules (Figure IV.4.5). These models present a

Table IV.4.2. Optical data of the octacyano systems **Q-CPV** and **Q-BTT**.

| Quinoidal Octacyano System | Experimental ^a | | TD-DFT ^b | | |
|----------------------------|-----------------------------|---|-----------------------------|-----------------------------|----------------------------------|
| | λ_{max} (nm) | ϵ ($\times 10^{-4}$ L·mol ⁻¹ ·cm ⁻¹) | λ_{max} (nm) | Oscillator Strength (a. u.) | Electronic Transition |
| Q-CPV | 344 (330/360) | 2.0 | 416 | 0.35 | HOMO-1→LUMO+3 (α/β) |
| | 570 (524) | | 583 | 0.22 | HOMO-1→LUMO+1 (α/β) |
| | 618 | | 596 | 1.66 | HOMO→LUMO (α/β) |
| | 683 | | 652 | 0.89 | HOMO-1→LUMO+1 (α/β) |
| Q-BTT | 335 | 4.2 | 310 | 0.19 | HOMO→LUMO+3 (α/β) |
| | 425 | | 397 | 0.48 | HOMO-1→LUMO+1 (α/β) |
| | 538 | | 493 | 0.38 | HOMO→LUMO+1 (α/β) |
| | | | 876 | 0.09 | HOMO→LUMO (α/β) |

^aMeasured in CH_2Cl_2 at room temperature. ^bTD-DFT calculations at (U)B3LYP/6-31G** level of theory. Geometry optimizations of **Q-CPV** and **Q-BTT** molecules were performed as singlet open-shell systems (spin unrestricted B3LYP).

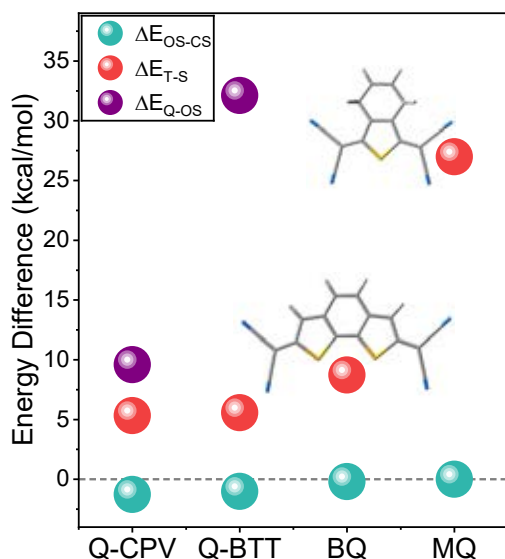


Figure IV.4.5. Formation energy differences (kcal/mol) between the singlet open-shell and the closed-shell configurations (green circles), and between the triplet and quintet states respect to the corresponding ground electronic state (red and purple circles, respectively) for **Q-CPV** and **Q-BTT** molecules, and **BQ** and **MQ** models, calculated at the (U)B3LYP/6-31G** level of theory.

closed-shell configuration of the ground electronic state and higher ΔE_{S-T} values respect to **Q-BTT**. In this sense, similar to the case of **Q-CPV**, the parallel coupling of both model molecules is the key to promote the diradical character.

A. II. Influence of the Spiro-conjugation on the Electronic Structure

As described in the previous section, the combination of the spiro linkage between the two quinoidal CPV moieties and their incipient diradical character result in a not trivial energy states diagram for this molecule. This energy diagram of **Q-CPV** is showed in Figure IV.4.6, together

with those of the two non-spiro models: **QM1CN** and **QM2CN**:

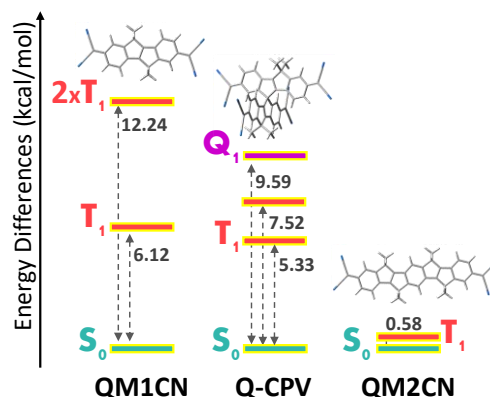


Figure IV.4.6. Formation energy differences (kcal/mol) between the ground electronic state (S_0) and the triplet (T_1) and quintet (Q_1 , only for the spiro-conjugated molecule) states of **QM1CN**, **QM2CN** and **Q-CPV** systems. Formation energies were calculated at the (U)B3LYP/6-31G** level of theory, and the second triplet state of **Q-CPV** was obtained as the vertical excitation energy by TD-DFT.^[4]

Regarding the singlet-triplet gap of the three systems, spiro **Q-CPV** behaves as an intermediate case between both non-spiro molecules, the closed-shell **QM1CN** and the diradical **QM2CN**. The low energy of a quintet state in **Q-CPV** suggests the formation of a tetraradicaloid species driven by the spiro coupling of two radicaloid CPV units. This *spiro-coupling effect* is manifested in the existence of two triplet states close in energy and in a quintet state 1.07 kcal/mol more stable than twice the triplet.

The singlet-triplet gap in **Q-CPV** was explored through EPR measurements and the molar magnetic susceptibility (χ_M) spectra (Figure IV.4.7), performed by the group of Professor Eiichi Nakamura:

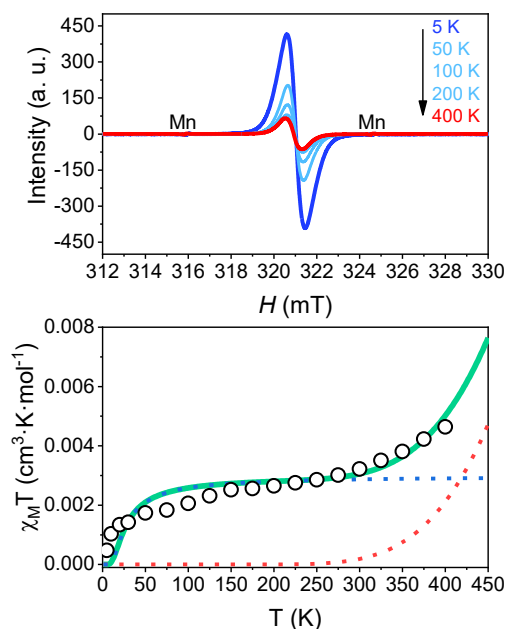


Figure IV.4.7. *Top*) EPR spectra of **Q-CPV** in solid state from 5 K to 400 K. Mn represents the reference signal of a Mn marker; *Bottom*) $\chi_M T/T$ plot calculated from the EPR intensity (open circles). Green line shows $\chi_M T/T$ curve reproduced by using the four-spin model composed of a singlet ground state (S), a triplet state (T), and a quintet state (Q) with an additional biradical impurity. Red and blue dashed lines represent the $\chi_M T/T$ curves from the main product and the impurity, respectively, and the green line indicates the sum.

The EPR behavior of **Q-CPV** with the temperature is the inverse than the observed for other diradical systems studied in previous chapters (as **OTPD₅** dianion or neutral **2DQQT**, see *Appendix VII.V*). In those cases, EPR intensity increases when increasing the temperature as a consequence of the thermal population of the low-lying triplet state. However, EPR intensity of **Q-CPV** molecule diminishes as the temperature is elevated from 5K to 400K (Figure IV.4.7, left panel).

In the case of the magnetic susceptibility, the $\chi_M T$ values increase with

the temperature, but not in an homogeneous way (see empty circles in Figure IV.4.7, right panel). $\chi_M T$ versus T plot displays an S-shaped form, in which three different slopes are observed. $\chi_M T$ behavior for temperatures higher than 225 K is well-reproduced taking into account the contributions from a singlet ground state and the presence of an excited triplet and quintet states (red dashed line in Figure IV.4.7, right panel), as presented in Figure IV.4.6. However, the $\chi_M T$ versus T plot in the full range of temperatures is described by a *four-spin model*^[5], in which a diradical impurity justifies the behavior at temperatures lower than 100 K (blue dashed line). This diradical impurity can be ascribed to a σ -dimer formed through the intermolecular interaction between two radical centres of two **Q-CPV** molecules. The ΔE_{S-T} for this system is 0.004 kcal/mol, denoting the small interaction between the two radical centres.

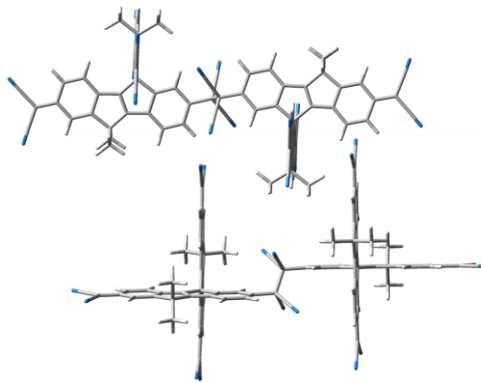


Figure IV.4.8. Optimized geometry of **Q-CPV** σ -dimer as singlet open-shell at the (U)B3LYP/6-31G** level of theory.

The ΔE_{S-T} and ΔE_{S-Q} values obtained through this model for **Q-CPV** molecule are 5.76 kcal/mol and 17.29 kcal/mol, respectively.

A. III. Energy of the Frontier Molecular Orbitals

Figure IV.4.9 displays the frontier molecular orbital energies of the CPVs family:

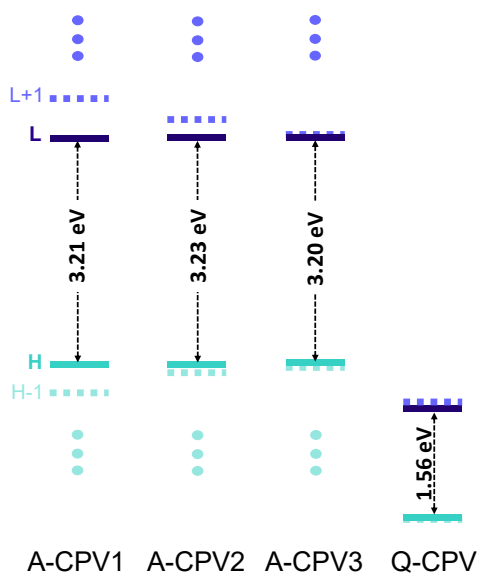


Figure IV.4.9. Energy of the frontier molecular orbitals of the CPV family. A-CPV molecules were optimized as closed-systems while Q-CPV was calculated as singlet open-shell configuration at the (U)B3LYP/6-31G** level of theory. Green lines correspond to the HOMOs; blue lines correspond to the LUMOs; dashed lines correspond to the HOMO-1 and LUMO+1 levels.

While aromatic spiro CPVs present similar optical bandgaps values, E_g is clearly narrowed in Q-CPV molecule. This behaviour has been already observed in the cross-conjugated systems when comparing aromatic OTPD_n molecules with the quinoidal 2DQoT. In addition, Q-CPV presents a high stabilization of the frontier molecular orbitals (FMO) compared to its aromatic counterparts.

In line with the FMO energies discussion in previous chapters, changes in

the E_g values in CPV family can be ascribed to the following factors:

- 1. The aromaticity or resonance stabilization energy.** This effect is evident when comparing the aromatic and quinoidal CPV molecules. The aromaticity stabilization is diminished when the π -electrons are involved in exocyclic $C_\alpha=C_\alpha$ double bonds, narrowing the HOMO-LUMO gap in quinoidal systems. This effect is experimentally demonstrated through the bathochromic shift of λ_{max} wavelength of Q-CPV in comparison with the aromatic molecules.

- 2. The planarity or rigidity of the system.** Despite in A-CPV2 and 3 the two π -systems forming the spiro molecules are rigidified in comparison with the rotational-free phenylene substituents in A-CPV1, their E_g values are very close

- 3. The substituent groups.** For Q-CPV, as in the case of the 2DQoT oligomers, the electron-withdrawing CN groups narrows the HOMO-LUMO gap.

Regarding the octacyano Q-CPV and Q-BTT systems, both molecules present optical band gaps of 1.56 eV and 1.74 eV, respectively (indicated in black in Figure IV.4.10). According to the discussion in Section A.I, the spiro-conjugation is the only differentiating factor that can explain this smaller optical band gap of Q-CPV. In this system, the interaction between the HOMO of the independent moieties to form the spiro molecule generates the corresponding symmetric and antisymmetric levels. The latter constitutes the new destabilized HOMO level in the spiro-bridged molecule,

explaining the narrower optical bandgap.^[6, 7]

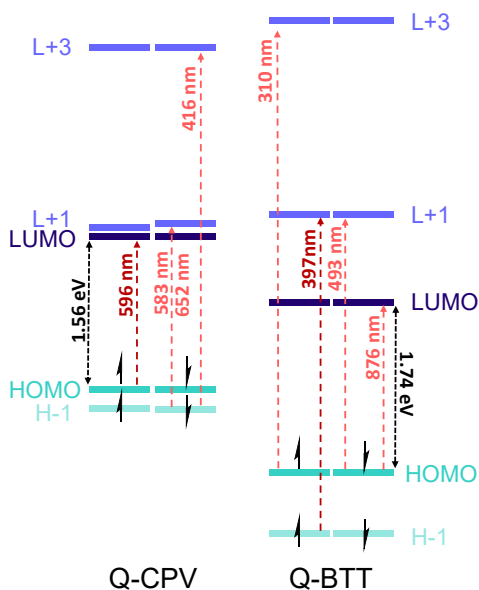


Figure IV.4.10. Energy of the frontier molecular orbitals and electronic transitions calculated at the TD-DFT/(U)B3LYP/6-31G** level of theory of singlet open-shell **QCPV** (left) and **Q-BTT** (right). HOMO levels are depicted in green, while LUMO levels are in blue. Electronic transitions corresponding to the experimental λ_{\max} wavelength are highlighted in dark red, and the HOMO-LUMO gap in black

A. IV. Atomic Coefficients

As described in *Section I.III. Spiro-Conjugation*, in this kind of systems, larger atomic coefficient values for the spiroconjugated atoms mean a larger π -electron density on them, providing the proper scenario for spiro-conjugation phenomenon to occur.^[6, 8] In addition, the spiro-conjugated $2p_z$ orbitals forming the HOMO-1 must present the suitable disposition to assure the through-space interaction. The contribution and sign of

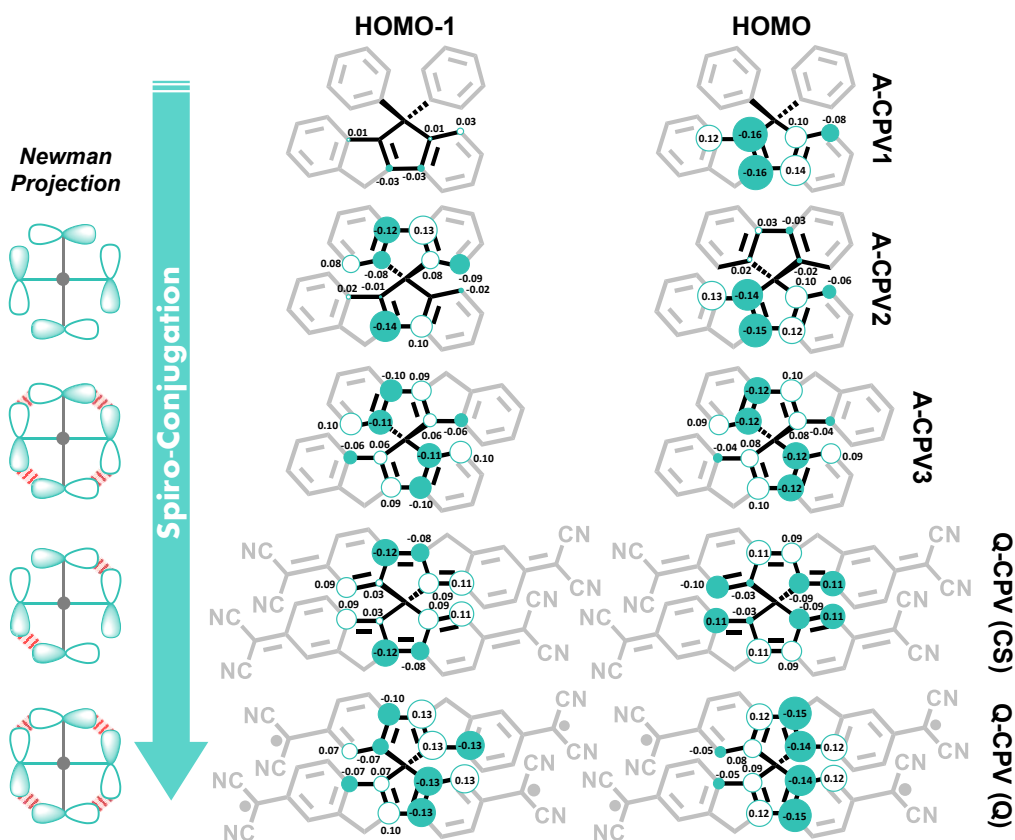
each atomic coefficient to the π -system are accessible parameters through theoretical calculations.

Scheme IV.4.5 presents the atomic coefficients of C $2p_z$ orbitals of the spiro motifs calculated at (U)B3LYP/6-31G** level of theory. For the aromatic systems, only the configuration corresponding to the ground electronic state, *i.e.*, the closed-shell form, was evaluated, while for **Q-CPV**, results for both, the closed-shell and the *fully* open-shell (quintet) configurations, are showed.

For **A-CPV1**, in which spiro-conjugation is not possible, the contribution of the evaluated atomic orbitals to the HOMO-1 is negligible, while this contribution is sizeable in the HOMO.

In the case of **A-CPV2**, despite the atomic coefficient values of the two spiro-conjugated C atoms on the fluorene moiety are appreciable, **CPV** unit displays a similar behaviour than in **A-CPV1**. Besides the low π -electron density on the spiro-conjugated atoms, they neither display the spatial disposition to accomplish the through-space interaction, as can be observed in the Newman projection in Scheme IV.4.5.

Ongoing to the symmetrical molecules, **A-CPV3** and **Q-CPV**, atomic coefficients of lobes with the same sign are face to face, allowing the through-space interaction between them. This situation is reproduced in the *fully* open-shell **Q-CPV** system, with even higher π -electron density on the spiro-conjugated C than the aromatic counterpart. However, the closed-shell configuration of the quinoidal



Scheme IV.4.5. Individual atomic coefficients of C 2pz orbitals in spiro systems for HOMO-1 and HOMO, together with the Newman projection of these orbitals for the spiro-conjugated C in the HOMO-1. Different colour of the orbital lobes indicates different sign, and their size are proportional to the corresponding atomic coefficients. Interactions between in phase orbitals are highlighted in red. Values for **A-CPV1**, **A-CPV2** and **A-CPV3** were obtained from the closed-shell configuration, while **Q-CPV** is presented for the closed-shell (CS) and the quintet (Q) configurations.

system does not display the complete in phase disposition of the evaluated orbital lobes.

open-shell configuration respect to the aromatic **A-CPV3**.

According to these results, and in agreement with the discussion performed along *Section A* for neutral molecules, spiro-conjugation is more likely to occur in the two symmetrical spiro systems, *i. e.*, **A-CPV3** and **Q-CPV**. The quinoidal nature of the second one reduces the π -electron confinement in the benzene rings, explaining the larger electron density in the spiro-conjugated C atoms in the *fully*

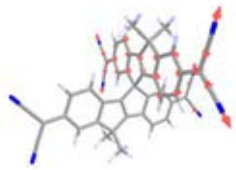
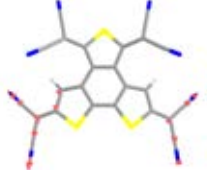
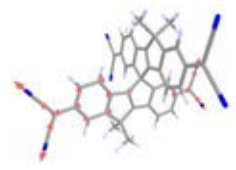
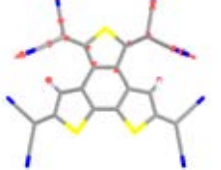
B. Molecular Structure

B. I. Vibrational IR Spectroscopic Properties

Dicyanomethylene groups of the two quinoidal systems, the spiro **Q-CPV** and the parallel **Q-BTT**, can be studied through IR spectroscopy.^[9] Figure IV.4.11 presents the CN stretching bands of the experimental IR spectra of **Q-CPV** and **Q-BTT** at room temperature, together with the corresponding theoretical spectra. The CN stretching vibrational modes (ν_{CN}) for both molecules are also displayed in Table IV.4.3.

The experimental IR spectrum of **Q-BTT** presents the ν_{CN} band at 2223 cm^{-1}

Table IV.4.3. Eigenvectors of the discussed vibrational modes for **Q-CPV** and **Q-BTT** systems.

| Q-CPV | Q-BTT |
|--|---|
|  2216 cm^{-1} |  2226 cm^{-1} |
|  2234 cm^{-1} |  2247 cm^{-1} |

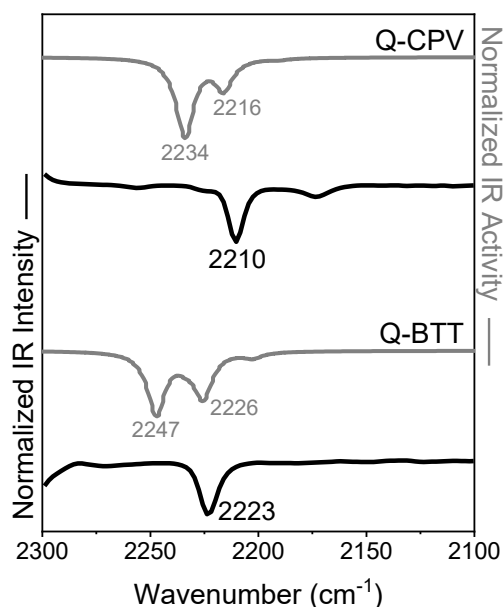


Figure IV.4.11. ν_{CN} region of FT-IR spectra of **Q-BTT** (bottom) and **Q-CPV** (top) in CH_2Cl_2 at room temperature. Black lines correspond to the experimental IR spectra while grey lines correspond to the theoretical IR spectra calculated at the (U)B3LYP/6-31G** level of theory and scaled down uniformly by a factor of 0.96.

(theoretically at 2247 cm^{-1} and 2226 cm^{-1}), while for **Q-CPV** ν_{CN} is placed at 2210 cm^{-1} (theoretically at 2234 cm^{-1} and 2216 cm^{-1}). Theoretical spectra correlate properly with the experimental results. However, in both cases only one ν_{CN} band was obtained experimentally, denoting the equivalence between the four dicyanomethylene moieties on each molecule. In the case of **Q-CPV**, the fact that only one ν_{CN} mode is detected evidences that the open-shell character is spread over the whole molecule, *i.e.*, it is compatible with a tetraradical species.

For **Q-BTT** molecule, when comparing with the quinoidal tetracyano-oligothienopyrrolediones (**2DQoT** family; ν_{CN} at 2204-2206 cm^{-1}), the higher wavenumber of the octacyano system indicates a lower π -electron delocalization towards the dicyanomethylene moieties.

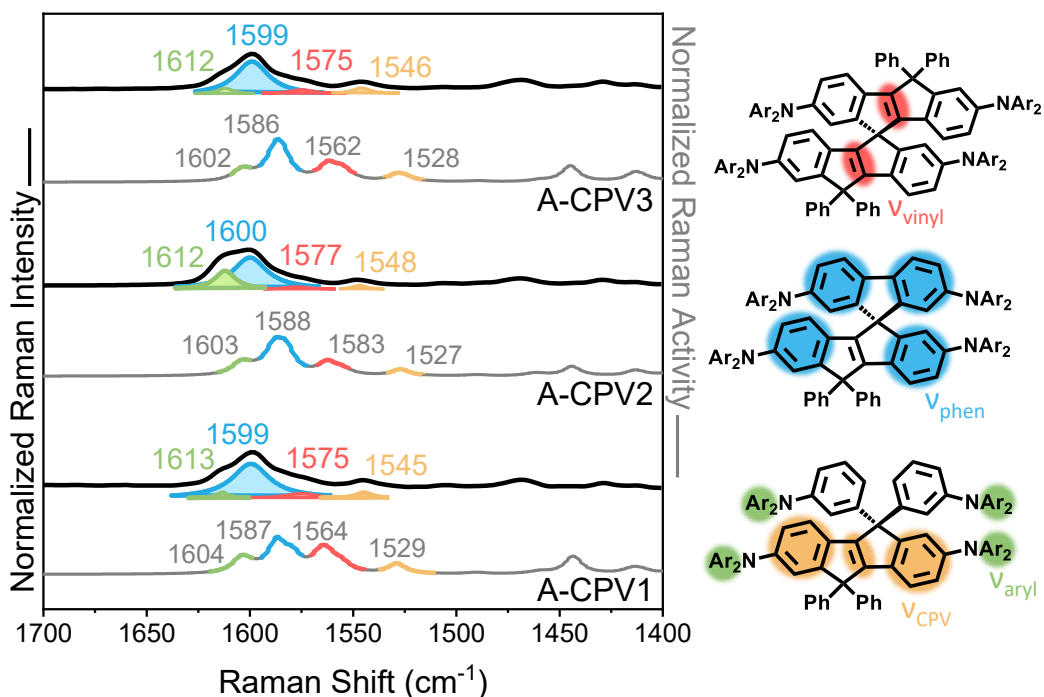


Figure IV.4.12. *Left*) FT-Raman spectra of aromatic CPV molecules in solid state at room temperature. Black lines correspond to the experimental Raman spectra while grey lines correspond to the theoretical Raman spectra calculated at the B3LYP/6-31G** level of theory and scaled down uniformly by a factor of 0.96. The wavenumbers of the experimental spectra have been assigned by deconvolution (Lorentzian shape, $R^2 > 0.99$): $\nu_{(C=C)}$ aryl in green, $\nu_{(C=C)}$ phenyl in blue, $\nu_{(C=C)}$ vinyl in red and ν_{CPV} in orange; *Right*) Scheme of the groups affected by the discussed vibrational normal modes.

B. II. Vibrational Raman Spectroscopic Properties

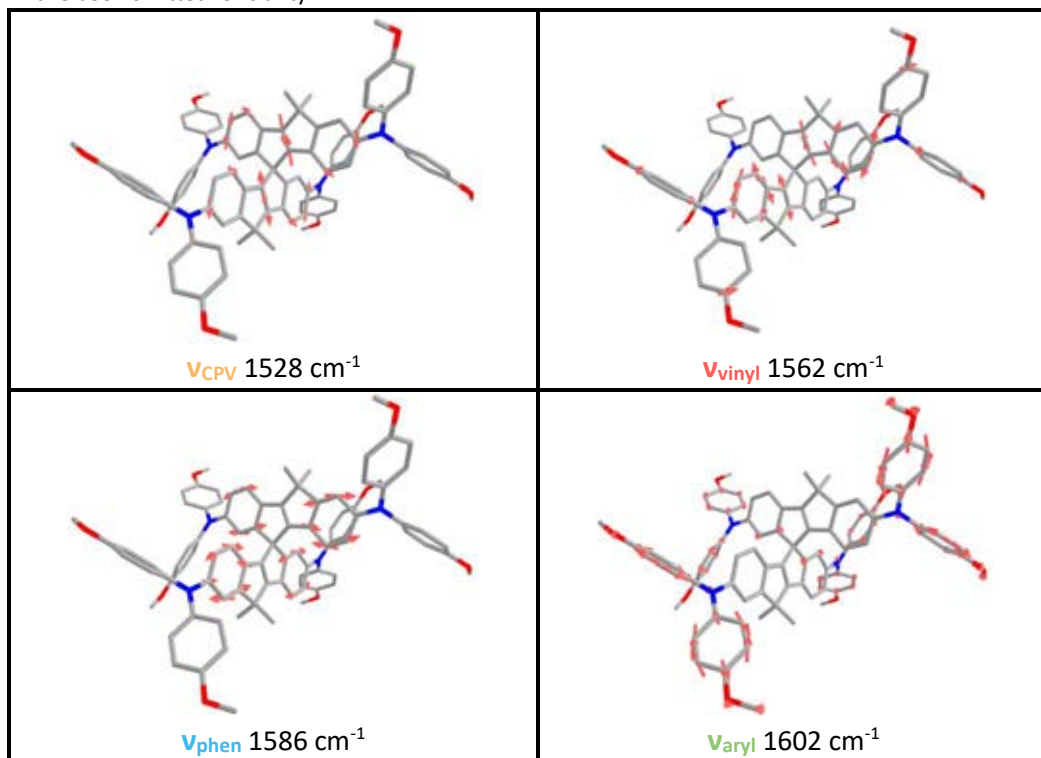
Figure IV.4.12 displays the solid-state FT-Raman spectra of the aromatic CPV molecules at room temperature. Eigenvectors of the theoretical vibrational normal modes related to the Raman bands are depicted in Table IV.4.4.

The most relevant Raman bands that account for the C–C/C=C π -conjugated backbone are placed between 1615–1540 cm^{-1} . Since these features are located in a small spectral region, the final Raman spectra constitute an envelope of the individual bands. For this reason, the assignment of the Raman wavenumbers

was carried out by deconvolution and comparing with the theoretical calculations and the available bibliography.^[10, 11]

In Figure IV.4.12, the highest energy band is assigned to the stretching vibration of the aryl rings of the geminal aminophenyl substituents (ν_{aryl} , in green in Figure IV.4.12 and Table IV.4.4). This vibration remains almost unaltered between the three molecules: 1613 cm^{-1} \rightarrow 1612 cm^{-1} \rightarrow 1612 cm^{-1} , from **A-CPV1** to **A-CPV3**.

The most intense band for the three systems is assigned to the collective CC stretching mode of the phenyl rings of the

Table IV.4.4. Eigenvectors of the discussed vibrational modes for **A-CPV3** molecule. Hydrogen atoms have been omitted for clarity.

CPV cores (ν_{phenyl} , in blue in Figure IV.4.12 and Table IV.4.4). In contrast, the Raman band related to the stretching vibration of the vinylic bonds (ν_{vinyl} in red) is enveloped by the ν_{phenyl} feature. These bands do not present significant variations from **A-CPV1** to **A-CPV3** (ν_{phenyl} : 1599 cm⁻¹ → 1600 cm⁻¹ → 1599 cm⁻¹; and ν_{vinyl} : 1575 cm⁻¹ → 1577 cm⁻¹ → 1575 cm⁻¹). However, ν_{vinyl} of **A-CPV** molecules are considerably down-shifted respect to the non-spiro **COPV** (1617 cm⁻¹ → 1583 cm⁻¹, from **COPV-1** to **COPV-6**, see Figure IV.4.13).^[10, 11] This trend of the ν_{vinyl} in **COPV** series is ascribed to the release of the strained vinylic bridge due to the equalization of the C–C/C=C bonds when enlarging the oligomer size. In fact, the larger π -electron delocalization in bis(arylamino) **COPV1**,

DA(COPV1), moves this ν_{vinyl} to 1579 cm⁻¹.^[12] By this way, even when comparing with the bis(arylamino) end-capped non-spiro counterpart, **A-CPV3** presents shorter ν_{vinyl} (1575 cm⁻¹). Consequently, a larger delocalization of the π -electron density in spiro **A-CPV** than in longer **COPV** and in **DA(COPV1)** can be deduced from their lower ν_{vinyl} wavenumbers. Regarding the ν_{phenyl} Raman bands, both spiro and non-spiro carbon-bridged phenylenevinylene present similar wavenumbers (1602 cm⁻¹ → 1598 cm⁻¹, from **COPV-1** to **COPV-6**; and 1600 cm⁻¹ in **DA(COPV1)**).

Finally, in Figure IV.4.12 the Raman band assigned to a stretching C=C_{vinyl} mode coupled to a CC_{phenyl} vibration is

highlighted in orange (denoted as ν_{CPV} , see Table IV.4.4). This band evolves from **A-CPV1** to **A-CPV3** as follows: $1545 \text{ cm}^{-1} \rightarrow 1548 \text{ cm}^{-1} \rightarrow 1546 \text{ cm}^{-1}$, in agreement with the higher values of ν_{phenyl} and ν_{vinyl} for **A-CPV2**.

These little changes of the stretching frequencies in the Raman spectra of **A-CPV** family are attributed to the dominance of the Raman activity of the CPV core, which is the same for all the aromatic **CPV** molecules.

In Figure IV.4.13, FT-Raman spectrum of spiro **A-CPV3** is compared with those of the non-spiro **COPV-1**, **COPV-2** and **COPV-3**.^[10, 11] Despite **A-CPV3** is formed by two **COPV-1** units linked by a tetrahedral carbon atom, its Raman shifts related with the discussed vibrational modes are closer to those of the longer oligomers of the **COPVn** series. Regarding Figure IV.4.13

right panel, while ν_{CPV} and ν_{phenyl} of **A-CPV3** present wavenumbers similar to those of **COPV-2** and **COPV-3**, respectively, ν_{vinyl} is even smaller than that of the longest **COPV-6** molecule. According to these results, the effective π -conjugation in the vinylenic bridge is considerably larger in the spiro system than in the non-spiro **COPV-1** and even in the end-capped **DA(COPV1)** counterpart. Thus, π -electron delocalization between the two CPV moieties of **A-CPV3** must occur to accounts for this *extra* delocalization in the innermost part of the molecule, that is, in the carbon atoms that participate in the spiro-conjugation phenomenon.

FT-Raman spectra of the quinoidal octacyano systems in solid state at room temperature are showed in Figure IV.4.14, and the eigenvectors of the vibrational modes at which Raman bands

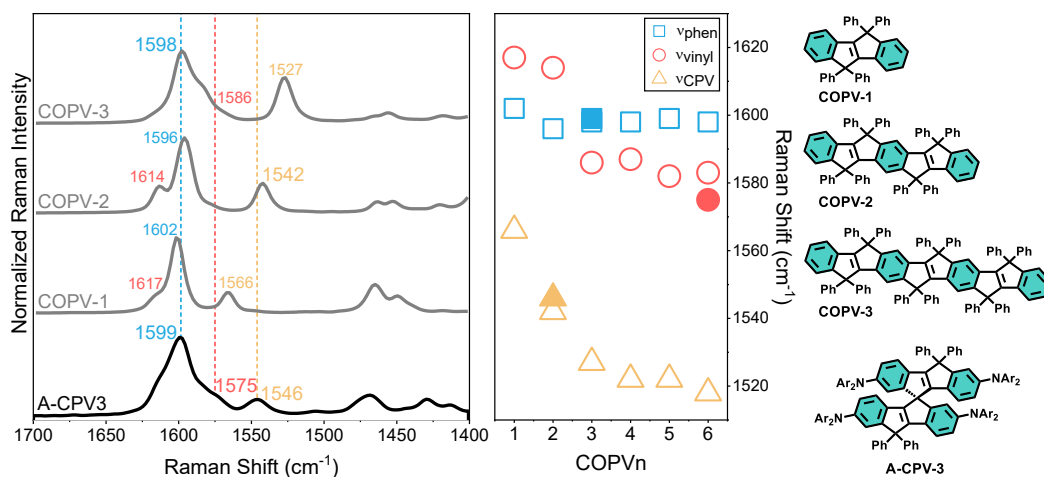


Figure IV.4.13. *Left*) FT-Raman spectra of **A-CPV3-pp** (black line) and **COPVn** (grey lines) molecules in solid state at room temperature.; *Middle*) COPV-size (empty figures) dependence of the wavenumber for the Raman bands related with the three discussed vibrational modes together with the wavenumbers corresponding to the **A-CPV3** spiro system (fulfilled figures): blue squares correspond to $\nu_{\text{(C=C) phenyl}}$, red circles correspond to $\nu_{\text{(C=C) vinyl}}$ and orange triangles correspond to ν_{CPV} ; *Right*) Chemical structures of **COPVn** molecules and **A-CPV3**.

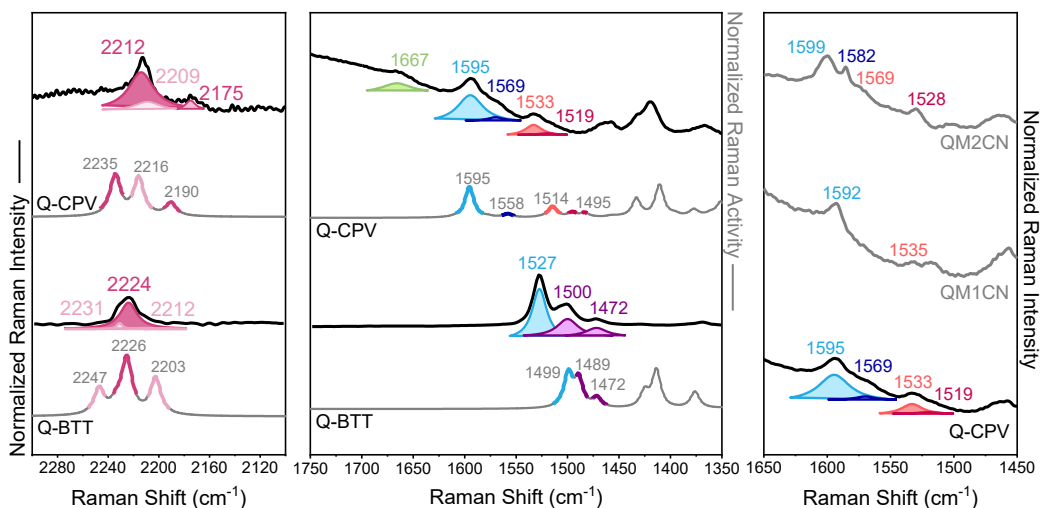


Figure IV.4.14. Left) Raman spectra of spiro **Q-CPV** and parallel **Q-BTT** molecules in solid state at room temperature in the ν_{CN} (left) and $\nu_{\text{C=C}}$ (middle) spectral region. Black lines correspond to the experimental Raman spectra while grey lines correspond to the theoretical Raman spectra calculated at the (U)B3LYP/6-31G** level of theory and scaled down uniformly by a factor of 0.96. The wavenumbers of the experimental spectra have been assigned by deconvolution (Lorentzian shape, $R^2 > 0.99$); Right) Raman spectra of non-spiro **QM1CN** and **QM2CN** molecules (grey lines) and spiro **Q-CPV** (black line) in solid state at room temperature. $\nu_{\text{C=C phenyl}}$ mode is highlighted in light and dark blue, $\nu_{\text{C=C aryl}}$ in green, $\nu_{\text{C=C bridge}}$ in light and dark red, ν_{CN} in light and dark pink and ν_{MQ} in purple.

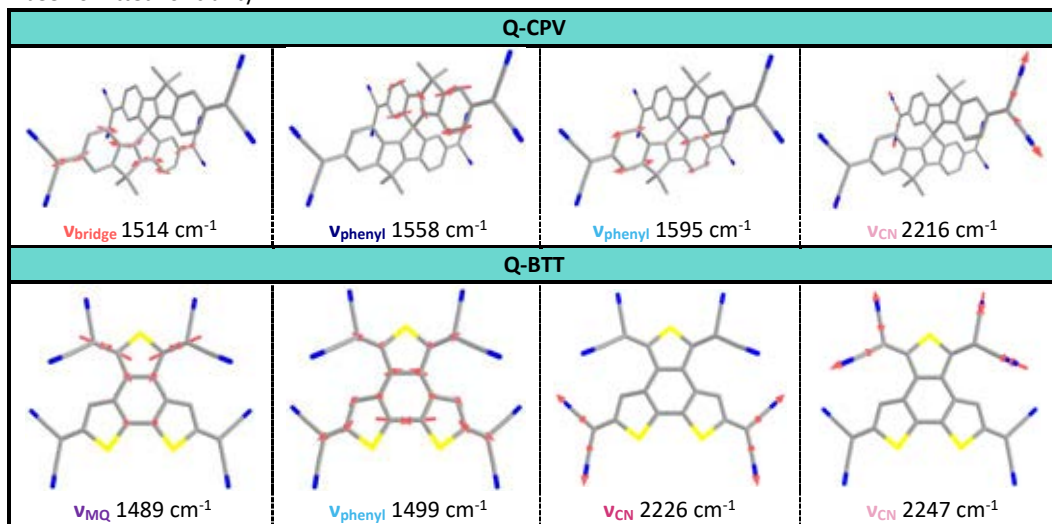
are ascribed to are depicted in Table IV.4.5. As in the case of the aromatic spiro molecules, the most intense feature in **Q-CPV** and **Q-BTT** Raman spectra are related to the ν_{phenyl} mode (highlighted in blue).

For **Q-CPV**, two different ν_{phenyl} and ν_{bridge} contributions are found, highlighting the presence of two C–C/C=C bonds patterns in the spiro-conjugated systems. The more energy ν_{phenyl} wavenumber (highlighted in light blue at 1595 cm^{-1}) belongs to the same indeno[2,1-a]indene moiety that the stretching vibration of the carbon bridge at 1533 cm^{-1} (ν_{bridge} mode in light red), which possess a quinoidal shape. On the contrary, the second CPV unit presents lower ν_{phenyl} and ν_{bridge} wavenumbers (at 1569 cm^{-1} and 1519 cm^{-1} , respectively), denoting a larger relaxation of the C–C/C=C bonds

alternation, that is, a larger π -electron delocalization. The two bands pattern for each vibrational mode, representing the quinoidal and the aromatic shapes, has been already observed for the diradical **QM2CN** system (see Figure IV.4.14, right panel), and has been described as the Raman fingerprint of the formation of a diradical species from a quinoidal structure.^[11]

Inversely to the ν_{phenyl} and ν_{bridge} modes, which experiment a shift to lower wavenumbers from the aromatic to the quinoidal spiro-systems, ν_{aryl} is significantly up-shifted (from 1612 cm^{-1} in **ACPV-3** to 1667 cm^{-1} in **QCPV**). This difference is because these bands do not arise from the same aryl groups. While in **ACPV** molecules ν_{aryl} Raman bands are provoked by the stretching vibrations of the benzene rings

Table IV.4.5. Eigenvectors of the discussed vibrational modes of **Q-CPV** and **Q-BTT**. Hydrogen atoms have been omitted for clarity.



in the geminal aminophenyl substituents, these groups are not present in the quinoidal system. In the case of **Q-CPV**, v_{aryl} is due to the lateral aryl units in the carbon bridge of the CPV core (in the central bicyclo [3.3.0] octene moiety). This band is not present in the theoretical Raman spectrum of **Q-CPV**, since aryl rings are substituted by methyl groups in the theoretical model to reduce the computational costs. However, it does emerge in the theoretical spectra of the aromatic systems.

Regarding the parallel quinoidal molecule **Q-BTT**, the Raman feature at 1527 cm^{-1} is ascribed to a combined vibrational mode involving the central benzene ring and the lateral thiophene units (v_{phenyl}). v_{phenyl} constitutes a low wavenumber value when comparing with similar systems bearing quinoidal benzene rings.

Tetracyanoquinodimethane molecule (TCNQ) presents a stretching vibration of the quinoidal benzene ring at

1602 cm^{-1} , which is down-shifted to 1596 cm^{-1} upon reduction to the dianion species.^[13] In this context, the wavenumber value of v_{phenyl} of **Q-BTT** seems to fit better with a partially aromatized benzene unit.

On the other hand, the stretching vibrations of the thiophene rings, at 1500 cm^{-1} and 1472 cm^{-1} , are mainly due to the **MQ** unit. These bands have wavenumber values of *pseudo* aromatic thiophenes, like those found for the diradical **2DQPT** molecule studied in the former chapter (1486 cm^{-1} and 1472 cm^{-1}).

Finally, features related to the stretching vibrations of the dicyanomethylene groups (v_{CN}) for both quinoidal molecules were also detected by Raman spectroscopy. Both octacyano systems present two groups of bands ascribed to the CN moieties (highlighted in light and dark pink in Figure IV.4.14). The most energy feature in **Q-CPV** (2212 cm^{-1}) corresponds to the same unit as the larger

ν_{phenyl} and ν_{bridge} wavenumbers, *i. e.*, the CPV moiety with a predominant quinoidal shape. This is also the case of **Q-BTT**, in which ν_{CN} at 2231 cm^{-1} belongs to the more quinoidal **MQ** unit while the stretching vibration at 2224 cm^{-1} is due to the **BQ** group, where the bond length alternation is smaller.

B. III. Bond Lengths Analysis

Figure IV.4.15 displays the variation of the length of the central vinylene bridge along the spiro CPV series, together with the BLA values of the π -conjugated sequences in **Q-BTT** molecule. These distances were calculated in the optimized geometries (**A-CPVn** as closed-shell systems, **Q-CPV** as singlet open-shell and quintet configurations, and **Q-BTT** as singlet open-shell) at the (U)B3LYP/6-31G** level of theory.

A general view of Figure IV.4.15 (left panel) shows that the vinylene bridge is slightly enlarged from **A-CPV1** to **A-CPV3** in the aromatic spiro systems. In the case of **Q-CPV**, (C=C)vinyl is shortened in the diradical moiety respect to the closed-shell one (red fulfilled circles). If the fully open-shell structure is considered (red empty circle), then (C=C)vinyl bond length is even shorter, denoting the large π -electron delocalization in **Q-CPV**. This change agrees with the downshift of the ν_{bridge} in the Raman spectra of **Q-CPV** ($1533/1519\text{ cm}^{-1}$) respect to the aromatic **A-CPV3** and the non-spiro **QM1CN** (1575 cm^{-1} and 1535 cm^{-1} , respectively).^[3]

Concerning the octacyano **Q-BTT** molecule (Figure IV.4.15, right panel), three different π -conjugated frameworks can be evaluated: i) the interdicyanomethylene sequence in the monothiophene moiety (denoted as **MQ**); ii) the interdicyanomethylene sequence in the bithiophene moiety (**BQ**), parallel to **MQ**; and iii) the framework between two opposite dicyanomethylene groups, crossing the other two sequences (denoted as *cross*). Regarding these data, a larger equalization of the C–C/C=C pattern was found for the **BQ** framework, according to the Raman discussion, while **MQ** presents the largest BLA value.

Joining together the optical and vibrational studies, the structure of the neutral **CPVs** and **Q-BTT** systems can be established. While the aromatic spiro molecules are described as closed-shell systems, with a well-defined C–C/C=C bond length alternation, this is not the case of the quinoidal molecule. **Q-CPV** presents an open-shell configuration of the ground state, and it can be seen as a tetraradicaloid system thanks to the spiro-conjugation of both diradical CPV units.

Q-BTT also displays a singlet open-shell ground state. Despite the two radical centres are mainly in the larger moiety (**BQ**), also some contribution of the diradical **MQ** form is observed. The delocalization of the diradical entity over the complete molecule suggests that some kind of interaction must exist between the two parallel units. The conjugation pattern that connects the two chromophores is a crossed framework between opposite dicyanomethylene groups.

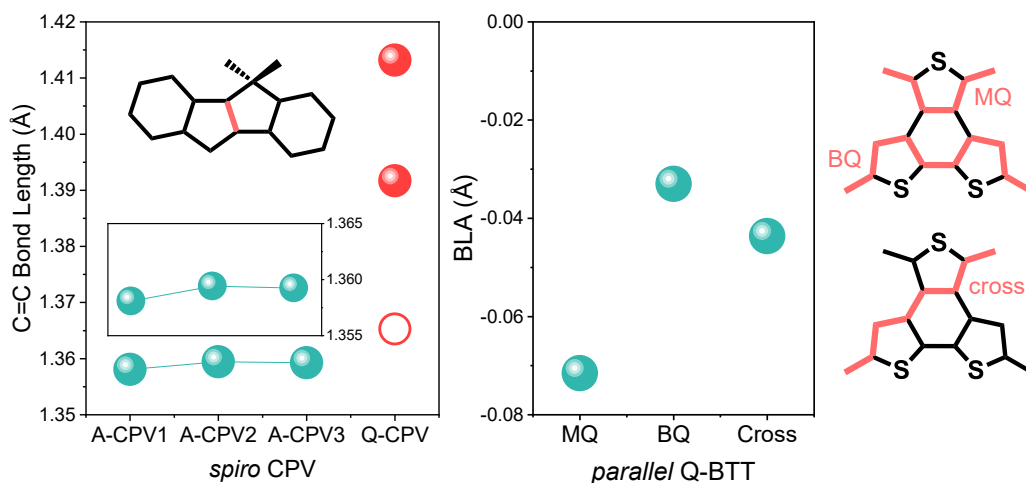
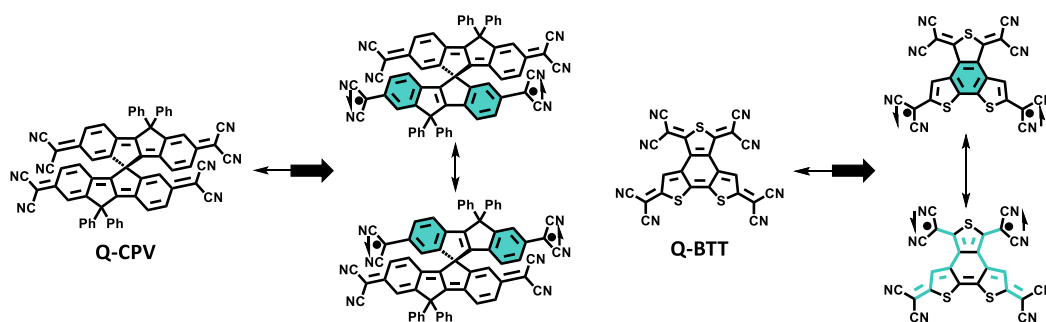


Figure IV.4.15. Lengths (Å) of the central (C=C) vinylic bond in the spiro series (*left*) and bond length alternation (BLA) values (Å) of the π -conjugated carbon bridges in **Q-BTT** (*right*) for the optimized molecular structures calculated at the (U)B3LYP/6-31G** level of theory, together with the schemes of the evaluated bond lengths (highlighted in red). Aromatic molecules were optimized with a closed-shell configuration while the quinoidal ones were optimized as singlet open-shell systems. Empty circles correspond to the quintet configuration in the spiro **Q-CPV** molecule.

Scheme IV.4.7 present the chemical structures proposed for the two quinoidal molecules.



Scheme IV.4.7. Closed-shell (*left*) and singlet open-shell (*right*) resonance structures of spiro **Q-CPV** and parallel **Q-BTT** molecules. The cross-conjugated framework that connects the **MQ** and **BQ** moieties in parallel **Q-BTT** is highlighted in green.

4.2 CHARGED SPECIES OF CPV FAMILY

A. Electronic Structure

A. I. Electrochemical Properties

Figure IV.4.16 and Table IV.4.6 present the cyclic voltammetry processes of CPVs and Q-BTT molecules in CH₂Cl₂ at room temperature.

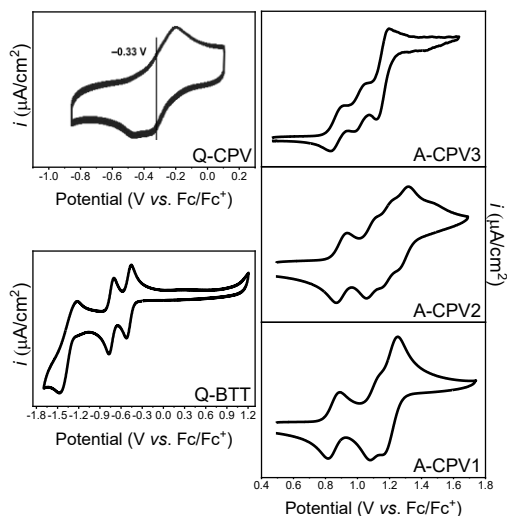


Figure IV.4.16. Cyclic voltammetry curves of **A-CPV** (right), and **Q-CPV** and **Q-BTT** (left) molecules in 0.1M Bu₄NPF₆ in CH₂Cl₂ at room temperature (vs. Fc/Fc⁺).

Table IV.4.6. Electrochemical data of of **A-CPV**, **Q-CPV** and **Q-BTT** molecules.

| | E ₁ ^{1/2a} (V) | E ₂ ^{1/2a} (V) | E ₃ ^{1/2a} (V) | E ₄ ^{1/2a} (V) |
|---------------|---------------------------------------|---------------------------------------|---------------------------------------|---------------------------------------|
| A-CPV1 | 0.85 | 1.11 | 1.20 ^b | — |
| A-CPV2 | 0.90 | 1.09 | 1.19 | 1.30 |
| A-CPV3 | 0.87 | 1.02 | 1.16 ^b | — |
| Q-CPV | -0.33 | | | |
| Q-BTT | -0.49 ^b | -0.74 ^b | -1.35 | — |

^aMeasured in 0.1M Bu₄NPF₆ in CH₂Cl₂ at room temperature (vs. Fc/Fc⁺); ^bTwo-electrons waves.

Figure IV.4.16 and Table IV.4.6 show that the **A-CPV1** and **A-CPV3** molecules are characterized by three anodic waves, the last one corresponding to a two-electrons process. In the case of **A-CPV2**, four anodic

waves were obtained. These results agree with the dominance in the oxidation process of the CPV core in **A-CPV1** and **A-CPV3**, while in **A-CPV2** also the fluorene moiety must be considered. Regarding the quinoidal molecule, **Q-CPV** presents a broad, unresolved wave with a half-wave potential of -0.33V. In general, the four spiro systems display complex cyclic voltammograms with overlapping between the different waves. In the next section, the existence of several isomers for some oxidized species, as well as, the similar chemical structures of the different charged species of each molecule (with small energy differences between them) are proposed. These facts can explain the shapes of the cyclic voltammograms of the spiro systems. Furthermore, the overlapping of the oxidation or reduction waves has been demonstrated to be a clear indicative of spiro-conjugation in this kind of systems.^[1, 14]

In the case of **Q-BTT**, two well-defined two-electrons cathodic waves were obtained. Therefore, the reduction process in **Q-BTT** takes place in two steps in which two-electrons are injected to the dicyanomethylene groups.

A. II. Optical Properties: UV-Vis-NIR Spectrochemical Processes

Charged species of CPVs family were explored through UV-Vis-NIR electronic absorption (Figures IV.4.17 to IV.4.20), and

theoretical calculations (Tables IV.4.7 to IV.4.8).

In Figures IV.4.17 and IV.4.18 and Table IV.4.7 UV-Vis-NIR spectroelectrochemical data of **A-CPV1** and **A-CPV2** are showed. For both molecules the oxidation processes present a similar pattern, as expected from their chemical structures.

For **A-CPV1** and **A-CPV2**, according to the studies performed by Nakamura *et al.*,^[1] the first oxidation step takes place in the carbon-bridged phenylenevinylene core (denoted as **CPV** in Figures IV.4.17 to IV.4.20). Consequently, oxidation of neutral **A-CPV-1** and **2** molecules provokes the formation of a **CPV** radical cation, with λ_{\max} wavelengths at 619, 652 nm/1534 nm and 617, 653 nm/1532 nm, respectively (pink spectra in Figures IV.4.17 and IV.4.18). This two-bands pattern is typical of polaronic species, and the NIR broad features can be ascribed to intervalence

charge transfer bands (IVCT bands). Similar to the oxidation of bis(arylamino) COPVs (**DA(COPVn)**),^[11, 12] in [**A-CPV1**]^{•+} and [**A-CPV2**]^{•+} the radical cation is delocalized between the two aminophenyl groups through the **CPV** core (**CPV^{•+}**), constituting a mixed valence state^[15, 16]. According to the Robin and Day classification^[15], spiro **A-CPV** systems can be labeled as class III mixed valence compounds since their redox centers are undistinguishable and mixed valence electronic transitions are observed in the visible region. However, this is not the case of unsubstituted **COPV** oligomers,^[10, 11] proving that this property arises as a consequence of the symmetrical disubstitution with the arylamino groups. The mixed valence properties have been already studied in similar systems were two redox centers with different oxidation states share the extra charge through the carbon backbone.^[16-18]

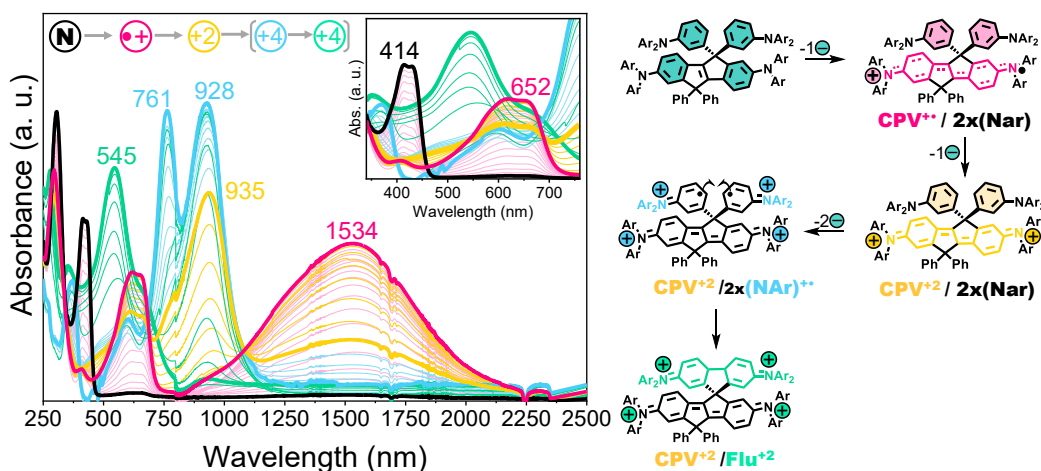


Figure IV.4.17. *Left*) UV-Vis-NIR spectra recorded during the electrochemical oxidation of **A-CPV1** in Bu₄N-PF₆ 0.1 M in CH₂Cl₂ at room temperature; *Right*) Chemical structures of **A-CPV1** upon the oxidation processes. Black lines correspond to the spectra of neutral molecule; pink lines correspond to the spectra of the completely formed radical cation, yellow lines correspond to the spectra of the completely formed bipolaron dication, and blue and green lines correspond to the spectra of the completely formed tetracation species. Light color lines correspond to the intermediate spectra between the former species in the oxidation process.

However, while the first oxidation step is developed in a similar way for both molecules, further oxidation of these radical cations evolves to different species. In **A-CPV-1**, the second electron is also extracted from the **CPV** moiety (CPV^{+2}), generating a bipolaronic dication (λ_{max} wavelengths at 935 nm) localized in the aminophenyl groups of the **CPV** system (yellow spectrum and structure in Figure IV.4.17). In the case of **A-CPV-2**, the second electron is removed from the fluorene moiety to diminish electrostatic interactions. In fact, the new feature at 526 nm in the absorption spectra of $[\text{A-CPV2}]^{+2}$ (yellow spectrum and structure in Figure IV.4.18) is attributed to the radical cation species of fluorene-based molecules.^[1, 19] Therefore, oxidation of $[\text{A-CPV2}]^{+}$ causes the formation of a second radical cation in the fluorene unit (denoted as **Flu⁺**), also delocalized between the two nitrogen atoms. The formation of these

two radical cations in **A-CPV2** is supported by the two-bands patterns in the optical spectrum, very similar to the radical cation shape, which is representative of polaron-pair dications.^[20] Deconvolution of the IVCT band in the NIR region (Figure IV.4.19) also demonstrates the contribution of

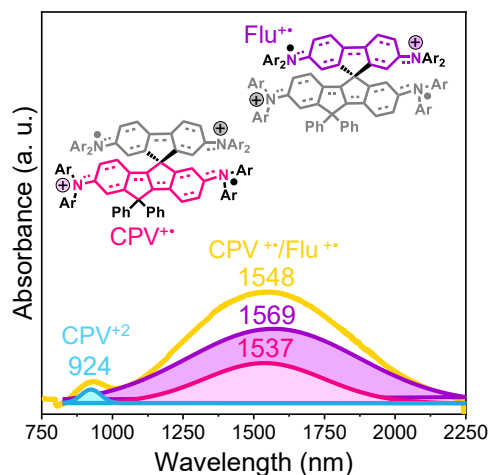


Figure IV.4.19. Deconvolution of the IVCT band of **A-CPV2** polaron-pair dication (Gaussian shape, $R^2 > 0.99$).

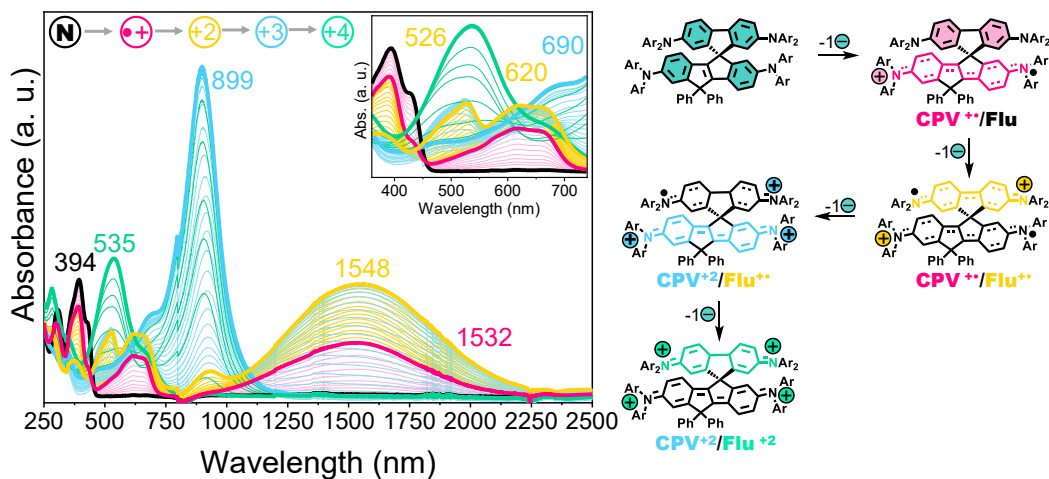


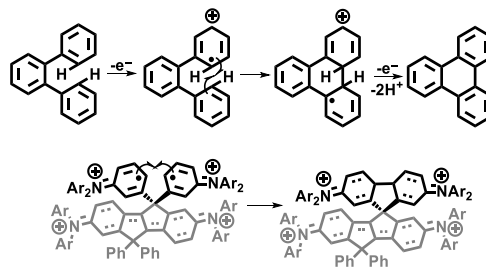
Figure IV.4.18. *Left*) UV-Vis-NIR spectra recorded during the electrochemical oxidation of **A-CPV2** in $\text{Bu}_4\text{N-PF}_6$ 0.1 M in CH_2Cl_2 at room temperature; *Right*) Chemical structures of **A-CPV2** upon the oxidation processes. Black lines correspond to the spectra of neutral molecule; pink lines correspond to the spectra of the completely formed radical cation, yellow lines correspond to the spectra of the completely formed polaron-pair dication, blue lines correspond to the spectra of the completely formed radical trication, and green lines correspond to the completely formed tetracation species. Light color lines correspond to the intermediate spectra between the former species in the oxidation process.

both fluorene and CPV radical cation species.

Nevertheless, almost simultaneously the third oxidation step begins in the **CPV^{•+}** moiety (forming a **CPV⁺²** unit) (blue contribution in Figure IV.4.19), giving rise to the radical trication species of **A-CPV2**.

According to the cyclic voltammetry, the third oxidation step in **A-CPV1** is a two-electron process which generates the tetracation species. The removal of one electron from each aminophenyl group bonded to the tetrahedral carbon produces an intense absorption band at 928 nm, which is related to that of **A-CPV2** at 899 nm (blue spectra and structures in Figures IV.4.17 and IV.4.18). These bands of the **A-CPV1** and **A-CPV2** oxidized species are similar due to the presence of a **CPV⁺²** moiety in both systems. The second, intense contribution at 761 nm in **[A-CPV2]⁺⁴** is characteristic of localized triphenylamine radical cation species.^[21, 22] Regarding the chemical structure proposed for the **A-CPV1** tetracation (blue structure in Figure IV.4.17), the two radical centres laying on the arylamino groups are closer enough to undergo a bond formation in a similar mechanism that dehydrogenation coupling reactions of aromatic compounds.^[23-25] The radical cation mechanism of Scholl reaction is displayed in Scheme IV.4.8, together with the radical coupling in **[A-CPV1]⁺⁴**.

According to this coupling, a fluorene moiety is now present in **A-CPV1** tetracation and, consequently, the same structure as that obtained upon the fourth oxidation step in **A-CPV2** is formed. The fact that both oxidation processes finish in



Scheme IV.4.8. Scheme of the radical cation mechanism of Scholl reaction (*top*) and bond formation in **A-CPV1** tetracation species (*bottom*).

the same tetracation species (green structures in Figures IV.4.17 and IV.4.18) is supported by the similar shape of their electronic absorption spectra (λ_{\max} wavelengths at 545 nm and 535 nm for **[A-CPV1]⁺⁴** and **[A-CPV2]⁺⁴**, respectively).

The oxidation mechanism of **A-CPV-3** molecule presents some differences respect to the previously discussed systems since the two spiro-conjugated units are identical: aromatic **CPV** moieties. In Figure IV.4.20 and Table IV.4.7, the four steps of the oxidation process of **A-CPV3** are displayed, together with the proposed chemical structures of the oxidized species.

In line with the other two aromatic molecules, oxidation of neutral **A-CPV3** gives rise to the well-known two-bands pattern of the polaron radical cation species (620/664 nm, 1560 nm, pink spectra in Figure IV.4.20). In **[A-CPV3]^{•+}** the radical cation is delocalized over one of the two **CPV** units, similar to **A-CPV1** and **A-CPV2** systems. Despite both spiro-conjugated chromophores are identical, only one of them is oxidized in the first step. Spiro-conjugation of the radical cation from the oxidized **CPV** moiety to the neutral one can explain the higher

Table IV.4.7. Optical data of UV-Vis-NIR spectroelectrochemical oxidation of **A-CPV** molecules in Bu₄N-PF₆ 0.1 M in CH₂Cl₂ at room temperature, together with their calculated electronic transitions at the (U)B3LYP/6-31G** level of theory.

| λ_{max} (nm) | A-CPV1 | | A-CPV2 | | A-CPV3 | | TD-DFT Electronic Transition ^b |
|--------------------------------|----------------------|----------------------|-------------------------------|---------------------------|------------------------|----------------------|---|
| | Exp. ^a | TD-DFT. ^b | Exp. ^a | TD-DFT. ^b | Exp. ^a | TD-DFT. ^b | |
| Neutral | 414/429 | 443 | 394/428 | 397/443 | 413/432 | 434/452 | |
| Radical Cation | 619/652 1534 | 567 1342 | 617/653 1532 | 602 1479 | 620/664 1560 | 618 1537 | H→S/S→L H-2→S/H→L |
| Dication | 614 935 (1521) | 554 834 1111 | 526 620/659 932 1548 | 531 572 825 1450 | 618 912 1531 | 571 847 1422 | H→L+1 H-4→L/H→L H-2→L H-1→L |
| Radical Trication | (601) 761/928 | — — | (690) 899 | 572 726 | 620/664 916 1560 | 583 843 1232 | S→L/S→L+1 H-5→S/H-2→S H→L/H→S |
| Tetra- Cation | 545 (673) | — — | 535 (670) | 702 — | 616 921 | 706 1034 | H-5→L+1/H-4→L H-1→L/H→L+1 |

^aMeasured in Bu₄N-PF₆ 0.1 M in CH₂Cl₂ at room temperature. ^bTD-DFT calculations at (U)B3LYP/6-31G** level of theory.

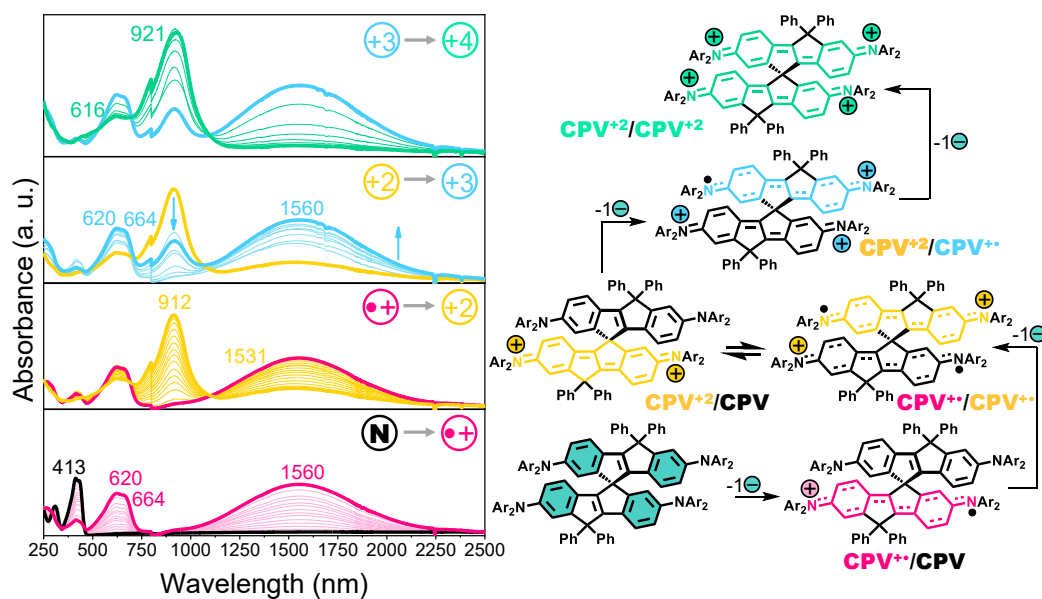


Figure IV.4.20. Left) UV-Vis-NIR spectra recorded during the electrochemical oxidation of **A-CPV3** in Bu₄N-PF₆ 0.1 M in CH₂Cl₂ at room temperature; Right) Chemical structures of **A-CPV3** upon the oxidation processes. Black line corresponds to the spectrum of neutral molecule; pink lines correspond to the spectra of the completely formed radical cation, yellow lines correspond to the spectra of the completely formed dication species, blue lines correspond to the spectra of the completely formed radical trication and green lines correspond to the tetracation species. Light color lines correspond to the intermediate spectra between the former species in the oxidation process.

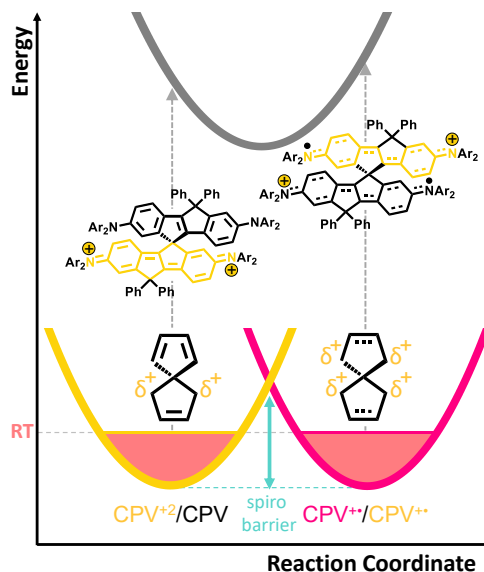
potential required to extract a second electron from the still neutral subunit. Radical cation of **A-CPV3** also presents properties of class III mixed valence states, as $[\mathbf{A-CPV1}]^{*+}$ and $[\mathbf{A-CPV2}]^{*+}$.

When carrying on with the oxidation sequence, a new intense band at 912 nm is developed, but the radical cation features do not disappear completely (see yellow spectra). As for $[\mathbf{A-CPV2}]^{*+}$, removal of the second electron can take place from two different units and, hence, forming different dicationic species:

- From the still neutral **CPV** unit, forming a polaron pair dication with one radical cation in each spiro conjugated system (structure $\mathbf{CPV}^{*+}/\mathbf{CPV}^{*+}$ in Figure IV.4.20). This species justifies the preservation of the radical cation λ_{\max} wavelengths (618 nm and 1531 nm).
- From the radical cation **CPV** unit ($\mathbf{CPV}^{*+}/\mathbf{CPV}$). Now, classical bipolaronic dication is obtained, explaining the absorption band at 912 nm, similar to that of $[\mathbf{A-CPV1}]^{*+}$, at 935 nm. This is the only dicationic species observed for the non spiro counterpart **DA(COPV1)** (λ_{\max} wavelengths at 913 nm).^[12]

Therefore, both species are present in the UV-Vis-NIR electronic absorption spectrum of $[\mathbf{A-CPV3}]^{*+}$. Formation of two electromers^[26, 27] of charged species as a consequence of the presence of two different π -conjugated frameworks was already observed for the radical anions of longer **2DQoT** systems in the previous chapter. Since both dicationic electromers

are detected simultaneously, they constitute two minima of the same energy in the potential energy surface of the electronic ground state of $[\mathbf{A-CPV3}]^{*+}$, represented in Scheme IV.4.9:



Scheme IV.4.9. Representation of the potential energy surface of the ground electronic state of the dication species of **A-CPV3** as deduced from the electronic absorption spectra.

The energy barrier between both electromers (denoted as *spiro* barrier) accounts for the energy required to spread the charge density towards the neutral spiro-conjugated unit. This *spiro* barrier can be surpassed thanks to the lower electrostatic repulsion in the segregated polarons structure.

From this point, the oxidation mechanism evolves different from the other two aromatic systems, and also from the non spiro **DA(COPV1)** (only two oxidation processes are observed for this molecule). Further oxidation of $[\mathbf{A-CPV3}]^{*+}$ seems to come back to the radical cation spectrum (blue spectra in Figure IV.4.20).

λ_{\max} wavelengths are at 620/664 nm and 1560 nm, exactly the same electronic transitions than in the radical cation, together with a third band at 916 nm (similar to the bipolaronic dication at 912 nm). With these comparisons in mind, the radical trication should present contributions from the radical cation and the bipolaron dication **CPV** moieties. Extraction of one electron from any of the two different dication structures (**CPV⁺⁺/CPV⁺⁺** or **CPV⁺²/CPV**) provokes the formation of a dicationic **CPV** unit spiro-conjugated to a radical cation **CPV** moiety: **CPV⁺²/CPV^{•+}**. Then, the combination of **CPV** oxidized forms for the dication and radical trication species is the same (**CPV⁺⁺** and **CPV⁺²** structures), explaining the similar UV-Vis-NIR absorption pattern.

Finally, a fourth oxidation step provokes the formation of a tetracation species in **A-CPV3** (green line in Figure IV.4.20). Now, the two spiro-conjugated **CPV** chromophores are bipolaronic dications: **CPV⁺²/CPV⁺²**. In consequence, the absorption spectrum of **[A-CPV3]⁺⁴** is very similar to that of the bipolaronic **[A-CPV1]⁺²** (λ_{\max} wavelengths at 921 nm and 935 nm, respectively).

Radical cation species of aromatic **CPV** systems can be compared in order to obtain a deeper insight of the distribution of the π -electron density since they present similar absorption spectra and structures. According to the evolution of the spiro-conjugation probability established in Section 4.1 for the neutral **A-CPV** molecules, λ_{\max} wavelengths of the radical cations are red-shifted from **[A-CPV1]^{•+}** to **[A-CPV3]^{•+}**, according to the proposed higher spiro-conjugation in the

symmetric molecule.

The electrochemical reduction processes of the quinoidal octacyano systems were also monitored through UV-Vis-NIR electronic absorption. The obtained results are showed in Figures IV.4.21 and IV.4.22 and Table IV.4.8.

For the spiro system, addition of one electron to neutral **Q-CPV** provokes the decrease of the 569/617/682 nm set of bands and the growth of a low-intensity, broad band at 1535 nm (pink spectra in Figure IV.4.21). Similar to the case of the aromatic **CPV** molecules, in **[Q-CPV]^{•-}** one of the two moieties carries one extra electron (pink structure in Figure IV.4.21, denoted as **CPV^{•-}/CPV**). The sets of bands at 344 nm and 617 nm are similar to those of the neutral **Q-CPV**, while the weak feature at 1535 nm is typical of the radical anionic species of tetracyanoquinoidal molecules.

The second reduction step can now take place in two different ways, similar to the oxidation of **[A-CPV3]^{•+}**: in the radical anion **CPV** unit or in the remaining neutral moiety. However, for **Q-CPV** electromers are not detected. The dianionic species presents the same bands of the radical anion at 344 nm, accompanied by the disappearance of the NIR band. These subtle differences between the spectra of these two species agree with the stabilization of one negative charge in each chromophore in **[Q-CPV]⁻²** (blue structure in Figure IV.4.21, denoted as **CPV^{•-}/CPV^{•-}**). The formation of the segregated dianion is favored by the partial aromatization of the quinoidal core and the reduction of the electrostatic

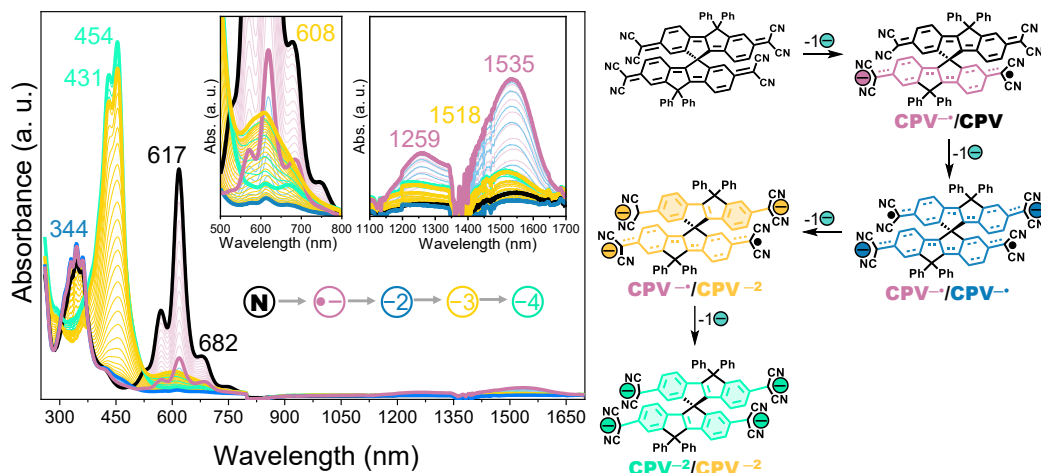


Figure IV.4.21. *Left*) UV-Vis-NIR spectra recorded during the electrochemical reduction of **Q-CPV** in $\text{Bu}_4\text{N-PF}_6$ 0.1 M in CH_2Cl_2 at room temperature; *Right*) Chemical structures of **Q-CPV** upon the reduction process. Black lines correspond to the spectra of neutral molecule; pink lines correspond to the spectra of the completely formed radical anion, blue lines correspond to the spectra of the completely formed dianion, yellow lines correspond to the completely formed radical trianion, and green lines correspond to the completely formed tetra-anion species. Light color lines correspond to the intermediate spectra between the former species in the reduction process.

Table IV.4.8. Optical data of UV-Vis-NIR spectroelectrochemical reduction of **Q-CPV** and **Q-BTT** systems in $\text{Bu}_4\text{N-PF}_6$ 0.1 M in CH_2Cl_2 at room temperature, together with their calculated electronic transitions at the (U)B3LYP/6-31G** level of theory.

| λ_{max} (nm) | Q-CPV | | Q-BTT | | Electronic Transition ^b |
|--------------------------------|---|-------------------------|-------------------------------|----------------------|---|
| | Exp. ^a | TD-DFT. ^b | Exp. ^a | TD-DFT. ^b | |
| Neutral | 344 (330/360) 617, 569, 682 (526, 751) | — | 335 425 538 | — | See Table 1 |
| Radical Anion | 344 (330/360) 618, 571, 684 1535 (1259) | 471 572, 784 1209 | — | — | H→L+1/H-1→L+1 S→L+1/H→L H-1→L/H→S |
| Dianion | 344 (330/360) — | 534 1125 | 347, 479 644 (593), 750 | 346 501 803 | HOMO→LUMO +1(α/β) HOMO-1→LUMO (α/β) HOMO→LUMO |
| Radical Trianion | 454, 431 608 (581) 1518 (1234) | 470 645 1336 | — | — | HOMO→LUMO+1 H→L+1/S→L HOMO-2→SOMO |
| Tetra-Anion | 454, 431 1511 (1234) | 439 — | 340 514/551 (608) | 309 497 — | H-1→L+1/H-1→L+2 HOMO→LUMO |

^aMeasured in $\text{Bu}_4\text{N-PF}_6$ 0.1 M in CH_2Cl_2 at room temperature. ^bTD-DFT calculations at (U)B3LYP/6-31G** level of theory

repulsion, avoiding the formation of the bipolaronic electromer.

In this scenario, the third reduction step can only come about through the injection of the third extra electron over a radical anion **CPV** unit (yellow structures, $\text{CPV}^{\cdot-}/\text{CPV}^{-2}$). **Q-CPV** radical trianion displays a strong absorption band at 431/454 nm together with a weak-medium absorption at 608 nm. The two-bands pattern is typical of radical species, and the most intense feature coincide with that of the dianionic species of the non-spiro **QM1CN** (λ_{max} wavelengths at 430-460 nm).^[2] Subsequent reduction of this species provokes the vanishing of the feature at 608 nm, reproducing exactly the electronic absorption spectrum of **QM1CN** dianion. Then, $[\text{Q-CPV}]^{-4}$ is formed by the spiro-conjugation of two dianionic quinoidal **CPV** moieties (green structure in Figure IV.4.21, $\text{CPV}^{-2}/\text{CPV}^{-2}$).

Regarding the octacyano **Q-BTT** system (Figure IV.4.22 and Table IV.4.8), and according to the cyclic voltammetry of this molecule, the reduction process takes place in two steps of two electrons each one.

Reduction of neutral **Q-BTT** gives rise to an intense band at 644 nm, together with a second one at 479 nm, through well-defined isobestic points (blue spectra in Figure IV.4.22). This step corresponds to the formation of a dianion species, according to the cyclic voltammetry. Regarding the chemical structure of **Q-BTT**, the three possible dianionic species are depicted in Scheme IV.4.10. Simultaneous injection of two electrons indicates that no charge density reorganization is required,

then each negative charge will be accommodated in each chromophore (blue structure and surface in Figure IV.4.22, denoted as $\text{MQ}^{\cdot-}/\text{BQ}^{\cdot-}$, and Scheme IV.4.10). In other words, a radical anion placed in each **BQ** and **MQ** units forms a polaron pair **Q-BTT** dianion. This form not only provides the maximum separation between the two extra electrons but also is supported by the aromaticity gain of the central benzene unit. For the bipolaronic dianion placed in the **BQ** moiety (purple structure and surface in Scheme IV.4.10), despite the aromatization of the benzene ring (and the adjacent thiophenes), the charge repulsion is higher than in the segregated dianion.

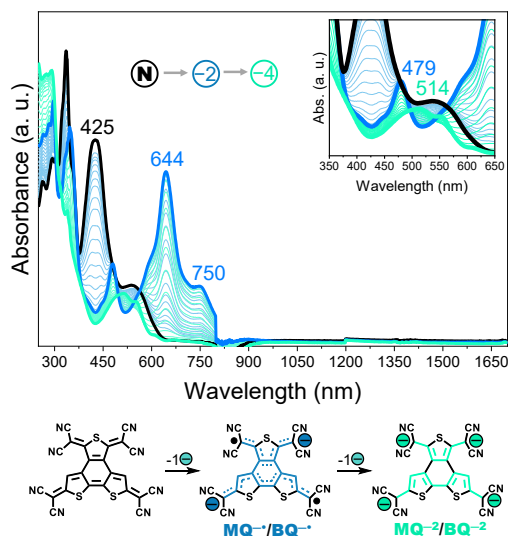
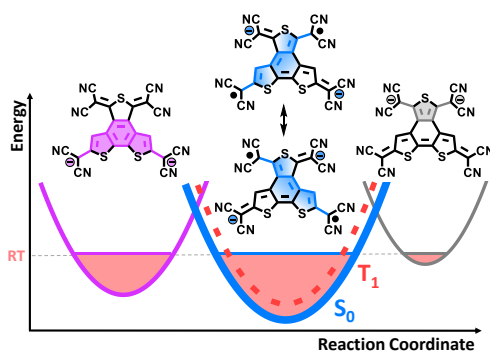


Figure IV.4.22. Top) UV-Vis-NIR spectra recorded during the electrochemical reduction of **Q-BTT** in $\text{Bu}_4\text{N-PF}_6$ 0.1 M in CH_2Cl_2 at room temperature; Bottom) Chemical structures of **Q-BTT** upon the reduction process. Black lines correspond to the spectra of neutral molecule; blue lines correspond to the spectra of the completely formed dianion; and green lines correspond to the completely formed tetra-anion species. Light color lines correspond to the intermediate spectra between the former species in the reduction process.



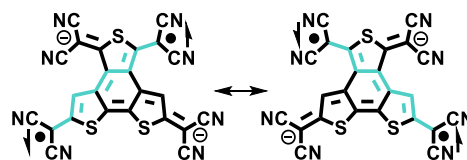
Scheme IV.4.10. Representation of the potential energy surfaces of the ground electronic states of the three possible dianion species of **Q-BTT**, and the corresponding chemical structures. Solid surfaces correspond to singlet states while the dashed line corresponds to the triplet configuration.

The less stable dianion is that in which the two extra electrons are injected in the **MQ** moiety (grey structure and surface). In this case, the aromaticity gain is only of one thiophene ring and the two extra charges are accommodated in the closest dicyanomethylene groups.

Upon reduction of the polaron-pair dianion, a second species is obtained with λ_{\max} wavelength at 514 nm (green spectra and structure). This reduction step in **Q-BTT** injects two extra electrons to the dianion, giving rise to a tetra-anion species.

In both quinoidal systems (**Q-CPV** and **Q-BTT**), the presence of two sets of two linearly conjugated dicyanomethylene groups are responsible of the stabilization of open-shell dianions. However, while the tetrahedral carbon atom avoids the through-bond interaction between the two **CPV** units, for **Q-BTT** the cross-conjugated framework established between the two parallel chromophores allows the interaction between the radical

centers. This cross-conjugated π -electron delocalization pathway between two opposite dicyanomethylene groups is depicted in Scheme IV.4.11:



Scheme IV.4.11. Cross-conjugated singlet open-shell resonance structures of **Q-BTT** dianion. The cross-conjugated framework is highlighted in green.

The interaction between the radical centres in the different divalent species is revealed in the singlet-triplet gap energy (ΔE_{S-T}). In Figure IV.4.23, the energy difference between the possible configurations of the spiro and parallel doubly charged systems are showed.

In agreement with the electronic absorption spectra, all the divalent species

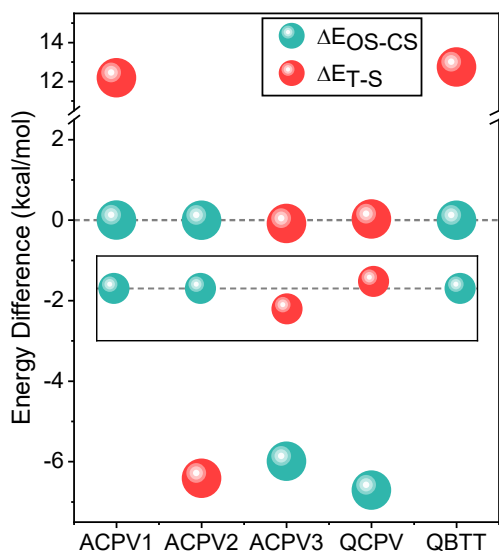
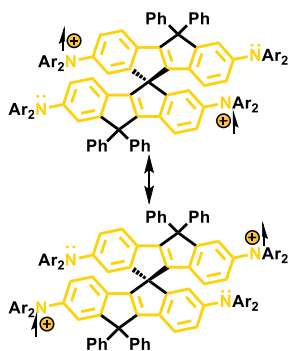


Figure IV.4.23. Formation energy differences (kcal/mol) between the singlet open-shell and closed-shell configurations (blue circle) and between the triplet and the most stable singlet state (red circles) of the divalent species under study, calculated at the (U)B3LYP/6-31G** level of theory.

are of open-shell nature, except **A-CPV1** dication, which presents a closed-shell configuration.

A significant fact is that the triplet states of $[\mathbf{A-CPV2}]^{-2}$ and $[\mathbf{A-CPV3}]^{-2}$ are lower in energy than the corresponding singlet open-shell configurations. This compliance with the Hund's Rule means that double spin polarization (DSP) mechanism is deactivated. In other words, for these two aromatic systems the two radical cations are delocalized in different **CPV** moieties and isolated from each other due to the tetrahedral, spiro carbon, avoiding the *chemical* interaction between them:



Scheme IV.4.12. Triplet state resonance chemical structures of **A-CPV3** dication. Each radical cation is delocalized between the two corresponding nitrogen atoms.

However, this is not the case of **Q-CPV**. In this system each radical anion forming the $[\mathbf{QCPV}]^{-2}$ species is placed in one chromophore units, as in the case of the aromatic systems **A-CPV2** and **A-CPV3**, but the delocalization of these centres involves the complete molecule, allowing the spin interaction in a singlet configuration. With this information in mind, the only possibility to account for the validity of the DSP mechanism is the spiro-conjugation

between the two **CPV** cores. It has to be noted that no single/double bond alternation framework can be established connecting the two radical centres in different **CPV** moieties. Consequently, the *through space* spiro linkage between the adjacent carbon atoms to the tetrahedral centre is responsible of the spin interaction. The weakness of this communication is revealed in the small energy stabilization of the singlet state respect to the triplet one.

The fact that the triplet state is destabilized respect to the singlet open-shell from $[\mathbf{A-CPV2}]^{-2}$ (T) to $[\mathbf{QCPV}]^{-2}$ (S-OS) manifests the progressive activation of the spiro-conjugation and, hence, the DSP mechanism, along the series.

Regarding the **Q-BTT** dianion, the small ΔE_{S-T} and, hence, the singlet open-shell character of its ground state, was demonstrated through electronic paramagnetic resonance. EPR spectrum at room temperature of this species is depicted in Figure IV.4.24, together with the half-field signal at 120 K (see inset), representative of triplet states. EPR spectrum of **Q-BTT** dianion displays 9 well-differentiated signals, which indicates that the radical centres are coupled with 4 equivalent nitrogen atoms. These results support the proposed polaron-pair structure for the dianion species of **Q-BTT**, with a thermally populated triplet state at room temperature, as depicted in Scheme IV.4.10. The small ΔE_{S-T} is ascribed to the out-of-plane distortion of the dicyanomethylene groups as a consequence of the steric hindrance between the two *parallelly*-coupled moieties.

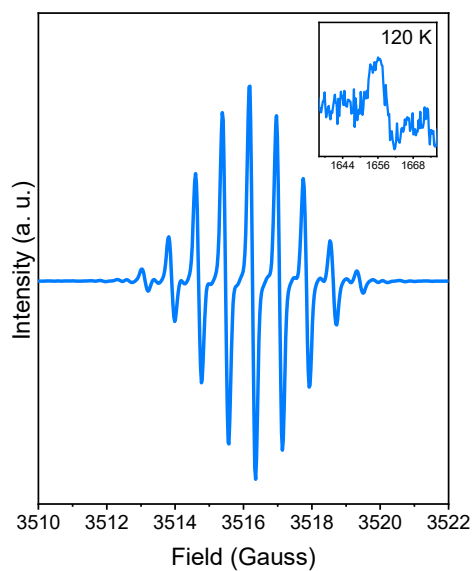


Figure IV.4.24. EPR spectrum of **Q-BTT** dianion at room temperature obtained electrochemically in CH_2Cl_2 , together with the half-field signal observed at 120 K (inset).

B. Molecular Structure

B. I. IR Spectroelectrochemical Reduction

The withdrawing character of the cyano groups in the quinoidal **Q-CPV** and **Q-BTT** make them the preferential location for the injected charges upon reduction. For this reason, these groups are very sensitive to the reduction progression, and their IR monitorization can help to understand the development of these processes.

IR spectroelectrochemical reduction of the spiro **Q-CPV** in the CN stretching region (ν_{CN}) at room temperature is displayed in Figure IV.4.25. Conversely to the net resolution of four species by UV-Vis-NIR spectroscopy, by infrared spectroscopy only two of these processes are distinguished. Reduction of neutral **Q-CPV**, which is characterized by one ν_{CN} at 2210 cm^{-1} , gives rise to a pattern with two IR ν_{CN} bands at 2171 and 2123 cm^{-1} (pink spectra in Figure IV.4.25). This spectral shape is typical of radical anion species of tetracyano quinoidal compounds^[13,28] and, according to the UV-Vis-NIR spectroelectrochemistry, it is compatible with both the radical anion or the polaron-pair dianion (one charge per **CPV** chromophore). These two species are indistinguishable by IR spectroscopy.

Further reduction of this species provokes the formation of two new IR bands at 2162 and 2115 cm^{-1} (blue spectrum). This set of bands is down-shifted regarding the previous radical anion/dianion features, indicating an stabilization of two charges per chromophore, either in one or in the two **CPV** moieties (corresponding to the radical

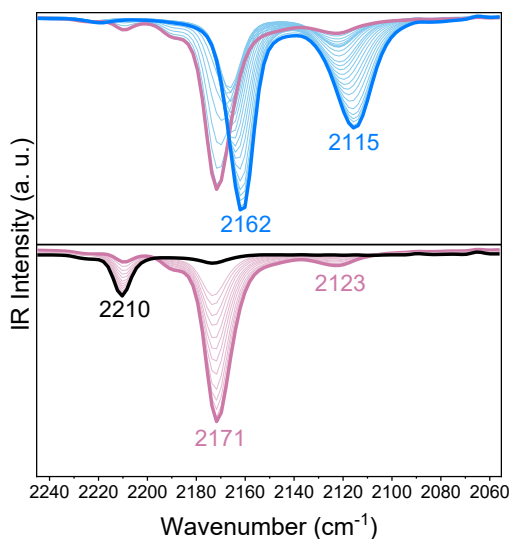


Figure IV.4.25. IR spectroelectrochemical reduction of **Q-CPV** molecule in $\text{Bu}_4\text{N-PF}_6$ 0.1 M in CH_2Cl_2 at room temperature. Black line corresponds to the spectrum of neutral molecule; pink lines correspond to the spectrum of the completely formed radical anion or dianion species, and blue line corresponds to the spectra of the completely formed radical trianion or tetra-anion species. Light color lines correspond to the intermediate spectra between the former species in the reduction process.

trianion or tetra-anion, respectively).

IR study of the reduced species was also performed for the parallel **Q-BTT** system. Electrochemical reduction of neutral **Q-BTT** generates one intense band at 2183 cm^{-1} through well-defined isosbestic points, assigned to the dianion species (blue spectrum in Figure IV.4.26). Since each *extra* negative charge is delocalized between each set of two dicyanomethylene groups, then only one ν_{CN} signature is detected through IR spectroscopy.

Upon reduction of the dianion to the tetra-anion species, two blue-shifted bands at 2160 cm^{-1} and 2106 cm^{-1} arise

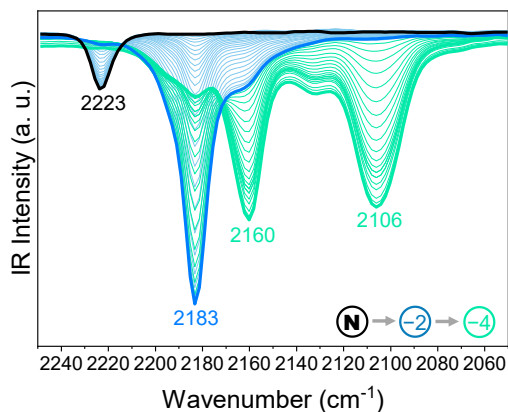


Figure IV.4.26. IR spectroelectrochemical reduction of **Q-BTT** molecule in $\text{Bu}_4\text{N-PF}_6$ 0.1 M in CH_2Cl_2 at room temperature. Black line corresponds to the spectrum of neutral molecule; blue line corresponds to the spectrum of the completely formed dianion, and green line corresponds to the spectrum of the completely formed tetra-anion species. Light color lines correspond to the intermediate spectra between the former species in the reduction process.

(green spectrum). In this case, π -electron delocalization through the linear frameworks, that is, between the dicyanomethylene groups of **MQ** and those of **BQ** chromophores, accounts for the ν_{CN} downshift in the tetra-anion species, presenting similar values than those of the radical trianion/tetra-anion of the spiro **Q-CPV**.

B. II. Transient Spectroscopic Properties

With the aim of having a better knowledge of the electronic distribution of charged species in **Q-BTT** system, where the two different parallel moieties **MQ** and **BQ** seem to influence each other, characterization through time resolved spectroscopies of this system was

performed by the group of Professor Dongho Kim.

In Figure IV.4.27 the time resolved absorption spectra of **Q-BTT** in CH_2Cl_2 at different delay times upon excitation at 530 nm are depicted, together with that corresponding to the dianion species.

Photoexcitation of **Q-BTT** system generates two-bands pattern absorption spectra (512 nm and 640 nm) that progressively decay when increasing the

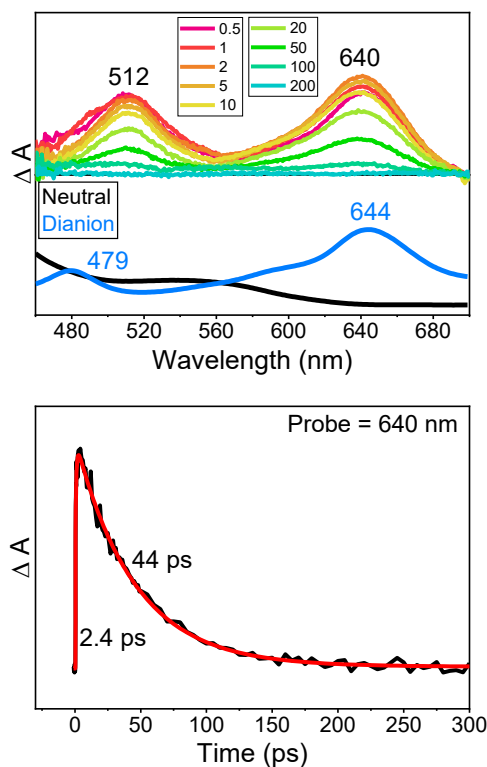


Figure IV.4.27. Top) UV-Vis-NIR transient absorption spectra of **Q-BTT** in CH_2Cl_2 at room temperature upon excitation at 530 nm. Different colours correspond to the different delay times (in ps). UV-Vis-NIR electronic absorption spectrum of neutral **Q-BTT** and the electrochemically obtained dianion in CH_2Cl_2 at room temperature are also displayed for reference; Bottom) Time evolution of the main excited state absorption band.

delay time. These excited states absorption bands closely simulate the UV-Vis-NIR electronic absorption spectrum of the dianion species (λ_{max} wavelengths at 479 nm and 644 nm, blue spectrum in Figure IV.4.27). Transient absorption spectra of TCNQ also displays an excited state absorption band at 460 nm with contribution of a long lifetime component (14-24 ps) ascribed to a charge transfer (CT) anionic state.^[29]

Time resolved IR (TR-IR) spectrum of **Q-BTT** was also obtained (Figure IV.4.28). In this case, the excited state displays a strong IR absorption band at 2175 cm^{-1} (pink spectra) that progressively evolves to 2185 cm^{-1} with time (green spectra). Then, the excited state band progresses over time towards the same ν_{CN} wavenumber of the dianion species. The ground state bleaching (GSB) band at 2225 cm^{-1} is likewise observed.

The study of the transient species of **Q-BTT** by electronic absorption as well as IR spectroscopy reveals the formation of a charge transfer state upon photoexcitation. The electronic distribution in this excited state is similar to that of the electrochemically obtained dianion species.

Recently, a tetracyano end-capped quinoidal system (**TMTQ**, see Scheme IV.4.13 for chemical structure) with similar transient state characteristics was studied by our group.^[30] For this molecule, a dianion-like CT excited state is generated because of Baird's aromatization gain, mediated by the diradical character and the electron-withdrawing dicyanomethylene groups. In

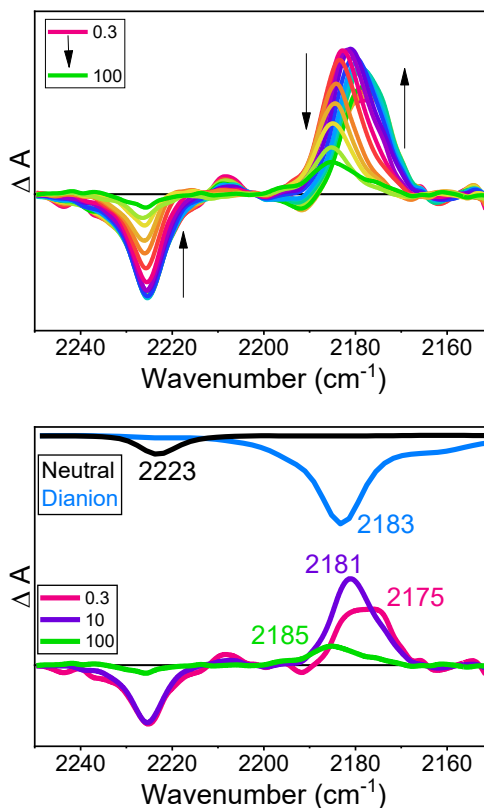
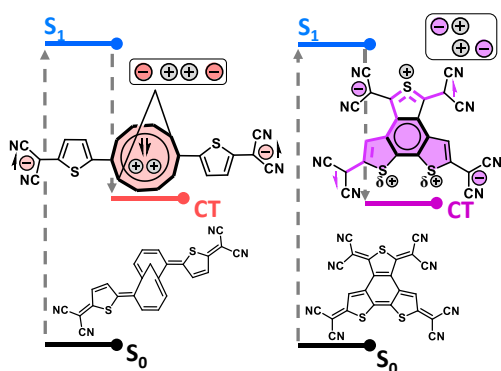


Figure IV.4.28. *Top*) ν_{CN} region of the time resolved IR spectra of **Q-BTT** in CH_2Cl_2 at room temperature at the same picoseconds delay times as those recorded for the excited state absorption bands. Different colours correspond to the different delay times (in ps).; *Bottom*) ν_{CN} region of the IR spectra of neutral (black line) and dianion (blue line) species of **Q-BTT**, together with the TR-IR spectra at 0.3 ps, 10 ps and 100 ps delay times

this scenario, a similar two-electron intramolecular CT state is proposed for **Q-BTT**, with a distribution of the negative charge density analogous to the polaron-pair dianion species (Scheme IV.4.13).

Q-BTT transient state moves two negative charges to *opposite* dicyanomethylene groups located in different chromophores, with positive charge densities over the sulphur atoms. Different from **TMTQ**, in **Q-BTT** the driving



Scheme IV.4.13. Qualitative scheme of the excited states of **TMTQ** (left) and **Q-BTT** (right). Charge density patterns are also schematized.

force for generating the zwitterionic excited state is the gain of Hückel aromaticity of the central benzene ring and secondly, the partial aromatization of the **BQ** thiophene rings. This driving force justifies the signal evolution in the TR-IR experiments. On the other hand, the cross-conjugated π -electron framework (highlighted in purple in Scheme IV.4.13) provides the through-bond connection between the radical centres needed to justify the singlet character of the excited state.

Despite the similar nature of the excited states of both quinoidal systems, while **TMTQ** is described as a linear CT system with a negative-positive—positive-negative charge density, **Q-BTT** is a parallel, asymmetric CT state with a negative—positive/positive—negative pattern. This different electronic distribution will probably confer unexplored excited states properties for the organic π -conjugated functional materials.

According to the transient spectroscopy results, the proposed

polaron-pair structure of the **Q-BTT** dianion is clearly evidenced. Each extra electron is linearly delocalized in each moiety (**BQ** and **MQ**), but always ensuring the central benzene aromaticity.

B. III. Raman Spectra of Charged Species

Raman spectra of charged species of aromatic **CPV** molecules in CH_2Cl_2 at room temperature are displayed in Figure IV.4.29. Radical cations, dications and radical trications were obtained by chemical oxidation with FeCl_3 and conveniently characterized by their UV-Vis-NIR absorption spectra.

As it was already observed for the neutral molecules, the relevant vibrational modes do not experiment significant changes between different systems, *i. e.*, radical cations and dications present similar wavenumbers for the aromatic family.

The stretching vibration of phenyl groups (ν_{phen} , blue bands in Figure IV.4.29) experiments a total shift of 9-10 cm^{-1} upon oxidation for the three molecules: for **A-CPV1**, $1599 \text{ cm}^{-1} \rightarrow 1592 \text{ cm}^{-1} \rightarrow 1590 \text{ cm}^{-1}$; for **A-CPV2**, $1600 \text{ cm}^{-1} \rightarrow 1592 \text{ cm}^{-1} \rightarrow 1591 \text{ cm}^{-1}$; and $1599 \text{ cm}^{-1} \rightarrow 1591 \text{ cm}^{-1} \rightarrow 1590 \text{ cm}^{-1} \rightarrow 1589 \text{ cm}^{-1}$ (10/6 cm^{-1}) for **A-CPV3**. This behaviour is consistent with the delocalization of the radical cation between the two amino groups. The electron transport through the **CPV** backbone provokes the enlarging of the double C=C bonds and the shortening of the single ones, giving rise to a pseudoquinoidal structure. This decrease

in the bond length alternation explains the Raman downshift of the bands ascribed to the ν_{phen} vibrational modes.

Similar to the case of the non-spiro **COPV** molecules,^[11] ν_{phen} is split in two bands upon oxidation for **A-CPV3** (highlighted in light and dark blue in Figure IV.4.29, right panel). Upon oxidation, one of the two **CPV** moieties is *pseudo*-quinoidized, explaining the existence of two kinds of phenyl rings in the **CPV** cores with different aromatic character (denoted as aromatic ν_{phen} , 1591 cm^{-1} , and quinoidal ν_{phen} , 1584 cm^{-1}). Further oxidation to dication and radical trication of **A-CPV3** provokes the down-shift and the relative intensification of the quinoidal ν_{phen} (1584 cm^{-1} → 1580 cm^{-1} → 1578 cm^{-1} ,

from radical cation to radical trication), in agreement with a larger quinoidization of the two **CPV** moieties.

The variations of ν_{phen} Raman bands also corroborate the formation of class III mixed valence states, already proposed in the *Electronic Structure* section, and in analogy with the substituted COPV, **DA(COPV2)**.^[11]

Wavenumbers related to the ν_{phen} normal modes of the aromatic **CPV** systems are found in the same spectral region than those of the quinoidal **CPV**, and its anionic species.

Resonance Raman spectra of **Q-CPV** upon chemical reduction with

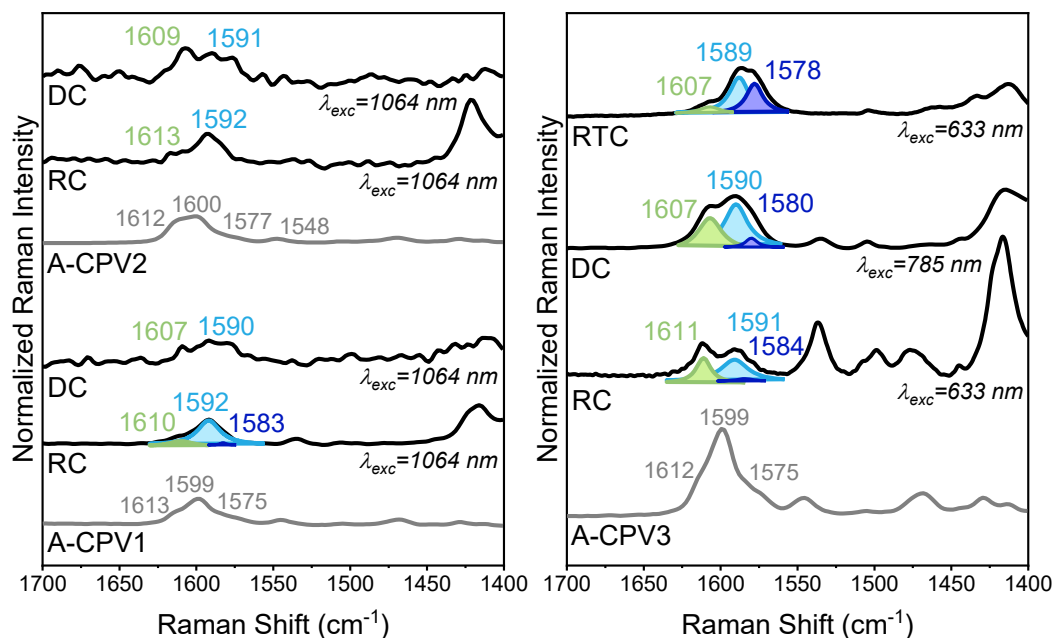


Figure IV.4.29. Resonance Raman spectra of cationic species of **A-CPV1** and **2** (left) and **A-CPV3** (right) CH_2Cl_2 at room temperature. Grey solid lines correspond to the solid-state spectra while black solid lines correspond to the experimental Raman spectra of radical cation (RC), dication (DC) and radical trication (RTC) species. Wavenumbers of experimental spectra have been assigned by deconvolution when possible (Lorentzian shape, $R^2 > 0.99$): $\nu_{(\text{C}=\text{C})_{\text{aryl}}}$ in green and $\nu_{(\text{C}=\text{C})_{\text{phenyl}}}$ in light and dark blue. The employed excitation wavelength (λ_{exc}) is indicated for each species.

triethylamine are shown in Figure IV.4.30. The correlation between ν_{phen} of aromatic and quinoidal spiro systems is another evidence of the structural quinoidization of **A-CPVs** upon oxidation.

For **Q-CPV** no significant variations were found for the radical anion Raman bands respect to the neutral ones (see Figure IV.4.30, ν_{phen} : 1595/1569 cm^{-1} \rightarrow 1592/1572 cm^{-1}). This result is not unexpected if the open-shell character of neutral **Q-CPV** is considered. In this scenario, the injection of one extra electron does not disturb excessively the already existent *pseudo*-aromatic structure.

The aromatic/quinoidal character of ν_{phen} Raman bands of **CPV** systems can be

easily seen when fitting their wavenumbers to a straight line limited by the values of the aromatic **A-CPV2** and the quinoidal **Q-CPV**, both in their neutral form (see left panel in Figure IV.4.30). While neutral **A-CPV** molecules are placed in the well-defined aromatic region, their radical cation and dication species present a less marked bond length alternation pattern (they are about 70% aromatic, light blue triangles). In this region is also located the ν_{phen} related to the diradical character of neutral **Q-CPV** (dark blue circle).

On the other hand, the second ν_{phen} observed wavenumbers of charged species (dark blue Raman bands and dark blue triangles in Figures IV.4.29 and IV.4.30) present lower percentages of aromaticity.

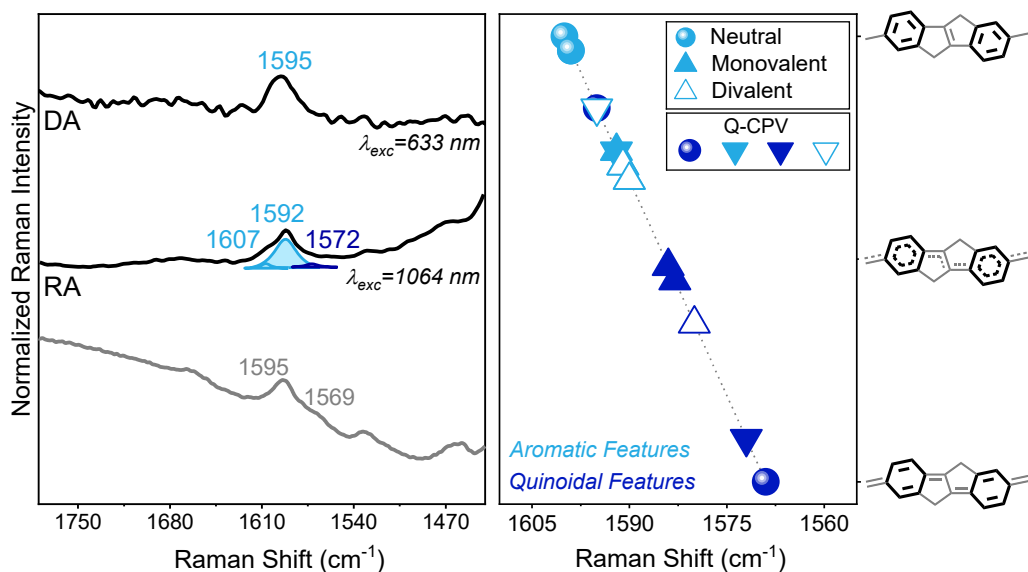


Figure IV.4.30. *Left*) Resonance Raman spectra of anionic species of **Q-CPV** in CH_2Cl_2 at room temperature. Grey solid line corresponds to the solid-state spectrum while black solid lines correspond to the experimental Raman spectra of the radical anion (RA) and dianion (DA) species. Wavenumbers of experimental spectra have been assigned by deconvolution when possible (Lorentzian shape, $R^2 > 0.99$). The employed excitation wavelength (λ_{exc}) is indicated for each species; *Right*) Linear fit of ν_{phen} Raman bands with aromatic (light blue) and quinoidal (dark blue) character for neutrals (fulfilled circles), monovalent (fulfilled triangles) and divalent (empty triangles) charged species of **CPV** systems. Dark blue circles and inverted triangles correspond to **Q-CPV**.

Radical cations and dication display a more quinoidal character, about 50% aromatic (or quinoidal). The delocalized mixed valence states of cationic species clearly account for these results.

Regarding the reduced species of **Q-CPV** (inverted triangles in Figure IV.4.30), ν_{phen} is progressively shifted towards the aromatic spectral region (higher wavenumbers) on going from the radical anion to the dianion species.

Finally, Raman spectroscopy was also employed in the study of the reduced species of the parallel **Q-BTT** molecule. Chemical reduction of this system was achieved with N-DMBI (reducing agent synthesized *ad hoc* for **2DQoT** family, see Chapter 3), and properly characterized through UV-Vis-NIR electronic absorption. Resonance Raman spectrum of **Q-BTT** dianion is displayed in Figure IV.4.31.

In this case, Raman feature related to the ν_{phen} normal mode experiments a substantial downshift when injecting two extra electrons: $1527\text{ cm}^{-1} \rightarrow 1495/1476\text{ cm}^{-1}$, from neutral to **Q-BTT** dianion species. Also the stretching vibrations involving the thiophene rings (now denoted as $\nu_{\text{thiophene}}$) shift to shorter wavenumbers upon reduction ($1500/1472\text{ cm}^{-1} \rightarrow 1386\text{ cm}^{-1}$). In this case, the vibrational modes of **MQ** and **BQ** moieties cannot be distinguished by Raman spectroscopy, *i. e.*, relevant Raman bands of the dianion involves both chromophores. These results completely agree with the proposed *fully* delocalized polaron-pair structure of **Q-BTT** dianion.

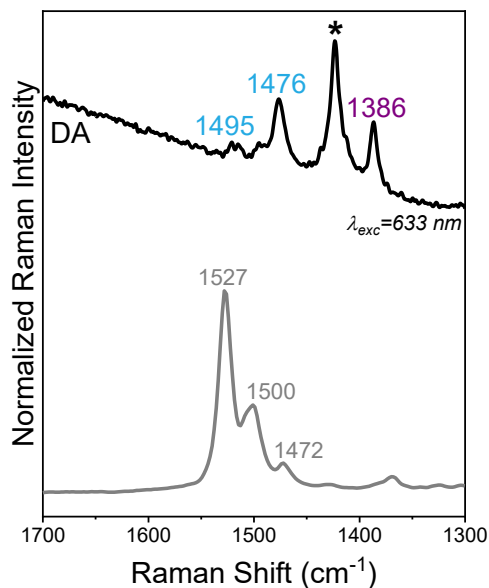


Figure IV.4.31. Resonance Raman spectra of **Q-BTT** dianion (DA, black solid line) in CH_2Cl_2 at room temperature (excitation wavelength at 633 nm), together with the solid-state spectrum of the neutral molecule (grey solid line). ν_{phenyl} mode is in light blue and $\nu_{\text{thiophene}}$ in purple. Raman band at 1423 cm^{-1} (*) corresponds to CH_2Cl_2 .

B. IV. Bond Lengths Analysis

In line with the bond length analysis performed for neutral species of **CPV** and **QBTT** systems, in Figure IV.4.32 the corresponding values of the charged species are depicted (together with those of the neutral molecules as reference).

Regarding the spiro series, aromatic **CPV** molecules present a substantial enlargement of the central vinylene bridge upon oxidation, according to the proposed quinoidization of the **CPV** core. However, when comparing the two oxidized species (radical cations and dications), different behaviours are found for the three

systems. In the case of **A-CPV1**, (C=C)vinyl bond is progressively enlarged on going from the neutral to the dication species. This change is consistent with a first *pseudo*-quinoidization of the **CPV** moiety in the radical cation species, followed by a complete quinoidization in the closed-shell dianion. Symmetric **A-CPV3** displays a similar behaviour due to the contribution of a closed-shell electromer to the dianion structure. Conversely, charged species of **A-CPV2** present similar (C=C)vinyl bond lengths, since the second electron is removed from the fluorene moiety, giving rise to a polaron-pair dication. Therefore, the already oxidized **CPV** unit remains almost unaltered upon the second oxidation step.

For the quinoidal **Q-CPV** system, the inverse trend respect to the aromatic molecules is observed. In this case, the shortening of the vinylenic bridge upon reduction to **Q-CPV** dianion species accounts for the aromatization of the **CPV** cores.

Finally, BLA values of the three evaluated frameworks in **Q-BTT** system shift from the quinoidal to the aromatic region upon reduction. The shortest BLA values were found for the dianion species according to the fully delocalized polaron-pair structure. The accommodation of one negative charge in each dicyanomethylene group in the tetra-anion provokes the complete aromatization of the **Q-BTT** molecule and, consequently, the increase in the BLA values.

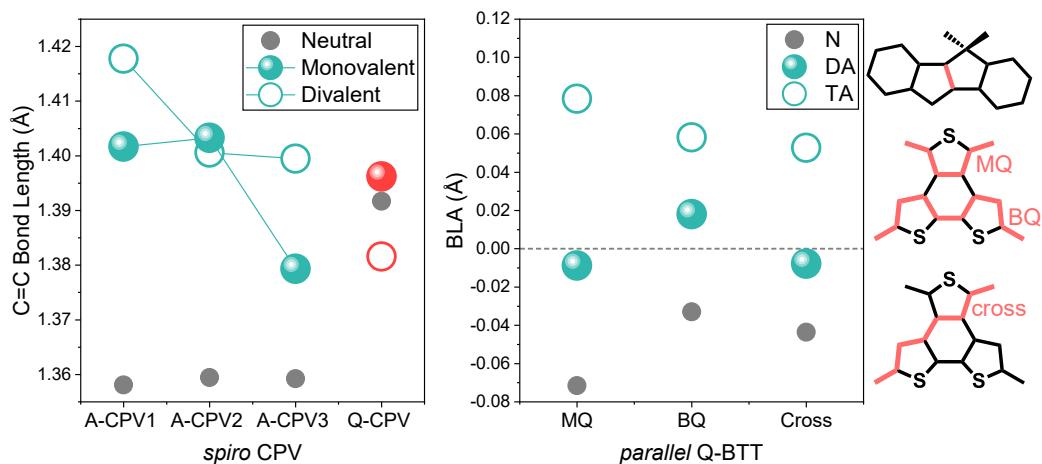


Figure IV.4.32. *Left*) Lengths (Å) of the central (C=C) vinylene bond in the spiro series for neutral (grey fulfilled circles), radical cations and radical anion (green and red fulfilled circles, respectively) and dications and dianion (green and red empty circles, respectively) species; *Middle*) Bond length alternation (BLA) values (Å) of the π -conjugated carbon bridges in **Q-BTT** neutral (grey fulfilled circles), dianion (green fulfilled circles) and tetra-anion (green empty circles) species; *Right*) Schemes of the evaluated bond lengths (highlighted in red). Optimized molecular structures of neutral and charged species were calculated at the (U)B3LYP/6-31G** level of theory.

4.3 CONCLUSIONS

Considering the results obtained in the study of the neutral and charged species of the aromatic **CPV** molecules and the quinoidal octacyano **Q-CPV** and **Q-BTT** systems, the following conclusions were extracted:

- The electronic absorption spectra are originated mainly by the indeno[2, 1-a]indene chromophore in the aromatic **CPV** systems, explaining their similitude. The main features of the absorption spectrum of the quinoidal spiro molecule, **Q-CPV**, are considerably red-shifted because of the quinoidization of the **CPV** core.
- Both octacyano systems, spiro **Q-CPV** and parallel **Q-BTT**, display aromatic absorption bands in their electronic absorption spectra, denoting the large contribution of an open-shell form to their chemical structure. In the case of **Q-CPV** molecule, the UV-Vis-NIR electronic absorption spectrum presents features similar to both non-spiro counterparts, the closed-shell **QM1CN** and the singlet open-shell **QM1CN** σ -dimer.
- The open-shell character of **Q-CPV** and **Q-BTT** ground electronic states was demonstrated through theoretical calculations, and a similar ΔE_{S-T} gap around 5 kcal/mol was obtained for both systems. The diradical formation can be explained by a synergistic effect of the aromaticity gain and the relaxation of their strained structures.

In the case of **Q-CPV**, spiro-conjugation phenomenon is a determining factor in the diradical stabilization. This *spiro-coupling effect*, that stabilizes a *fully* open-shell structure for **Q-CPV** (a tetraradical species, quintet configuration) is manifested in the population of low-lying triplet and quintet states at room temperature, which was observed through EPR measurements, as well as when comparing with the non-spiro **QM1CN** and **QM2CN** molecules.

- Cross-conjugation in **Q-BTT** and spiro-conjugation in **Q-CPV** are responsible of the different optical band gap between both quinoidal octacyano systems. Spiro-conjugation interaction between the HOMO levels of both **CPV** chromophores generates the corresponding symmetric and antisymmetric energy levels in **Q-CPV**, narrowing the HOMO-LUMO gap respect to the non-spiro molecules. In the case of **Q-BTT**, the delocalization of the π -electron density over the longer **BQ** moiety is pushed to the **MQ** unit by the cross-conjugation between the dicyanomethylene groups. Consequently, the optical band gap is larger than that of a linearly conjugated quinoidal bithiophene molecule because of the competition between the cross-conjugated frameworks, as it was already demonstrated in the study of **OTPD_n** series.

- The diradical contribution to the chemical structure of neutral **Q-CPV** and **Q-BTT** was also revealed in the IR and Raman vibrational spectroscopies, together with the bond length studies.
- Oxidation and reduction processes were performed for both aromatic and quinoidal systems, respectively. Oxidation of aromatic spiro molecules generates polaron radical cation structures over the **CPV** core for the three molecules. These radical cations are delocalized between the two aminophenyl groups, constituting class III mixed valence systems. This delocalization was also supported by the down-shift of the Raman vibrational bands upon oxidation of the neutral aromatic **A-CPV** molecules.
- However, removing a second electron from the polaron radical cation evolves different for the three aromatic **A-CPV**. For **A-CPV1**, the second electron is extracted from the radical cation **CPV** core, giving rise to a bipolaron dication species. In the case of **A-CPV2**, the second electron is extracted from the fluorene moiety due to electrostatic effects. **A-CPV3** displays the two kind of dication species, or electromers, in which the two charges are accommodated in the same **CPV** unit (bipolaron structure) or one in each moiety (polaron pair structure).
- Further oxidation of **A-CPV2** and **3** dication species generates the radical trication, in which two charges are over the **CPV** core while the third one is delocalized over the fluorene or the second **CPV** moieties, respectively. In the case of **A-CPV1** the third reduction step consists on a two-electrons process that finally results in a tetra-cation structure similar to that of the **A-CPV2** tetra-cation species.
- Subsequent oxidation of the radical trication **A-CPV2** and **3** species provokes the formation of tetra-cation species in which one extra positive charge is located on each amino group.
- For the quinoidal spiro system, reduction of the neutral **Q-CPV** molecule gives rise to a polaron-like radical anion, similar to the aromatic radical cations. Further reduction of the radical anion gives rise to the polaron-pair dianion, where one negative charge is delocalized over each **CPV** moiety. Then, injection of a third electron only can take place in one way, with two localized negative charges in the dicyanomethylene groups of one **CPV** moiety, and the second one with a radical anion delocalized through the carbon-based backbone. The final reduced species consist on a tetra-anion with one negative charge on each dicyanomethylene group.
- In parallel **Q-BTT** the *pseudo*-aromatization of the central benzene ring drives the formation of a polaron-pair dianion in a first reduction step. The singlet open-shell character of **Q-BTT** dianion was demonstrated with the presence of a thermally accessible triplet state by EPR. Next reduction step of **Q-BTT** dianion provokes the formation of a tetra-anion structure

similar to that obtained for the **Q-CPV** tetra-anion species.

- While ground electronic states of **A-CPV2** and **A-CPV3** dication species are characterized as triplets, spiro-conjugation phenomenon allows the singlet open-shell stabilization in the **Q-CPV** dianion. Spiro-conjugation is manifested in both symmetric **A-CPV3** and **Q-CPV** systems through the progressive stabilization of the singlet open-shell configuration respect to the triplet one. However, its efficacy is larger in **Q-CPV** dianion (singlet ground state) due to the structure aromatization, that increases the π -electron density on the carbon atoms linked to the spiro bridge.
- In **Q-BTT** dianion, the cross-conjugated framework is responsible of the singlet open-shell configuration of the two radical centres. Excited state absorption studies, performed through transient UV-Vis-NIR absorption and time resolved IR spectroscopies, supports both, the existence of an effective cross-conjugated pathway between **MQ** and **BQ** moieties, and the open-shell character of the dianion.
- The structures of the reduced species of the quinoidal systems were also studied by IR spectroscopy, and the obtained spectra nicely reproduce the results found by UV-Vis-NIR electronic absorption.
- The progressive quinoidization and aromatization of the **CPV** cores upon oxidation/reduction of **A-CPVn** and **Q-CPV**, respectively, was supported by Raman spectroscopy as well as the bond length changes of the central vinylenic bridge.
- According to these results, it can be established that, while spiro-conjugation is not manifested in **A-CPV1** molecule, this phenomenon is progressively favoured from asymmetric **A-CPV2** to symmetric **A-CPV3**, and **Q-CPV** is the best situation for its activation.

REFERENCES

- [1] *Three-Dimensionally Homoconjugated Carbon-Bridged Oligophenylenevinylene for Perovskite Solar Cells*, Q. Yan, Y. Guo, A. Ichimura, H. Tsuji and E. Nakamura, *J. Am. Chem. Soc.*, **2016**, *138*, 10897–10904.
- [2] *Air- and Heat-Stable Planar Tri-p-quinodimethane with Distinct Biradical Characteristics*, X. Zhu, H. Tsuji, K. Nakabayashi, S. Ohkoshi, and E. Nakamura, *J. Am. Chem. Soc.*, **2011**, *133*, 16342–16345.
- [3] *Carbon-Bridged Phenylene-Vinylene: On the Common Diradicaloid Origin of Their Photonic and Chemical Properties*, R. C. González-Cano, S. Di Motta, X. Zhu, J. T. López Navarrete, H. Tsuji, E. Nakamura, F. Negri and J. Casado, *J. Phys. Chem. C*, **2017**, *121*, 23141–23148.
- [4] *Exploration of Ground and Excited Electronic States of Aromatic and Quinoid S,S-Dioxide Terthiophenes. Complementary Systems for Enhanced Electronic Organic Materials*, J. Casado, M. Z. Zgierski, P. C. Ewbank, M. W. Burand, D. E. Janzen, K. R. Mann, T. M. Pappenfus, A. Berlin, E. Pérez-Inestrosa, R. Ponce Ortiz and J. T. López Navarrete, *J. Am. Chem. Soc.*, **2006**, *128*, 10134–10144.
- [5] *Exchange Interactions between Two Nitronyl Nitroxide or Iminyl Nitroxide Radicals Attached to Thiophene and 2,2'-Bithienyl Rings*, T. Mitsumori, K. Inoue, N. Koga and H. Iwamura, *J. Am. Chem. Soc.*, **1995**, *117*, 2467–2478.
- [6] *Spiroconjugation*, H. E. Simmons and T. Fukunaga, *J. Am. Chem. Soc.*, **1967**, *89*, 5208–5215.
- [7] *The spirarenes*, R. Hoffmann, A. Imamura and G. D. Zeiss, *J. Am. Chem. Soc.*, **1967**, *89*, 5215–5220.
- [8] *Aromaticity and Other Conjugation Effects*, R. Gleiter and G. Haberhauer, Wiley-VCH, Weinheim: Germany, **2012**.
- [9] *Quinoidal Oligothiophenes: Towards Biradical Ground State Species*, R. Ponce Ortiz J. Casado, S. Rodríguez González, V. Hernández, J. T. López Navarrete, P. M. Viruela, E. Ortí, K. Takimiya and T. Otsubo, *Chem. Eur. J.*, **2010**, *16*, 470–484.
- [10] *Carbon-Bridged Oligo(phenylenevinylene)s: Stable π -Systems with High Responsiveness to Doping and Excitation*, X. Zhu, H. Tsuji, J. T. López Navarrete, J. Casado and E. Nakamura, *J. Am. Chem. Soc.*, **2012**, *134*, 19254–19259.
- [11] *Planarization, Fusion, and Strain of Carbon-Bridged Phenylenevinylene Oligomers Enhance π -Electron and Charge Conjugation: A Dissectional Vibrational Raman Study*, P. Mayorga Burrezo, X. Zhu, S.-F. Zhu, Q. Yan, J. T. López Navarrete, H. Tsuji, E. Nakamura and J. Casado, *J. Am. Chem. Soc.*, **2015**, *137*, 3834–3843.
- [12] *Bis(aminoaryl) Carbon-Bridged Oligo(phenylenevinylene)s Expand the Limits of Electronic Couplings*, P. Mayorga Burrezo, N.-T. Lin, K. Nakabayashi, S.-i. Ohkoshi, E. M. Calzado, P. G. Boj, M. A. Díaz García, C. Franco, C. Rovira, J. Veciana, M. Moos, C. Lambert, J. T. López Navarrete, H. Tsuji, E. Nakamura and J. Casado, *Angew. Chem.*, **2017**, *129*, 2944–2948.
- [13] *The Vibrational and Electronic Spectra of the Mono-, Di-, and Trianion Salts of*

- TCNQ, M. S. Khatkale and J. P.I Devlin, *J. Chem. Phys.*, **1979**, *70*, 1851–1859.
- [14] *Axially Chiral Spiro-Conjugated Carbon-Bridged p-Phenylenevinylene Congeners: Synthetic Design and Materials Properties*, H. Hamada, Y. Itabashi, R. Shang and E. Nakamura, *J. Am. Chem. Soc.*, **2020**, *142*, 2059–2067.
- [15] *Mixed Valence Chemistry - A Survey and Classification*, M. B. Robin, O. Day, *Adv. Inorg. Chem. Radiochem.*, **1967**, *10*, 247–422.
- [16] *Organic Mixed Valence*, J. Hankache and O. S. Wenger, *Chem. Rev.*, **2011**, *111*, 5138–5178.
- [17] *Delocalization-to-Localization Charge Transition in Diferrocenyl-Oligothiophene-Vinylene Molecular Wires as a Function of the Size by Raman Spectroscopy*, S. Rodríguez González, M. C. Ruiz Delgado, R. Caballero, P. De la Cruz, F. Langa, J. T. López Navarrete and J. Casado, *J. Am. Chem. Soc.*, **2012**, *134*, 5675–5681.
- [18] *Oligomers of Cyclopentadithiophene-Vinylene in Aromatic and Quinoidal Versions and Redox Species with Intermediate Forms*, P. Mayorga Burrezo, R. Domínguez, J. L. Zafra, T. M. Pappenfus, P. de la Cruz, L. Welte, D. E. Janzen, J. T. López Navarrete, F. Langa and J. Casado, *Chem. Sci.*, **2017**, *8*, 8106–8114.
- [19] *Generation and Spectroscopic Profiles of Stable Multiarylaminium Radical Cations Bridged by Fluorenes*, C.-C. Chang, H. Yueh and C.-T. Chen, *Org. Lett.*, **2011**, *13*, 2702–2705.
- [20] *Polarons, Bipolarons, and Side-By-Side Polarons in Reduction of Oligofluorenes*, L. Zaikowski, P. Kaur, C. Gelfond, E. Selvaggio, S. Asaoka, Q. Wu, H.-C. Chen, N. Takeda, A. R. Cook, A. Yang, J. Rosanelli and J. R. Miller, *J. Am. Chem. Soc.*, **2012**, *134*, 10852–0863.
- [21] *The Class II/III Transition in Triarylamine Redox Systems*, C. Lambert and G. Nöll, *J. Am. Chem. Soc.*, **1999**, *121*, 8434–8442.
- [22] *Bridge-mediated Hopping or Superexchange Electron-transfer Processes in Bis(triarylamine) Systems*, C. Lambert, G. Nöll and J. Schelter, *Nat. Mater.*, **2002**, *1*, 69–73.
- [23] *Investigation of the Mechanism of the Intramolecular Scholl Reaction of Contiguous Phenylbenzenes*, P. Rempala, J. Kroulík and B. T. King, *J. Org. Chem.*, **2006**, *71*, 5067–5081.
- [24] *Comparison of Oxidative Aromatic Coupling and the Scholl Reaction*, M. Grzybowski, K. Skonieczny, H. Butenschön and D. T. Gryko, *Angew. Chem. Int. Ed.*, **2013**, *52*, 2–33.
- [25] *Insights into the Scholl Coupling Reaction: A Key Transformation of Relevance to the Synthesis of Graphenes and Related Systems*, M. S. Little, S. G. Yeates, A. A. Alwattar, K. W. J. Heard, J. Raftery, A. C. Edwards, A. V. S. Parry and P. Quayle, *Eur. J. Org. Chem.*, **2017**, *3*, 1694–1703.
- [26] “Electromers” of the Tetramethyleneethane Radical Cation and Their Nonexistence in the Octamethyl Derivative: Interplay of Experiment and Theory, B. Müller, T. Bally, F. Gerson, A. de

Meijere, and M. von Seebach, *J. Am. Chem. Soc.*, **2003**, *125*, 13776–13783.

[27] *Isomerism: The Same but Different*, T. Bally, *Nat. Chem.*, **2010**, *2*, 165–166.

[28] *Tetracyanoethylene (TCNE): The Characteristic Geometries and Vibrational Absorptions of Its Numerous Structures*, J. S. Miller, *Angew. Chem. Int. Ed.*, **2006**, *45*, 2508–2525.

[29] *Ultrafast spectroscopic characterization of 7,7,8,8-tetracyanoquinodimethane (TCNQ) and its radical anion (TCNQ)*, L. Ma, P. Hu, C. Kloc, H. Sun, M. E. Michel-Beyerle and G. G. Gurzadyan, *Chem. Phys. Lett.*, **2014**, *609*, 11–14.

[30] *Two-Electron Transfer Stabilized by Excited-State Aromatization*, J. Kim, J. Oh, S. Park, J. L. Zafra, J. R. DeFrancisco, D. Casanova, M. Lim, J. D. Tovar, J. Casado and D. Kim, *Nat. Commun.*, **2019**, *10*, 4983–4990.

V. CONCLUDING REMARKS ON POLYCONJUGATED SYSTEMS

V. CONCLUDING REMARKS ON POLYCONJUGATED SYSTEMS

Over the *Results and Discussion* Section of the present Ph. D. Thesis, the characterization of the electronic and molecular structure of organic systems with several π -conjugated sequences and the effect on their electronic properties, have been performed. The study of each type of π -conjugation framework, namely linear π -conjugation, cross-conjugation, spiro-conjugation and parallel π -conjugation, has led us to specific conclusions and remarks about the particular system under study. This final section provides an overview of the alteration of the linear π -conjugation when several π -sequences are simultaneously present in the system.

Changes on the Linear π -Conjugation by Cross-Conjugated Frameworks

The effect of a second π -conjugated sequence orthogonal to the main π -conjugated carbon-based backbone has been evaluated in aromatic and quinoidal oligothiophene systems with inter-dione cross-conjugated frameworks (**OTPD_n** and **2DQoT**, respectively). The 2D extension of the π -electron density for both systems has been caused by the competition between the two orthogonal π -conjugated sequences. The weight of the cross-conjugated pathway is raised with the presence of *extra* electronic density, *i. e.* in reduced species, as well as in diradical forms.

Usually, the presence of a cross-conjugated sequence in neutral systems provokes the confinement of the π -

electron density (or the radical centres in the case of diradical systems) in the innermost part of the molecules. This effect can be suppressed by two ways: i) attaching highly electron-withdrawing groups in small molecules (which is the case of **2DQTT**, in which the larger electron-accepting character of the dicyanomethylene moieties blocks the action of the cross-conjugated inter-dione framework); ii) stabilizing the linearly π -conjugated structure, for example, with an aromaticity energy gain. In **2DQPT**, the influence of the electron-accepting dicyanomethylene groups is diminished towards the central thiophene rings because of the longer distances. Nevertheless, the open-shell character of this system stabilizes the linear *versus* the cross-conjugated resonant form through the aromatization of five thiophene rings, accommodating the radical centres in the dicyanomethylene moieties.

For the charged species, two different behaviours for the aromatic and quinoidal oligothiophenes have been observed due to the diradical character of the second series. While in aromatic **OTPD_n** molecules the injection of one *extra* electron generates a classical polaron radical anion, which is delocalized over the linear oligothiophene backbone, the activation of the cross-conjugated framework in diradical **2DQoT** molecules brings the possibility of two different radical anion species. Reduction of **2DQQT** and **2DQPT** to the corresponding radical anions generates two electronic isomers, only differentiated in the localization of the

radical anion centre: through the linear inter-dicyanomethylene pathway or over the cross-conjugated inter-dione one.

On the other hand, injection of a second electron to generate divalent species provokes the opposite behaviour. In the quinoidal **2DQoT**, the accommodation of the second *extra* electron in the linear inter-dicyanomethylene sequence is favoured by the aromaticity gain of the thiophene rings. Conversely, dianion species of longer **OTPD_n** molecules display polaron pair structures, in which each radical anion centre forming the dianion is accommodated in a cross-conjugated inter-dione sequence, thus reducing the spatial repulsion between identical charges. As in the case of the neutral forms, in the diradical **2DQQT** and **2DQPT** systems, the open-shell configuration shifts the π -electron delocalization towards the cross-conjugated frameworks.

Besides, the presence of an alternative orthogonal sequence in longer oligomers of **2DQoT** series brings the possibility of a third reduction step, since a third electron can host in the cross-conjugated pathway. This process is not favoured in **OTPD_n** since no electron-withdrawing groups (different from the carbonyl ones) are available, so that the third *extra* electron would reduce the aromatic energy of the thiophene rings.

For the open-shell molecules, the Double Spin Polarization (DSP) mechanism is activated by the double conjugation of the cross-conjugated radical centres with the π -electrons of the linear oligothiophene backbone. However, this

effect can be diminished when adding cross-conjugated moieties between the two radical centres. The presence of this “neutral” inter-dione sequences disrupts the *chemical* connection between the two radical centres, destabilizing the singlet ground electronic state respect to the triplet form. This mechanism is schematized in Figure V.1.

For these systems, the combination of the cross-conjugation properties with an incipient diradical character have been demonstrated to produce new outstanding features (as the cholesteric-like aggregation mode in doped **2DQQT**, Figure V.1) with direct applications in functional organic devices.

Cross-conjugation was also evaluated in a polyconjugated closed-shell system: a tetra-aminophenyl ethene (referred as **TPE**). We have demonstrated that the bis-protonated **TPE** presents well-defined conductance through the cross-conjugated framework, as well as through the linear *cis/trans* pathways. These results proved the applicability of the cross-conjugation phenomena in organic electronics.

Changes on the Linear π -Conjugation by Through-Space Spiro-Conjugation

Through-space π -interactions have been explored through aromatic and quinoidal spiro-conjugated systems. **CPV** family allowed the study of this 3D π -conjugation varying the two spiro-linked chromophores. On the other hand, the quinoidal **CPV** molecule has been compared with a similar quinoidal

octacyano system formed by two *parallelly* π -conjugated moieties (**Q-BTT**), but in this case with an intramolecular cross-conjugated connection instead of the spiro one.

For neutral species, spiro-conjugation is shown in the quinoidal **Q-CPV** molecule because of its open-shell character (purple inset in Figure V.1.). The aromatization of the quinoidal structure upon generation of the diradical (or tetraradical) form increases the π -electron density over the carbon atoms linked to the tetrahedral centre, favouring their spiro-conjugation to the equivalent atoms in the second moiety. The open-shell character of **Q-CPV** is promoted by a synergistic effect between the aromaticity gain, the relaxation of the strained 3D structure and the aforementioned spiro-conjugation. These features directly affect the functional properties of these materials, narrowing both the HOMO-LUMO gap and the singlet-triplet gap respect to the non-spiro counterparts.

When comparing **Q-CPV** with the non-spiro **Q-BTT**, a narrower optical band gap is found for the former. Spiro-conjugation between the HOMO levels of the two chromophores generates the corresponding symmetric and antisymmetric linear combinations in **Q-CPV**, thus reducing the HOMO-LUMO gap. However, as it has been demonstrated in **OTPD_n** series, the presence of cross-conjugated frameworks between the dicyanomethylene groups of different moieties in **Q-BTT** reduces the extension of the π -electron density through the longer quinoidal bithiophene unit. Consequently,

the HOMO-LUMO gap is larger than in the case of a non-cross-conjugated bithiophene, and also than the spiro **Q-CPV** molecule.

Similar to the case of **OTPD_n** and **2DQoT** cross-conjugated systems, while quinoidal **Q-CPV** molecule displays spiro-conjugation in the neutral form, this interaction is observed in the aromatic **A-CPV-3** upon oxidation to the polaron pair dication. Again, the alternative π -conjugation sequence is activated respect to the linear framework by the presence of extra charge density in oxidised species as well as in diradical forms.

Nevertheless, injection of a second electron in **Q-CPV** reinforces the through-space interaction in the dianion species, contrary to **2DQoT** systems. In both cases, the formation of the dianion provokes the aromatization of the carbon-based backbone. However, while in the case of **2DQoT**, the aromatization of the linear oligothiophene reduces the contribution of the cross-conjugated framework to the π -electron delocalization, in **Q-CPV** the aromatic form increases the π -electron density on the carbon atoms linked to the spiro bridge, thus improving the effectivity of the spiro-conjugation. This effect is also shown in the activation of the DSP mechanism, since the singlet character of the open-shell dianion cannot be justified by any through-bond interaction (Figure V.1).

Q-BTT dianion species also presents an inverse influence of the cross-conjugated sequence respect to the **OTPD_n** family. While in the cross-conjugated oligothiophenes the presence of

orthogonal pathways diminishes the effect of the DSP, the property that allows the operation of the DSP mechanism between the two radical anions placed in parallel moieties in **Q-BTT** is precisely the cross-conjugation (yellow inset in Figure V.1.).

In this scenario, it can be concluded that in diradical polyconjugated systems, the activation/deactivation of the DSP mechanism must be examined considering the kind of alternative π -conjugation modes. In linearly π -conjugated oligomers crossed by orthogonal pathways, the cross-conjugation properties can disrupt the double conjugation through the bridge

(i. e., the DSP mechanism is deactivated, favouring the triplet ground state). However, when the cross-conjugated framework connects two π -systems, is precisely this orthogonal pathway the feature that activates the DSP phenomenon for diradical or segregated divalent species. Finally, for spiro-conjugated systems, similarly to the parallel cross-conjugated chromophores, higher through-space interactions favour the DSP mechanism and, hence, the singlet open-shell ground state, for species in which the radical centres are located in different moieties.

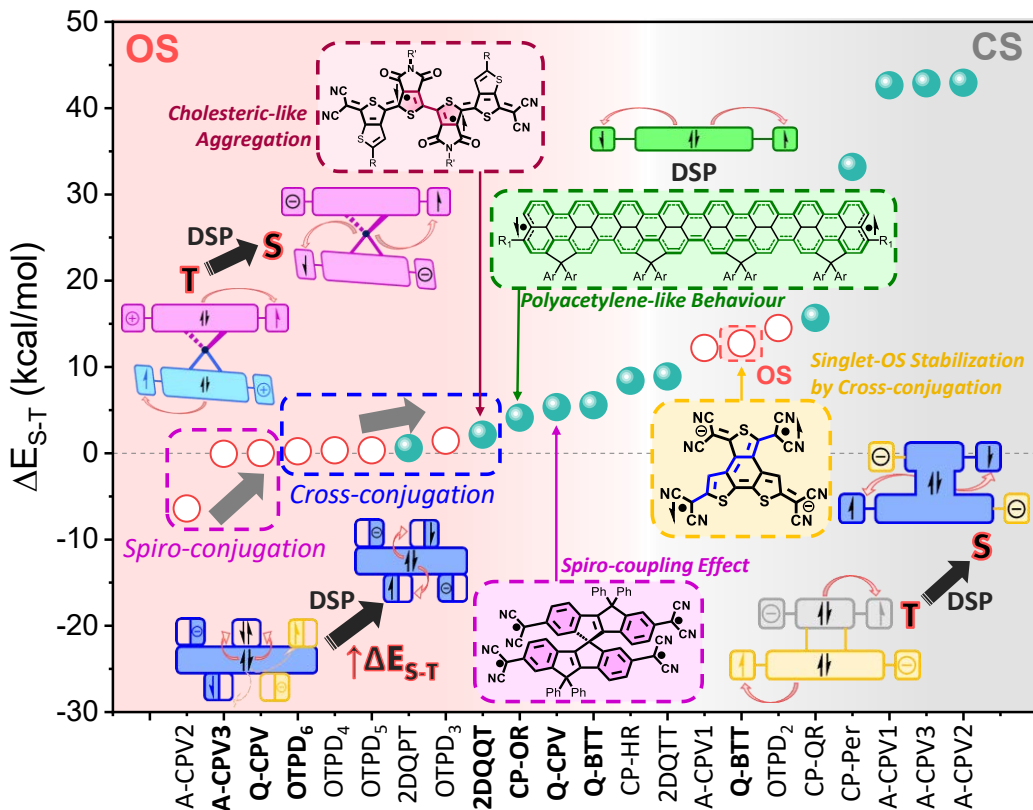


Figure V.1. Singlet-triplet gap (in kcal/mol) of the most relevant neutral (green fulfilled circles) and doubly charged (red empty circles) species of the different molecules studied in the present Ph.D. Thesis, together with the schematization of the activation of the Double Spin Polarization (DSP) mechanism for each polyconjugated system.

VI. RESUMEN Y CONCLUSIONES

VI. RESUMEN Y CONCLUSIONES

Introducción

Los sistemas orgánicos π -conjugados han estado en el foco de atención de la comunidad científica desde el descubrimiento de sus propiedades semiconductoras y, por tanto, de su potencial uso como materiales funcionales en dispositivos electrónicos orgánicos.^[1-4] El enorme y rápido desarrollo en la aplicación de este tipo de moléculas solo se ha podido conseguir a través de un amplio conocimiento de su estructura química y de las propiedades derivadas de la misma.

Estas propiedades semiconductoras de las moléculas π -conjugadas son consecuencia de la deslocalización de sus electrones π a través del esqueleto de carbono. Por tanto, el establecimiento de los mecanismos de deslocalización electrónica y de los factores que perturban la densidad de electrones π son de crucial importancia en el discernimiento de la relación estructura-propiedades. Dicha relación permitirá un perfeccionamiento del funcionamiento de estos materiales y el desarrollo de métodos de síntesis *ad hoc* para las aplicaciones deseadas.

En el campo de estudio de la deslocalización de los electrones π , la existencia de una longitud de conjugación efectiva para los oligómeros y polímeros semiconductores ha facilitado enormemente la caracterización de las propiedades de dichos materiales. A dicha longitud de conjugación efectiva (n_{ECL} , del inglés *Effective Conjugation Length*) se produce una convergencia de las

propiedades electrónicas y ópticas de los oligómeros y polímeros π -conjugados.^[5, 6] Así, el estudio sistemático de la evolución de dichas propiedades al aumentar el número de unidades monoméricas hasta tamaños próximos a la n_{EC} , y la extrapolación de las mismas a la cadena ideal de longitud infinita, es conocido como *aproximación oligomérica*,^[7] y es el método más extendido para el análisis de este tipo de materiales. De esta forma, es posible establecer relaciones estructura-propiedades en sistemas poliméricos a través del estudio de moléculas más sencillas. Por tanto, la aproximación oligomérica permite conocer las características de la deslocalización de los electrones π , y de sus propiedades, a través de una cadena linealmente conjugada. La tendencia o evolución de estas propiedades al aumentar el número de unidades puede ser comparada entre diferentes familias de moléculas, de forma que se puedan establecer ciertas guías para la síntesis “a medida” según la aplicación deseada.

Sin embargo, junto a la cadena de conjugación lineal principal pueden coexistir secuencias alternativas de deslocalización de electrones π . Aunque la contribución de las estructuras resonantes correspondientes a la deslocalización a través de estas rutas secundarias no sea elevada, su existencia puede modificar de forma significativa las propiedades ópticas, electrónicas y moleculares derivadas de la cadena conjugada lineal principal. Así, el conocimiento de cómo estos modos de conjugación perturban la densidad de

electrones π en moléculas policonjugadas puede permitir la modulación racional de la contribución relativa de cada ruta de conjugación, dando lugar a nuevas propiedades y aplicaciones en el campo de la electrónica orgánica que no son accesibles a través de sistemas monoconjugados.

En este escenario, los diferentes sistemas policonjugados pueden describirse en función de cómo la ruta de conjugación π alternativa interacciona con el esqueleto lineal principal.

El caso más común de coexistencia de diferentes cadenas de conjugación son las **moléculas cross-conjugadas**, que son sistemas en los que dos secuencias de conjugación comparten un enlace múltiple (o un fragmento de enlaces conjugados).^[8] Por consiguiente, en estos sistemas dos secuencias de enlaces CC sencillos y dobles alternantes, aisladas entre sí a través de dos enlaces sencillos consecutivos, están a su vez conjugadas a un tercer sistema π . En otras palabras, la secuencia *cross*-conjugada puede ser descrita como una ruta de deslocalización de los electrones π alternativa y ortogonal a la secuencia linealmente conjugada principal. Así, se establece una competencia por dicha deslocalización entre ambas secuencias, por lo que todas las propiedades derivadas de la conjugación a través de la cadena principal se verán afectadas. La alteración de la densidad π -electrónica por la presencia de una secuencia *cross*-conjugada respecto a moléculas que solo presentan conjugación lineal puede manifestarse a través de los siguientes parámetros: i) la variación de la longitud

media de enlaces alternantes (o BLA, del inglés *Bond Length Alternation*) al aumentar el tamaño del oligómero; ii) una disminución de la longitud de conjugación efectiva; y iii) una menor reducción del *gap* HOMO-LUMO al aumentar el número de unidades monoméricas. Así, tanto la longitud de conjugación efectiva como el *gap* HOMO-LUMO pueden permanecer prácticamente invariantes al aumentar el número de unidades en sistemas *cross*-conjugados.

Además de este tipo de sistemas policonjugados, puede darse interacción entre sistemas π -conjugados a través del espacio que modifiquen la conjugación lineal de los dos esqueletos de carbono implicados. En general, el concepto de *homoconjugación* se refiere a la interacción entre dos sistemas π conectados por un átomo aislante.^[9, 10] Para que este tipo de interacción exista es necesario que la molécula adopte una conformación espacial determinada. . Puede ocurrir, por ejemplo, que los dos sistemas homoconjugados se encuentren en dos planos perpendiculares entre sí unidos únicamente a través de un átomo de carbono sp^3 tetraédrico. A este tipo de homoconjugación se le denomina **spiro-conjugación**.^[11, 12]

Una propiedad interesante de este tipo de sistemas es que, cuando ambas unidades *spiro*-conjugadas contribuyen con un número par de dobles enlaces y el número total de electrones π en la molécula es igual a $4N$ (con N siendo un número entero), entonces el nivel HOMO resultante aumenta su energía respecto a las unidades individuales y, por tanto, el

gap óptico disminuye.^[12, 13]

Además del *gap* HOMO-LUMO, el valor del BLA también se ve afectado por la presencia de *spiro*-conjugación. Sin embargo, la integral de solapamiento entre los orbitales *spiro*-conjugados representa solo el 20% del valor correspondiente al solapamiento π - π entre átomos adyacentes situados en el mismo plano.^[12] Por tanto, no es de extrañar que la disminución del BLA como consecuencia del aumento de la deslocalización π pueda pasar desapercibida en moléculas *spiro*-conjugadas.

La presencia de estas secuencias de policonjugación es especialmente relevante en el límite de ruptura de enlaces π , es decir, en moléculas con una elevada deslocalización de dichos electrones π .^[14] Un aumento de esta deslocalización π (*i. e.*, disminución del BLA) al aumentar el número de unidades monoméricas puede conllevar en última instancia una **transformación aromático ↔ quinoide** del sistema heteroaromático bajo estudio. Dicha tautomerización es posible gracias a la formación de **especies dirradicales**. De esta forma, a través de la transformación desde moléculas de capa cerrada (o *closed-shell* en la terminología en inglés) a sistemas de capa abierta (*open-shell*) en dirradicales tipo *Kekulé*^[15] es posible evaluar la contribución relativa de cada secuencia π -conjugada a la estructura real de la molécula.

Debido a que una nueva entidad química, el sistema dirradical, entra en juego en este proceso, se abre un nuevo abanico de propiedades para los sistemas

policonjugados. Uno de los fenómenos más importantes que pueden experimentar los dirradicales *Kekulé* es la activación del mecanismo de **doble polarización de espín** (o DSP, de sus siglas en inglés *Double Spin Polarization*). Según la DSP, las moléculas de capa abierta pueden presentar una configuración singlete de su estado electrónico fundamental, violando la regla de máxima multiplicidad de Hund,^[15, 16] como consecuencia de la doble deslocalización de los electrones π del puente (*i. e.*, el esqueleto π -conjugado) en los orbitales no enlazantes del dirradical, frente a una única posible deslocalización en los estados triplete.^[16-18] Por consiguiente, cualquier factor que interrumpa la conjugación de los electrones π a través del esqueleto de carbono evitará la activación del mecanismo de DSP. Precisamente es en esta interrupción de la π -conjugación donde entran en juego las diferentes secuencias de deslocalización de los sistemas policonjugados. Las rutas alternativas de conjugación de los electrones π retiran densidad electrónica del puente lineal y, por tanto, interrumpen o debilitan la doble deslocalización de dichos electrones en los orbitales moleculares no enlazantes del dirradical. De esta forma, la diferencia de energía entre los estados singlete y triplete de las moléculas capa abierta (denominado *gap* singlete-triplete) se ve directamente afectada por la presencia de rutas alternativas de deslocalización π , constituyendo una herramienta de gran utilidad para evaluar la contribución relativa de dichos modos de conjugación.



Objetivos

La presente tesis doctoral está enfocada al estudio de las estructuras electrónicas y moleculares de sistemas orgánicos que presentan varias secuencias de conjugación de los electrones π , así como de sus propiedades ópticas y electrónicas y su uso potencial en dispositivos electrónicos orgánicos.

Para conseguir este propósito, las estructuras electrónicas y moleculares de siete sistemas diferentes han sido caracterizadas mediante espectroscopías ópticas y vibracionales. En todos los casos los resultados obtenidos se han apoyado en cálculos químico-cuánticos y, siempre que ha sido posible, con técnicas como resonancia paramagnética electrónica, conductancia de moléculas individuales o absorción de estados excitados. La investigación de estos sistemas orgánicos se ha realizado atendiendo a los diferentes esquemas de conjugación que presentan los electrones π . El estudio de cada uno de estos esquemas ha sido abordado desde estructuras iniciales aromáticas y quinoideas capaces de experimentar una transformación hacia sistemas de capa abierta, es decir, dirradicales.

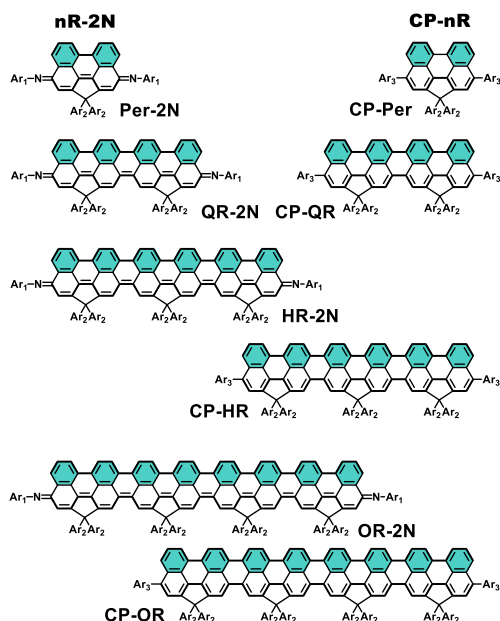
En la *Sección A* se ha realizado la caracterización de dos series de ciclopentaoligorrilenos linealmente monoconjugados, una de ellas de carácter aromático (**CP-nR**) y la segunda, quinoide (**nR-2N**). Ambas familias fueron sintetizadas por el grupo del Profesor Jishan Wu, perteneciente a la *University of Singapore* (Singapur). El hecho de que ambas familias presenten una transformación de capa cerrada a capa

abierta en estado neutro al aumentar el tamaño del oligómero ha permitido realizar una descripción completa del comportamiento de la densidad de electrones π en una secuencia de conjugación lineal, tanto de carácter aromático como quinoide. El estudio de estas familias permite el establecimiento de una serie de pautas generales acerca del comportamiento de los electrones π en un sistema dirradical linealmente conjugado, lo que permitirá luego evaluar su alteración con la presencia de secuencias π -conjugadas alternativas.

La *Sección B* está dedicada al estudio de sistemas policonjugados a través del enlace, concretamente de moléculas *cross*-conjugadas, representadas por dos series de oligotienopirrolo-dionas aromáticas (**OTPD_n**) y quinoideas (**2DQoT**), proporcionadas por el grupo del Profesor Xiaozhang Zhu de la *Chinese Academy of Science* (Beijing, China). De forma complementaria, también se ha evaluado la *cross*-conjugación en sistemas de capa cerrada en una familia de etilenos 4-aminofenil-sustituídos (**nPE**), sintetizadas por el grupo del Profesor José Luis Segura (Universidad Complutense de Madrid, España). El estudio de las características ópticas, electrónicas y estructurales tanto de las moléculas neutras como de sus especies reducidas nos permitirá evaluar el nivel de interferencia entre las dos secuencias *cross*-conjugadas y de las propiedades derivadas de la misma.

Finalmente, en la *Sección C* se describen fenómenos de conjugación π a través del espacio en sistemas *spiro* aromáticos (**A-CPVn**) y quinoide (**Q-CPV**). Además, se

realizará la comparación de la molécula quinoide **Q-CPV** con un sistema similar, un octaciano-benzotritiofeno con dos secuencias inter-dicianometileno paralelas (**Q-BTT**). La molécula **Q-BTT** presenta también una secuencia *cross*-conjugada que conecta las dos unidades π paralelas. La síntesis de las moléculas **CPV spiro**-conjugadas fue realizada por el grupo del Profesor Eiichi Nakamura (*School of Science, The University of Tokyo*, Japón); mientras que el sistema **Q-BTT** fue preparado por el grupo del Profesor Nazario Martín (Universidad Complutense de Madrid e Instituto IMDEA Nanociencia, España).



Esquema 1. Estructura química de las familias de bis(imino)oligorileno quinoide (**nR-2N**, izquierda) y oligorileno aromático fusionado (**CP-nR**, derecha) estudiadas en el Capítulo 1 de Resultados.

Resultados y Discusión

Sección A. Dirradicales Linealmente π -Conjugados

Capítulo 1. El caso de Oligorileno Aromáticos y Quinoide.

En este capítulo se ha investigado la deslocalización de los electrones π en un esqueleto linealmente conjugado a través de la evolución de las estructuras electrónica y molecular de dos familias de oligorileno neutros, desde el monómero perileno hasta el tetrámero. La primera familia presenta un carácter aromático (**CP-nR**), mientras que la segunda es de naturaleza quinoide y está constituida por bis(imino)-cilopentaoligorileno (**nR-2N**). En ambas familias, las unidades de perileno están covalentemente fusionadas, dando lugar a una estructura completamente plana. Además, los dos

fragmentos de naftaleno que forman la unidad de perileno están a su vez fusionados mediante un anillo de cinco miembros. Esta unión impone una curvatura de la estructura plana del esqueleto oligorilénico que aumenta progresivamente al aumentar la longitud del oligómero (es decir, la curvatura es más pronunciada en los rilenos más largos).

De acuerdo con los espectros de absorción electrónica UV-Vis-NIR, en ambas familias se aprecian características típicas de sistemas dirradicales para las moléculas de mayor tamaño (los trímeros, **CP-HR** y **HR-2N**, y los tetrámeros, **CP-OR** y **OR-2N**). Esto indica una transformación del estado electrónico fundamental de capa cerrada a una configuración de singlete capa abierta al aumentar el tamaño de ambos tipos de oligorileno. En el caso de la serie quinoide **nR-2N**, la

configuración de singlete capa abierta se manifiesta en la aparición de una doble transición electrónica $H,H \rightarrow L,L$ como consecuencia de la presencia de un estado excitado singlete de baja energía.^[19]

Por otra parte, el ajuste de acuerdo con la ecuación de Meier^[5, 6] de las longitudes de onda de los máximos de absorción de ambas series da lugar a longitudes de conjugación efectiva elevadas ($n_{ECL}=45$ y $n_{ECL}=28$ para **CP-nR** y **nR-2N**, respectivamente). Esta extensión de la conjugación efectiva, facilitada tanto por las estructuras planas de ambas familias de oligorrilenos como por el ángulo de curvatura que presentan, tiene un origen diferente para cada familia y explica la diferencia entre ambos valores de n_{ECL} . En el caso de la serie **nR-2N**, la deslocalización de los electrones π está favorecida por su propia estructura química de tipo quinoide. Sin embargo, la transformación a estructuras de capa abierta de las moléculas de mayor longitud, en las que la densidad electrónica tiende a quedar confinada en los anillos aromáticos, hace que dicha serie alcance más rápidamente el límite de saturación de Meier (n_{ECL}). En el caso de la familia **CP-nR**, el comportamiento es el contrario: las estructuras capa-abierta de los miembros dirradicaloides de mayor longitud es de tipo quinoide, es decir, facilita la deslocalización exocíclica de los electrones π . Por tanto, a medida que aumenta la longitud de cadena, también lo hace el carácter quinoide, lo que conlleva una mayor longitud de conjugación efectiva.

Para la familia **nR-2N** la transformación de capa cerrada a capa abierta está justificada por la ganancia de aromaticidad

del esqueleto rilénico quinoide (es un fenómeno entálpico). Sin embargo, en la serie aromática **CP-nR**, la estabilización de estructuras capa abierta para las moléculas de mayor tamaño es debida al pequeño *gap* HOMO-LUMO, que provoca a su vez una reducción de la diferencia de energía entre los estados singlete y triplete.^[20] En este caso, la población del estado triplete provoca la estabilización entrópica de la especie capa-abierta.

Los estudios vibracionales IR y Raman confirman el carácter dirradical de las moléculas de mayor longitud en las dos familias de oligorrilenos. El progresivo desplazamiento hacia menores números de ondas de las bandas Raman características de estos sistemas, al aumentar el tamaño de los mismos, indica una mayor deslocalización de los electrones π a través del esqueleto lineal.^[21] Este resultado también queda demostrado en la variación de los valores de BLA.

Sin embargo, los tetrámeros **CP-OR** y **OR-2N** presentan un comportamiento Raman diferente al del resto de su serie. Mientras que los espectros Raman de las moléculas más cortas están dominados claramente por un régimen *bencenoide*, en el caso de las moléculas de mayor longitud, el comportamiento de las bandas vibracionales es de tipo *poliacetilénico*. De esta forma, en completo acuerdo con la descripción de los estados electrónicos fundamentales de estas moléculas, mientras que la deslocalización de los electrones π en las moléculas más pequeñas tiene lugar preferentemente en los anillos de benceno, en el caso de los tetrámeros, dicha deslocalización se

produce preferentemente a través de los bordes tipo “silla” de la molécula.^[22] El comportamiento tipo poliacetileno de **CP-OR** también se manifiesta en la presencia de un sobretono de la banda más intensa en el espectro Raman.

La secuencia de π -conjugación lineal a través los bordes tipo “silla” establece la conexión entre los dos centros radicalarios que explica la configuración singlete del estado fundamental de estos sistemas, es decir, permite la activación del mecanismo de doble polarización de espín. El fenómeno de DSP se ve favorecido por las estructuras planas de estas moléculas, y por la ausencia de grupos secundarios que puedan retirar densidad π -electrónica del puente rilénico.

Sección B. Dirradicales *Cross*-Conjugados

Capítulo 2. El Caso de las Oligotienopirrolo-dionas Aromáticas: Dianiones *Cross*-Conjugados.

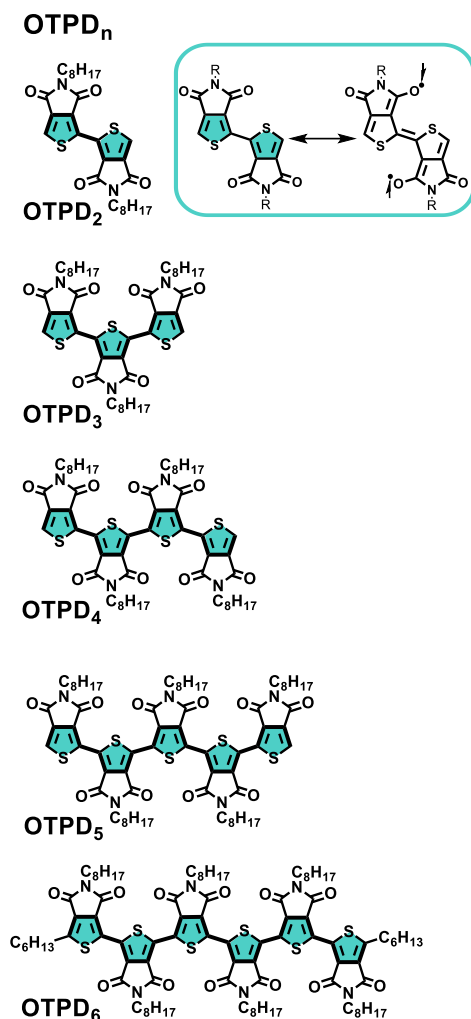
En este capítulo de la *Sección B* se describen las especies neutras y reducidas de una familia de oligotienopirrolo-dionas aromáticas *cross*-conjugadas (**OTPD_n**), desde el dímero hasta el hexámero. La principal secuencia de π -conjugación la constituye la cadena de oligotiofenos, mientras que los modos *cross*-conjugados aparecen entre los grupos carbonilo vecinales de dos unidades TPD consecutivas (secuencia inter-diona). La influencia de la deslocalización *cross*-conjugada se ha analizado al variar la carga *extra* inyectada en estas moléculas (desde

las especies neutras hasta los dianiones).

En los sistemas neutros, la existencia de una secuencia ortogonal provoca el confinamiento de la densidad de electrones π hacia el centro de la molécula, disminuyendo la longitud de conjugación efectiva de la serie ($n_{ECL}=14$) y, por consiguiente, disminuyendo la reducción del *gap* HOMO-LUMO al aumentar la cadena. Para esta familia no se encontraron variaciones de la configuración de su estado electrónico fundamental, y todas las moléculas neutras son descritas como sistemas de capa cerrada.

En el análisis de las especies cargadas, en una primera etapa de reducción de los oligómeros **OTPD_n**, se obtienen en todos los casos los correspondientes radicales aniones con la clásica estructura tipo polarón. Los espectros vibracionales Raman, así como los valores de BLA, sugieren que la presencia de las secuencias inter-diona provocan que la carga *extra* inyectada se localice preferentemente en el centro de la molécula.

La posterior reducción de estos radicales aniones se observó solo para los oligómeros de mayor longitud de la serie. Los dianiones de los oligómeros **OTPD₄**, **OTPD₅** y **OTPD₆**, se muestran como polarones segregados o como un par de polarones, con una configuración en su estado fundamental de singlete capa abierta. La única estructura química posible que da cuenta de estas características es aquella en la que cada polarón se deslocaliza en una secuencia descrita entre dos grupos carbonilos vecinales de unidades TPD contiguas, es



Esquema 2. Estructura química de la serie de oligotienopirrolodionas aromáticas *cross*-conjugadas (OTPD_n) estudiadas en el Capítulo 2 de Resultados. La secuencia *cross*-conjugada se muestra en el inset.

decir, cada polarón se encuentra en un fragmento *cross*-conjugado inter-diona.

Estos dos centros radicalarios que conforman el par de polarones están *químicamente* conectados a través del puente de oligotiofenos π -conjugados, explicando el carácter singlete del estado fundamental de acuerdo con el mecanismo de DSP. Sin embargo, la

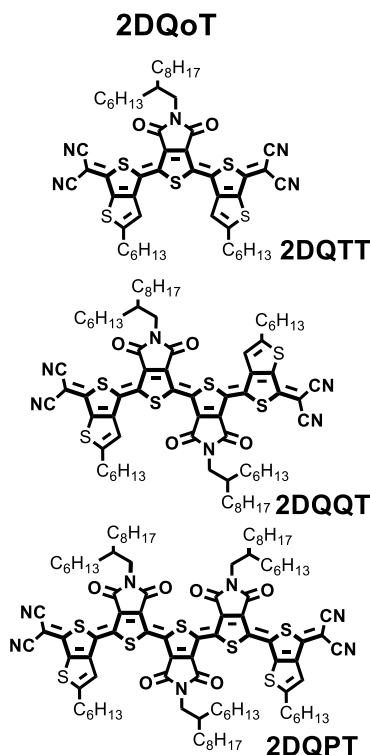
presencia de secuencias inter-diona “neutras” entre estos dos fragmentos “reducidos” interrumpe la conjugación a través del esqueleto de oligotiofenos (*i. e.*, el mecanismo de DSP) y, por tanto, disminuye el *gap* singlete-triplete.

Capítulo 3. El Caso de las Oligotienopirrolodionas Quinoideas: El efecto de La Longitud de Cadena.

En analogía con los estudios realizados en el Capítulo 2, en esta sección se realiza el análisis de la *cross*-conjugación en una familia de oligotienopirrolodionas quinoideas (**2DQoT**, desde el trímero hasta el pentámero).

Al comparar los resultados de ambas familias, se deben tener en cuenta dos diferencias principales: i) la estructura quinoide en **2DQoT** fuerza que la secuencia *cross*-conjugada se establezca entre grupos carbonilos opuestos o distales de dos unidades TPD adyacentes; y ii) un aumento progresivo del carácter dirradical al aumentar la longitud de los oligómeros emerge gracias a la aromatización de los anillos de tiofeno. De esta forma, el trímero **2DQTT** se caracteriza como un sistema capa cerrada, mientras que el pentámero **2DQPT** presenta un marcado carácter dirradical. El tetrámero **2DQQT** muestra un comportamiento intermedio, con un carácter dirradical incipiente.

Los dirradicales **2DQQT** y **2DQPT** presentan una configuración singlete capa abierta de su estado electrónico fundamental gracias al mecanismo de DSP. Sin embargo, la presencia de las secuencias



Esquema 3. Estructura química de la serie de oligotienopirrolodionas quinoides *cross*-conjugadas (**2DQoT**) estudiadas en el Capítulo 3 de Resultados.

cross-conjugadas altera la deslocalización de los electrones π a través del esqueleto de oligotiofenos, disminuyendo el *gap* singlete-triplete al avanzar en la serie (de **2DQTT** a **2DQPT**). Además, la presencia de dichos modos de conjugación alternativos dirige la localización de los centros radicales en el caso de **2DQQT**. La competencia entre las secuencias de conjugación lineal y ortogonal empuja los centros radicalarios hacia los anillos de tiofeno centrales de la molécula. Para **2DQPT**, las dos secuencias inter-diona existentes se cancelan entre sí. Este hecho, unido al mayor carácter dirradical del pentámero, hace que los centros radicalarios en este caso se sitúen en los grupos dicianometileno de los extremos.

Esta forma se ve altamente favorecida por la aromatización de cinco anillos de tiofeno.

En cuanto a las especies cargadas, la reducción de **2DQTT** da lugar a la formación de un único radical anión, mientras que en el caso de las moléculas **2DQQT** y **2DQPT**, las secuencias *cross*-conjugadas son responsables de la generación de dos tipos de radicales aniones diferentes. Estas especies monovalentes constituyen isómeros electrónicos (o electroisómeros)^[23] pues solo se diferencian en la deslocalización de sus electrones π : a través de la secuencia lineal entre grupos dicianometileno o través de las secuencias *cross*-conjugadas entre grupos carbonilo. Sin embargo, la reducción de estos radicales aniones solo da lugar a especies dianiónicas tipo bipolarón, con independencia de la longitud del oligómero. Esta estructura es estabilizada en las tres moléculas por la ganancia de aromaticidad del esqueleto de oligotiofenos. Además, es posible obtener una tercera especie reducida en la que el tercer electrón inyectado se aloja en una de las secuencias inter-diona *cross*-conjugadas.

Por otra parte, las moléculas de la serie **2DQoT** han sido evaluadas como materiales semiconductores tipo *n*, presentado excelentes valores de conductividad eléctrica y de estabilidad ambiental, especialmente **2DQQT**. Estos resultados están íntimamente relacionados con la combinación del carácter dirradical y de las propiedades de *cross*-conjugación que se produce en estas moléculas. La sinergia entre estos dos fenómenos, que presentan una extensión

diferente para cada molécula, da lugar a un modo de agregación particular para cada sistema. En el caso de **2DQTT** y **2DQPT**, las dos configuraciones extremas (capa cerrada y dirradical), provoca la formación de agregados π - π desplazados y de σ -polimerización, respectivamente. Para **2DQQT**, el incipiente carácter dirradical junto con las propiedades conferidas por la presencia de una única secuencia inter-diona *cross*-conjugada, da lugar a una agregación π - π colestérica o helicoidal. Esta organización presenta las mejores características de estabilidad y conductividad en su aplicación como material semiconductor tipo n.

Puesto que las secuencias *cross*-conjugadas en ambos tipos de oligotiofenos, **OTPD_n** y **2DQoT**, se han manifestado cuando la configuración del estado electrónico fundamental es de capa abierta, en el *Capítulo 3* también se ha realizado un estudio complementario de la *cross*-conjugación en moléculas de capa cerrada. Para ello, se ha estudiado un tetra 4-aminofenil-etileno (**TPE**) policonjugado, junto a sus derivados di-sustituídos lineal (**trans-BPE**) y *cross*-conjugado (**cross-BPE**). Las propiedades de *cross*-conjugación en **TPE** han sido demostradas mediante la aparición de una conductancia bien definida para el isómero de **TPE** bis-protonado en la secuencia *cross*-conjugada, además de la conductancia asignada a los canales lineales. Además, la transmisión a través del canal *cross*-conjugado se ve reforzada por la contribución de una transmisión a través del espacio que aparece solo para este isómero.

La dependencia de la conductancia con

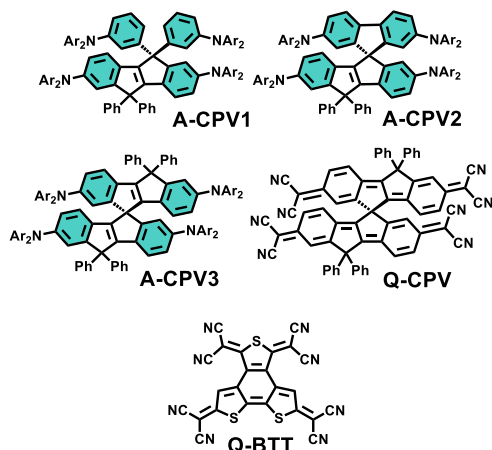
el modo de conjugación, y su control racional, ofrecen la posibilidad de emplear sistemas *cross*-conjugados similares como interruptores ON/OFF en materiales transportadores de carga.

Sección C. Dirradicales *Spiro*-Conjugados

Capítulo 4. El Caso de los Dirradicales Octaciano: π -Conjugación Spiro versus Paralela

En este último bloque se evalúan las interacciones intramoleculares a través del espacio entre densidades π -electrónicas de sistemas linealmente conjugados. Para ello, se han empleado moléculas formadas por dos sistemas π *spiro*-conjugados. En el *Capítulo 4*, se describen las estructuras electrónica y molecular de una familia de fenilenovinilenos rigidificados con puentes de carbono (CPV) *spiro*-conjugados, tanto en su forma neutra como para sus especies cargadas. Dicha serie está constituida por tres sistemas aromáticos (**A-CPV_n**) y por una única molécula quinoide *spiro*-conjugada, **Q-CPV**.

En el caso de la molécula **Q-CPV**, el carácter quinoide se debe a la presencia de dos grupos dicianometileno en cada unidad de CPV (es decir, ocho grupos CN en total). La influencia de estos grupos en la deslocalización de los electrones π también es analizada en un octaciano-benzotritiofeno quinoide (**Q-BTT**), en el cual existen dos secuencias π -conjugadas paralelas entre grupos dicianometileno. A diferencia del *spiro*-conjugado **Q-CPV**, en el sistema **Q-BTT** los dos sistemas lineales



Esquema 4. Estructura química de la serie de fenilenoquinonileno rigidificados con puentes de carbono *spiro*-conjugados (**A-CPV** y **Q-CPV**) y del octaciano-benzotritiofeno quinoide (**Q-BTT**) estudiadas en el Capítulo 4 de Resultados.

están conectados a través de una secuencia *cross*-conjugada descrita entre grupos dicianometileno opuestos (se trata, por tanto, de una interacción a través del enlace).

Para los sistemas neutros, el resultado más relevante es la presencia de características dirradicales en los espectros de absorción electrónica de los dos sistemas octaciano, **Q-CPV** y **Q-BTT**, indicando la elevada contribución de la correspondiente forma de capa abierta a su estructura. La configuración de singlete de su estado fundamental, así como su *gap* singlete-triplete similar, ha sido demostrada mediante cálculos teóricos. La estabilización de la estructura capa abierta en ambas moléculas puede explicarse mediante el efecto sinérgico entre la ganancia de aromaticidad y la relajación de las estructuras tensionadas. En el caso de **Q-BTT** el dirradical se extiende por todo el esqueleto (con una mayor contribución de la forma con los centros radicales sobre la

unidad **BQ** más larga). Esta distribución del dirradical es posible gracias a las secuencias *cross*-conjugadas que conectan ambos cromóforos **MQ** y **BQ**. Por otra parte, la existencia de un estado quintuplete de baja energía en el sistema *spiro*-conjugado quinoide demuestra la alta contribución de una especie tetra-radical capa-abierta. La existencia de dicha especie también se demuestra mediante estudios de EPR.

Precisamente, son esta secuencia *cross*-conjugada en **Q-BTT** y la *spiro*-conjugación en **Q-CPV** los factores responsables del diferente *gap* óptico entre ambos sistemas octaciano. La interacción por *spiro*-conjugación entre los niveles HOMO de los dos cromóforos CPV genera los correspondientes niveles de energía simétrico y antisimétrico en la molécula final **Q-CPV**, por lo que el *gap* HOMO-LUMO se reduce respecto a las unidades CPV individuales. Por el contrario, en el caso de la molécula **Q-BTT**, la deslocalización de la densidad de electrones π sobre la unidad **BQ** más larga se extiende hacia el monotiofeno **MQ** a través de los modos *cross*-conjugados que conectan ambos cromóforos.

Considerando la serie de moléculas *spiro*-conjugadas, a partir del estudio de las propiedades ópticas y electrónicas, así como de los resultados de cálculos químico-cuánticos, se puede establecer el siguiente aumento de la *spiro*-conjugación para las moléculas neutras: **A-CPV1** < **A-CPV2** < **A-CPV3** < **Q-CPV**. La mayor expresión de este fenómeno en el sistema quinoide se debe a la contribución de la especie capa-abierta, en la cual existe una

mayor densidad π -electrónica sobre los átomos que sufren *spiro*-conjugación.

Por otra parte, la oxidación de los sistemas *spiro* aromáticos dan lugar a cationes radicales con estructura tipo polarón en el núcleo CPV para las tres moléculas. Estos cationes radicales se deslocalizan entre los dos grupos diarilamina opuestos, dando lugar a sistemas de valencia mixta de clase III. Dicha deslocalización se manifiesta también en los espectros Raman, en los que los modos de vibración analizados experimentan un desplazamiento hacia menores números de ondas en la oxidación de las moléculas neutras aromáticas.

Sin embargo, la extracción de un segundo electrón de estos radicales cationes tiene lugar en diferentes circunstancias para los tres sistemas aromáticos. En **A-CPV1**, el segundo electrón es extraído del núcleo CPV previamente oxidado, formando un dicatión tipo bipolarón. En el caso de **A-CPV2**, la segunda etapa de la oxidación se desarrolla en la unidad de fluoreno para minimizar los efectos de repulsión de carga. Por otra parte, **A-CPV3** presenta dos tipos de especies dicatiónicas, pero el hecho de que ambos cromóforos *spiro*-conjugados sean iguales (unidades de CPV) hace que no exista una estabilización preferente de ninguna de las dos estructuras, el bipolarón o el par polarónico.

Continuando con el proceso de oxidación, en el tricatión radical dos cargas se encuentran alojadas en la unidad CPV (más larga), mientras que la tercera se

sitúa en el fluoreno en **A-CPV2**, o en la segunda unidad de CPV en **A-CPV3**.

Para **A-CPV1**, el último proceso de oxidación es de carácter bi-electrónico. De esta forma, finalmente se obtiene la especie tetracatión para los tres sistemas aromáticos *spiro*-conjugados. En **A-CPV1** y **A-CPV2** dicha especie está formada por una unidad de fluoreno dicatiónica unida a una unidad CPV también doblemente cargada. Para **A-CPV3**, cada unidad CPV se describe como un dicatión bipolarónico.

La comparación entre las energías de formación de los dicatiónes revela la presencia de interacciones a través del espacio en **A-CPV3**, que empujan la densidad π -electrónica hacia el centro de la molécula. Por tanto, se demuestra la existencia de *spiro*-conjugación efectiva para la estructura de par polarónico del dicatión **A-CPV3**.

Respecto al sistema *spiro*-conjugado quinoide, la reducción de la molécula neutra **Q-CPV** da lugar a la formación de un radical anión, como en el caso de su análogo aromático. La posterior reducción de esta especie evoluciona a un dianión tipo par polarónico. La inyección de un tercer electrón da lugar a una única especie de trianión radical, en el que una unidad CPV *aromatizada* posee dos electrones *extra* en los grupos dicianometilenos, mientras que en la otra existe una carga negativa deslocalizada sobre el esqueleto de carbono. Finalmente, un cuarto electrón es alojado en esta segunda unidad de CPV.

La presencia de una secuencia *cross*-conjugada en el sistema **Q-BTT** introduce diferencias significativas en el proceso de

reducción con respecto al sistema **Q-CPV**. En este caso, la aromatización del anillo de benceno central dirige la formación del dianión segregado en un proceso de inyección de dos electrones. Una segunda reducción de dos electrones da lugar al tetra-anión de la molécula **Q-BTT**, en la que cada carga negativa se encuentra en un grupo dicianometileno, de forma similar a la especie equivalente de la molécula **Q-CPV**.

En el caso del polarón segregado de la especie dianiónica de **Q-CPV**, puesto que las densidades π de las dos unidades CPV están desconectadas por la presencia del átomo de carbono tetraédrico en ambas moléculas, la única posibilidad de establecer una conexión *química* entre los centros radicales, y asegurar el carácter singlete del estado fundamental, es mediante una interacción a través del espacio. De esta forma la *spiro*-conjugación se manifiesta en el dianión **Q-CPV** debido a la aromatización de su estructura, que aumenta la densidad π -electrónica sobre los átomos de carbono unidos al puente tetraédrico. Nótese que en el dicatión segregado de la molécula **ACPV-3** (cuyo estado fundamental es triplete), la formación de esta especie deslocalizada provoca la *quinoidización* de la estructura aromática, por lo que se produce una retirada de densidad π de los átomos capaces de experimentar *spiro*-conjugación. Los procesos de aromatización /quinoidización descritos para estas moléculas han sido observados en el desplazamiento de las bandas Raman de las correspondientes especies cargadas.

En el caso del dianión tipo par polarónico de **Q-BTT**, la secuencia *cross*-

conjugada proporciona el marco adecuado para la activación del mecanismo de DSP, confiriendo la configuración de singlete al estado electrónico fundamental. Los estudios de absorción del estado excitado, realizados mediante absorción electrónica UV-Vis-NIR de especies transitorias y espectroscopía IR resuelta en el tiempo, apoyan la presencia de un modo de *cross*-conjugación efectivo entre las dos unidades **MQ** y **BQ** de la molécula **Q-BTT**.

Observaciones Finales

En esta sección final se intenta proporcionar una visión general de la alteración de la π -conjugación lineal cuando coexiste con diferentes secuencias de deslocalización π alternativas en un mismo sistema.

Alteración de la Conjugación π Lineal mediante la Presencia de Secuencias Cross-Conjugadas

La extensión en 2D de la densidad de electrones π en los sistemas *cross*-conjugados estudiados ha sido demostrada y atribuida a la competencia establecida entre las secuencias de conjugación lineal y ortogonal. El peso relativo del modo *cross*-conjugado se ve incrementado cuando existe una apreciable contribución dirradical, debido al carácter aceptor de electrones de los grupos carbonilo que forman dicha secuencia.

De forma general, la presencia de una secuencia *cross*-conjugada provoca el

confinamiento de la densidad π -electrónica (o de los centros radicalarios) en la parte central de la molécula. Este efecto puede evitarse de dos formas: i) mediante la presencia en el esqueleto lineal de grupos con un mayor carácter aceptor en moléculas pequeñas (como es el caso del sistema **2DQTT**); y ii) estabilizando la estructura π -conjugada lineal, por ejemplo, mediante la ganancia de aromaticidad (éste es el caso de la molécula dirradical **2DQPT**).

Para las especies cargadas, el carácter dirradical de las moléculas quinoideas da lugar a dos comportamientos diferentes. Por una parte, en las moléculas **OTPD_n** aromáticas se obtienen, en una primera etapa, radicales aniones con estructuras clásicas de polarones, mientras que en el caso de las moléculas quinoideas **2DQQT** y **2DQPT** se obtienen dos tipos de radicales aniones en función de su deslocalización (electrómeros): en el oligotiofeno lineal o en la secuencia inter-diona *cross*-conjugada.

En una segunda etapa de reducción, las especies dianiónicas presentan el comportamiento inverso. Mientras que los dianiones de los sistemas **2DQoT** son de tipo bipolarón (capa cerrada), las moléculas más largas de la familia aromática exhiben una estructura de polarones segregados (capa abierta), en la que los dos radicales aniones se encuentran en dos secuencias inter-diona. Además, en las moléculas **2DQoT**, la presencia de los fragmentos inter-diona permite una tercera etapa de reducción, en la que una de las cargas del trianion radical se acomoda en una secuencia

ortogonal.

En el caso de las estructuras de capa abierta, el mecanismo de DSP se activa mediante la doble conjugación de los electrones π del puente de oligotiofeno. Sin embargo, este fenómeno se ve comprometido al introducir secuencias *cross*-conjugadas adicionales entre aquellas en las que se encuentran situados los centros radicales. De esta forma, la presencia y número de secuencias *cross*-conjugadas en este tipo de sistemas puede modular el *gap* singlete-triplete.

Alteración de la Conjugación π Lineal mediante la Presencia de Interacciones de Spiro-Conjugación

En las especies neutras de los sistemas estudiados, la *spiro*-conjugación se manifiesta en la molécula quinoide **Q-CPV** debido a su configuración capa abierta. La aromatización de las unidades CPV en la formación de la especie dirradical provoca un aumento de la densidad π -electrónica en los átomos de carbono capaces de experimentar *spiro*-conjugación. Del mismo modo ocurre para la especie dianiónica tipo par polarónico de esta molécula.

El dianión segregado de la molécula **Q-CPV** presenta también interacciones de tipo *spiro*, por las mismas razones que la especie neutra dirradical. Al contrario que en los sistemas **2DQoT**, en los que la aromatización de la estructura en las especies dianiónicas anula las propiedades de *cross*-conjugación, en **Q-CPV** es precisamente la forma aromática del dianión la que incrementa la efectividad de

la *spiro*-conjugación. Esta interacción a través del espacio se manifiesta mediante la activación del mecanismo de DSP, que da lugar a un dianión singlete capa abierta.

En el dianión **Q-BTT** la *cross*-conjugación también influye de forma inversa a la observada en la familia **OTPD_n**. Mientras que en la familia de oligotiofenos aromáticos la presencia de varios fragmentos *cross*-conjugados disminuye el efecto del mecanismo de DSP, en el sistema **Q-BTT** es la secuencia *cross*-conjugada entre los dos cromóforos la que permite la activación de dicho fenómeno.

En este escenario, se puede concluir que en sistemas policonjugados dirradicaloides, la activación/desactivación del mecanismo de DSP debe ser examinada atendiendo al modo y disposición de la secuencia de π -conjugación alternativa existente. En oligómeros linealmente π -conjugados cruzados por una secuencia π ortogonal, la propiedad de *cross*-conjugación interrumpe la doble conjugación a través del puente. Sin embargo, cuando la secuencia *cross*-conjugada conecta dos sistemas π lineales paralelos, es precisamente su presencia la que promueve el fenómeno de DSP. Finalmente, en el caso de sistemas *spiro*-conjugados, una mayor extensión de la interacción espacial tipo *spiro* favorece el mecanismo de DSP y, por tanto, la configuración singlete del dirradical, siempre que ambos centros se encuentren en unidades *spiro*-conjugadas diferentes, como es el caso del dianión segregado de **Q-CPV**.

Referencias

- [1] *Organic Semiconductors for Solution-Processable Field-Effect Transistors (OFETs)*, S. Allard, M. Forster, B. Souharce, H. Thiem, and U. Scherf, *Angew. Chem. Int. Ed.*, **2008**, *47*, 4070–4098.
- [2] *Handbook of Thiophene-Based Materials*, I. F. Perepichka and D. F. Perepichka, Eds.; John Wiley & Sons, LTd: United Kingdom, **2009**.
- [3] *Organic Photovoltaics*, S. Shaik, B. Kippelen and J. L. Brédas, *Energy Environ. Sci.*, **2009**, *2*, 251–261.
- [4] *Organic Optoelectronic Materials: Mechanisms and Applications*, O. Ostroverkhova, *Chem. Rev.*, **2016**, *116*, 13279–13412.
- [5] *Effective Conjugation Length and UV/Vis Spectra of Oligomers*, H. Meier, U. Stalmach and H. Kolshorn, *Acta Polymer.*, **1997**, *48*, 379–384.
- [6] *Conjugation Oligomers with Terminal Donor-Acceptor Substitution*, H. Meier, *Angew. Chem. Int. Ed.*, **2005**, *44*, 2482–2506.
- [7] *Electronic Materials: The Oligomer Approach*, M. Bürkle, K. Müllen and G. Wegner, Eds.; John Wiley & Sons, LTd: United Kingdom, **2008**.
- [8] *Cross-Conjugation*, P. A. Limacher and H. P. Luthi, *Comput Mol Sci.*, **2011**, *1*, 477–486.
- [9] *IUPAC. Compendium of Chemical Terminology, 2nd ed. (the "Gold Book")*. Compiled by A. D. McNaught and A. Wilkinson. Blackwell Scientific Publications, Oxford (**1997**). Online version

(2019-) created by S. J. Chalk. ISBN 0-9678550-9-8.

<https://doi.org/10.1351/goldbook>.

[10] *Homoconjugation and Homoaromaticity. IV. The Trishomocyclopropenyl Cation. A Homoaromatic Structure*, S. Winstein and J. Sonnenberg, *J. Am. Chem. Soc.*, **1961**, *83*, 3244–3251.

[11] *Aromaticity and Other Conjugation Effects*, R. Gleiter and G. Haberhauer, Wiley-VCH, Weinheim: Germany, **2012**.

[12] *Spiroconjugation*, H. E. Simmons and T. Fukunaga, *J. Am. Chem. Soc.*, **1967**, *89*, 5208–5215.

[13] *The Spirarenes*, R. Hoffmann, A. Imamura and G. D. Zeiss, *J. Am. Chem. Soc.*, **1967**, *89*, 5215–5220.

[14] *Quinoidal/Aromatic Transformation in π -Conjugated Oligomers: Vibrational Raman Studies on the Limit of Rupture of π -Bonds*, P. Mayorga Burrezo, J. L. Zafra, J. T. López Navarrete and J. Casado, *Angew. Chem. Int. Ed.*, **2017**, *56*, 2250–2259.

[15] *Diradicals*, M. Abe, *Chem. Rev.*, **2013**, *113*, 7011–7088.

[16] *The Double (or Dynamic) Spin Polarization in π -Diradicals*, P. Karafiloglou, *J. Chem. Educ.*, **1989**, *66*, 816–818.

[17] *Para-Quinodimethanes: A Unified Review of the Quinoidal-Versus-Aromatic Competition and its Implications*, J. Casado, *Top Curr Chem (Z)*, **2017**, *375*, doi:10.1007/s41061-017-0163-2.

[18] *Dirradicales: Moléculas “Rotas”*, J. Casado, *An. Quím.*, **2019**, *115*, 371–380.

[19] *Biradicaloid and Polyenic Character of Quinoidal Oligothiophenes Revealed by the Presence of a Low-Lying Double-Exciton State*, S. Di Motta, F. Negri, D. Fazzi, C. Castiglioni, and E. Valeria Caneis, *J. Phys. Chem. Lett.*, **2010**, *1*, 3334–3339.

[20] *The Energy Barrier in Singlet Fission Can Be Overcome Through Coherent Coupling and Entropic Gain*, W. Chan, M. Ligges and X. Zhu, *Nature Chem.*, **2012**, *4*, 840–845.

[21] *Raman Spectroscopy of Polyconjugated Molecules and Materials: Confinement Effect in One and Two Dimensions*, C. Castiglioni, M. Tommasini and G. Zerbi, *Phil. Trans. R. Soc. Lond. A*, **2004**, *362*, 2425–2459.

[22] *Raman Spectra of trans- and cis-Polyacetylenes Excited with Nd:Yag Laser 1064- and 532-nm Pulses*, M. Tasumi, H. Yoshida, M. Fujiwara, H. Hamaguchi and H. Shirakawa, *Synth. Met.*, **1987**, *17*, 319–324.

[23] *Isomerism: The Same but Different*, T. Bally, *Nat. Chem.*, **2010**, *2*, 165–166.

VII. APPENDICES

APPENDIX VII.I. ACRONYMS

| | |
|--|--|
| (U) | Unrestricted |
| 2D | Two dimensions (used for the π -electron delocalization) |
| 2Me-THF | 2-MethylTetrahydroFuran |
| 3D | Three dimensions (used for the π -electron delocalization) |
| BLA | Bond Length Alternation |
| CPV | Carbon-bridged PhenyleneVinylene |
| CS | Closed Shell |
| CT | Charge Transfer |
| DFT | Density Functional Theory |
| DSP | Double Spin Polarization |
| ECC | Effective Conjugation Coordinate |
| E_g | Optical band gap |
| EPR/ESR | Electron Paramagnetic/Spin Resonance |
| ESA | Excited State Absorption |
| Flu | Fluorene |
| FMOs | Frontier Molecular Orbitals |
| HOMO | Highest Occupied Molecular Orbital |
| IR | Infrared |
| IVCT | Intervalence Charge Transfer |
| LUMO | Lowes Unoccupied Molecular Orbital |
| MO | Molecular Orbital |
| NBMO | Non Bonding Molecular Orbital |
| NIR | Near Infrared |
| OS | Open Shell |
| QM1CN | Quinoidal tetracyano carbon-bridged phenylenevinylene |
| SOMO | Singly Occupied Molecular Orbital |
| TA | Transient Absorption |
| TbT | Thieno[3,4-b]thiophene |
| TCNQ | Tetracyanoquinodimethane |
| TMTQ | Oligomer composed of a central 1,6-methano[10]annulene and 5-dicyanomethyl-thiophene peripheries |
| TPD | Thieno[3,4-c]Pyrrole-4,6-Dione |
| TR | Time Resolved |
| UV | Ultraviolet |
| VBT | Valence Bond Theory |
| Vis | Visible |
| ΔE_{S-T} | Singlet-triplet gap |
| λ_{exc} | Excitation wavelength (usually referred to Raman Spectroscopy) |
| λ_{max} wavelength | Absorption maxima wavelength |
| Ψ | Wavefunction |

APPENDIX VII.II. KEYWORDS

Definitions of the following keywords have been extracted from the bibliography referenced in the corresponding chapters, or from the IUPAC Gold Book Website (<https://goldbook.iupac.org/>).

| | |
|---|---|
| Homoconjugation | π -electrons interaction between p orbitals separated by an insulating atom. |
| Spiroconjugation | Kind of homoconjugation where the two interacting π -systems are in perpendicular planes with a common atom of tetrahedral geometry. |
| Cross-Conjugation | π -conjugation phenomenon in which two conjugation paths share a multiple bond (or in which three unsaturated groups, two of which although conjugated to a third unsaturated centre, are not conjugated to each other). |
| Linear π-Conjugation | Carbonated chains with an alternating simple and double bond CC pattern in which π -electrons are delocalized over the sp^2 framework formed by the C—C σ -bonds. |
| Parallel Conjugation | π -conjugation phenomenon in which two linearly conjugated units are linked. |
| Effective Conjugation Length | Number of repetitive monomeric units at which the optical properties converge. The effective conjugation length (n_{ECL}) is defined as the oligomer length at which the wavelength of the absorption maxima is equal or less than 1 nm larger than the one of the previous oligomer. |
| π-Electron Delocalization | Concept employed to describe a π -bond in a conjugated system, which is not localized between two atoms, instead, each link has a “fractional double bond character” or bond order. |
| Diradical | Molecular specie having two unpaired electrons, in which at least two different electronic states with different multiplicities [anti-parallel spins (singlet state) or parallel spins (triplet state)] can be identified. Despite in the literature the term Biradical is used as synonym of Diradical , the first |

one refers to species with two unpaired electrons which electron exchange interaction is negligible, *i. e.*, the two radical centres act nearly independently of each other.

Open-Shell Systems

Atomic or molecular systems in which the electrons are not completely assigned to orbitals in pairs.

Closed-Shell Systems

Even-electron atomic or molecular systems whose electron configurations consist of doubly occupied orbitals.

Double Spin Polarization (DSP) Mechanism

Phenomenon that accounts for the stabilization of the singlet electronic state respect to the triplet one (that does not change its energy) in open-shell systems, violating the Hund's rule. According to the DSP mechanism, π -electrons of the bridge can be delocalized towards the NBMO twice in the singlet open-shell configuration, while only once for the triplet species due to their parallel spins.

Kekulé Diradicals

Diradical systems that can be described by several resonant structures, one of them with a closed-shell configuration.

Non-Kekulé Diradicals

Diradical systems that are fully conjugated, but each of whose Kekulé structures contains at least two atoms that are not π -bonded.

Polyconjugated Systems

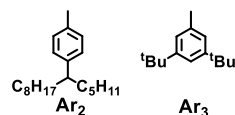
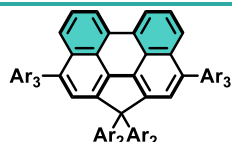
π -conjugated systems in which more than one π -electron delocalization framework is available.

APPENDIX VII.III. CHEMICAL STRUCTURES AND IUPAC NOMENCLATURE

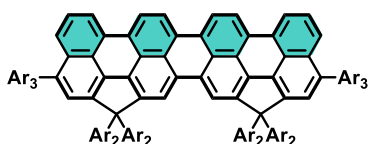
Section A. Linearly π -Conjugated Diradicals

Chapter 1. The Case of Aromatic and Quinoidal Oligorylenes.

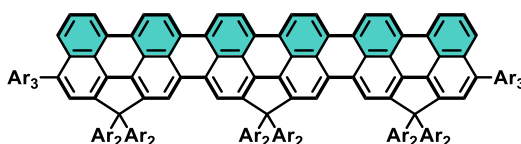
CP-nR Series



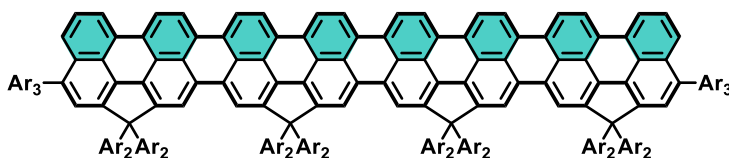
CP-Per: 3,10-bis(3,5-di-*tert*-butylphenyl)-1,1-bis(4-(tetradecan-6-yl)phenyl)-1*H*-cyclopenta[ghi]perylene



CP-QR: quaterrylene derivative



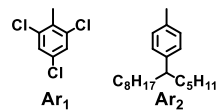
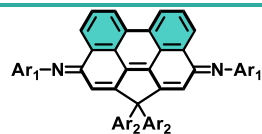
CP-HR: hexarylene derivative



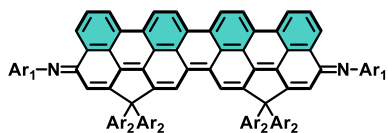
CP-OR: octarylene derivative

The abbreviated name **CP-nR** of this family corresponds to the acronym of **Cy**clo**P**enta-**n**-**R**ylene, with *n* being the number of perylene units.

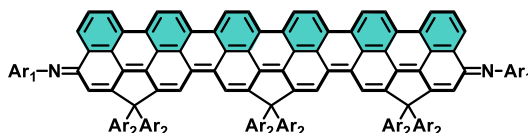
nR-2N Series



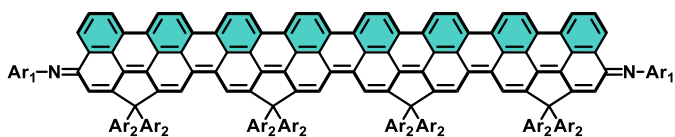
Per-2N: (3*Z*,10*E*)-1,1-bis(4-(tetradecan-6-yl)phenyl)-*N*³,*N*¹⁰-bis(2,4,6-trichlorophenyl)-1*H*-cyclopenta[ghi]perylene-3,10-diimine



QR-2N: quaterrylene bis(imine) derivative



HR-2N: hexarylene bis(imine) derivative



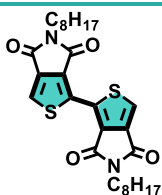
OR-2N: octaylene bis(imine) derivative

The abbreviated name of this series refers to the number of perylene units (**nR**) and the end-capping imine groups (**2N**).

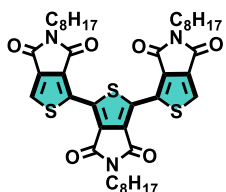
Section B. Cross-Conjugated Diradicals

Chapter 2. The Case of Aromatic Oligothienopyrrolediones: Cross-Conjugated Dianions.

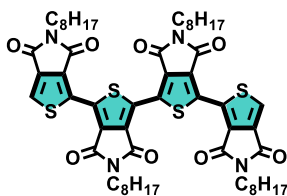
OTPD_n Series



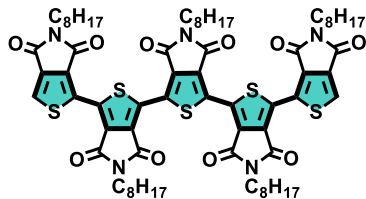
OTPD₂: 5,5'-dioctyl-4*H*,4'*H*-[1,1'-bithieno[3,4-*c*]pyrrole]-4,4',6,6'(5*H*,5'*H*)-tetraone



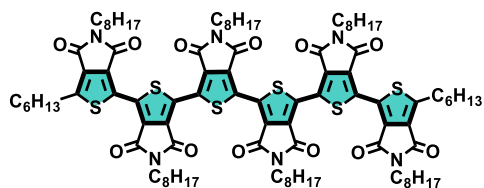
OTPD₃: 5,5',5''-trioctyl-4*H*,4'*H*,4''*H*-[1,1':3',1''-terthieno[3,4-*c*]pyrrole]-4,4',4'',6,6',6''(5*H*,5'*H*,5''*H*)-hexaone



OTPD₄: 5,5',5'',5'''-tetraoctyl-4*H*,4'*H*,4''*H*,4'''*H*-[1,1':3',1''':3'',1''''-quaterthieno[3,4-*c*]pyrrol]-4,4',4'',4''',6,6',6''(5*H*,5'*H*,5''*H*,5'''*H*)-octaone



OTPD₅: 5,5',5'',5''',5''''-pentaoctyl-4*H*,4'*H*,4''*H*,4'''*H*,4''''*H*-[1,1':3',1''':3'',1''''':3''''',1''''''-quinquethieno[3,4-*c*]pyrrole]-4,4',4'',4''',4''''(5*H*,5'*H*,5''*H*,5'''*H*,5''''*H*)-decaone

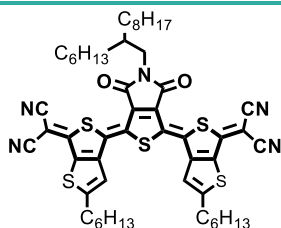


OTPD₆: 5,5',5'',5''',5''''-hexaoctyl-4*H*,4'*H*,4''*H*,4'''*H*,4''''*H*,4'''''*H*-[1,1':3',1'':3'',1''':3''',1''''':3''''',1''''':3''''',1''''''-sexithieno[3,4-*c*]pyrrole]-4,4',4'',4''',4''''',4''''''',6,6',6'',6''',6''''',6''''''(5*H*,5'*H*,5''*H*,5'''*H*,5''''*H*,5'''''*H*)-dodecaone

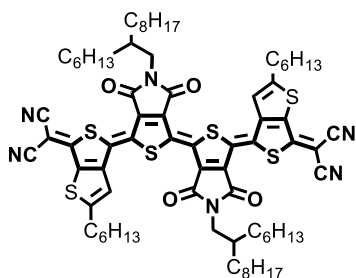
The abbreviated name **OTPD_n** of this family corresponds to the acronym of **OligoThienoPirroleDione**, with *n* being the number of thienopyrroledione units.

Chapter 3. The Case of Quinoidal Oligothienopyrrolediones: The Effect of Size.

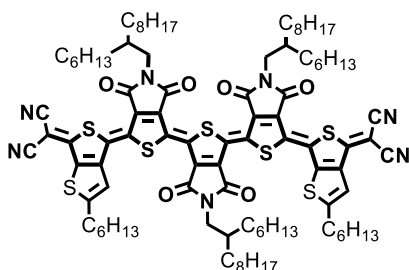
2DQoT Series



2DQTT: 2,2'-((4*E*,4'*E*)-(5-(2-hexyldecyl)-4,6-dioxo-5,6-dihydro-1*H*-thieno[3,4-*c*]pyrrole-1,3(4*H*)-diylidene)bis(2-hexylthieno[3,4-*b*]thiophene-4,6(4*H*)-diylidene))dimalononitrile



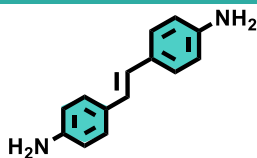
2DQQT: 2,2'-((4*E*,4'*E*)-((*Z*)-5,5'-bis(2-hexyldecyl)-4,4',6,6'-tetraoxo-5,5',6,6'-tetrahydro-[1,1'-bithieno[3,4-*c*]pyrrolylidene]-3,3'(4*H*,4'*H*)-diylidene)bis(2-hexylthieno[3,4-*b*]thiophene-4,6(4*H*)-diylidene))dimalononitrile



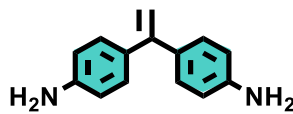
2DQPT: 2,2'-((4*E*,4'*E*)-((1*Z*,1''*Z*)-5,5',5''-tris(2-hexyldecyl)-4,4',4'',6,6',6''-hexaaxo-5,5',5'',6,6',6''-hexahydro-4'*H*-[1,1':3',1''-terthieno[3,4-*c*]pyrrole]-3,3''(4*H*,4''*H*)-diylidene)bis(2-hexylthieno[3,4-*b*]thiophene-4,6(4*H*)-diylidene))dimalononitrile

The abbreviated name of this series refers to the **2-Dimension** extension of π -conjugation in the **Quinoidal oligoThiophene** system (**2DQoT**).

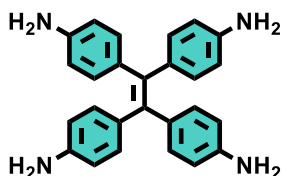
nPE Series



trans-BPE: 1,2 bis(4,4'-aminophenyl)-
trans-ethene



cross-BPE: 1,1 bis(4,4'-aminophenyl)-
ethene



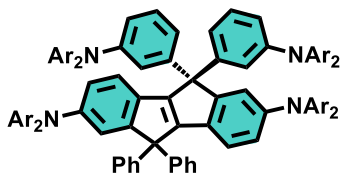
TPE: 1,1,2,2-tetrakis(4-aminophenyl)ethene

The abbreviated names of these molecules correspond to the acronyms of BisPhenylene-substituted Ethene (**BPE**) and TetraPhenylene-substituted Ethene (**TPE**).

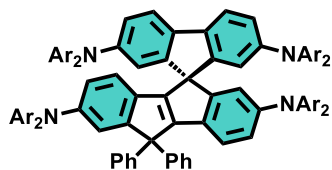
Section C. Spiro-Conjugated Diradicals

Chapter 4. The Case of Octacyano Diradicals: Spiro versus Parallel π -Conjugation

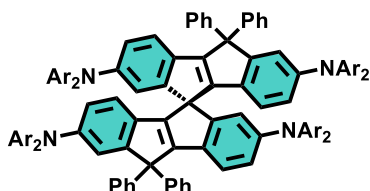
Spiro-CPV Series



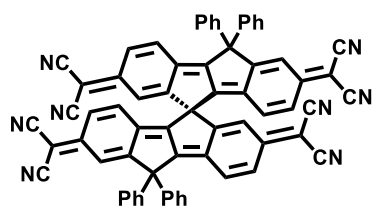
A-CPV1: 5,5-bis(3-(bis(4-methoxyphenyl)amino)phenyl)- N^2,N^2,N^7,N^7 -tetrakis(4-methoxyphenyl)-10,10-diphenyl-5,10-dihydroindeno[2,1-a]indene-2,7-diamine



A-CPV2: (*S*)- $N^2,N^2,N^2',N^2',N^5,N^5,N^7',N^7'$ -octakis(4-methoxyphenyl)-10',10'-diphenyl-10'*H*-spiro[fluorene-9,5'-indeno[2,1-a]indene]-2,2',5,7'-tetraamine

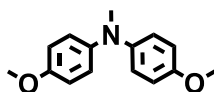


A-CPV3: (*R*)- $N^2,N^2,N^2',N^2',N^7,N^7,N^7',N^7'$ -octakis(4-methoxyphenyl)-10,10,10',10'-tetraphenyl-10*H*,10'*H*-5,5'-spirobi[indeno[2,1-a]indene]-2,2',7,7'-tetraamine



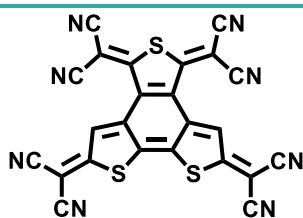
Q-CPV: (*R*)-2,2',2'',2'''-(10,10,10',10'-tetraphenyl-2*H*,2'*H*-5,5'-spirobi[indeno[2,1-*a*]inden]-2,2',7,7'(10*H*,10'*H*)-tetraylidene)tetramalononitrile

Ar:



The abbreviated name the spiro-CPV molecules corresponds to the acronym of Carbon-bridged *para*-PhenyleneVinylene, with **A** referring to the Aromatic systems and **Q** to the Quinoidal octacyano molecule.

Parallel Quinoidal System



Q-BTT: 2,2',2'',2'''-(benzo[1,2-*b*:6,5-*b*':3,4-*c*']trithiophene-2,4,6,8-tetraylidene)tetramalononitrile

The abbreviated name **Q-BTT** is the acronym of Quinoidal BenzoTriThiophene.

APPENDIX VII.IV. GROUND ELECTRONIC STATE OPTIMIZED GEOMETRIES

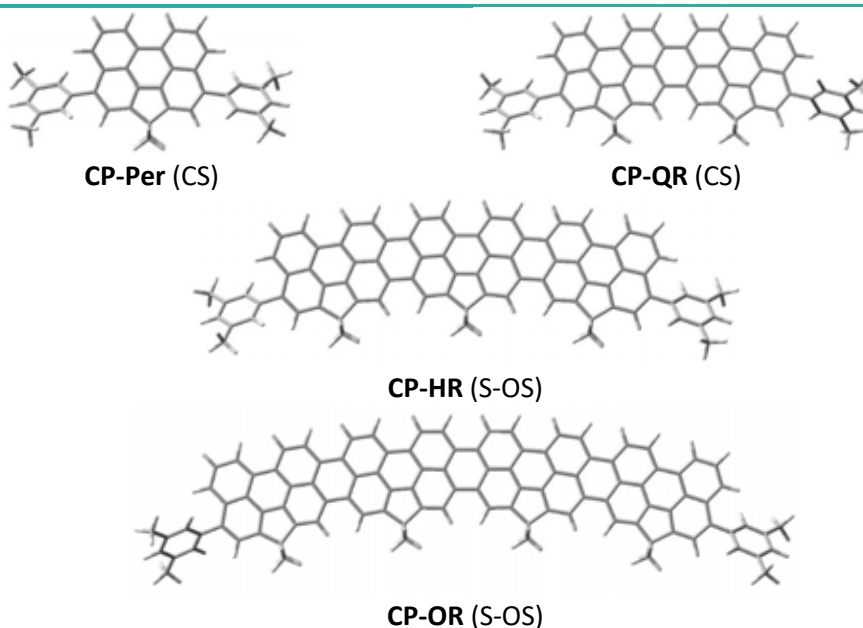
DFT calculations in the present Ph.D. Thesis were performed with the Gaussian16 suite of programs. Molecular geometry optimizations were performed with the B3LYP functional and the 6-31G** standard basis set. The Broken-Symmetry approximation in the unrestricted DFT methodology (BS-UDFT) was employed for the theoretical study of the energies and geometries of open-shell systems. In these cases, 6-31G** basis set was also used (level of theory denoted as $(U)B3LYP/6-31G^{**}$) due to the good results described in bibliography and in order to perform a consistent comparison with the closed-shell systems.

Energy optimizations were performed by allowing all geometric parameters to vary independently. The optimum energy structures were found to be a true minimum in the ground state potential energy surface. Generally, substituent hydrocarbon chains or aryl groups are replaced by methyl units to reduce computational costs.

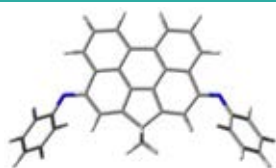
Section A. Linearly π -Conjugated Diradicals

Chapter 1. The Case of Aromatic and Quinoidal Oligorylenes.

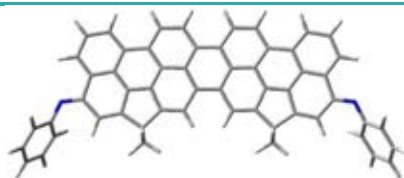
CP-nR Series



nR-2N Series



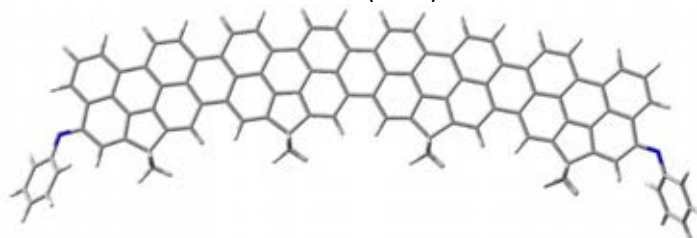
Per-2N (CS)



QR-2N (CS)



HR-2N (S-OS)

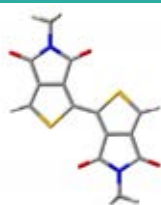


OR-2N (S-OS)

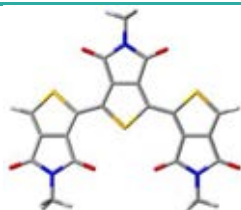
Section B. Cross-Conjugated Diradicals

Chapter 2. The Case of Aromatic Oligothienopyrrolediones: Cross-Conjugated Dianions.

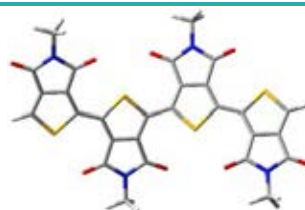
OTPD_n Series



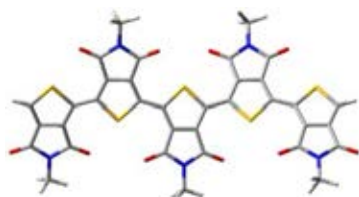
OTPD₂ (CS)



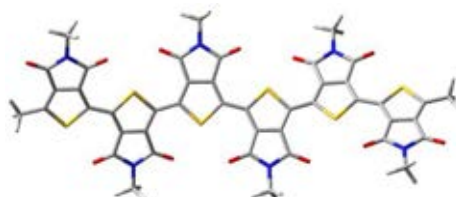
OTPD₃ (CS)



OTPD₄ (CS)



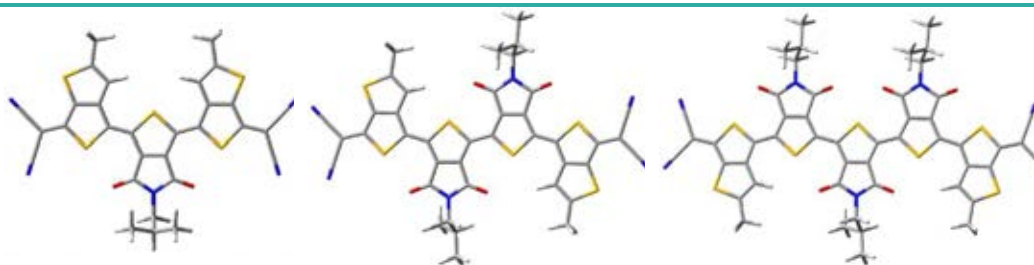
OTPD₅ (CS)



OTPD₆ (CS)

Chapter 3. The Case of Quinoidal Oligothiopyrrolediones: The Effect of Size.

2DQoT Series

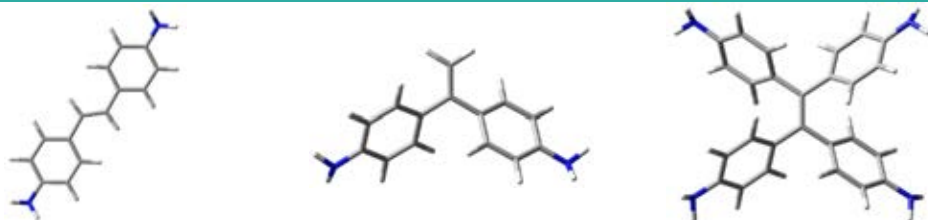


2DQTT (CS)

2DQQT (S-OS)

2DQPT (S-OS)

nPE Series

*trans*-BPE*Cross*-BPE

TPE

Section C. Spiro-Conjugated Diradicals

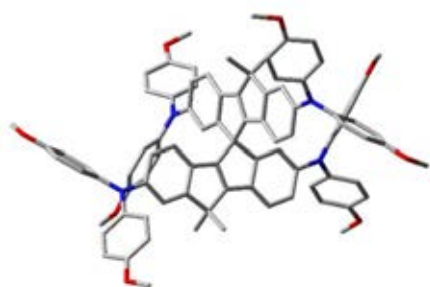
Chapter 4. The Case of Octacyano Diradicals: Spiro versus Parallel π -Conjugation.

Spiro-CPV Series

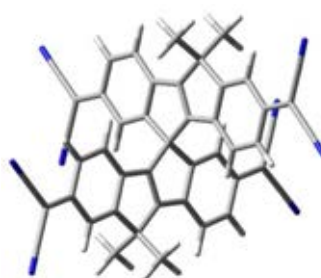


A-CPV1 (CS)

A-CPV2 (CS)



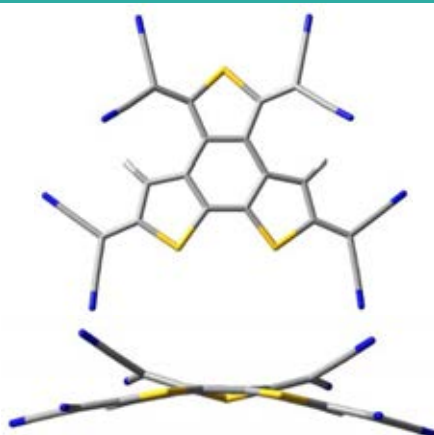
A-CPV3 (CS)



Q-CPV (S-OS)

In aromatic molecules hydrogen atoms have been omitted for clarity.

Parallel Quinoidal System



Q-BTT (S-OS)

Observe that **MQ** and **BQ** moieties forming **Q-BTT** molecule are not in the same plane. This distortion is imposed by the steric crowding between the dicyanomethylene groups of the two subunits. As a consequence, the double bonds connecting the dicyanomethylene groups to the thiophenes are weakened, favouring the incipient diradical character of the **Q-BTT** system.

APPENDIX VII.V. ELECTRON PARAMAGNETIC RESONANCE (EPR) SPECTRA

Section A. Linearly π -Conjugated Diradicals.

Chapter 1. The Case of Aromatic and Quinoidal Oligorylenes.

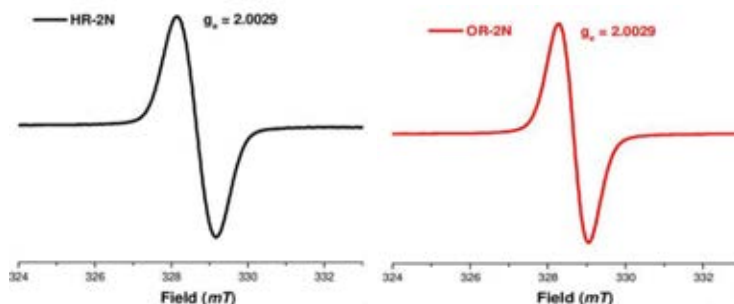


Figure VII.V.1. EPR spectra of **HR-2N** (left) and **OR-2N** (right) quinoidal oligorylenes in solid state at room temperature.

EPR measurements of **nR-2N** quinoidal oligorylenes were performed by the group of Professor Jishan Wu from the *National University of Singapore* (Singapore). The thermally populated low-lying triplet states at room temperature of these molecules demonstrate the contribution of an open-shell configuration to their ground electronic states.

Section B. Cross-Conjugated Diradicals.

Chapter 2. The Case of Aromatic Oligothienopyrrolediones: Cross-Conjugated Dianions.

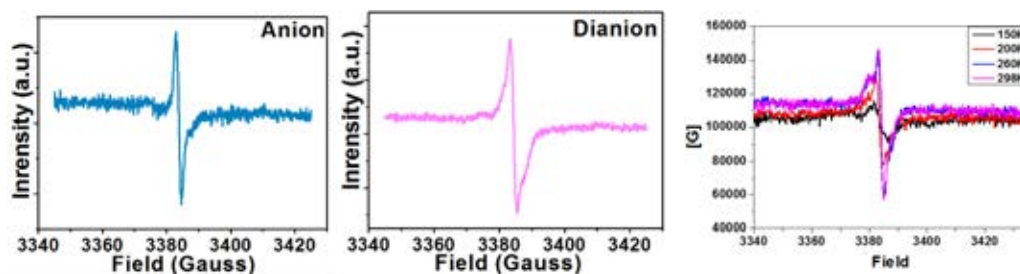


Figure VII.V.2. Left) EPR spectra of radical anion (blue line) and dianion (pink line) species of **OTPD₅** in tetrahydrofuran at room temperature; Right) EPR spectra of **OTPD₅** dianion in tetrahydrofuran with increasing temperature.

EPR measurements of **OTPD_n** and **2DQoT** oligothiophene series were performed by the group of Professor Xiaozhang Zhu from the *Chinese Academy of Science* (Beijing, China).

Chemical reduction of **OTPD₅** was performed using lithium naphthalide as reductant and monitored through UV-Vis electronic absorption. UV-Vis absorption spectra from the chemical reduction are consistent with those obtained electrochemically.

EPR signal of **OTPD₅** dianion suggests the formation of an open shell specie. EPR measurements of dianion with increasing temperature are conducted from 150 K to 298 K observing that the intensity of EPR signal also increased in parallel, which is consistent with the thermal population of the low energy lying triplet for **OTPD₅** dianion.

Chapter 3. The Case of Quinoidal Oligothiopyrrolediones: The Effect of Size.

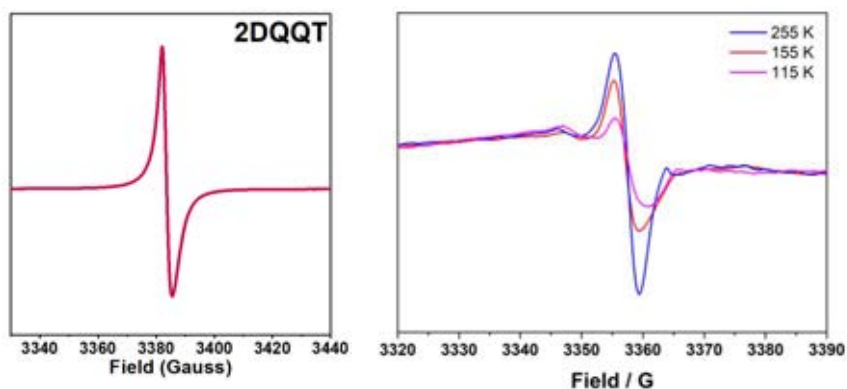


Figure VII.V.3. Left) EPR spectrum of **2DQQT** in solid state; Right) EPR spectra of **2DQQT** in tetrahydrofuran at different temperatures.

EPR behaviour of neutral **2QQT** is indicative of its incipient diradical character. EPR spectra of pristine and doped **2DqoT** films are showed and discussed in *Chapter 3*.

Section C. Spiro-Conjugated Diradicals.

Chapter 4. The Case of Octacyano Diradicals: Spiro versus Parallel π -Conjugation.

EPR measurements of **Q-BTT** molecule were performed in the *Instituto de Ciencia de los Materiales de Barcelona (ICMAB-CSIC, Barcelona, España)*, in the group of Professor Jaume Veciana and supervised and guided by Dr. Vega Lloveras, who also

performed the simulated spectra. Reduction of **Q-BTT** was carried out electrochemically at concentrations of 10^{-6} M solutions in 0.1M of tetrabutylammonium-hexafluorophosphate ($\text{Bu}_4\text{N-PF}_6$) in fresh, distilled CH_2Cl_2 . The reduction process was monitored through UV-Vis-NIR electronic absorption.

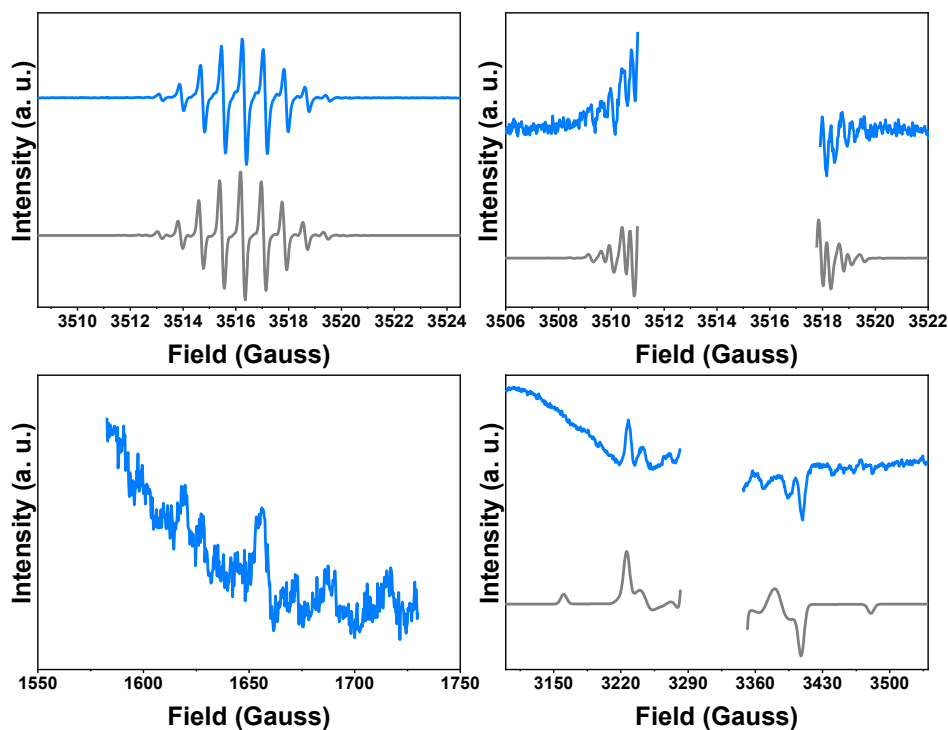


Figure VII.V.4. EPR spectra of **Q-BTT** dianion obtained electrochemically in CH_2Cl_2 at room temperature (*top, left*) and the zoom of the corresponding dipolar fine structure (*top, right*), together with the half-field signal (*bottom, left*) and the dipolar fine structure (*bottom, right*) observed at 120 K in frozen solution. Experimental spectra are in blue while the corresponding simulations are in grey.

First electrochemically reduced species of **Q-BTT** generates an EPR spectrum of 9 main lines due to the coupling of the unpaired electrons with four nitrogen nuclei, consistent with the formation of the proposed segregated dianion. The triplet nature of this spectrum was corroborated by the detection of the half-field signal in the frozen solution. The dipolar coupling of the unpaired electrons with the sulphur nuclei was also observed at both temperatures, reinforcing the proposed mechanism for the transient spectroscopy studies. The simulated spectra corroborate these results.

Further reduction of **Q-BTT** dianion did not produce any other EPR activity.

APPENDIX VII.VI. UV-Vis-NIR SPECTROELECTROCHEMICAL PROCESSES

Section B. Cross-Conjugated Diradicals

Chapter 2. The Case of Aromatic Oligothiopyrrolediones: Cross-Conjugated Dianions.

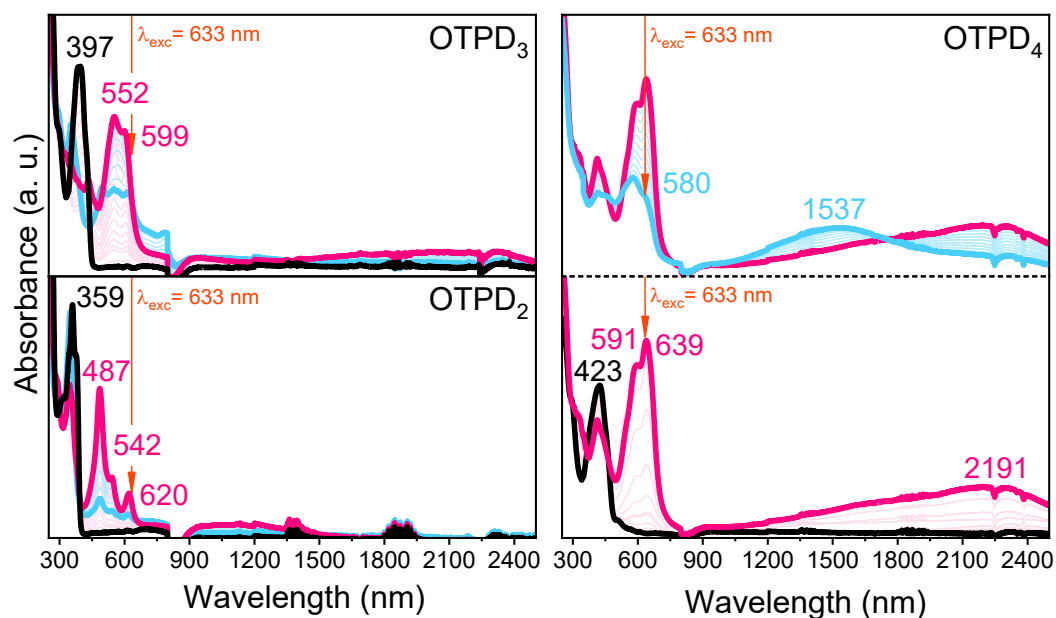
OTPD_n Series

Figure VII.VI.1. UV-Vis-NIR spectroelectrochemical reduction of **OTPD₂**, **OTPD₃** and **OTPD₄** oligomers in Bu₄N-PF₆ 0.1M in CH₂Cl₂ at room temperature. Black lines correspond to the spectra of neutral molecules; pink lines correspond to the completely formed radical anion species; blue lines correspond to the completely formed dianion species (only for **OTPD₄**). Light colour lines correspond to the intermediate spectra between the former species in the reduction process.

For **OTPD_n** molecules, electrochemical reduction of the neutral species produces polaronic radical anions. For the longest oligomers (**OTPD₄**, **OTPD₅** and **OTPD₆**), further reduction of the radical anions gives rise to a two-bands pattern in the UV-Vis-NIR spectra, typical of polaron-pair dianions.

Red arrows indicate the excitation wavelengths employed to obtain the Raman spectra of radical anion (633 nm, detected for **OTPD₄**, **OTPD₅** and **OTPD₆**) and dianion (633 nm, detected for **OTPD₅** and **OTPD₆**) species.

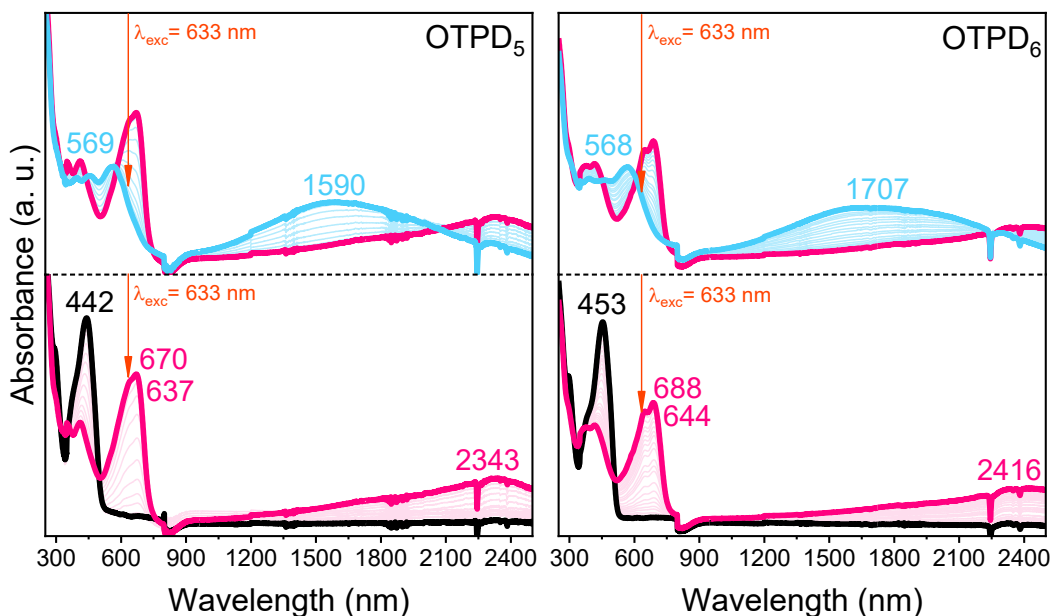


Figure VII.VI.2. UV-Vis-NIR spectroelectrochemical reduction of **OTPD₅** and **OTPD₆** oligomers in $\text{Bu}_4\text{N-PF}_6$ 0.1M in CH_2Cl_2 at room temperature. Black lines correspond to the spectra of neutral molecules; pink lines correspond to the completely formed radical anion species; blue lines correspond to the completely formed dianion species. Light colour lines correspond to the intermediate spectra between the former species in the reduction process.

Chapter 3. The Case of Quinoidal Oligothienopyrrolediones: The Effect of Size.

2DQoT Series

Electrochemical reduction of neutral **2DQoT** molecules produces the corresponding radical anion species in which the *extra* electron is delocalized between the end-capping dicyanomethylene moieties. Further reduction of **2DQQT** and **2DQPT** linear radical anion gives rise to a second anionic species in which the *extra* electron is delocalized through inter-dione sequences: cross-conjugated radical anions. Next reduction step is followed by the formation of bipolaron dianion species for the three systems. Finally, radical trinaion species are detected for **2DQTT** and **2DQQT**.

Red and brown arrows indicate the excitation wavelengths employed to obtain the Raman spectra of radical anion species (785 nm for **2DQTT**, and 633 nm for **2DQQT** and **2DQPT**), obtained chemically.

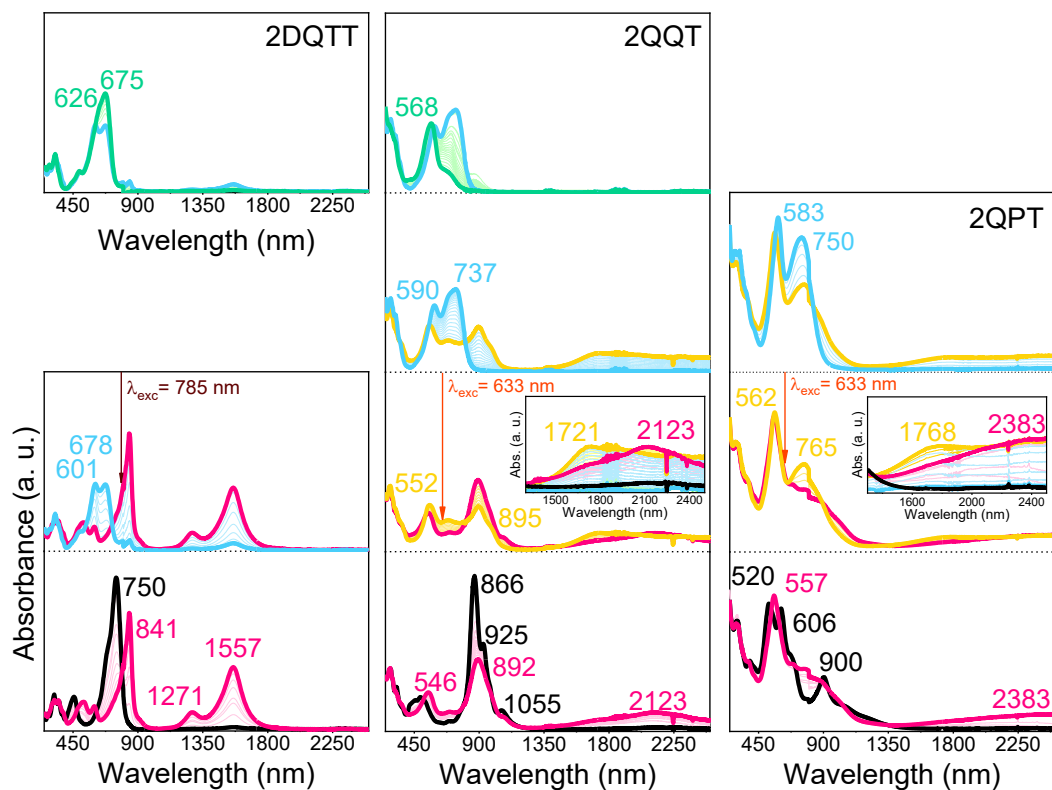


Figure VII.VI.3. UV-Vis-NIR spectroelectrochemical reduction of **2DQoT** oligomers in $\text{Bu}_4\text{N-PF}_6$ 0.1M in CH_2Cl_2 at room temperature. Black lines correspond to the spectra of neutral molecules; pink lines correspond to the completely formed linear radical anion species; yellow lines correspond to the completely formed cross-conjugated radical anion species; blue lines correspond to the completely formed dianion species; green lines correspond to the completely formed radical trianion species. Light colour lines correspond to the intermediate spectra between the former species in the reduction process.

nPE Series

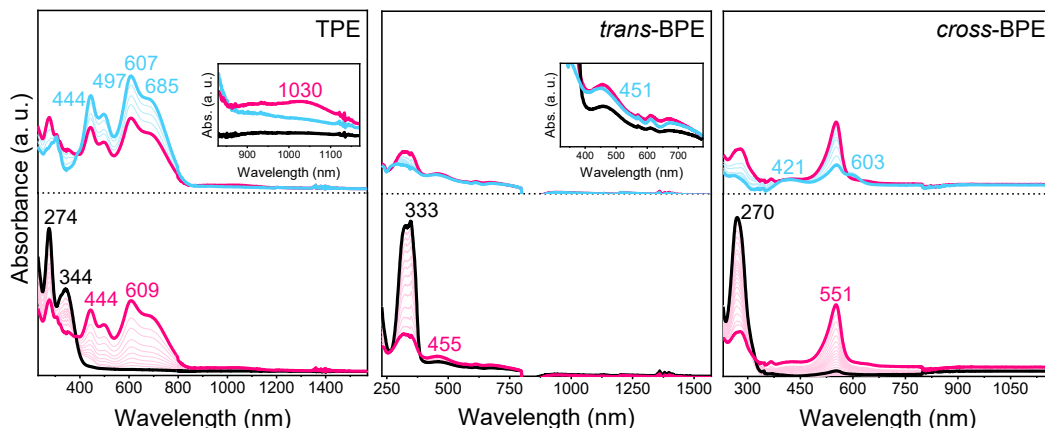


Figure VII.VI.4. UV-Vis-NIR spectroelectrochemical oxidation of nPE oligomers in $\text{Bu}_4\text{N-PF}_6$ 0.1M in CH_2Cl_2 at room temperature. Black lines correspond to the spectra of neutral molecules; pink lines correspond to the completely formed first oxidized species and blue lines correspond to the completely formed second oxidized species. Light colour lines correspond to the intermediate spectra between the former species in the oxidation process.

Section C. Spiro-Conjugated Diradicals

Chapter 4. The Case of Octacyano Diradicals: Spiro versus Parallel π -Conjugation.

Spiro-CPV Series

Electrochemical oxidation of neutral **A-CPVn** molecules produces in a first step the radical cation species, which is delocalized in the CPV cores for the three systems. Next oxidation step produces a bipolaron dianion in **A-CPV1**, and a polaron-pair dianion in **A-CPV2**. In the case of **A-CPV3**, both dianion species are formed. For **A-CPV1**, the following reduction step is a two-electron process that generates a tetracation species. Radical trication of **A-CPV2** (two electrons extracted from the CPV core, while only one is retired from the fluorene moiety) and **A-CPV3** are obtained after oxidation of the dicationic species. Finally, both subunits are doubly charged forming a tetracation species in the last oxidation step for the two molecules. **A-CPV1** tetracation evolves to the same structure as **A-CPV2** tetracation.

Red and brown arrows indicate the excitation wavelengths employed to obtain the Raman spectra of radical cation, dication and radical trication (only for **A-CPV3**) species obtained chemically.

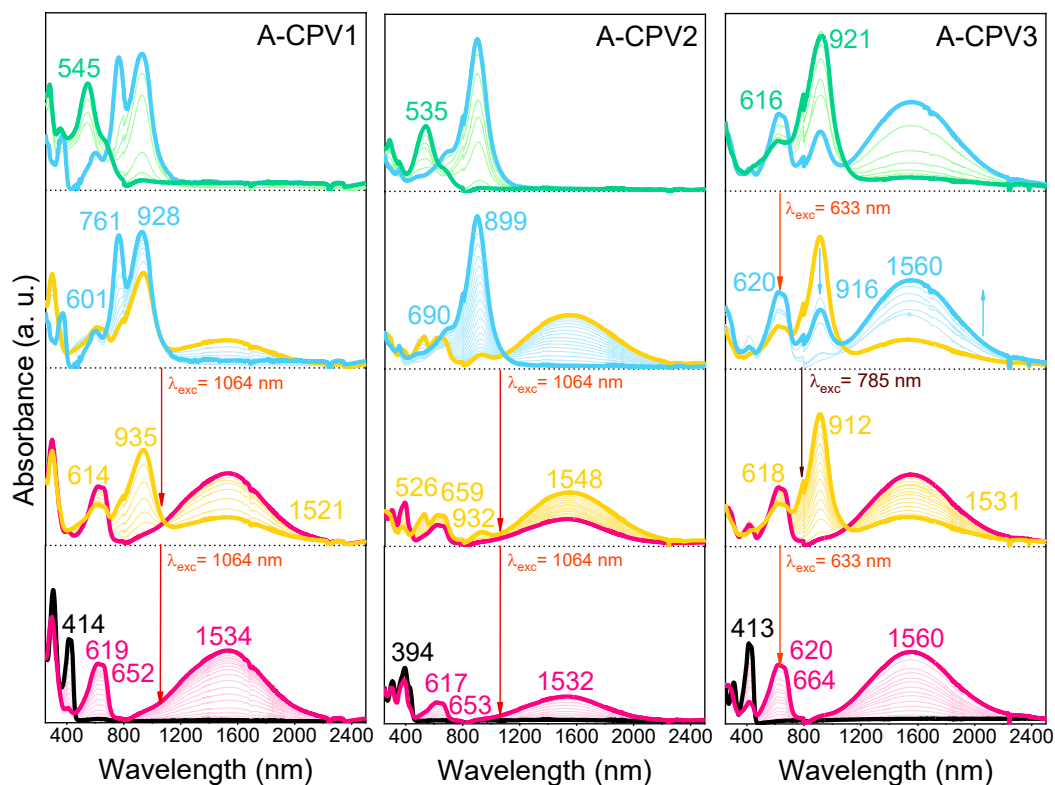


Figure VII.VI.5. UV-Vis-NIR spectroelectrochemical oxidation of **A-CPV1**, **A-CPV2** and **A-CPV3** molecules in $\text{Bu}_4\text{N-PF}_6$ 0.1M in CH_2Cl_2 at room temperature. Black lines correspond to the spectra of neutral molecules; pink lines correspond to the completely formed radical cation species; yellow line corresponds to the completely formed dication specie; blue lines correspond to the completely formed radical trication and tetracation species for **A-CPV2/ A-CPV3** and **A-CPV1**, respectively; green lines correspond to the completely formed tetracation species. Light colour lines correspond to the intermediate spectra between the former species in the oxidation process.

Octacyano Systems

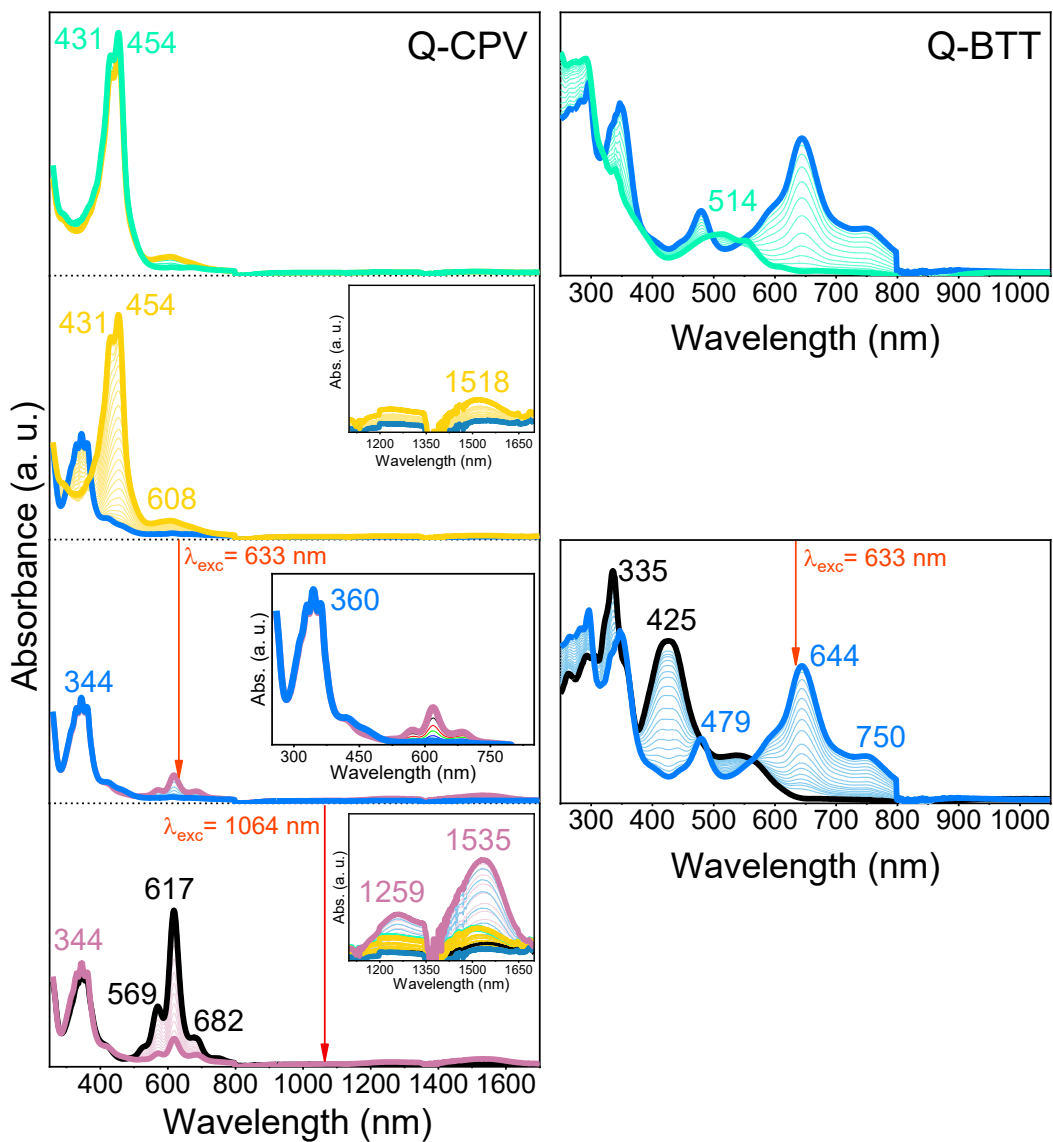


Figure VII.VI.6. UV-Vis-NIR spectroelectrochemical reduction of **Q-CPV** and **Q-BTT** molecules in $\text{Bu}_4\text{N-PF}_6$ 0.1M in CH_2Cl_2 at room temperature. Black lines correspond to the spectra of neutral molecules; pink lines correspond to the spectra of the completely formed radical anion, blue lines correspond to the spectra of the completely formed dianions, yellow lines correspond to the completely formed radical trianion, and green lines correspond to the spectra of the completely formed tetra-anion species. Light colour lines correspond to the intermediate spectra between the former species in the reduction process.

Electrochemical reduction of spiro **Q-CPV** generates in a first step the radical anion in one of the two CPV cores, while the second reduction step produces the segregated dianion (one *extra* electron in each CPV moiety). Further reduction produces the radical

trianion species, and finally, the injection of a fourth electron results in the tetra-anion species. Observe that the optical spectra of radical anion and dianion, and radical trianion and tetra-anion are very similar.

Red arrows indicate the excitation wavelengths (1064 nm and 633 nm) employed to perform the Raman spectra of radical anion and dianion species, respectively, obtained chemically.

On the other hand, electrochemical reduction of parallel **Q-BTT** takes place in two processes of two electrons each one. First reduction step produces the polaron-pair dianion, while the second step gives rise to the closed-shell tetra-anion species.

Red arrow indicates the excitation wavelengths (633 nm) employed to perform the Raman spectra of the dianion species, obtained chemically.

APPENDIX VII.VII. PUBLICATIONS

This section presents the publications derived from the development of the different projects discussed in this Ph. D. Thesis.

Section A. Linearly π -Conjugated DiradicalsChapter 1. *The Case of Aromatic and Quinoidal Oligorylenes.*

- **Long Rylene Nanoribbons Express Polyacetylene-like Signatures at their Edges.** Samara Medina Rivero, Sofia Canola, Wangdong Zeng, Francisco J. Ramírez, José L. Zafra, Jishan Wu*, Fabrizia Negri* and Juan Casado*, *Phys. Chem. Chem. Phys.*, **2019**, *21*, 7281—7287.
- **Stable Nitrogen-Centered Bis(imino)rylene Diradicaloids.** Wangdong Zeng, Yongseok Hong, Samara Medina Rivero, Jinseok Kim, José L. Zafra, Hoa Phan, Tullimilli Y. Gopalakrishna, Tun Seng Heng, Jun Ding, Juan Casado*, Dongho Kim* and Jishan Wu*, *Chem. Eur. J.*, **2018**, *24*, 4944—4951.

Section B. Cross-Conjugated Diradicals

Chapter 2. *The Case of Aromatic Oligothiopyrrolediones: Cross-Conjugated Dianions.*

- **Thieno[3,4-*c*]pyrrole-4,6-dione Oligothiophenes Have Two Crossed Paths for Electron Delocalization.** Dafei Yuan, Samara Medina Rivero, Paula Mayorga Burrezo, Longbin Ren, María E. Sandoval-Salinas, Sławomir J. Grabowski, David Casanova, Xiaozhang Zhu* and Juan Casado*, *Chem. Eur. J.*, **2018**, *24*, 13523—13534.

Chapter 3. *The Case of Quinoidal Oligothiopyrrolediones: The Effect of Size.*

- **Cholesteric Aggregation at the Quinoidal-to-Diradical Border Enabled Stable *n*-Doped Conductor.** Dafei Yuan, Dazhen Huang, Samara Medina Rivero, Abel Carreras, Cheng Zhang, Ye Zou, Xuechen Jiao, Christopher R. McNeill, Xiaozhang Zhu*, Chong-an*, Daoben Zhu, David Casanova* and Juan Casado*, *Chem.*, **2019**, *5*, 964—976.
- **Stable Cross-Conjugated Tetrathiophene Diradical.** Cheng Zhang, Samara Medina Rivero, Wuyue Liu, David Casanova, Xiaozhang Zhu* and Juan Casado*, *Angew. Chem. Int. Ed.*, **2019**, *58*, 11291—11295.



Long rylene nanoribbons express polyacetylene-like signatures at their edges†

Cite this: *Phys. Chem. Chem. Phys.*, 2019, 21, 7281

Samara Medina Rivero,^a Sofia Canola,^{b,c} Wangdong Zeng,^d Francisco J. Ramirez,^a José L. Zafra,^{b,a} Jishan Wu,^{b,*d} Fabrizia Negri^{c,*bc} and Juan Casado^{b,*a}

Oligorylenes have been the focus of research during the journey toward intrinsically conducting polyrylene. Recently, the description of diradicaloid and tetraradicaloid properties in long oligorylene molecules has revived the old question about their electronic structures which is of current interest in the context of the properties of graphene nanoribbons. Here we show that the armchair edges of smaller oligorylenes are embedded within aromatic units and they transform into armchair *cis*-polyacetylenic structures for octarylene and longer. Concomitantly, the short zig-zag edges of oligorylenes stabilize diradicaloid and multiradical states. This electronic transformation is proved experimentally by Raman spectroscopy and supported by theoretical modelling.

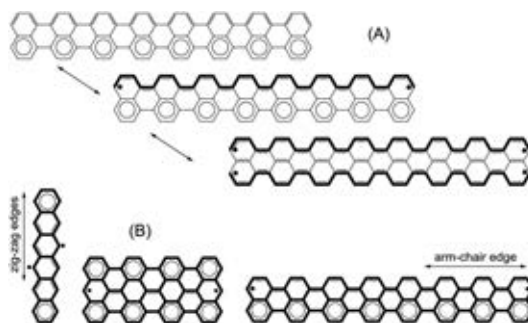
Received 3rd February 2019,
Accepted 1st March 2019

DOI: 10.1039/c9cp00679f

rsc.li/pccp

Introduction

Polyrylene has been the subject of interest since the discovery of conducting polymers, as it was predicted to be an electrical conductor without the need for external doping.¹ In parallel, oligomers of rylene, oligorylenes,² have also been the focus of research not only as molecular models of polyrylene, but also for important reasons such as: (i) they represent exceptional molecular models of graphene nanoribbons³ with finite gaps and semiconducting properties; that is, they are ideal for oligomer approach studies dealing with chain length and size dependent rationalization of electronic properties; and (ii) they can serve as open-shell graphene-like models given that they feature “semiconducting” armchair states and “metallic” edge states associated with the existence of “unpaired” electron density or radicaloid state domains (Scheme 1).^{4,5} In octarylene, the oligorylene with eight naphthalenes in Scheme 1, a simple chemist’s view in terms of electronic canonical forms enlightens the fundamental properties under discussion.



Scheme 1 (A) Closed-shell, diradical and tetraradical canonical forms of octarylene. (B) Diradical canonical forms of hexacene, quarteranthene, and octarylene drawn with the zig-zag and armchair edges in the vertical and horizontal axes, respectively.

Hence, the understanding of the electronic and molecular structures of polyrylene in terms of open-shell forms consisting of fused *cis*-polyacetylene-like lateral ribbons (bonds in bold in Scheme 1A for octarylene) has been an age-old aspiration of chemists to explain the low band gap characteristics of an “ideal” polymer. From this polyacetylene viewpoint, both ribbons sustain soliton-like structures or (multi)radicaloid states which are features intrinsically related to the more recent theoretical prediction of diradical and tetraradical characters in long rylene⁶ and, in general, to the radicaloid character of some of the edge states of graphene nanoribbons. In this regard, hexacene⁷ and quarteranthene⁸ are known polycyclic aromatic hydrocarbons, similar to oligorylenes, in which the diradical character is accommodated in the zig-zag edges with 12 and 6 carbon-carbon bond sizes, respectively (Scheme 1B).

^a Department of Physical Chemistry, University of Málaga, Campus de Teatinos s/n, Málaga 29071, Spain. E-mail: casado@uma.es

^b Università di Bologna, Dipartimento di Chimica ‘G. Ciamician’, Via F. Selmi, 2, 40126 Bologna, Italy

^c INSTM, Udr Bologna, Italy. E-mail: fabrizia.negri@unibo.it

^d Department of Chemistry, National University of Singapore, 3 Science Drive 3, 117543, Singapore. E-mail: chmwuj@nus.edu.sg

† Electronic supplementary information (ESI) available: Experimental description of the instruments and spectroscopic measurements together with theoretical details of the quantum calculations including theoretical Raman spectra and assignments of the Raman bands in terms of vibrational eigenvectors. See DOI: 10.1039/c9cp00679f

Diradicaloids

Stable Nitrogen-Centered Bis(imino)rylene Diradicaloids

Wangdong Zeng,^[a, b] Yongseok Hong,^[c] Samara Medina Rivero,^[d] Jinseok Kim,^[c] José L. Zafra,^[d] Hoa Phan,^[a] Tullimilli Y. Gopalakrishna,^[a] Tun Seng Heng,^[e] Jun Ding,^[e] Juan Casado,^{*,[d]} Dongho Kim,^{*,[c]} and Jishan Wu^{*,[a]}

Abstract: The synthesis of stable open-shell singlet diradicaloids is critical for their practical material application. So far, most reported examples are based on carbon-centered radicals, which are intrinsically reactive, and there are very few examples of stable nitrogen-centered diradicaloids. In this full paper, a series of soluble and stable bis(imino)rylenes up to octarylene were synthesized on the basis of newly developed dibromorylene intermediates. It was found that from hexarylene onward, these quinoidal rylenes showed open-shell singlet ground states and could be thermally populated

to paramagnetic triplet aminyl diradicals. They are stable due to efficient spin delocalization onto the rylene backbone as well as kinetic blocking of the aminyl sites by the bulky and electron-deficient 2,4,6-trichlorophenyl groups. They exhibited very different electronic structures, diradical character, excited-state dynamics, one-photon absorption, two-photon absorption, and electrochemical properties from their respective aromatic rylene counterparts. These bis(imino)rylenes represent a rare class of stable, neutral, nitrogen-centered aminyl diradicaloids.

Introduction

Recently, there has been growing interest in open-shell singlet diradicaloids/polyradicaloids that exhibit unique magnetic activity and have potential applications in organic electronics, photonics, and spintronics.^[1] So far, most reported diradicaloids^[2–7] and polyradicaloids^[8] have been based on carbon-centered radicals, which are usually highly reactive. Phenoxyl^[9] and porphyrinoid-based^[10] diradicaloids usually demonstrate better stability. In addition, diradicaloids based on triphenylamine cations^[11] and boron anions^[12] have also been reported, but they are usually sensitive to moisture and oxygen. Neutral, nitrogen-centered aminyl singlet diradicaloids^[13] and high-spin

polyradicals^[14] have reasonable stability if the aminyl center is properly protected by bulky substituents. However, examples are very limited. We recently demonstrated that cyclopenta (CP)-ring fused rylene ribbons displayed very unusual open-shell singlet diradical character from hexarylene onward (Figure 1 a).^[15] From the viewpoint of aromaticity, the formation of a diradical is not favorable because upon going from the closed-shell aromatic resonance form to the open-shell quinoid-

[a] Dr. W. Zeng, Dr. H. Phan, Dr. T. Y. Gopalakrishna, Prof. J. Wu
Department of Chemistry, National University of Singapore, 3 Science Drive 3, 117543, Singapore (Singapore)
E-mail: chmwuj@nus.edu.sg

[b] Dr. W. Zeng
Institute of Materials Science and Engineering, Hunan University of Science and Technology, Xiangtan 411201 (P. R. China)

[c] Y. Hong, J. Kim, Prof. D. Kim
Spectroscopy Laboratory for Functional π -Electronic Systems and Department of Chemistry, Yonsei University, Seoul 03722 (Korea)
E-mail: dongho@yonsei.ac.kr

[d] S. Medina Rivero, Dr. J. L. Zafra, Prof. J. Casado
Department of Physical Chemistry, University of Malaga, Campus de Teatinos s/n, 229071 Malaga (Spain)
E-mail: casado@uma.es

[e] Dr. T. S. Heng, Prof. J. Ding
Department of Materials Science & Engineering, National University of Singapore, 119260, Singapore (Singapore)

Supporting Information and the ORCID identification number(s) for the author(s) of this article can be found under <https://doi.org/10.1002/chem.201706041>.

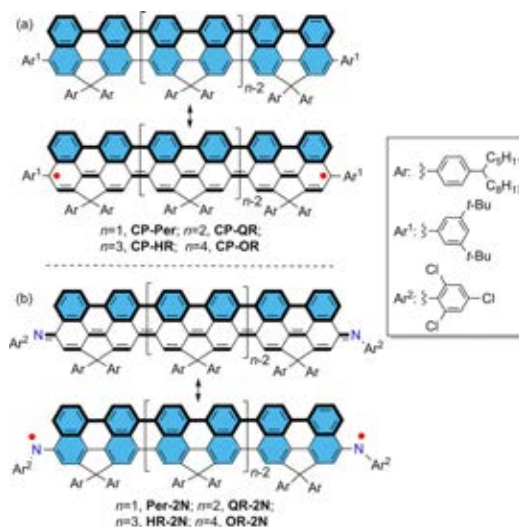


Figure 1. Closed-shell and open-shell diradical resonance forms of a) the aromatic CP-rylenes and b) the new bis(imino)rylenes.

Oligomers

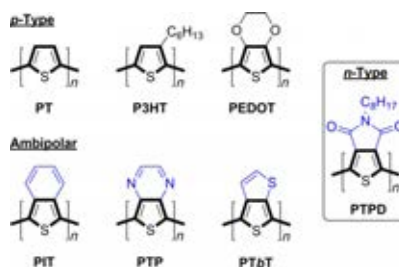
Thieno[3,4-*c*]pyrrole-4,6-dione Oligothiophenes Have Two Crossed Paths for Electron DelocalizationDafei Yuan,^[a, c] Samara Medina Rivero,^[b] Paula Mayorga Burrezo,^[b] Longbin Ren,^[a, c] María E. Sandoval-Salinas,^[d, e] Sławomir J. Grabowski,^[e] David Casanova,^[e] Xiaozhang Zhu,^{*[a, c]} and Juan Casado^{*[b]}

Abstract: A new series of electron-deficient oligothiophenes, thieno[3,4-*c*]pyrrole-4,6-dione oligothiophenes (OTPD_n), from the monomer to hexamer, is reported. The optical and structural properties in the neutral states have been analyzed by absorption and emission spectroscopy together with vibrational Raman spectroscopy. In their reduced forms, these molecules could stabilize both anions and dianions in similar ways. For the dianions, two independent modes of electron

conjugation of the charge excess were observed: the inter-dione path and the interthiophene path. The interference of these two paths highlighted the existence of a singlet diradical ground electronic state and the appearance of low-energy, thermally accessible triplet states. These results provide valuable insights into the device performance of TPD-based materials and for the rational design of new high-performance organic semiconductors.

Introduction

During the last decades, thiophene-based π -functional materials have played a crucial role in the development of high-performance organic electronic/optoelectronic devices.^[1] Although bare thiophene is electron rich, it can be transformed into valuable building blocks with widely tuneable electronic properties by attaching specific substituents around the thiophene (Scheme 1). Substitution in its 3 and 4 positions (i.e., β positions) is particularly effective, for example, poly(3-hexylthiophene-2,5-diyl) (P3HT)^[2] and poly(3,4-ethylenedioxythiophene) (PEDOT),^[3] which consist of electron-rich 3-hexylthiophene and 3,4-ethylenedioxythiophene, respectively. These are important



Scheme 1. Series of homopolymers that consist of thiophene building blocks but possess dissimilar electronic properties.

p-type semiconductors for applications into polymer solar cells as a landmark electron-donor material, and in some cases, these are also widely applied as transparent conductive polymers, such as PEDOT:poly(styrenesulfonate).^[4] By fusing pro-aromatic benzene, pyrazine, and thiophene rings in the β positions of thiophene, the resultant benzo[*c*]thiophene, thieno[3,4-*b*]pyrazine, and thieno[3,4-*b*]thiophene show high quinoid-enhancing effects and amphoteric redox behavior, from which homopolymers have been produced, such as poly(isothianaphthene) (PIT),^[5] poly(thieno[3,4-*b*]pyrazine) (PTP),^[6] and poly(thieno[3,4-*b*]thiophene) (PTbT),^[7] which have relatively small optical band gaps (Scheme 1). β -functionalization with pyrrole diones gives rise to the thieno[3,4-*c*]pyrrole-4,6-dione (TPD) monomer, which is a net electron-accepting moiety that produces poly(thieno[3,4-*c*]pyrrole-4,6-dione) (PTPD)^[8] with very low-energy unoccupied orbitals. To date, π -functional materials designed by donor–acceptor (D–A) and quinoid strategies have occupied a dominant position in organic photovoltaic chemistry,^[9] therefore, quinoid-enhancing TbT and electron-deficient TPD compounds are highly valuable building

[a] D. Yuan, L. Ren, Prof. X. Zhu
Beijing National Laboratory for Molecular Sciences
CAS Key Laboratory of Organic Solids, Institute of Chemistry
Chinese Academy of Sciences, Beijing 100190 (China)
E-mail: xzzhu@iccas.ac.cn

[b] S. Medina Rivero, P. Mayorga Burrezo, Prof. J. Casado
Department of Physical Chemistry, University of Málaga
Campus de Teatinos s/n, Málaga, 29071 (Spain)
E-mail: casado@uma.es

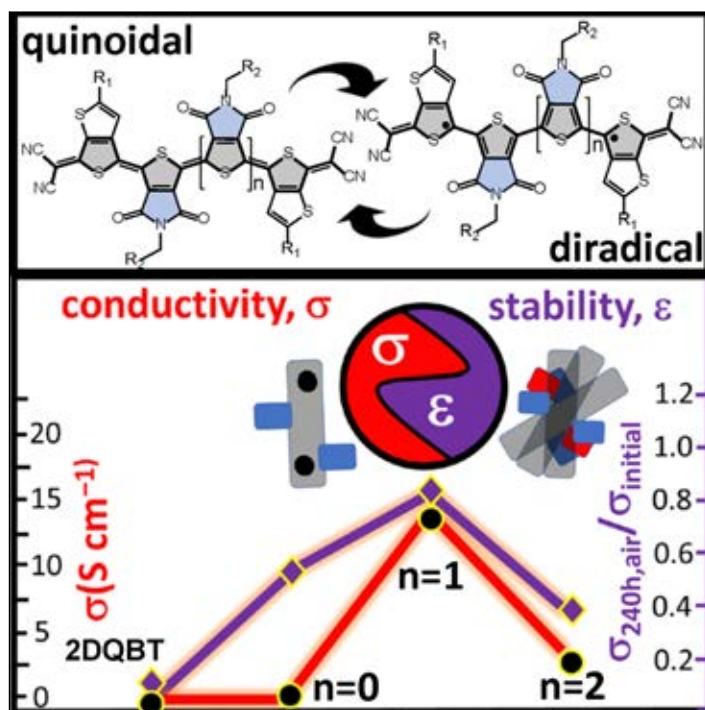
[c] D. Yuan, L. Ren, Prof. X. Zhu
University of Chinese Academy of Sciences, Beijing 100190 (China)

[d] M. E. Sandoval-Salinas
Departament de Ciència de Materials i Química Física
Institut de Química Teòrica i Computacional (IQTCUB)
Universitat de Barcelona, Martí i Franquès 1-11, Barcelona 08028 (Spain)

[e] M. E. Sandoval-Salinas, S. J. Grabowski, Prof. D. Casanova
Kimika Fakultatea, Euskal Herriko Unibertsitatea (UPV/EHU)
Donostia International Physics Center
Paseo Manuel de Lardizabal 4, Donostia 20018 (Spain)

Supporting information and the ORCID identification number(s) for the author(s) of this article can be found under:
<https://doi.org/10.1002/chem.201801880>.

Article

Cholesteric Aggregation at the Quinoidal-to-Diradical Border Enabled Stable n -Doped Conductor

Highly stable n -doped conductors based on quinoidal oligothiophenes are achieved. The suitable synergy between intra- and inter-molecular effects dictates the exceptional properties of 2DQQT. Uniquely, its incipient diradical character and cholesteric-like aggregation both enhance electrical conductivity (i.e., $14.0\ S\ cm^{-1}$) and unprecedented air stability. At the molecular level, our findings demonstrate that small diradical character and deep LUMO energy levels, lower than $-4.6\ eV$, are conditions suitable for achieving stable n -type doping.

Dafei Yuan, Dazhen Huang,
Samara Medina Rivero, ...,
Daoben Zhu, David Casanova,
Juan Casado

xzzhu@iccas.ac.cn (X.Z.)
dicha@iccas.ac.cn (C.-a.D.)
david.casanova@ehu.eus (D.C.)
casado@uma.es (J.C.)

HIGHLIGHTS

Air-stable n -doped conductors
from diradical oligothiophenes

Synergistic action of incipient
diradical character and
cholesteric-type aggregation

Outstanding performance as
electrical and thermoelectric
materials

Yuan et al., Chem 5, 964–976
April 11, 2019 © 2019 Elsevier Inc.
<https://doi.org/10.1016/j.chempr.2019.02.010>

Radicals

International Edition: DOI: 10.1002/anie.201904153
German Edition: DOI: 10.1002/ange.201904153

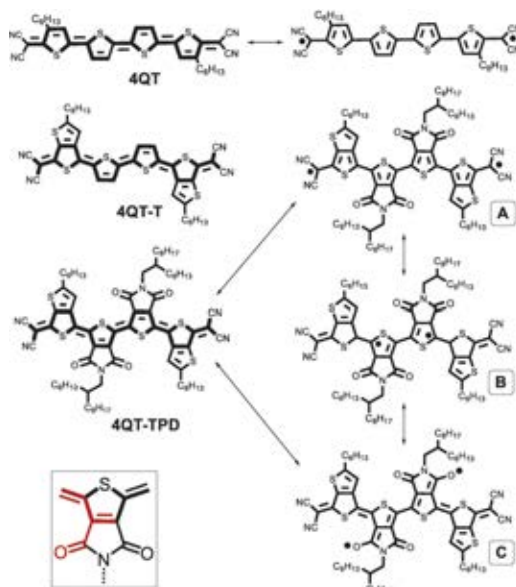
Stable Cross-Conjugated Tetrathiophene Diradical

Cheng Zhang[†], Samara Medina Rivero[†], Wuyue Liu, David Casanova, Xiaozhang Zhu,^{*} and Juan Casado^{*}

Abstract: A tetracyano quinoidal tetrathiophene, having a central bi(thieno[3,4-*c*]pyrrole-4,6-dione) acceptor, has been studied. The recovered aromaticity of the thiophenes produces a diradical species with cross-conjugation between the inter-dicyano and inter-dione acceptor paths. A diradical character of $y_0 = 0.61$ and a singlet–triplet gap of -2.76 kcal mol⁻¹ were determined. Competition between the two cross-conjugated paths enhances the disjointed character of the SOMOs and results in the confinement of the diradical to the molecular center, enabling a thermodynamic diradical stabilization featuring a half-life of 262 hours. Cross-conjugation effects have been also addressed in the anionic species (up to a radical trianion).

Diradicals based on π -conjugated molecules (i.e., Kekulé-type) are of continuous interest in chemistry because of their unique connection with the nature of the chemical bond.^[1] In addition, they are in the spotlight of current organic electronic applications.^[2] The diradical character can be tailored in several ways, such as with the number of pro-aromatic rings or with the inclusion of proper functionalization (Scheme 1).^[3] Unfortunately, the increase of diradical character often sacrifices the chemical stability, therefore strategies conserving diradical character and improving molecular fatigue are highly welcome. Herein we describe a stable cross-conjugated diradical.

Tetracyanoquinodimethane oligothiophenes (i.e., quinoidal oligothiophene series, **nQT** where n = number of thiophenes) are well-known in the field of Kekulé diradicals, and form these diradicals by recovery of the aromaticity on the



Scheme 1. Chemical structures of the studied quinoidal tetrathiophenes in their closed-shell and diradical canonical forms (A, B, and C). The insert highlights in red the cross-conjugated subunits.

thiophene rings (Scheme 1). Furthermore, given the small aromatic character of thiophene, a large tunability of the diradical character and of the singlet–triplet gaps (ΔE_{ST} gaps) is facilitated in **nQT**.^[4,5] In the **nQT** oligomer series, the tetramer in Scheme 1 is the first element with evidence of diradical properties.^[5] Differently functionalized quinoidal tetramers have been reported with the objective of modifying the solubility and optoelectronic properties.^[4,5] However, the evaluation of the diradical character on quinoidal tetramers and its dependence on the substitution and π -electron structure of thiophene has not been addressed in detail yet.

Herein, we modify a quinoidal tetracyano tetrathiophene core with thieno[3,4-*b*]thiophene^[6] and thieno[3,4-*c*]pyrrole-4,6-dione^[7] (TPD) groups, forming **4QT-TPD** (Scheme 1). **4QT-TPD** has been reported to be a material that is easily *n*-doped and has high chemical stability, high electrical conductivity, and outstanding thermoelectrical properties.^[8] A notable feature of **4QT-TPD** is cross-conjugation. For a given number of π -bonds, cross-conjugation reduces their effective π -delocalization compared with the case in which all bonds are in linear disposition (linear conjugation). **4QT-TPD** thus displays diradical delocalization along two crossed axes of conjugation (Scheme 1), the long axis between the dicyano

[*] Dr. C. Zhang^{†,††}, W. Liu, Prof. X. Zhu
Beijing National Laboratory for Molecular Sciences, CAS Key Laboratory of Organic Solids, Institute of Chemistry, Chinese Academy of Sciences, Beijing 100190 (P. R. China)

and
School of Chemistry and Chemical Engineering, University of Chinese Academy of Sciences, Beijing 100049 (China)
E-mail: xzzhu@iccas.ac.cn

S. Medina Rivero^{†,††}, Prof. J. Casado
Department of Physical Chemistry, University of Málaga, Andalucía-Tech, Campus de Teatinos s/n, 29071 Málaga (Spain)
E-mail: casado@uma.es

Dr. D. Casanova
Donostia, International Physics Center (DIPC) & IKERBASQUE—Basque Foundation for Science
20018 Donostia- San Sebastián, Euskadi (Spain)

[†] These authors contributed equally to this work.

[††] co-first author

Supporting information and the ORCID identification number(s) for the author(s) of this article can be found under:
<https://doi.org/10.1002/anie.201904153>.

